Paloma Álvarez Suárez

Drebrin and myosin VI: Cytoskeletal regulators of the development of the postsynaptic machinery at the murine neuromuscular junction

PhD thesis

Completed in the Laboratory of Molecular Basis of Cell Motility,
Nencki Institute of Experimental Biology,
Polish Academy of Sciences

Supervisor:
Prof. Maria Jolanta Rędowicz, Ph.D., D.Sc.
Auxiliary supervisor:
Dr. Marta Gawor, Ph.D.

Warsaw, 2022

TABLE OF CONTENTS

ACKNOWLEDGEMENTS

I would like to thank:

My supervisor, Prof. Maria Jolanta Rędowicz, PhD, DSc, for all the support and guidance through my scientific journey and for providing me with the opportunity to successfully complete my research. Her invaluable help and wisdom have made every step of this adventure easier, particularly in the hardest times.

My auxiliary supervisor, Dr. Marta Gawor, for showing me from the early start what a truly passionate mentor is. For all the scientific input at the bench and all the informal conversations at lunch time. For the intellectual and emotional support and, most importantly, for teaching me critical thinking, tolerance, and perseverance inside and outside the lab.

My parents, María José Suárez Cascajares and José Luis Álvarez Prida, for inculcating me the values and beliefs that have guided me so far through life and my professional career. For their constant support and genuine interest in listening to endless explanations of successful and failed experiments.

MSc. Dawid Gościk, for all the care, love, patience, and compassion that have enabled me to complete this challenge and prepared me to conquer any other to come. Words cannot describe the luck and gratitude of finding a true soulmate in such unexpected way.

Dr. María Banqueri López, for being my anchor to sanity throughout my entire journey as a researcher and beyond. For making life in Warsaw a bit more like home and continuously making me grow as a scientist and as a person.

MSc. Agnieszka Nadel, for being a unicorn in a field of horses and for her contagious good vibes, that could light up a room even when all experiments were failing.

My family and friends, Ángela, Alejandra, Ana, Inés, Ben, Jorge, Silvia, and all the rest, for their emotional support and constant cheer that made so many kilometers feel like nothing.

My Polish family, Krystyna, Roman, Marta, Kasia, and Konrad Gościk, Sarah Fuhrmann and Kuba Sobek, for taking me in.

MSc. Esther Jiménez García, for accompanying me in the last and hardest part of this journey, and teaching me how to better take care of my mental health.

My labmates from the former Laboratory of Synaptogenesis, for all the good times enjoyed and all the bad times overcome together.

My current labmates from the Laboratory of Molecular Basis of Cell Motility, for welcoming and supporting new members as if they were always there.

All the mice and rats whose lives were sacrificed in the name of science for the execution of this PhD thesis and all side projects.

Without you, none of this would have been possible.

Esta tesis doctoral está dedicada a mis padres, por creer siempre en mí

ABSTRACT

The neuromuscular junction (NMJ) is a chemical synapse of the peripheral nervous system that enables skeletal muscle contraction through acetylcholine-mediated neurotransmission. This synaptic structure is composed of three main elements, motor neuron, myofiber, and Schwann cells, that tightly regulate one another throughout ontogenesis via multiple signaling pathways. Disruption of these pathways can result in neuromuscular disorders that reduce the efficiency of muscle contraction and lead to muscle fatigue, wasting, and, in some cases, premature death. The cause of many neuromuscular disorders remains unknown to this date and any cure or treatment is often missing. Studying the molecular mechanisms underlying NMJ function in physiological and pathological contexts could shed light on these unmet clinical needs and even lay the path to discovering therapeutic targets. Impairments in cellular processes regulating the presence of acetylcholine receptors (AChRs) on the myofiber surface are one of the most devastating for proper NMJ function. Most importantly, many signaling pathways and developmental processes involved in receptor clustering and maintenance remain poorly understood, and researchers continue to unveil new roles for proteins whose relevance at the NMJ had been unknown before.

The actin cytoskeleton and actin-remodeling proteins are at the core of many postsynaptic-regulating processes, including local delivery and recycling of synaptic components, stabilization of postsynaptic complexes, and recruitment of other cytoskeletal filaments. Through my PhD research, I identified and characterized for the first time some of the functions of the cytoskeletal regulators drebrin and myosin VI in the formation and maintenance of the postsynaptic machinery. Specifically, I found that drebrin plays an important role in AChR clustering and maturation through its ability to rearrange actin filaments. Moreover, its mechanisms of action at the postsynaptic machinery seem to involve microtubule organization and interaction with rapsyn, a key AChR clustering mediator and stabilizer. Myosin VI, on the other hand, does not seem to be crucial neither for NMJ formation nor maturation, however its absence in mice significantly impairs NMJ structure and leads to reduced muscle strength, particularly in females.

Altogether, my results provide an insight into the mechanisms through which drebrin mediates AChR cluster formation, maturation, and maintenance, as well as the functional consequences of myosin VI loss in the skeletal muscle of mice.

STRESZCZENIE

Złącze nerwowo-mięśniowe (ZNM) to chemiczna synapsa obwodowego układu nerwowego, która pośredniczy w skurczu mięśni szkieletowych poprzez neurotransmisję za pośrednictwem acetylocholiny. Ta struktura synaptyczna składa się z trzech głównych składowych: motoneuronu, włókien mięśniowych i komórek Schwanna, które w ontogenezie ściśle regulują się nawzajem za pośrednictwem wielu ścieżek sygnałowych. Zakłócenie tych szlaków może skutkować zaburzeniami nerwowo-mięśniowymi, które zmniejszają wydajność skurczu mięśni i prowadzą do męczliwości mięśni, wyniszczenia, a w niektórych przypadkach do przedwczesnej śmierci. Przyczyna wielu zaburzeń nerwowo-mięśniowych pozostaje do tej pory nieznana i wciąż nie ma skutecznych leków i terapii. Poznanie mechanizmów molekularnych leżących u podstaw działania ZNM w warunkach fizjologicznych i patologicznych może rzucić światło na te niespełnione potrzeby kliniczne, m.in. poprzez odkrycie nowych celów terapeutycznych. Zaburzenia procesów komórkowych regulujących obecność receptorów acetylocholinowych (AChR) na powierzchni włókien mięśniowych są jednymi z najbardziej destrukcyjnych dla prawidłowego funkcjonowania ZNM. Co ważne, wiele ścieżek sygnałowych i procesów rozwojowych zaangażowanych w grupowanie i stabilność receptorów pozostaje słabo poznanych, a naukowcy nadal odkrywają nowe funkcje białek, których rola na ZNM była wcześniej nieznana.

Cytoszkielet aktynowy i białka biorące udział w rearanżacji filamentów aktynowych są zaangażowane w wiele postsynaptycznych procesów regulacyjnych, w tym w lokalne dostarczanie i recyrkulację komponentów synapsy, stabilizację kompleksów postsynaptycznych i rekrutację innych składowych cytoszkieletu. W moich badaniach będących podstawą rozprawy doktorskiej po raz pierwszy zidentyfikowałam i scharakteryzowałam niektóre funkcje białek cytoszkieletu: drebryny i miozyny VI w tworzeniu i organizacji maszynerii postsynaptycznej. W szczególności odkryłam, że drebryna, dzięki swojej zdolności do oddziaływania z filamentami aktynowymi, odgrywa ważną rolę w grupowaniu i dojrzewaniu klastrów AChR. Co więcej, mechanizmy organizacji maszynerii postsynaptycznej, w które zaangażowana jest drebryna wydają się obejmować organizację mikrotubul i interakcję z rapsyną, białkiem stanowiącym kluczowy element rekrutacji i stabilizacji AChR. Z kolei niekonwencjonalna miozyna VI, zależne od aktyny białko motoryczne, nie wydaje się być kluczowa w tworzeniu i dojrzewaniu ZNM, jednak jej brak u myszy skutkuje zmianami w struturze złącza, które prowadzą do zmniejszenia siły mięśni kończyn tylnych myszy, w szczególności u samic.

Podsumowując, moje wyniki dostarczają nowej wiedzy o mechanizmach udziału drebryny w tworzeniu, dojrzewaniu i stabilności klastrów AChR, jak również o funkcjonalnych konsekwencjach utraty miozyny VI w mięśniach szkieletowych myszy.

OWN PUBLICATIONS

Part of the work contained in this thesis has been published in peer-reviewed, indexed scientific journals:

Alvarez-Suarez, P., Nowak, N., Protasiuk-Filipunas, A., Yamazaki, H., Prószyński, T.J., Gawor, M. (2021). Drebrin regulates AChR clustering and organization of microtubules at the postsynaptic machinery. *International Journal of Molecular Sciences*, special issue Molecular Research on Muscle Protein and Myopathies, 22 (9387). DOI: 10.3390/ijms22179387. IF = 5.923.

Lehka, L., Topolewska, M., Wojton, D., Karatsai, O., **Alvarez-Suarez, P.**, Pomorski, P., Redowicz, M.J. (2020). Formation of Aberrant Myotubes by Myoblasts Lacking Myosin VI Is Associated with Alterations in the Cytoskeleton Organization, Myoblast Adhesion and Fusion. *Cells*, 9 (7), 1673. DOI: 10.3390/cells9071673. IF = 6.600.

Alvarez-Suarez, P., Gawor, M., and Prószyński, T. J. (2020). Perisynaptic Schwann cells - the multitasking cells at the developing neuromuscular junctions. *Seminars in Cell and Developmental Biology*, 104, 31-38. DOI: 10.1016/j.semcdb.2020.02.011. IF = 6.138

Other work published during the PhD studies:

Sampedro-Piquero, P., **Alvarez-Suarez, P.**, Postigo, A., Cuesta, M., and Begega A. (2020). Impact of Aerobic Exercise on Stress Resilient Behaviour Across the Lifespan. In *Healthy Lifestyles and Healthy Eating* (1st ed.) Nova Science. ISBN: 978-1-53618-399-3.

Sampedro-Piquero, P., **Alvarez-Suarez, P.**, Moreno-Fernandez, R.D., Garcia-Castro, G., Cuesta, M., and Begega A. (2018). Environmental Enrichment Results in Both Brain Connectivity Efficiency and Selective Improvement in Different Behavioral Tasks. *Neuroscience*, 388, 374-383. DOI: 10.1016/j.neuroscience.2018.07.036. IF = 3.244

This research was funded by the National Science Centre, Poland:

grant number UMO-2016/21/D/NZ4/03069 (awarded to M.G.)

grant number UMO-2018/29/N/NZ3/02682 (awarded to P.A-S.)

LIST OF ABBREVIATIONS

+TIP	Microtubule plus-end-tracking protein
Abl	Non-receptor tyrosine-protein kinase
ACh	Acetylcholine
AChE	Acetylcholinesterase
AChR	Acetylcholine receptor
ADF-H	Actin-depolymerizing factor homology domain
AKAP	A-kinase anchor protein
ALS	Amyotrophic lateral sclerosis
AMPA	α-amino-3-hydroxy-5-methyl-4-isoxazolepropionic acid
AMPAR	AMPA-type glutamate receptor
APC	Adenomatous polyposis coli protein
APP	β-amyloid precursor protein
Arp2/3	Actin-related proteins 2 and 3 complex
ATP	Adenosine 5'-triphosphate
BTX	Bungarotoxin
CaMKII	Calcium/Calmodulin-dependent protein kinase II
CC	Coiled-coil domain
CCE	Chicken embryo extract
Cdk5	Cyclin-dependent kinase 5
CLASP	Cytoplasmic linker-associated protein
CLIP	Cytoplasmic linker protein
CMS	Congenital myasthenic syndrome
CNS	Central nervous system
CRAC	Ca^{2+} release-activated Ca^{2+} channel
Dbn1	Drebrin gene in mice
DBN1	Drebrin gene in humans
DBN-1	Drebrin-like homolog in *C. elegans*
DBNL	Drebrin-like protein in humans
DGC	Dystrophin-glycoprotein complex
DHPR	Dihydropyridine receptor
DIA	Diaphragm muscle
DMD	Duchenne's muscular dystrophy
DMEM	Dulbecco's Modified Eagle's Medium
DNM2	Dynamin-2 gene in humans
DOCK7	Dedicator of cytokinesis 7
Dok7	Downstream of tyrosine kinase 7
DTT	Dithiothreitol
DXKO	Drebrin global knockout mouse strain
EB	End-binding protein
ECM	Extracellular matrix
EDL	Extensor digitorum longus
EPP	Endplate potential
FBS	Fetal bovine serum
GA	Gastrocnemius muscle
GGT	Geranylgeranyltransferase
GIPC1	GAIP (G α-interacting protein) C-terminus-interacting protein
GTP	Guanosin-5'-triphosphate
Hel	Helical domain
HS	Horse serum
IP_3R	Inositol triphosphate receptor
IQ motif	Light-chain binding motif

Lrp4	Low-density lipoprotein receptor-related protein
LTD	Long-term depression
LTP	Long-term potentiation
MACF1	Microtubule actin cross-linking factor 1
mAP	Muscle action potential
MAP	Microtubule-associated protein
MHC	Myosin heavy chain
MT1-MMP	Membrane type 1 matrix metalloproteinase
MT	Microtubule
MuSK	Muscle-specific kinase
MVI	Myosin VI
Myo6	Myosin VI gene in mice
nAP	Nerve action potential
Nav1.4	Muscle-specific voltage-gated Na^+ channels
NFAT	Nuclear factor of activated T cell
NM	Nemaline myopathy
NMJ	Neuromuscular junction
PAK1	Serine/threonine-protein kinase
PFA	Paraformaldehyde
PI3K	Phosphoinositide 3-kinase
PKA	Protein kinase A

PKC	Protein kinase C
PNS	Peripheral nervous system
PP	Proline-rich domain
p/s	penicillin and streptomycin
PSC	Perisynaptic Schwann cell
PSD-95	Postsynaptic density protein 95
PTEN	Phosphatase and tensin homolog
RAPSN	Rapsyn gene in humans
RCF	Relative centrifugal force (G-force)
RPM	Revolutions per minute
RT	Room temperature
Ryr1	Ryanodine receptor 1
SAP97	Synapse-associated protein 97
SC	Schwann cell
SOD1	Superoxide dismutase 1 gene in humans
SOL	Soleus muscle
Spikar	Spine and karyoplasm protein
SR	Sarcoplasmic reticulum (endoplasmic reticulum in muscle tissue)
ST	Sternomastoid muscle
SV	Snell's waltzer mouse strain, global myosin VI knockout
TA	Tibialis anterior muscle
TS	Triangularis sterni muscle

"*Science, for me, gives a partial explanation for life*.
In so far as it goes, it is based on fact, experience and experiment."

Rosalind Franklin,

co-discoverer of the DNA double helix structure

CHAPTER 1: INTRODUCTION

The nervous system is responsible for the ability of the organism to interact with the environment and the numerous stimuli that it is constantly receiving. It is organized to detect changes in both the internal and the external environments, evaluate and integrate information, and finally, to respond through effector cues, such as the endocrine and muscular systems. The ability to move is a crucial aspect of survival and reproduction for many species, and even the simple act of breathing is controlled by the muscular system in response to a nervous input. This is true to such extent that a failure in the muscular system to respond to these input signals often has fatal consequences for the organism. The analysis of these systems and their interactions is crucial for understanding both normal animal behavior and the development of pathology, such as neurological disorders and muscular dystrophies.

1.1. Organization of the Peripheral Nervous System

Evolution has provided animals with increasingly complex nervous systems that tend to centralize nervous networks and accumulate them in the anterior part of the nervous cord, with prolongations that reach throughout the entire organism to receive and emit signals and communicate with other systems (Arendt et al., 2008). The vertebrate nervous system is divided into two main sub-systems: the central nervous system (CNS) and the peripheral nervous system (PNS). The CNS includes the encephalon (brain, cerebellum, and brainstem) and the spinal cord, while the PNS consists of CNS-stemming nerves and ganglia located outside of the brain and the spinal cord (**Fig. 1.1A**). In turn, the PNS is divided in the autonomous (involuntary) and somatic (voluntary) systems (Purves et al., 2018).

The motor component of the somatic PNS comprises all motor nerves that send information in order to contract skeletal muscles. These motor nerves correspond to bundles of axons from neurons whose cell body is located in either the motor nuclei of the brainstem or the ventral horn of the spinal cord gray matter (cranial and spinal nerves, respectively). These so-called α motor neurons (or motoneurons) are controlled directly by local circuits within the spinal cord and the brainstem, but also indirectly by neurons in higher CNS centers (upper motoneurons) that regulate local circuits to enable the execution of complex and coordinated movements. Sensory neurons also emit direct

information to local circuit neurons to regulate motor reflexes that operate independently from higher brain structures. In the end, skeletal muscles receive information from a variety of sources integrated by the α motoneurons (**Fig. 1.1B**). Both axons and axon terminals of α motoneurons are encapsulated by peripheral glial cells called Schwann cells (SC), that assist motor nerve functions (Purves et al., 2018).

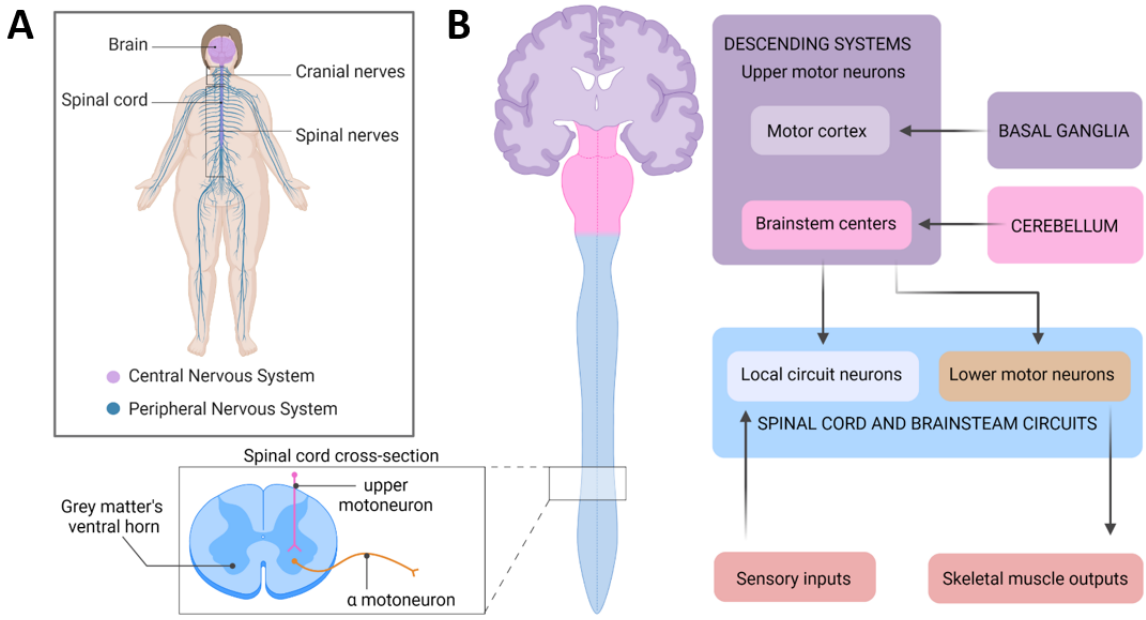

Figure 1.1. Organization of the nervous system. (A) Overall view of the central and peripheral nervous systems. **(B)** Neural structures controlling voluntary movement of skeletal muscles. Illustration created with BioRender.com.

Developing an electrically excitable muscle membrane (sarcolemma) was the evolutionary solution for a more efficient use of the motor input, thus further focalizing the point of contact between motoneurons and muscle fibers (Slater, 2017). In mammals, a given adult muscle fiber is generally innervated by only one α motoneuron, with the exception of multinnervated extraocular and limb muscles, trunk and limbs intrafusal fibers, and temporary developmental stages of multinnervation (Schiaffino & Reggiani, 2011). Conversely, one α motoneuron usually innervates several fibers from the same muscle (Buchthal & Schmalbruch, 1980).

1.1.1. The neuromuscular junction

A single α motoneuron and all the muscle fibers it innervates constitute the so-called motor unit, the smallest unit force that can be recruited for movement. This way, the number of motor units recruited at a given time is used to control the amount of force that a muscle generates. The focal point where an axon terminal contacts with the

muscle fiber is called neuromuscular junction (NMJ) and forms a chemical synapse relying, in mammals, on the neurotransmitter acetylcholine (ACh) (**Fig. 1.2**) (Purves et al., 2018). Apart from skeletal muscle fiber and α motoneuron, NMJ structure and function is tightly regulated by non-myelinating perisynaptic Schwann cells (PSCs) that cover the synaptic area, altogether creating a tripartite synapse (Alvarez-Suarez et al., 2020; Araque et al., 1999).

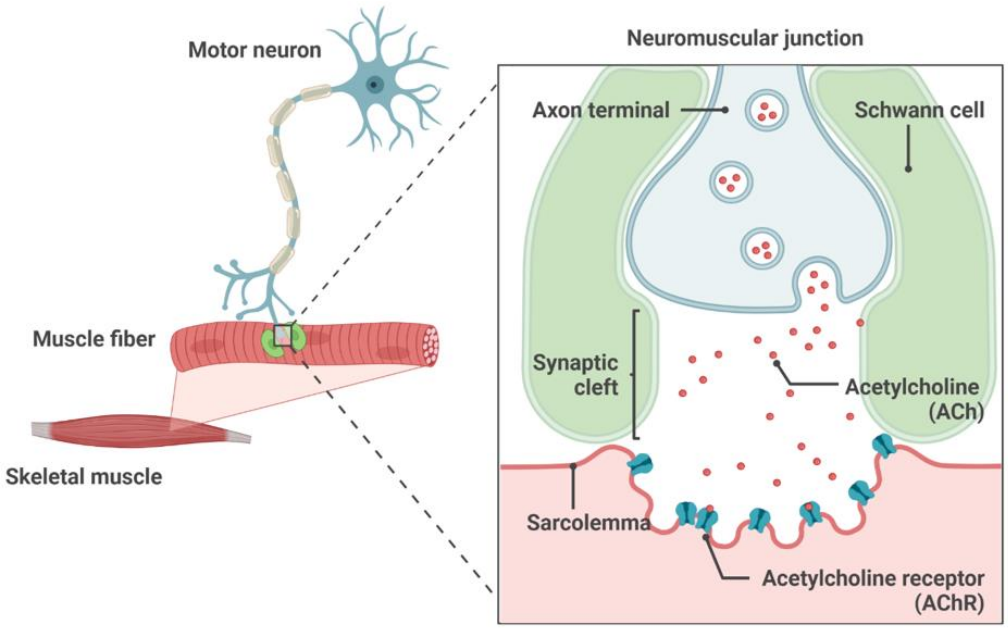

Figure 1.2. Schematic illustration of the neuromuscular junction components. Illustration created with BioRender.com.

An action potential travelling through the neuronal axon (nAP) leads to depolarization of the motoneuron membrane, opening of voltage-gated calcium channels, and the subsequent influx of calcium ions (Ca^{2+}) from the extracellular fluid. The increase in Ca^{2+} concentration triggers the fusion of ACh-containing synaptic vesicles with the presynaptic membrane of the motoneuron terminal and the release of ACh into the narrow space between pre- and postsynaptic elements, called synaptic cleft (**Fig. 1.3A_1**). The postsynaptic membrane is highly specialized to mirror the morphology of the presynaptic terminal, and is extensively folded in mammals to maximize the efficiency of the transmission (**Fig. 1.3B-C**). Junctional folds directly appose presynaptic active zones, where synaptic vesicles accumulate in a laminin subunit α4-dependent manner (Patton et al., 2001). The ACh molecules diffuse through the synaptic cleft in less than 1 ms, and bind to ligand-gated cation channels called acetylcholine receptors (AChRs). These receptors are accumulated at the crests of the muscle junctional folds

and their activation leads to the influx of sodium (Na^+), potassium (K^+), and Ca^{2+} ions and, in turn, changes in the polarization of the muscle membrane (endplate potential or EPP). To guarantee the efficacy of the neurotransmission and the contraction of the muscle, neurons release a high content of neurotransmitter, so that the EPP is several folds higher than the required to reach the threshold for generating a muscle action potential. This feature, called safety factor, allows for certain loss of function before the neurotransmission is completely impaired. The local depolarization caused by the EPP activates voltage-gated Na^+ channels (Nav1.4) located at the bottom of the junctional folds, leading to a bigger influx of cations inside the cell and depolarization of the muscle membrane (muscle action potential or mAP). Therefore, Na^+ channels at the bottom of junctional folds act as amplifiers of the signal and their high density contributes to the safety factor (**Fig. 1.3A_2**) (Purves et al., 2018; Slater, 2017; Tintignac et al., 2015; Verschuuren et al., 2016).

The mAP travels across the specialized sarcolemma and into T tubules, invaginations of the sarcolemma that are in close vicinity of the sarcoplasmic reticulum (SR, muscle endoplasmic reticulum) (Chal & Pourquié, 2017). Since the SR membrane is covered in voltage-gated Ca^{2+} channels, the mAP triggers the release of Ca^{2+} from within the SR to the cytoplasm through coupled activation of DHPR (dihydropyridine receptor) and Ryr1 (ryanodine receptor 1) channels (**Fig. 1.3A_3**). Calcium ions bind to proteins of the contractile machinery (sarcomere) and, eventually, induce a contraction in the muscle fiber (Huxley & Simmons, 1971) (*for more information about muscle contraction, see section 1.2.1.*). Opposite to many other neurotransmitters, the signal transmission is terminated not by reuptake of ACh, but by rapid hydrolytic activity of the enzyme acetylcholinesterase (AChE) that is present at the synaptic cleft (**Fig. 1.3D**). Therefore, it prevents repeated activation of AChR channels upon a single nAP (Purves et al., 2018).

Most of the current knowledge about chemical synaptic transmission was obtained from experiments on the murine NMJ, because it constitutes an excellent synapse model. Neuromuscular junctions are simpler whilst larger than central synapses (Takikawa & Nishimune, 2022). Moreover, they rely on unidirectional neurotransmission of one neuron to one muscle fiber, in comparison to multiple neuronal connections and neurotransmitters conveyed into neurons that are part of a network in the case of CNS (Tintignac et al., 2015).

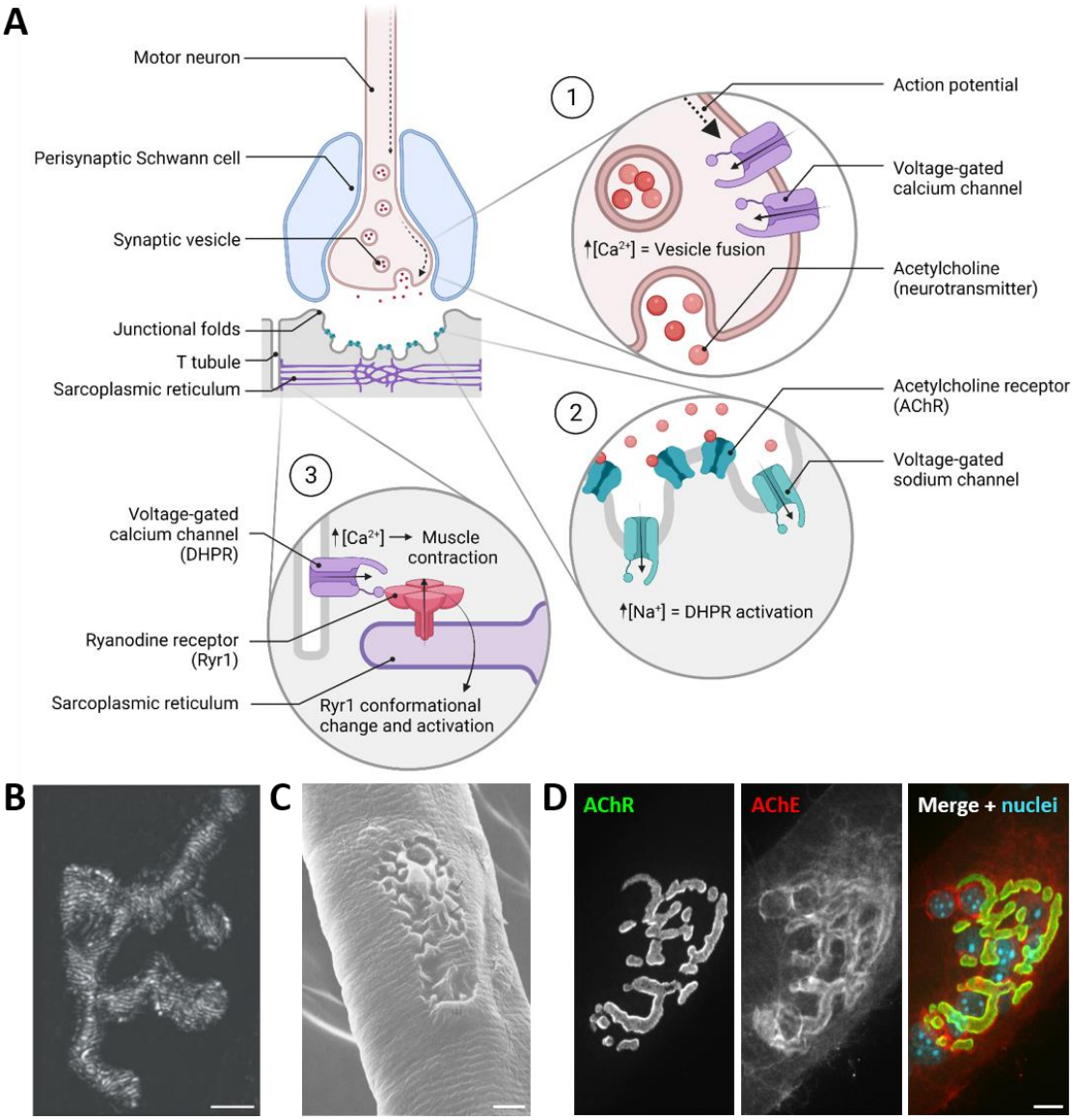

Figure 1.3. Transmission of the signal at the neuromuscular junction. (A) Schematic representation of the NMJ (upper left corner) and the three main events of the neurotransmission: **1)** entry of Ca^{2+} in the presynaptic terminal upon the arrival of a nAP and triggering of fusion of synaptic vesicles with the cell membrane, leading to the release of the neurotransmitter into the synaptic clef; **2)** binding of ACh to its receptor on the muscle surface (AChR) that generates an EPP, triggering the activation of voltage-gated Na^{2+} channels that amplify the signal (mAP); **3)** muscle contraction triggered by the cytoplasmic release of Ca^{2+} stored in the SR. Illustration created with BioRender.com. **(B)** Visualization of the topography of AChRs in the adult mouse NMJ through high-resolution confocal microscopy, where the observed striped pattern is due to the extensive junctional folding of the postsynaptic membrane. Scale bar = 4 µm. Image adapted with permission of the authors (Marques et al., 2000). **(C)** Junctional folds on the muscle surface of the Chinese hamster observed with scanning electron microscopy. Scale bar = 5 µm. Image adapted with permission of the authors (Desaki & Uehara, 1981). **(D)** Distribution pattern of acetylcholinesterase (AChE, red) in the synaptic cleft of the mouse NMJ, visualized together with postsynaptic neurotransmitter receptors (AChR, green) and synaptic nuclei (blue) in a spinning-disk confocal microscope. Scale bar = 10 µm. Own image.

Additionally, NMJs are more accessible due to their peripheral location, facilitating the application of histological and electrophysiological methods and allowing for both structural and functional studies (Webster, 2018). In particular, murine NMJs have a significantly larger surface (400 μm^2 in mice vs. 200 μm^2 in humans) and a higher content of neurotransmitter released in synaptic vesicles than human NMJs, which makes them convenient to manipulate in experimental settings. Importantly, murine NMJs reflect most of the morphological features and molecular mechanisms of human NMJs (Boehm et al., 2020), such as the extensive folding of the postsynaptic membrane (Slater, 2017), or the agrin-induced signaling pathways involved in synapse formation and morphological maturation (Burgess et al., 1999; Sanes & Lichtman, 1999). Thus, animal models give us the possibility to study not only the mechanism of neuromuscular signaling in physiological conditions, but also to understand pathological impairments in neuromuscular transmission and explore therapeutic treatments to ameliorate them in appropriate experimental settings (Fralish et al., 2021; Webster, 2018). As it will be revised throughout this introduction, a great volume of the literature has focused on understanding pathological and non-pathological processes throughout mouse lifespan that affect NMJ-dependent efficiency of muscle contraction.

1.2. Mouse skeletal muscle development

Many neuromuscular diseases in humans, including congenital myasthenic syndromes (CMS), have been linked to the same genes that were described in rodent models as part of NMJ formation and maintenance (Fralish et al., 2021; Webster, 2018). For that reason, understanding the molecular pathways in the mouse synaptic development can contribute to the potential therapeutic treatment of myopathies in humans.

The formation of skeletal muscle cells (myogenesis) of the trunk and limbs starts in mice around the 9th embryonic day (E9.5) (Fürst et al., 1989) (**Fig. 1.4**). During embryogenesis, the neural tube grows along with two surrounding strips of paraxial mesoderm, a tissue divided in blocks called somites. Somites are composed of several types of columnar epithelial cells, of which the dermomyotome eventually differentiates into muscle tissue, connective tissue, and dermis (Fürst et al., 1989; Krauss, 2017). In response to signals from surrounding tissues, somite-derived muscle progenitor cells initiate a differentiation program that is characterized by the expression of transcription factors Pax3 and Pax7 (Kassar-Duchossoy et al., 2005). Then, these progenitor cells start expressing Myf5 and MyoD factors and become determined to differentiate into muscle-

lineage cells, namely myoblasts. Myoblasts already express specialized cytoskeletal proteins, such as myosin heavy chains (MHC), skeletal muscle actin isoforms (α-actin-1), and desmin (Fürst et al., 1989). Most importantly, they have the potential of proliferating and fusing into multinucleated myotubes and then myofibers upon the expression of MyoD and myogenin (Chal & Pourquié, 2017; Fürst et al., 1989).

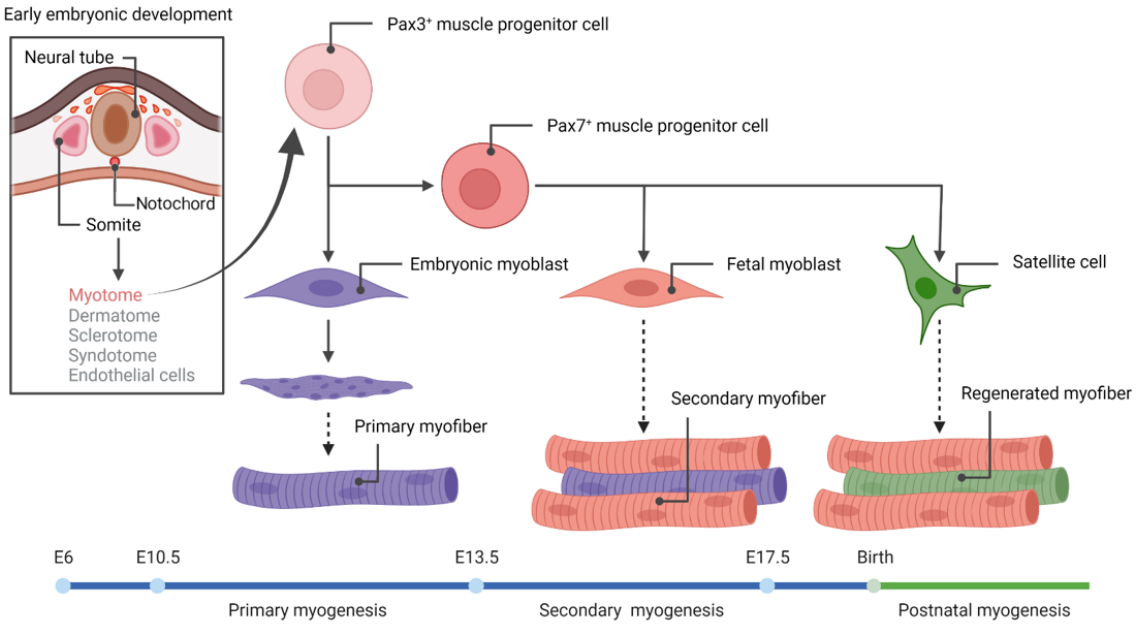

Figure 1.4. Representation of myogenesis in mice. Key time points in the embryonic development of skeletal muscle are represented in the blue time scale (between embryonic days E6-E21). Dotted arrows represent intermediate steps in differentiation, not described in the text for simplicity purposes. Illustration created with BioRender.com.

Myogenesis takes place in two phases during embryogenesis (**Fig. 1.4**). At E10.5-12.5 in mouse, primary myofibers are formed from Pax3$^+$ muscle progenitor cells and are followed by the arrival of motor axons to the central area of the future muscle (Kassar-Duchossoy et al., 2005). In the vicinity of this area, myofibers have started delivering AChRs to the cell surface, where they form aneural, solitary small clusters (Flanagan-Steet et al., 2005; Lin et al., 2001). Between E14.5 and E17.5, a subpopulation of muscle progenitor cells, located around the motor axon contact points, starts expressing Pax7 and, after expressing late myogenic markers, eventually differentiates into secondary myofibers. The motoneurons immediately start innervating these myofibers so that all mature skeletal myocytes are electrically coupled (Chal & Pourquié, 2017; Evans et al., 1994; Kassar-Duchossoy et al., 2005). This is particularly important since functional innervation and electrical activity are crucial for proper NMJ formation and muscle maintenance (Borodinsky & Spitzer, 2006). By E18.5 in the mouse diaphragm

development, all AChR clusters are bigger and innervated by an axon terminal, while the aneural clusters have disassembled (Lin et al., 2001). A third subpopulation of progenitor cells, also expressing Pax7, remains undifferentiated throughout postnatal development to give rise to adult muscle stem cells (satellite cells) (Kassar-Duchossoy et al., 2005). At the end of the myogenic process, each mature skeletal myofiber is innervated by one motoneuron, and contains numerous nuclei as a result of myoblast and myotube consecutive fusions, which are regulated by actin dynamics and proteins involved in endocytosis (Chal & Pourquié, 2017).

1.2.1. Skeletal muscle fibers in the adult mouse

As previously mentioned, the basic unit of the contractile machinery in skeletal muscle fibers is the sarcomere, constituted of alternating arrays of thin (mainly composed of actin) and thick (mainly composed of skeletal muscle myosin) filaments (**Fig. 1.5**). The sarcomeric structure repeats across the myofiber in a characteristic striated pattern due to the distribution of thick and thin filaments forming: 1) central A-bands (hexameric bipolar myosin filaments), with adjacent filaments being cross-linked at the center by proteins of the central M-line, and 2) lateral I-bands, composed of actin filaments that partially overlap with the A-bands and extend into the Z-discs at both endings of the sarcomere. The Z-discs provide a mechanical link between actin filaments of opposite polarity from adjacent sarcomeres, and thick filaments are anchored to the Z-discs via the spring-like giant protein called titin (Luther, 2009; Squire, 1997).

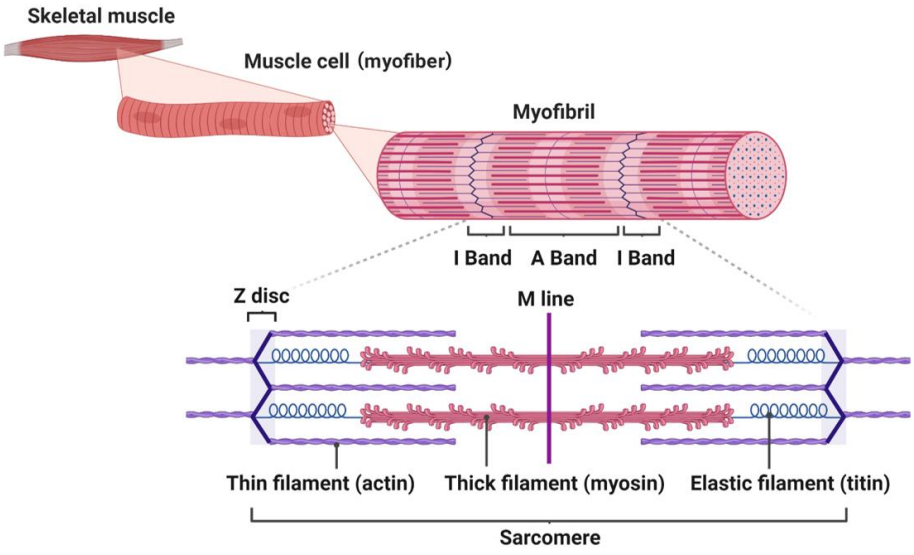

Figure 1.5. Sarcomere structure in skeletal muscle. Reprinted from "Myofibril structure", by BioRender.com (2022). Retrieved from https://app.biorender.com/biorender-templates.

When Ca^{2+} are released into the muscle cytoplasm to induce muscle contraction, a major Ca^{2+}-dependent mechanism is triggered by Ca^{2+} interaction with the actin-binding complex of troponin-tropomyosin, inducing a series of conformational changes that expose the binding site of actin filaments to the myosin head. The ATP-dependent interaction between myosin and actin filaments occurs in an asynchronous manner, and myosin heads appear to slide along actin filaments towards Z-discs. As a result, opposing Z-discs of a given sarcomere are pulled towards each other, shortening the contractile unit. The synchronized shortening of all sarcomeres from a given myofiber and all myofibers of a given muscle leads to the shortening of the muscle itself (Lieber et al., 2017; Squire, 1997; Sweeney & Hammers, 2018).

In the adult, all fibers composing a given motor unit are of the same fiber type (Edström & Kugelberg, 1968). Traditionally, skeletal muscles were classified depending on their proportion of fast-twitch (white) and slow-twitch (red) fibers, in correlation with their glycolytic and oxidative metabolism, respectively (Needham, 1926). This original classification gradually evolved by including parameters such as fatigue resistance, metabolic properties (activity of mitochondrial enzyme succinate dehydrogenase B), speed of contraction, and myosin heavy chain (MHC)-encoding genes (*MYH*), isoforms, and ATPase activity (Peter et al., 1972; Schiaffino & Reggiani, 2011). Based on the current classification, the four major fiber types in the adult skeletal muscle of mammals are described in **Table 1.1**. However, hybrid or sole expression of *MYH* genes in different fibers of a given muscle results in a spectrum of fiber types (1, 1/2A, 2A, 2A/2X, 2X, 2X/2B, and 2B). Type 2A fibers are often referred to as *intermediate* fibers because they share properties of both slow- and fast-twitch fiber types (Schiaffino & Reggiani, 2011; Zhang et al., 2010). Fiber types are variously distributed in limbs, trunk, and head, and their relative proportion varies depending on the species and the body size: small animals tend to have predominantly 2B and 2X fibers with abundant oxidative enzymes, while bigger mammals, such as humans, have muscles with low levels of oxidative enzymes, which are predominantly composed of 1 and 2A fiber types.

Interestingly, fiber type can impact the morphological characteristics of the NMJ, including axon terminal shape and complexity, endplate area, and topology of the junctional folds (Deschenes et al., 1994; Seene et al., 2017). Moreover, the reciprocal developmental regulation between pre- and postsynaptic elements, that is maintained across age and fiber type (Deschenes et al., 2013), takes place at a different timing

depending on the content of slow- or fast-twitch fibers (Lee, 2019), thus emphasizing the importance of the analysis of multiple muscle types in neuromuscular studies.

Table 1.1. Mammalian skeletal muscle fiber types.

Property	Fiber type 1	Fiber type 2A	Fiber type 2B	Fiber type 2X
Speed of contraction	Slow-twitch	Fast-twitch	Fast-twitch	Fast-twitch
Fatigue resistance	Fatigue-resistant	Fatigue-resistant	Fast-fatigable	Fast-fatigable
Metabolism	Oxidative	Oxidative-Glycolytic	Glycolytic	Glycolytic
Muscle myosin isoform (gene)	Myosin I (*MYH7*)	Myosin IIa (*MYH2*)	Myosin IIb (*MYH4*)	Myosin IIx (*MYH1*)

Information from Schiaffino and Reggiani (2011) and Zhang et al. (2010).

Regardless of the type, each fiber is surrounded by a specialized muscle basal lamina whose composition differs between synaptic and extrasynaptic compartments. The synaptic portion of the basal lamina also includes secreted molecules from both the axon terminal and the PSCs that encapsulate the synapse (Patton, 2003). Besides ubiquitously expressed components of the extracellular matrix (ECM), such as laminin subunit α2, fibronectin, and entactin, the synaptic basal lamina contains AChE, laminin subunits α4, α5 and β2, heparin sulfate proteoglycans (agrin, perlecan), some collagen variants (IV, VI, XIII) and neuregulin, among other key modulators of pre- and postsynaptic development (Dempsey et al., 2019; Patton, 2003; Sanes & Lichtman, 1999) (*for more information about regulators of NMJ development, see section 1.3.2.*). Myonuclei located below the neuromuscular point of contact (subsynaptic myonuclei) also display a different transcriptional pattern than extrasynaptic myonuclei, including AChR subunit-encoding genes and other proteins of the postsynaptic machinery (Sanes & Lichtman, 1999).

1.2.2. Synaptogenesis and NMJ maturation

Both synaptic compartments (i.e. motoneuron and myofiber) develop separately, but their interaction during early development plays a crucial role in the establishment of the neuromuscular synapse (Borodinsky & Spitzer, 2006; Sanes & Lichtman, 1999). Notably, signals from PSCs have been proven in recent years to be equally important, not only for synapse formation but also maintenance, neurotransmission, and repair (Alvarez-Suarez et al., 2020; Barik et al., 2016; Feng & Ko, 2008; Gould et al., 2019; Reddy et al., 2003). Although glial and neuronal inputs and outputs during development

will be omitted or only mentioned briefly throughout this text in order to focus on the postsynaptic compartment, it is noteworthy that NMJ homeostasis strongly depends on the tightly synchronized modulation of the three elements of this tripartite synapse.

In the canonical pathway for NMJ formation (**Fig. 1.6**), binding of nerve-derived agrin is the presynaptic signal that induces postsynaptic changes by interaction with muscle transmembrane protein Lrp4 (low-density lipoprotein receptor-related protein 4), which in turn binds to another muscle transmembrane protein, MuSK (muscle-specific kinase) (Glass et al., 1996; Kim et al., 2008). Agrin-Lrp4 tetramers induce transphosphorylation and activation of MuSK, leading to an intracellular signaling cascade that promotes AChR clustering and stabilization at the postsynaptic membrane (Zong et al., 2012). The exact mechanism for the initial MuSK phosphorylation and subsequent activation remains unclear. Nevertheless, it is already known that adaptor-like protein Dok7 (downstream of tyrosine kinase 7) is indispensable for both MuSK basal activity and agrin-mediated activation, and acts as a cytoplasmic ligand of MuSK (Inoue et al., 2009; Okada et al., 2006). Dok7 binds to phosphorylated MuSK and dimerizes, also causing MuSK dimerization, which facilitates the transautophosphorylation loop required for MuSK activation (Bergamin et al., 2010). Although still requiring further analysis, some *in vitro* studies have elucidated several enzyme effectors downstream of MuSK-Dok7, such as Abl, GGT, Rho GTPases, and PAK1 (Li et al., 2018).

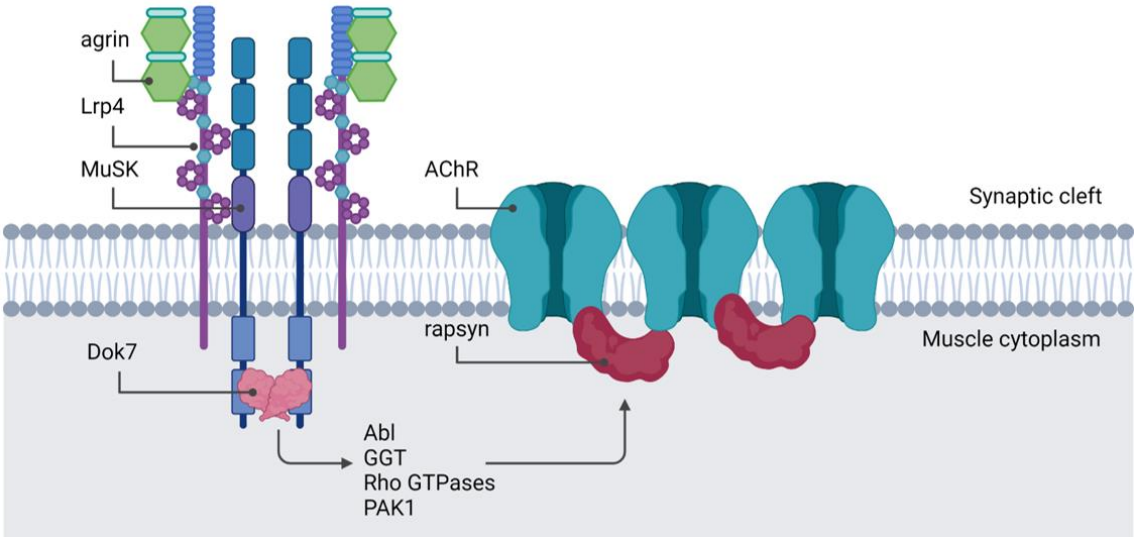

Figure 1.6. Signaling pathway for neuromuscular junction formation. Canonical pathway featuring the five indispensable molecules involved in synaptic membrane organization and AChR clustering: agrin - Lrp4 - MuSK - Dok7 - rapsyn. Illustration created with BioRender.com.

A notable exception to this pathway is the formation of aneural AChR clusters, called muscle pre-patterning, which takes place on the muscle surface prior to motoneuron arrival during embryogenesis (Yang et al., 2001). Although most of them are disassembled upon nerve-induced electrical activity (Anderson & Cohen, 1977), those clusters located nearby a region of neuronal contact transform into bigger, organized AChR clusters due to agrin stimulation (Flanagan-Steet et al., 2005). So far, there is evidence in favor of the hypotheses that 1) Lrp4-MuSK basal activity is indispensable for aneural clusters formation, 2) Dok7 mediates MuSK basal activity, and 3) MuSK basal activity is independent of agrin signaling (Li et al., 2018).

MuSK activation is also regulated by extracellular mechanisms. For example, motoneuron APP (β-amyloid precursor protein) interacts with the extracellular domain of Lrp4 to increase agrin-induced AChR clustering (Choi et al., 2013). Muscle-derived extracellular components, such as laminin subunit β2, collagen XIII, perlecan, byglycan, and AChE interact with agrin, the dystrophin-glycoprotein complex (DGC), MuSK, and/or AChR subunits to either anchor the postsynaptic machinery or facilitate agrin signaling (Gawor & Prószyński, 2018). Finally, Wnt proteins regulate AChR clustering and NMJ formation in a variety of ways and with opposing effects depending on the protein variant and the cell origin of the Wnt molecule (Barik et al., 2014; Henriquez et al., 2008; Li et al., 2008; Shen et al., 2018). Nevertheless, Wnt-MuSK interaction through MuSK cysteine-rich domain has been demonstrated to be necessary for MuSK basal activity and thus, muscle pre-patterning (Jing et al., 2009). A downstream key effector of MuSK activation is the scaffolding protein rapsyn. Rapsyn anchors AChR subunits to the postsynaptic membrane by simultaneously interacting with ACh receptors and cytoskeletal subsynaptic proteins or regulators, such as DGC, actin filaments, and intermediate filaments (Apel et al., 1995; Xing et al., 2020). Moreover, a recent study has shown that rapsyn also has an E3 ligase enzymatic activity that promotes AChR neddylation (Li et al., 2016). Although the underlying mechanism remains unclear, this post-translational modification, that antagonizes AChR ubiquitination, could promote AChR stability by reducing its turnover rate (Li et al., 2016).

Once the AChR cluster has been established, it maintains a concave oval or round shape (plaque) for the rest of the prenatal development (E17-E19) and the first days of postnatal development (P7-P10) (Marques et al., 2000; Sanes & Lichtman, 2001). Then, small perforations appear in the plaque-like cluster as a result of localized AChR disassembly and endocytosis (Sanes & Lichtman, 2001), which is triggered by focal

degradation of the ECM. Membrane type 1 matrix metalloproteinase (MT1-MMP) is inserted into the muscle membrane by actin polymerization and microtubule (MT) recruitment processes, and mediates the proteolytic degradation of cluster-stabilizing ECM components (Chan et al., 2020; Dai et al., 2000) (*for more information about actin and MT dynamics, see section 1.3*). In parallel, a presynaptic maturation process, called synaptic elimination, induces the progressive retraction of supernumerary terminals, so that only one axon innervates each muscle fiber (Lee et al., 2017; Redfern, 1970). Eventually, AChR clusters organize into branches of striped-patterned receptors (**Fig. 1.3B**), with AChR-free spaces between them, forming a pretzel-like topology (Sanes & Lichtman, 1999). Therefore, low-density AChR areas are the first sign at the postsynaptic machinery of the NMJ maturation process from plaque to pretzel-like shape (**Fig. 1.7**) (Marques et al., 2000; Sanes & Lichtman, 2001).

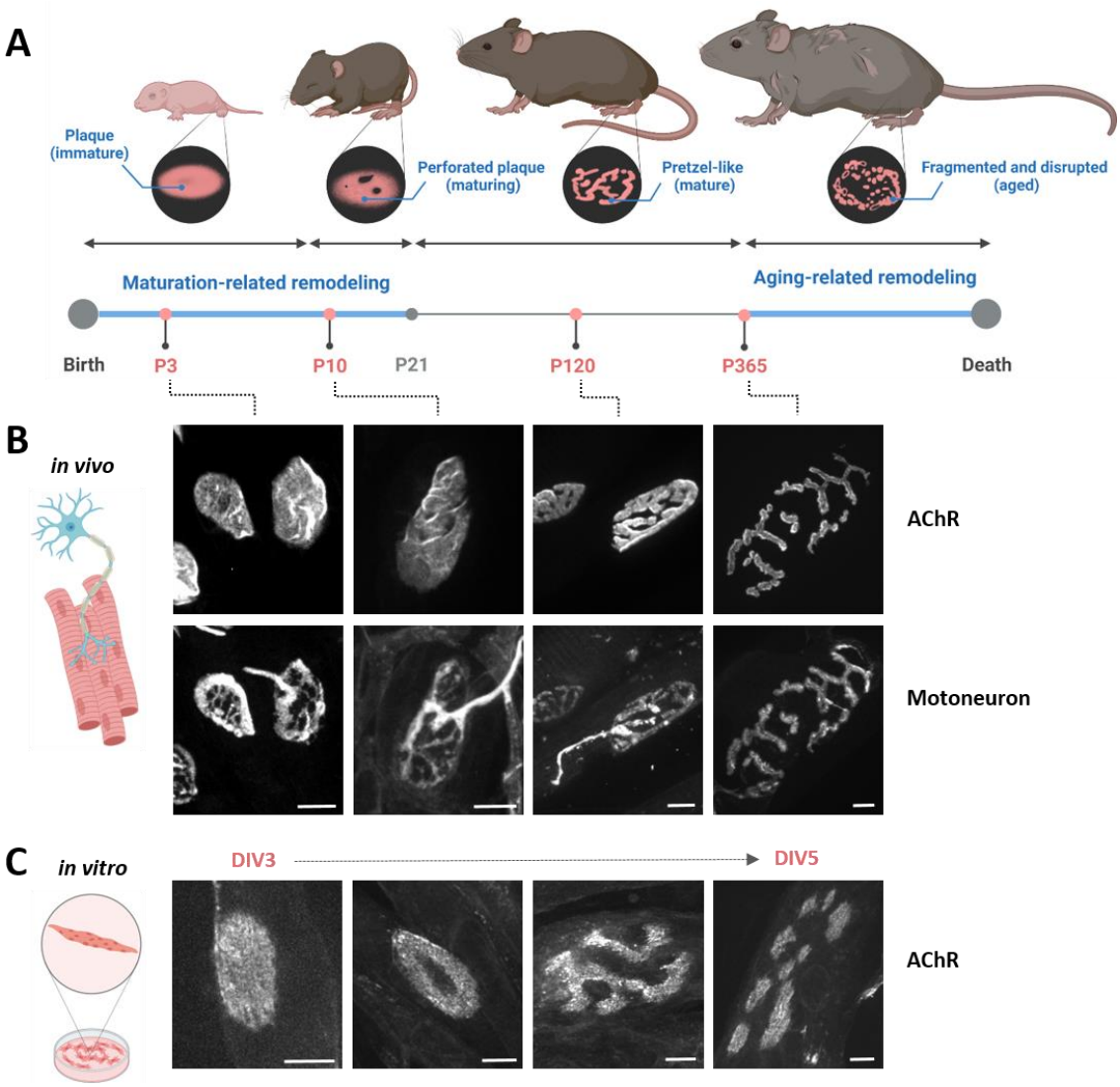

Figure 1.7. Neuromuscular postnatal maturation. (A) Age time points throughout mouse lifespan in which neuromuscular remodeling takes place. Illustration created with BioRender.com. **(B)** Postsynaptic morphological maturation from plaque to pretzel *in vivo* at postnatal days P3-P10-

P120-P365 in wild-type mice, visualized with fluorescent staining of postsynaptic neurotransmitter receptors (AChR, labelled with bungarotoxin, BTX) and presynaptic motor neuron (labelled with neurofilament- and synaptophysin-specific antibodies). **(C)** Postsynaptic morphological maturation *in vitro* between DIVs 3-5 of C2C12 mytoubes cultured on a laminin-coated surface, resembling the plaque-to-pretzel transition of AChRs *in vivo*. Own images. **Abbreviations:** DIV = days of culture *in vitro*.

Several factors are involved in the patterning of branches, such as presynaptic entry site and intrusive myelination (Balice-Gordon & Lichtman, 1993), the radial appearance of the primary junctional folds, or the orientation of the muscle fiber (Marques et al., 2000). Opposite to the plaque-shaped stage, the increasing morphological complexity of the postsynaptic receptors in later stages is mirrored by both the motoneuron (**Fig. 1.7B**) and the PSCs (Sanes & Lichtman, 2001). In conjunction with the appearance of morphological defects, the percentage of overlapping between pre- and postsynaptic components starts to gradually decrease from 10-14 months of age in mice (Cheng et al., 2013), which may suggest an increased interdependence of all three synaptic components in adult developmental stages.

While the initial arrangement of the postsynaptic machinery provides the organism with a functional synapse, the maturation-related changes are crucial for the progressive growth of the synapse (Marques et al., 2000; Sanes & Lichtman, 2001). Although some experimental evidence concludes differently (Willadt et al., 2016), this elaborated morphology appears to be related to increased efficiency of the neurotransmission (Slater, 2008). Thus, its disruption has been associated with neuromuscular dysfunction and myasthenic disorders (Caillol et al., 2012; Fralish et al., 2021; Lee et al., 2011; Pratt et al., 2014; Rafuse et al., 2000; Ratliff et al., 2018; Valdez et al., 2010). It is worth mentioning that targeted depletion of any of the key proteins in NMJ formation (agrin, Lrp4, MuSK, Dok7, or rapsyn) leads to the disintegration of the postsynaptic machinery (Barik et al., 2014; Eguchi et al., 2016; Kong et al., 2004; Samuel et al., 2012), supporting the idea that these proteins are indispensable not only for synaptogenesis but also for NMJ maintenance (Li et al., 2018).

1.2.3. Postsynaptic development *in vitro*

Studying synapses inside a living organism poses multiple technical challenges, therefore, numerous research groups work on the development of *in vitro* models resembling NMJ organization and function, such as cell and organoid cultures. In these culture systems, much emphasis is put on including all NMJ components to recreate the

tripartite synapse existing *in vivo* (Bellmann et al., 2019; Das et al., 2007; Hörner et al., 2021; Ionescu et al., 2016). Organoid cultures derived from human tissues constitute an emerging solution for modeling both healthy NMJs and neuromuscular diseases, which is particularly useful in clinical contexts (Faustino Martins et al., 2020; Pereira et al., 2021). Despite the reduced complexity of *in vitro* cell models in comparison to organoid cultures and *in vivo* environments (Alvarez-Suarez et al., 2020; Li et al., 2018), studying muscle cell cultures can help to understand muscle-specific intrinsic mechanisms of synaptic formation and maintenance, such as those regulating spontaneous formation of aneural clusters during embryonic development (Kummer et al., 2004). Moreover, simplified *in vitro* studies to great extent eliminate the compensatory mechanisms that interfere in functional studies in more complex *in vitro* models or *in vivo.*

Formation of the postsynaptic machinery *in vitro* requires induction with proteins, such as soluble agrin for nerve-derived AChR clustering, laminin for muscle-derived AChR clustering, or laminin trimers 121, 211, 221, 511, and 521 for boosting specific cluster maturation structures (Pęziński et al., 2020). Interestingly, the effects of certain laminins are able to mimic the NMJ maturation process from plaque to pretzel (**Fig. 1.7C**) (Kummer et al., 2004; Pęziński et al., 2020). In fact, laminin subunit β4 knockout mice are characterized by morphologically immature AChR clusters (Noakes et al., 1995). Notably, also MuSK signaling is necessary for substrate-dependent formation and maturation of AChR clusters (Mazhar & Herbst, 2012). AChR cluster maturation *in vitro* involves the formation of actin-rich structures called synaptic podosomes (Proszynski et al., 2009). Podosomes are mostly known for remodeling the ECM in a variety of cell types and participating in cell migration (Veillat et al., 2015). However, synaptic podosomes are also involved in the postsynaptic maturation process (Bernadzki et al., 2014), where they are characterized by accumulated F-actin bundles (**Fig. 1.8**). These structures protrude through the muscle membrane into the extracellular space, disrupting the extracellular mechanisms responsible for the stability of AChR clusters and leading to increased endocytosis rate of AChRs (Chan et al., 2020; S. Lin et al., 2020; Proszynski et al., 2009). Furthermore, proteins involved in podosome formation *in vitro*, dynamin-2 and MT1-MMP, were recently demonstrated to be crucial for postsynaptic organization and morphological maturation *in vivo* (Chan et al., 2020; S. Lin et al., 2020). Similar to other podosomes (Veillat et al., 2015), synaptic podosomes are highly organized structures (**Fig. 1.8A**).

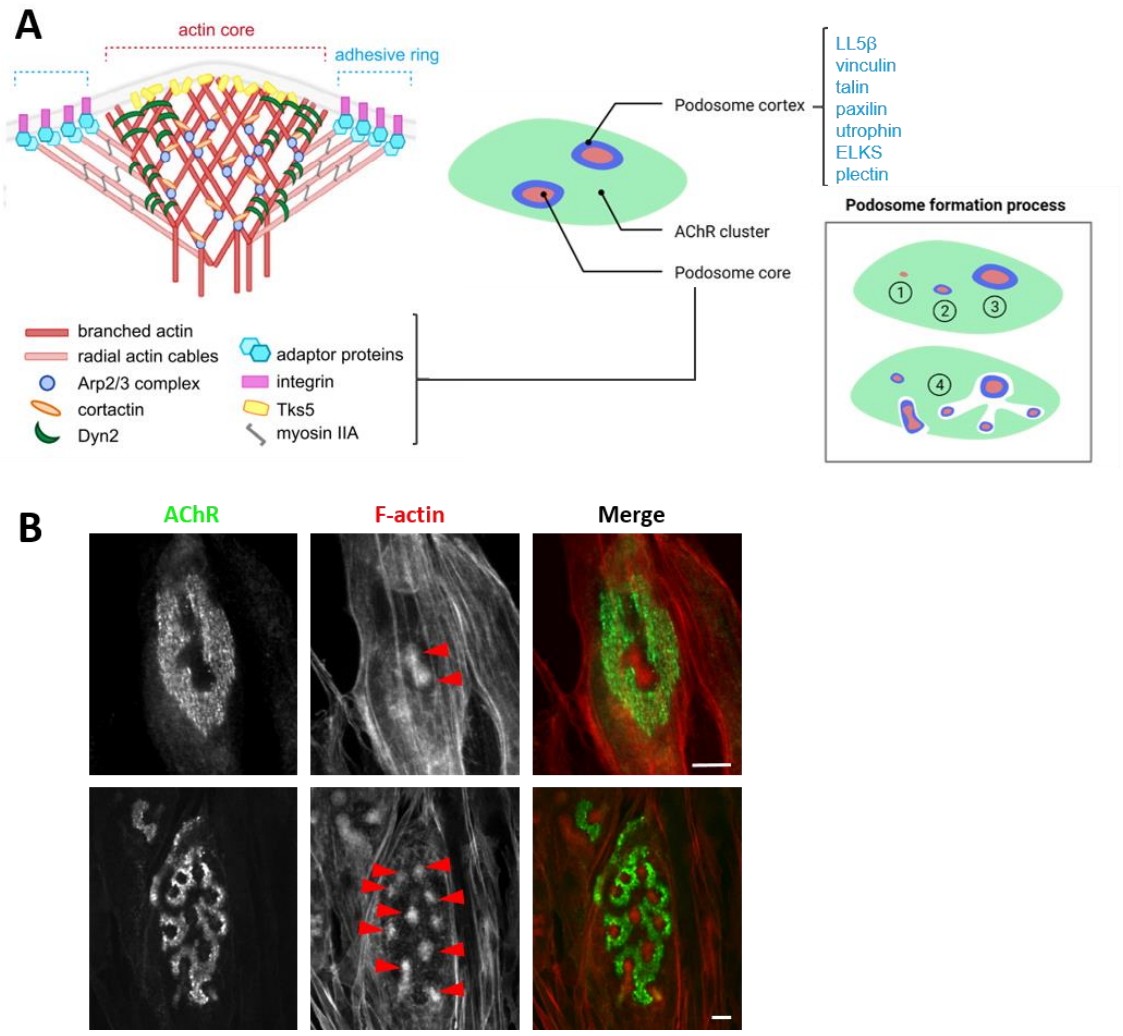

Figure 1.8. Synaptic podosome formation *in vitro*. (A) Schematic representation of podosome structures in cross-section (left) and top (right) views. Images adapted with permission of the authors (Lin et al., 2020; Proszynski et al., 2009). **(B)** Podosome association *in vitro* with AChR (green) clusters at early (top panel) and late (bottom panel) maturation stages of C2C12 myotubes cultured on a laminin-coated surface. Red arrowheads indicate individual podosomes of various sizes (F-actin, red). Scale bars = 10 µm. Own image (upper panel) and M. Gawor's image (bottom panel). **Abbreviations:** Dyn2 = dynamin-2.

Synaptic podosomes are composed of a core of F-actin and other actin-regulating proteins (Arp2, NCK, cortactin, non-muscle myosin IIA, dynamin-2, Asef2, filamin A, Amotl2, and Tks5), as well as a cortex of focal adhesion components (talin, vinculin, LL5β, paxilin, utrophin, plectin, ELKS) (Bernadzki et al., 2014; Proszynski et al., 2009). Moreover, synaptic podosomes are highly dynamic structures and they can appear, disappear, remodel, fuse, or split over the course of a few minutes to several hours. Importantly, these changes correlate with the AChR remodeling process depicted in **Fig. 1.7C** (Proszynski et al., 2009). Therefore, studying the postsynaptic machinery

maturation *in vitro* is possible in the absence of neurons and PSCs due to the formation of synaptic podosomes in aneural systems.

1.3. Cytoskeletal dynamics in the nervous system: actin and microtubule networks

The assembly of neural circuits requires coordination of multiple developmental processes and intracellular machineries to support cell migration, cell polarity, axon outgrowth, and finally, synapse formation and maintenance (Nelson et al., 2013). Central to these events is the cytoskeleton, a scaffold composed of numerous proteins that accumulate in the cytoplasm to organize and stabilize the internal domain. The cytoskeleton of animal cells contains three major filament systems, microtubules (MT), intermediate filaments, and actin filaments (**Fig. 1.9**), which are responsible for the cell spatial organization and mechanical properties. Cytoskeletal elements are involved in reacting to external mechanical stimuli and generating internal forces that drive changes in cell location and shape (Alberts et al., 2005). For simplicity purposes, only actin and MT systems will be further elaborated in the text, however, it is noteworthy that intermediate filaments play multiple important roles in the cell, particularly in mechanotransduction, migration, and development (Sanghvi-Shah & Weber, 2017). In summary, the cytoskeleton is not only the "bones" of the cell, but also its "muscles".

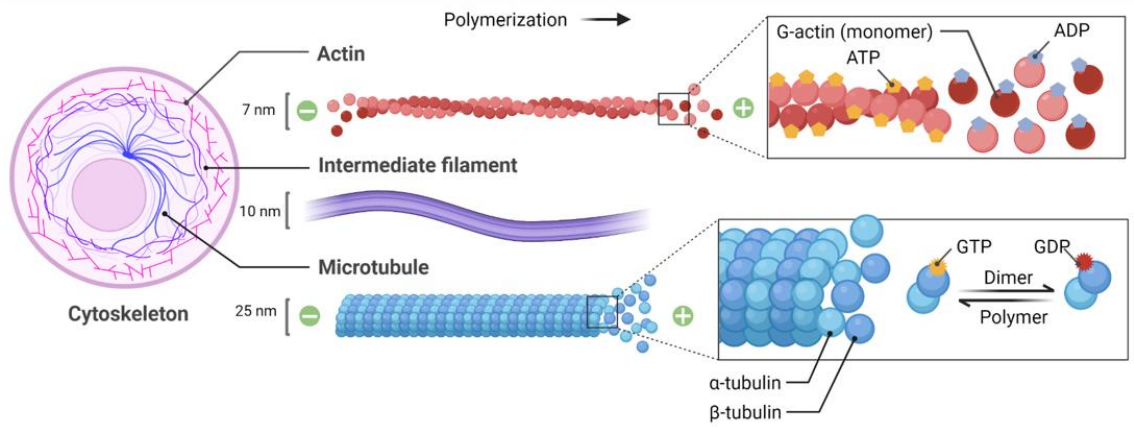

Figure 1.9. Cytoskeletal filaments in the cell: actin, intermediate filaments, and microtubules. Zoomed areas depict growing ends (plus) of both actin (top panel) and microtubule (bottom panel) filaments and their energy-dependent polymerization process. Illustration created with BioRender.com.

Actin is a globular protein of 42 KDa in its monomeric form (G-actin), however a portion of the actin pool of cells is found in a polymerized state, forming double-stranded helical filaments (F-actin) that arrange in branched and cross-linked networks, parallel bundles

or anti-parallel contractile structures (Blanchoin et al., 2014). Monomeric actin polymerizes spontaneously into polarized filaments in an ATP-dependent manner, with 10-times faster polymerization in the plus (barbed) end. The reason for this difference is that the ATP-binding cleft is oriented towards the minus (pointed) end and therefore, ATP-bound actin is less "exposed" for hydrolysis in the plus end (**Fig. 1.9, top panel**). More than 100 different proteins interact with actin to maintain the availability of monomers, regulate the dynamics of polymerization/depolymerization by limiting the length of filaments (capping and severing proteins) or promoting their growth (nucleating proteins), and sustain filament networks (bundling proteins) (Pollard & Cooper, 2009). Moreover, motor proteins can regulate and interact with actin to induce filament shortening or intracellular movement, as well as with MTs (Alberts et al., 2005; Krendel & Mooseker, 2005) (*for more information about motor proteins, see section 1.3.4.*).

Microtubules are stiff, hollow tubes composed usually of 13 parallel protofilaments formed by heterodimers of alternating α and β tubulin subunits of 55 KDa. Within the same MT, α and β tubulin subunits all point in the same direction and provide these filaments with structural polarity, with α-tubulin exposed on the minus end and β-tubulin exposed on the plus end (Alberts et al., 2005). Both tubulin subunits are bound to GTP in their monomeric state, but β-tubulin GTP is hydrolyzed into GDP during or shortly after assembly into a MT (**Fig. 1.9, bottom panel**). Binding GDP instead of GTP induces a conformational change in the β subunit that reduces the intra- and interdimer forces, thus increasing the probability of depolymerization in GDP-bound β-tubulins (Desai & Mitchison, 1997; Wang & Nogales, 2005). When GTP hydrolysis is delayed, the probability of polymerization increases, and creates a "GTP-cap" at the growing end of the MT. However, stochastic hydrolysis of the GTP-cap leads to so-called catastrophic events, in which MTs rapidly disassemble, and sometimes even disappear completely. Therefore, MTs exist in a state of dynamic instability that would randomly form and destroy filaments if it was not for a myriad of proteins that interact with MTs to control their intrinsic instability (Horio & Murata, 2014; Roostalu et al., 2020). Among these MT-interacting proteins, microtubule plus-end-tracking proteins (+TIPs), that dynamically accumulate at the growing plus end, can influence both MT dynamics and the accessibility for interaction with other proteins (Akhmanova & Hoogenraad, 2005). Some +TIP protein families involved in cytoskeletal regulation of the nervous system are

dyneins, CLIPs (cytoplasmic linker proteins), CLASPs (cytoplasmic linker-associated proteins), and EBs (end-binding proteins) (Akhmanova & Hoogenraad, 2005).

The development of the nervous system depends on these highly dynamic cytoskeletal components for multiple cellular processes. Functional impairments of actin, MTs, or their regulators can lead to various neurological disorders and myopathies.

1.3.1. Cytoskeletal regulation of chemical synapses

Chemical synapses have multiple, and often complementary, regulatory mechanisms based on cytoskeleton dynamics. The reason for this is that synaptic plasticity requires a system with the ability to respond in diverse manners to many different stimuli from outside and within the cell. The main focus of this section will be the postsynaptic cytoskeletal regulators and remodeling mechanisms, setting the foundation for comparisons between central and peripheral synapses. However, one should keep in mind the many presynaptic processes that are also tightly controlled by actin- and/or MT-regulating proteins, as well as the reciprocal regulation between pre- and postsynaptic compartments (Bodaleo & Gonzalez-Billault, 2016; Gentile et al., 2022; Nelson et al., 2013).

Dendritic spines constitute the postsynaptic specialization of the majority of excitatory synapses in the CNS. The structure and function of dendritic spines is governed and supported by the underlying F-actin cytoskeleton, including spine formation and maintenance, synaptic adhesion, neurotransmitter receptor turnover, and synaptic plasticity (Hering & Sheng, 2001). Therefore, these highly responsive physiological conditions require constant remodeling, assembly, stabilization, and depolymerization of actin filaments, mediated by nucleating proteins (Arp2/3, formins, profilin) (Chazeau et al., 2014), nucleation-promoting factors (N-WASP, WAVE1) (Pilpel & Segal, 2005), depolymerizing factors and cofilins (Racz & Weinberg, 2006), and stabilizing proteins (CapZ, Eps8) (Kitanishi et al., 2010; Menna et al., 2013). Synaptic plasticity at the CNS implies alterations in neurotransmitter receptor density at the postsynaptic membrane (Bruneau et al., 2009), which are mediated by multiple actin-remodeling proteins and their interactors (Spence & Soderling, 2015). The activity of all these actin regulatory elements is, in turn, modulated by the molecular switches of Rho-family GTPases (Tolias et al., 2011), which have been also involved in neuromuscular pre- and postsynaptic organization (Medina-Moreno & Henríquez, 2021; Shi et al., 2010; Weston et al., 2003).

In summary, actin cytoskeleton dynamics is at the core of learning, memory, and many other high cognitive functions, as well as voluntary and involuntary movements.

The MT network and its crosstalk with the actin cytoskeleton supports such processes as neurite formation, axon determination and neuronal polarity, synaptogenesis, stabilization of receptor clusters, and selective targeting of synaptic proteins to the synaptic membrane (Dogterom & Koenderink, 2019; Lasser et al., 2018). For example, the formation of dendritic branches is mediated by actin polymerization from MT plus-ends due to the formation of a protein complex containing +TIP proteins, EB1 and CLIP170, and actin-nucleating protein, formin (Dogterom & Koenderink, 2019). Similarly, MT plus-end protein, CLASP2, was shown to be involved in neurite outgrowth, dendritic arborization, synaptic morphology, and neurotransmitter receptor insertion into the postsynaptic membrane (Beffert et al., 2012). One of the major roles of MTs at the postsynaptic compartment relies on their dynamically-regulated recruitment to dendritic spines (Gu et al., 2008). Importantly, activity-evoked F-actin polymerization at the base of dendritic spines and actin interaction with +TIP protein EB3 seem to explain MT targeting to recently activated spines (Schätzle et al., 2018).

1.3.2. Cytoskeletal regulation of postsynaptic machinery formation and maintenance at the neuromuscular junction

Many of the aforementioned mechanisms and protein families are also part of the machinery that regulates synapse formation, remodeling, and maintenance at the NMJ. Therefore, research focusing on the cytoskeletal dynamics of the CNS can provide potential targets for studies in the PNS. The neuromuscular postsynaptic machinery is anchored to the membrane via multiple protein interactions with extracellular or intracellular components (**Fig. 1.10**). The main mediators of postsynaptic cytoskeleton interactions are scaffolding protein rapsyn, focal adhesion proteins, and the dystrophin-glycoprotein complex (DGC).

The DGC is composed of multiple molecules (dystrophin, sarcoglycans, dystroglycan, α- and β-dystrobrevin, syntrophin, sarcospan, caveolin-3, and nitric oxide synthase) that act as hubs for protein recruitment (Lapidos et al., 2004). For example, dystroglycan subunits bind to extracellular agrin and laminin (Rahimov & Kunkel, 2013), as well as transmembrane MuSK and AChRs, but also rapsyn, podosome-associated Tks5, and DGC-hub protein dystrophin (**Fig. 1.10B**) (Gawor & Prószyński, 2018). One of the two muscle-specific isoforms of α-dystrobrevin, α-dystrobrevin-1, is enriched at the NMJ and directly

interacts with proteins crucial for neuromuscular integrity (Gingras et al., 2016; Grady et al., 2003), such as MT-recruiting liprin-α1 (Bernadzki et al., 2017) and Arhgef5, regulator of actin dynamics that interacts with Rho GTPases (Bernadzki et al., 2020). Functional dystrophin homolog, utrophin, cross-links actin filaments directly with AChRs and rapsyn, thus stabilizing the postsynaptic receptors to the cortical actin cytoskeleton (Aittaleb et al., 2017; Gawor & Prószyński, 2018).

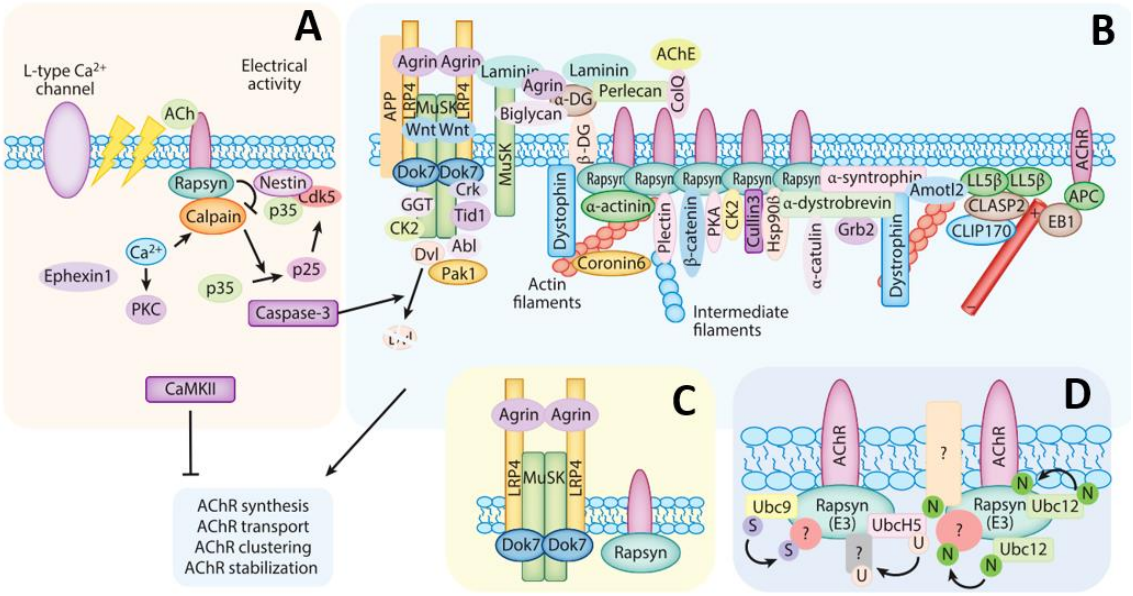

Figure 1.10. Intracellular pathways for AChR clustering. (A) Electrical activity in response to AChR activation and subsequent Ca^{2+} influx inhibit AChR synthesis, transport, clustering, and stability in entire muscle fibers. This process requires Cdk5, CaMKII, and PKC and may involve ephexin1. Cdk5 is regulated by a calpain-rapsyn complex and membrane-associated nestin. ACh-activated caspase-3 can disperse AChR clusters by degrading Dvl. **(B)** Agrin binds to Lrp4 to activate MuSK, which can be activated by Dok7. Agrin signaling can be regulated by proteins interacting with Lrp4/MuSK, such as extracellular proteins APP, Wnt, laminin, and biglycan and intracellular proteins Abl, Tid1, Dvl/Pak1, GGT, CK2, and Crk (via Dok7). Rapsyn has two functions: as an adaptor protein to bridge AChRs to the cytoskeleton and to the dystrophin-dystroglycan complex; and as an E3 ligase whose enzymatic activity is required for AChR clustering (see panel D). The function and stability of rapsyn are regulated by PKA, Hsp90β, and α-syntrophin/α-dystrobrevin. LL5β and CLASP2 are required for MT capture to AChR clusters and for intracellular AChR trafficking. APC associates with AChR and EB1 at the MT plus-end to regulate AChR clustering. **(C)** Molecules critical for NMJ formation (*see section 1.2.2.*). **(D)** Rapsyn serves as an E3 ligase, whose substrates can include proteins involved in NMJ structure and function. Modifications mediated by rapsyn may include neddylation, ubiquitination, and/or sumoylation. Question marks indicate unidentified substrate proteins of rapsyn. **Abbreviations:** ACh = acetylcholine; AChR = acetylcholine receptor; APC = adenomatous polyposis coli; APP = amyloid beta precursor protein; CaMKII = calcium/calmodulin-dependent protein kinase II; CK2 = casein kinase 2; Crk = CT10 regulator of kinase; DG = dystroglycan; Dok7 = downstream of tyrosine kinase 7; Dvl = Dishevelled; GGT = geranylgeranyltransferase; Lrp4 = low- density lipoprotein receptor-related protein 4; MuSK = muscle-specific kinase; N = nedd8; Pak1 = P21-activated kinase 1; PKA = protein kinase A; PKC = protein kinase C; S = sumo; Tid1 = tumorous

imaginal discs protein tid56 homolog; U = ubiquitin. Image and figure legend adapted with permission of the authors (Li et al., 2018).

As previously described in section 1.2.2., rapsyn plays a central role in NMJ formation and postsynaptic machinery assembly: mutations of rapsyn gene in humans (*RAPSN*) are at the root of a number of CMSs and cause AChR deficit (Ohno et al., 2002). Moreover, rapsyn knockout mice die soon after birth (Gautam et al., 1995), similarly to agrin-deficient mice (Gautam et al., 1996). The underlying mechanisms by which neurotransmitter receptors are clustered and anchored to the postsynaptic membrane are dependent on rapsyn at different levels. First, agrin enhances rapsyn-AChR interaction (Moransard et al., 2003) in a process promoted by rapsyn binding to β-catenin and α-catenin-associated cytoskeleton, as well as rapsyn binding to F-actin cross-linker, α-actinin (Dobbins et al., 2008; Zhang et al., 2007). Then, rapsyn stimulates phosphorylation of α and β AChR subunits through activation of Src class tyrosine kinases (Mohamed & Swope, 1999). Furthermore, AChR anchorage to the postsynaptic membrane is mediated by rapsyn linking to the cytoskeleton-anchored DGC (Apel et al., 1995). Rapsyn-dependent clustering of AChRs is regulated by many cytoskeletal interactors. For example, the physiological implications of rapsyn direct binding to MACF1 (microtubule actin cross-linking factor 1) (Antolik et al., 2007) were not fully understood until recent evidence of its role as a synaptic organizer of MT-associated proteins EB1, MAP1b, and focal adhesion protein, vinculin. Genetic mutations in *MACF1* have been linked to CMSs in humans, and MACF1 plays an important role in maintaining NMJ maturation, efficient synaptic transmission, and motor performance in mice (Oury et al., 2019). Moreover, MACF1 seems to govern synaptic myonuclei localization in mice by regulating the postsynaptic MT network in order to maintain the integrity of the postsynaptic machinery (Ghasemizadeh et al., 2021).

Microtubules are recruited under the postsynaptic machinery to mediate focal delivery of synaptic proteins in a process dependent of +TIP protein CLASP2 (Basu et al., 2014, 2015). Briefly, agrin activation of MuSK leads to phosphoinositide 3-kinase (PI3K)-mediated dephosphorylation of CLASP2, which can then interact with MT-coupled protein CLIP-170 (Schmidt et al., 2012). At the same time, LL5β is also recruited to the synaptic membrane in a PI3K-dependent manner, where it regulates actin-mediated focal delivery of AChR-containing vesicles, and interacts with CLASP2 directly (Basu et al., 2015). Recruitment of MTs to the cell cortex through complex formation with actin-regulating proteins, LL5β and ELKS, has also been demonstrated in HeLa cells

(Lansbergen et al., 2006), and LL5β has been shown to be indispensable for assembly of the postsynaptic apparatus (Kishi et al., 2005). Likewise, multiple studies in *Drosophila* have shown how the MT network and MT-regulating proteins crucially impact neuromuscular formation, stability, signal transmission, and subsynaptic assembly, among others (Godena et al., 2011; Lee et al., 2009; Liebl et al., 2005; Mao et al., 2014; Pielage et al., 2008). Finally, the interaction between EB1 and APC has been shown to tightly regulate MT and actin dynamics in different cell types (Juanes et al., 2020; Nakamura et al., 2001; Wen et al., 2004). Importantly, APC directly interacts with AChRs and regulates their clustering at the postsynaptic machinery in cultured myotubes (Wang et al., 2003). Altogether, these studies strongly support the idea that postsynaptic machinery assembly and stabilization are facilitated by cross-linking between actin and MT networks. However, the complexity of cytoskeleton dynamics suggests that the role of many other regulatory elements remains poorly understood in the NMJ context.

1.3.3. Drebrin as a cytoskeletal regulator of intercellular communication

Drebrin (developmentally-regulated brain protein) is an actin regulator of cell-cell communication systems, including adherens junctions, immunological synapses, gap junctions, and neuronal synapses (Majoul et al., 2007; Shirao & Sekino, 2017). Drebrin is highly conserved among vertebrates and invertebrates: both fruit flies (*Drosophila melanogaster*) and nematodes (*Caenorhabditis elegans*) express drebrin orthologs called drebrin-like protein (DBNL) and drebrin-like homolog (DBN-1), respectively (Butkevich et al., 2015; Koch et al., 2014). In mammals, drebrin gene (*DBN1* in humans) encodes two major isoforms as a result of alternative splicing, named after the dominant expression patterns throughout chicken brain development: drebrin E (embryonic) and drebrin A (adult), the latter containing a drebrin A-specific domain (**Fig. 1.11**) (Shirao et al., 1990; Shirao & Obata, 1986).

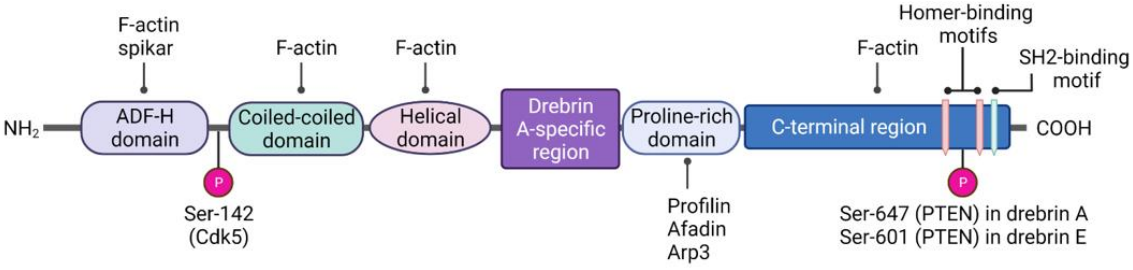

Figure 1.11. Drebrin functional domains. Schematic representation of functional domains in the rat drebrin A and E polypeptides, adapted with permission of the authors (Chen et al., 2017). Domains are not represented proportionately to their molecular weight. Illustration created with BioRender.com.

The first developmental structure in which drebrin is expressed is the myotome, that later on forms the skeletal muscle (Shirao & Obata, 1986). At the developing brain, isoform conversion from drebrin E to drebrin A occurs in parallel to synaptogenesis, and targeting of synaptic proteins to the postsynaptic compartment depends on AMPAR-mediated clustering of drebrin and F-actin (**Fig. 1.12**). Accordingly, drebrin downregulation leads to delayed synapse formation (Aoki et al., 2005; Takahashi et al., 2003, 2006, 2009). Drebrin E is expressed in the embryonic brain and, specifically, in the migrating neuronal cell body, until drebrin A expression is induced and distributed to the cell processes (Song et al., 2008). However, drebrin E is also expressed in the adult organism in many non-neuronal tissues and cell types, such as skeletal muscle, heart, T-cells, placenta, lung, seminiferous epithelium, kidney, pancreas, skin fibroblasts, gingival fibroblasts, and bone-derived cells (Fisher et al., 1994; Li et al., 2011; Peitsch et al., 1999; Pérez-Martínez et al., 2010). In these tissues, drebrin E acts as a linker between membrane proteins and the cortical actin in order to regulate different types of intercellular communication (**Fig. 1.13**). On the other hand, drebrin A is exclusively found in neuronal synapses, where it accumulates inside dendritic spines in a complex with F-actin, gelsolin, and myosins I, II, and V (Hayashi et al., 1996; Shirao et al., 1987).

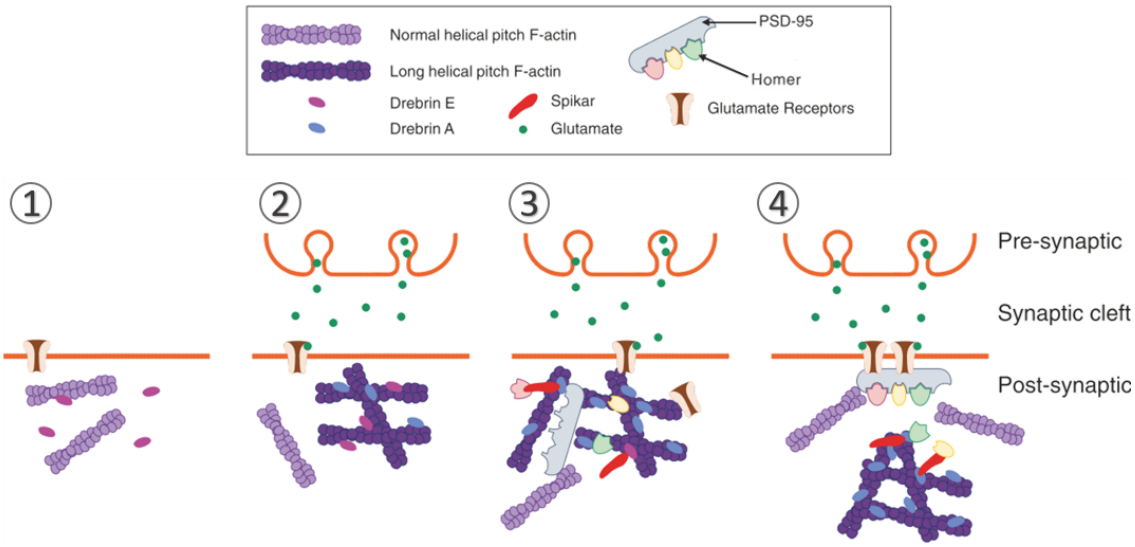

Figure 1.12. Role of drebrin in activity-dependent formation of the postsynaptic compartment of dendritic spines. (1) Dynamic F-actin is transported to the cortical cytoplasm of the dendritic shaft and dendritic filopodia, **(2)** drebrin A accumulates at future postsynaptic sites through AMPA receptor activity and forms drebrin A-decorated F-actin, **(3)** F-actin builds up a platform for assembly of glutamate receptors, CaMKII, spikar, and scaffold proteins such as PSD-95 (postsynaptic density protein 95) and Homer, and **(4)** the postsynaptic density structure is constructed in a mature spine, from which drebrin A-decorated F-actin is located relatively far away (Aoki et al., 2005; Takahashi et al., 2003, 2006, 2009). Image and figure legend adapted by permission from Springer Nature [Advances in Experimental Medicine and Biology] (Shirao & Sekino, 2017), Springer Japan KK (2017).

Drebrin contains an actin-depolymerizing factor homology (ADF-H) domain, a coiled-coil domain (CC), a helical domain (Hel), and a C-terminal "blue box" domain, all of which have sequences for F-actin interaction (**Fig. 1.11**) (Hayashi et al., 1999; Majoul et al., 2007; Worth et al., 2013). In the last few decades, many drebrin-interacting partners have been identified and some of the mechanisms through which drebrin displays such variety of functions have been elucidated (**Fig. 1.13**).

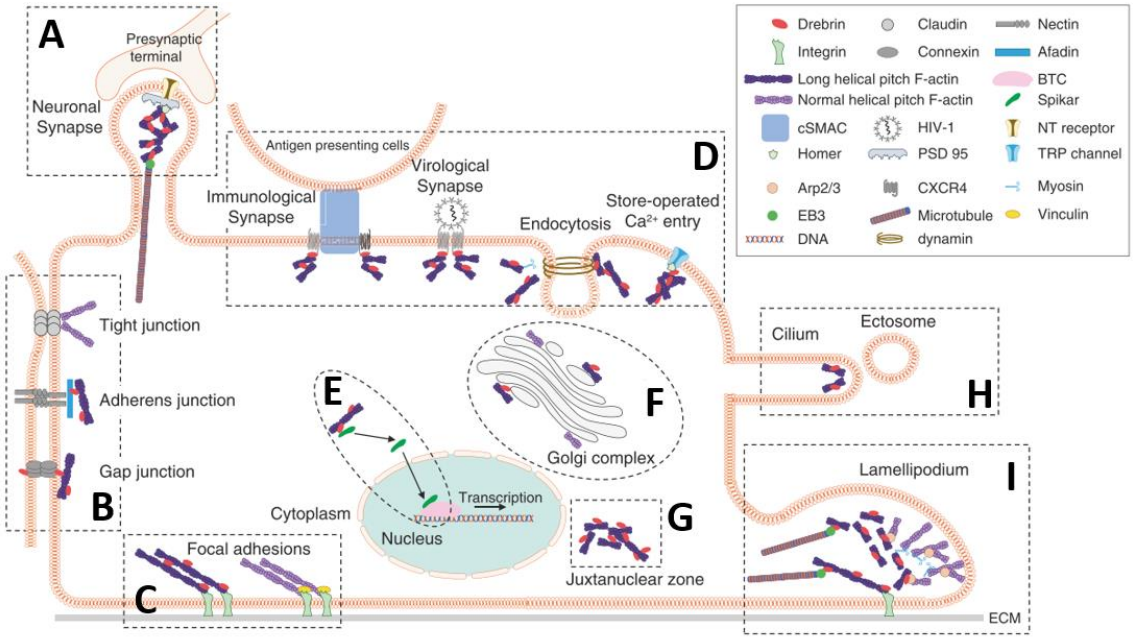

Figure 1.13. Cellular functions of drebrin. (A) Drebrin forms a stable F-actin pool at postsynaptic sites of excitatory synapses and participates in postsynaptic maturation. **(B)** Drebrin stabilizes nectin via afadin at adherens junctions and regulates gap junction via connexin43 (Butkevich et al., 2004; Rehm et al., 2013). **(C)** Drebrin is not localized at vinculin-positive focal adhesions, but some focal adhesions are stabilized by drebrin (Peitsch et al., 1999). **(D)** Association of drebrin and chemokine receptor CXCR4 is enhanced by antigenic stimulation at immunological synapses and inhibits the entry of HIV-1 at virological synapses and endocytosis (Gordón-Alonso et al., 2013; Li et al., 2017; Pérez-Martínez et al., 2010). Drebrin is also necessary for the store-operated Ca^{2+} channel function (Mercer et al., 2010). **(E)** Spikar, a transcription coactivator, enters into the nucleus when it dissociates from drebrin (Yamazaki et al., 2014). **(F)** Drebrin is a specific component of the small GTP-binding protein, ARF-dependent actin pool on the Golgi complex (Fucini et al., 2000). **(G)** Drebrin is localized at the juxtanuclear drebrin-enriched zone, which is supposedly involved in cell migration (Peitsch et al., 2006). **(H)** Drebrin mediates ectosome release from the tip of cilia (Nager et al., 2017). **(I)** Drebrin is localized at the transitional zone between lamellipodia and MTs at the tip of cell processes (Geraldo et al., 2008; Mizui et al., 2009). **Abbreviations:** ARF = ADP-ribosylation factor, BTC = basal transcription complex, cSMAC = central supramolecular activation cluster, ECM = extracellular matrix, HIV = human immunodeficiency virus, NT = neurotransmitter, TRP = transient receptor potential. Long and normal helical pitches of F-actin are 40 nm and 36 nm, respectively. Image and figure legend adapted by permission from Springer Nature [Advances in Experimental Medicine and Biology] (Shirao & Sekino, 2017), Springer Japan KK (2017).

As these functional domains suggest, drebrin main function is to bind and bundle actin filaments, and thus it has the ability to stabilize and regulate the remodeling of the F-actin cytoskeleton (Sharma et al., 2011; Worth et al., 2013). For instance, the stable pool of F-actin located at the core of dendritic spines is bound to drebrin A (Aoki et al., 2005; Hayashi et al., 1996; Honkura et al., 2008). Upon long-term potentiation (LTP) and NMDAR-dependent Ca^{2+} influx, drebrin-decorated F-actin is removed from the spine core and re-enters it after spine morphological changes occur (Mizui et al., 2014). The ADF-H domain also binds to spikar (spine and karyoplasm protein) (**Fig. 1.14**), a rat ortholog of human *ZMYND8*, encoding protein kinase C-binding protein 1, that regulates spine density and accumulates in the postsynaptic machinery in a drebrin-dependent manner (Yamazaki et al., 2014). Based on this evidence, it has been proposed that glutamatergic synapses switch between morphological stability and reactivity depending on the presence or absence, respectively, of drebrin-decorated F-actin (Shirao & Sekino, 2017). Therefore, drebrin A seems to be involved not only in synapse formation, but also in synaptic plasticity at excitatory central synapses (Koganezawa et al., 2017). Moreover, the loss of drebrin A and, subsequently, the control over dendritic spine stability/reactivity, is associated with cognitive decline observed in both aging and Alzheimer disease (Harigaya et al., 1996; Hatanpaa et al., 1999).

Additional evidence of drebrin involvement in actin dynamics comes from the interaction of drebrin E with the Arp2/3 complex (**Fig. 1.14**) in the testis. Drebrin E binds through its proline-rich (PP) domain to Arp2/3 and regulates actin bundles, participating in cell polarity through vesicle trafficking-mediated membrane plasticity and junction remodeling (Chen et al., 2017; Li et al., 2011). The PP domain is also known to bind to actin-nucleating protein, profilin, and actin-binding scaffold protein, afadin (Mammoto et al., 1998; Rehm et al., 2013). Close to the C-terminal, a PPXF binding motif can interact with Homer (**Fig. 1.14**), one of the most abundant scaffolding proteins at the dendritic spine postsynaptic density, which has been demonstrated to influence actin cytoskeleton organization (Shiraishi-Yamaguchi et al., 2009). Homer links neurotransmitter receptors to the actin cytoskeleton and the actin-regulating Rho family of GTPases (Shiraishi et al., 1999), and its tetramers promote the actin bundling activity of drebrin (Li et al., 2019).

Interestingly, drebrin seems to play a role in actin and MT cross-linking, as its localization within dendritic spines is limited to the transition zone between F-actin- and MT-rich regions, and it interacts with +TIP protein EB3 (**Fig. 1.14**) in growth-cone filopodia of

developing neurons (Geraldo et al., 2008). When the interaction between drebrin E and MTs is impaired, the actin cytoskeleton dynamics is reduced, affecting neuritogenesis and axon extension during neuronal development (Geraldo et al., 2008; Zhao et al., 2017).

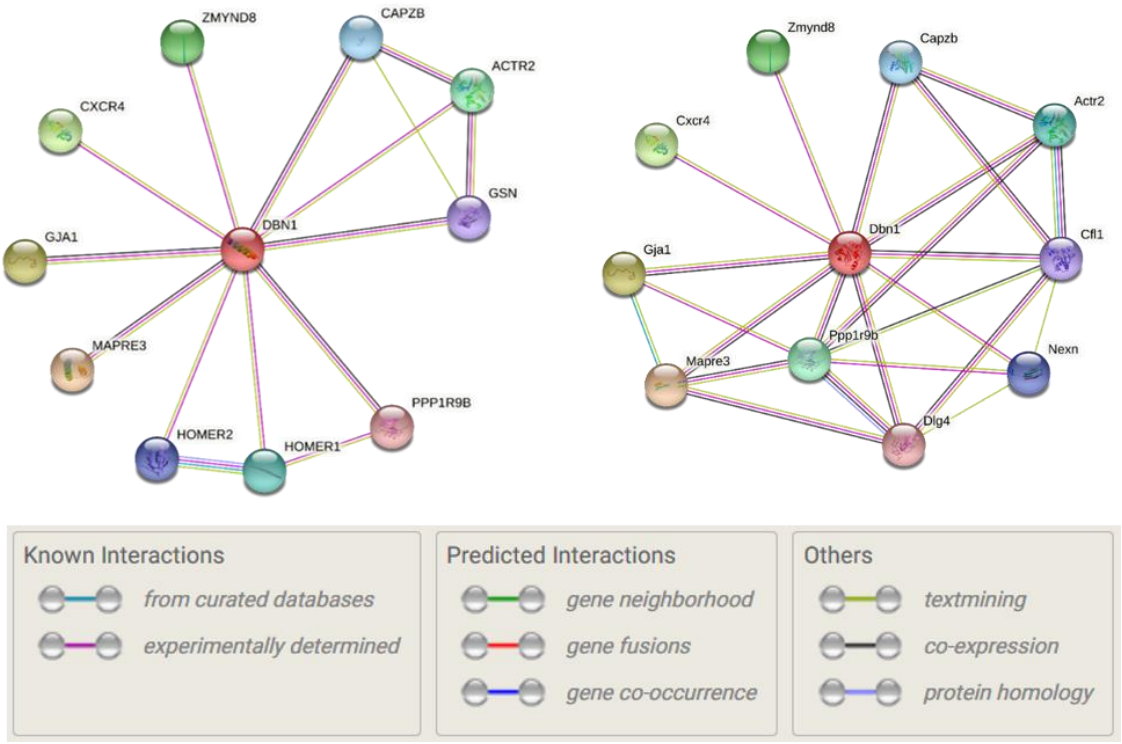

Figure 1.14. Drebrin interacting partners. Drebrin human (left) and mouse (right) interacting partners (non-exhaustive list). **Encoded proteins:** *ACTR2/Actr2* = Arp2 (Actin-related protein 2), *CAPZB/Capzb* = Capping protein muscle Z line, *Cfl1* = Cofilin-1, *CXCR4/Cxcr4* = C-X-C chemokine receptor type 4, *DBN1/Dbn1* = Drebrin, *Dlg4* = Disks large homolog 4, *GJA1/Gja1* = Gap junction alpha-1 protein, *GSN* = Gelsolin, *HOMER1/2* = Homer1/2 proteins, *MAPRE3/Mapre3* = +TIP EB3, Nexn = Nexilin, *PPP1R9B/Ppp1r9b* = Neurabin-2, *ZMYND8/Zmynd8* = Protein kinase C-binding protein 1. Figure created with String database of protein-protein interactions (www.string-db.org).

There are two known phosphorylation sites in drebrin protein: Ser142, phosphorylated by Cdk5 (cyclin-dependent kinase 5), and Ser647/601, dephosphorylated by PTEN (phosphatase and tensin homolog) (**Fig. 1.11**) (Kreis et al., 2013; Worth et al., 2013). Reversible phosphorylation/dephosphorylation of drebrin at Ser142 was involved in radial migration of cortical neurons (Tanabe et al., 2014). Notably, a mechanistic model for explaining the cross-linking activity of drebrin involves a Cdk5-dependent conformational change of drebrin structure that enhances the interaction with EB3 (Worth et al., 2013). The activity-dependent invasion of MTs into dendritic spines is facilitated by EB3-drebrin interaction (Hu et al., 2008; Schätzle et al., 2018). Importantly,

disruption in the Cdk5/drebrin/EB3 pathway was linked to disease development, such as invasive prostate cancer and Alzheimer disease (Dart et al., 2017; Gordon-Weeks, 2016). In summary, a wide body of evidence, mainly at the CNS, supports the involvement of drebrin in the regulation of cytoskeletal dynamics by stabilizing F-actin and cross-linking it with the MT network.

In skeletal muscle, however, the role of drebrin is poorly understood. Up to this date, it was only described in three contexts: 1) muscle contraction in *C. elegans* (Butkevich et al., 2015), 2) linking transcriptional and morphological aspects of myoblast differentiation and fusion into myotubes of murine origin (Mancini et al., 2011) and 3) axon terminal arborization and presynaptic bouton formation in *Drosophila* NMJ (Koch et al., 2014). Actin cytoskeleton dynamics is at the core of an evolutionarily conserved mechanism for myoblast fusion, involving WAVE, WASP, and Arp2/3 actin-remodeling complexes and, specifically in mammals, cytoskeletal regulators integrin β1, talin, cadherin, Cdc42, and EB3 (Krauss, 2017). Importantly, the muscle-specific transcriptional program leading to myoblast differentiation does not seem to precede alterations in cytoskeletal architecture, but it is rather coordinated simultaneously with actin and MT remodeling. In sparse-growing myoblasts, drebrin accumulates in F-actin-rich regions, such as cell projections and cell cortex, while it concentrates at cell-cell contacts and the tips of nascent myotubes when the initial stages of myoblast fusion take place (Mancini et al., 2011). On the other hand, when drebrin is depleted, the levels of both early and late differentiation markers, such as myogenin and muscle myosin heavy chain, respectively, are strongly reduced, and the formed myotubes are thinner, smaller, and contain significantly less myonuclei than control cells (Mancini et al., 2011). It is noteworthy that known drebrin-interacting partners are also involved in myogenic differentiation and myotube formation, including EB3, Homer, and CXCR4 (Griffin et al., 2010; Stiber et al., 2005; Straube & Merdes, 2007). Nevertheless, and despite the well-known involvement of drebrin in postsynaptic regulation at the CNS, the potential role of drebrin at the NMJ has not been explored yet.

1.3.4. Myosin VI as a versatile unconventional actin-based motor

In addition to their aforementioned structural roles, polarized cytoskeletal filaments often act as tracks or guidelines for directional intracellular movements mediated by molecular motors. These motor proteins are capable of transforming chemical energy (i.e. ATP hydrolysis) into mechanical movement, resulting from conformational changes

within myosin molecules (Alberts et al., 2005; Krendel & Mooseker, 2005). This movement is used for a variety of cellular functions, such as inducing tension in cytoskeletal filaments and carrying a cargo (vesicles, organelles, and other cellular components). Generally, motor proteins move along MTs for long-range transport (kinesins and dyneins) or actin filaments for short-range transport (myosins) (Langford, 1995). The myosin superfamily is an evolutionarily conserved group of actin-based motors that are divided in at least 35 classes (**Fig. 1.15**), however only 12 classes are expressed in mammals (Berg et al., 2001; Odronitz & Kollmar, 2007). Myosins play diverse functions in eukaryotic cells, including cell migration and adhesion, intracellular transport and localization of macromolecules and organelles, signal transduction, synaptic plasticity, and tumor suppression (Krendel & Mooseker, 2005).

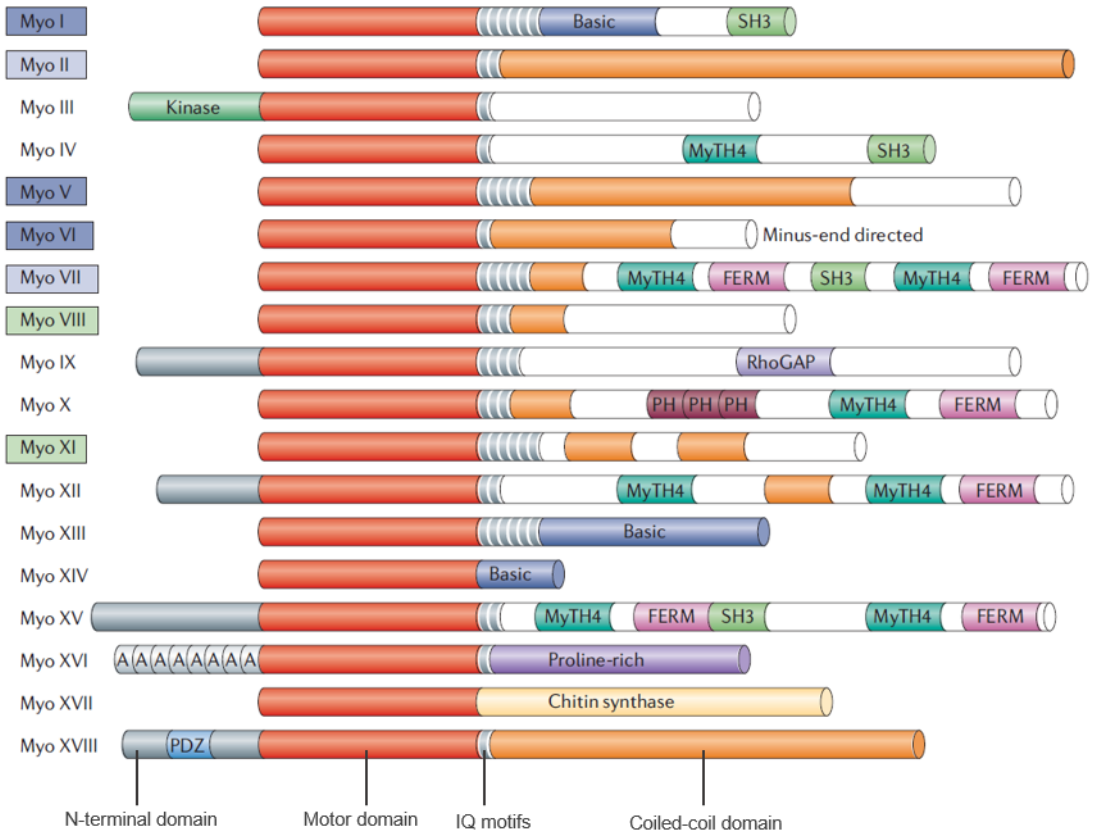

Figure 1.15. Superfamily of myosins. Overview of first 18 myosin classes and their functional domains. Motor families in which all (light blue) or some (dark blue for animals, light green for plants) members are involved in membrane trafficking are highlighted. **Abbreviations:** A = Ankyrin repeats, FERM = Protein 4.1. ezrin, radixin, moesin domain, MyTH4 = Myosin tail-homology-4 domain, PH = Pleckstrin-homology domain, SH3 = SRC-homology-3 domain. Image adapted with permission of the authors (Soldati & Schliwa, 2006).

Conventional skeletal muscle myosin was the first member of the superfamily described and, as a key component of the contractile machinery, it is the most abundant motor protein in skeletal muscle (Alberts et al., 2005; Kühne, 1864). Additionally to conventional skeletal muscle myosins (class II), several classes of unconventional myosins (I, V, VI, VII, IX, and XVIII) have been found in skeletal muscle and myogenic cells (Redowicz, 2007). Despite their functional diversity, the structure of all myosins includes: 1) a conserved N-terminal motor domain (head) that is responsible for binding to actin and ATP, 2) a neck composed of a variable number of light-chain binding (IQ) motifs, and 3) a highly variable C-terminal tail, responsible for cargo binding and dimerization, and determining the affinity to specific cargoes or other binding partners (**Fig. 1.15**) (Krendel & Mooseker, 2005; Soldati & Schliwa, 2006). In opposition to conventional myosins, the tail of unconventional myosins does not form filaments, although some classes, such as myosins V and VI, can dimerize (**Fig. 1.16B**) (Benashski et al., 1997; Woolner & Bement, 2009). Unconventional myosins are involved in sensing F-actin tension, tethering organelles to F-actin upon their MT-mediated delivery to the cell membrane, organizing F-actin during endocytosis, maintaining the mitotic spindle structure, and transporting cargo along cytoskeletal filaments (Woolner & Bement, 2009).

Unconventional myosin VI (MVI) is present in all metazoans, as it appeared rather early in evolution, and thus homologs of this protein can be found in nematodes, flies, and vertebrates (Thompson & Langford, 2002). Although maintaining its main functional domains (**Fig. 1.16A**), MVI is transcribed into different tissue-specific isoforms via alternative splicing of the tail sequence and the number of isoforms differs between organisms (Buss et al., 2004). In opposition to the majority of myosins, MVI is the only actin motor to be described moving towards the pointed minus end of actin filaments (Spudich & Sivaramakrishnan, 2010; Wells et al., 1999). Several characteristics of MVI predict its ability to effectively and rapidly transport cargoes: 1) MVI can form dimers and multiple MVI molecules can cooperate together to facilitate movement in a F-actin network, 2) ATP binds to them slowly and with slow affinity and 3) like myosins V and X, MVI has a high-duty ratio (time spent attached to the filament) (De la Cruz et al., 1999, 2001; Homma & Ikebe, 2005; Sivaramakrishnan & Spudich, 2009). Therefore, major functions of a minus-end-directed motor such as MVI can involve inward transport of cargo (endocytosis) and the maintenance of membrane invaginations at the base of cell protrusions (Krendel & Mooseker, 2005).

Furthermore, MVI plays important roles in developmental processes of multicellular organisms, such as organization of the syncytial blastoderm in early embryogenesis of *Drosophila* (Mermall & Miller, 1995), or spermatogenesis (Hicks et al., 1999; Isaji et al., 2011; Zakrzewski et al., 2017). Together with other unconventional myosins (Ia, VIIa, XV), MVI is involved in differentiation and function of mechanotransducing inner ear hair cells, and mutations in the genes encoding these myosins lead to non-syndromic hearing loss in fruit flies, mice and humans (Avraham et al., 1995; Donaudy et al., 2003; Liu et al., 1997; Todi et al., 2005; Wang et al., 1998). Myosin VI, in particular, plays a crucial role in membrane organization of the hair cell stereocilia mediating minus-end directed tension between the plasma membrane and the cortical actin cytoskeleton (Hasson et al., 1997; Hegan et al., 2015; Self et al., 1999).

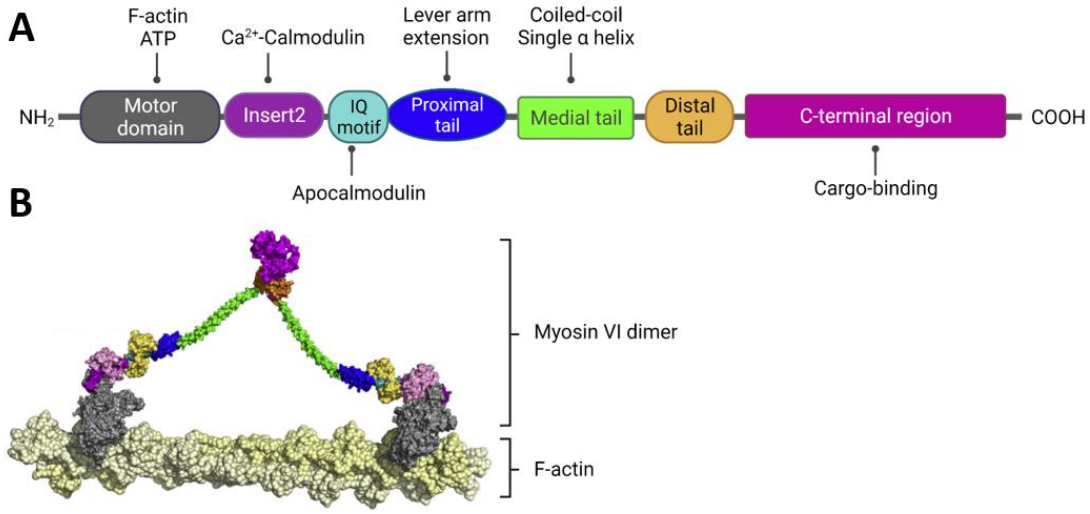

Figure 1.16. Myosin VI functional domains and movement along actin. (A) Schematic representation of functional domains and main interacting molecules in full-length MVI protein as described in Mukherjea et al. (2009). Domains are not represented proportionately to their molecular weight. Illustration created with BioRender.com. **(B)** Model of MVI dimerization by using stable single α helices as lever arm extensions (Spink et al., 2008). Color corresponds to functional domains depicted in A. Figure reprinted from (Mukherjea et al., 2009) with permission from Elsevier.

Depending on its tissue-specific isoforms, MVI has been associated to diverse functions in many cell types. Some of the known roles of MVI are related to broad intracellular trafficking pathways, such as early steps of endocytosis of both clathrin-coated or uncoated vesicles in mammalian epithelial cells with and without apical microvilli, respectively (Aschenbrenner et al., 2003; Buss et al., 2001). During early development, MVI cooperates with the MT network for secretion of lipid-modified proteins in *Drosophila* S2R+ cells (late embryonic cells) (Finan et al., 2011). More specific roles of

MVI include regulation of actin dynamics and formation of F-actin barriers by targeted localization of actin-nucleating complex Arp2/3 in *Drosophila* spermatids (Rogat & Miller, 2002). In addition, MVI regulates endocytosis of cell surface receptors in mammalian kidney epithelial cells (Naccache et al., 2006).

Importantly, MVI is found in both brain and striated muscle tissues and has been implicated in both neuromuscular synaptic transmission and in myoblast differentiation, (Karolczak et al., 2015a; Kisiel et al., 2011). In hippocampal neurons, depletion of MVI leads to fewer and shorter dendritic spines, as well as fewer presynaptic boutons (Kneussel & Wagner, 2013). In a complex with GIPC1 (GAIP C-terminus-interacting protein), MVI mediates presynaptic short-term plasticity, possibly by promoting synaptic vesicle recycling (Yano et al., 2006). Furthermore, MVI interacts with DOCK7 (dedicator of cytokinesis 7) in neurosecretory cells to mediate neurite outgrowth (Sobczak et al., 2016). Additionally, postsynaptic MVI binds directly to the β-splice isoform of SAP97 (synapse-associated protein 97) (Wu et al., 2002), a scaffold protein that mediates the interaction between glutamate AMPAR and receptor-stabilizing protein PSD-95, and disruption of this interaction impairs the number of neurotransmitter receptors on the postsynaptic surface (Nash et al., 2010). Notably, SAP97 forms a complex with AKAP79 (A-kinase anchor protein 79) that participates in receptor recycling (Gardner et al., 2007). In myogenic cells, MVI has been shown to bind AKAP9 (Karolczak et al., 2015b). Furthermore, *Snell's waltzer* mice (*SV*), carrying a mutation in the *Myo6* gene that leads to a functional knockout of MVI, are characterized by reduced activity-induced endocytosis of AMPARs (Osterweil et al., 2005). Based on the multiple similarities between central AMPAR-PSD-95 and neuromuscular AChR-rapsyn anchorage systems (Bruneau et al., 2009), it seems reasonable to expect similar interactions and roles of MVI in peripheral synapses.

Indeed, mutations in the *Drosophila* homolog of *Myo6* gene lead to shorter NMJs, reduced presynaptic bouton number, and altered synaptic vesicle localization (Kisiel et al., 2011). Moreover, MVI accumulates at the postsynaptic machinery in cultured murine myotubes and rat skeletal muscle (Karolczak et al., 2013, 2015a). Furthermore, experimental evidence links the density and recycling of AChRs at the postsynaptic surface with AKAP protein and stimulation of PKC or inhibition of PKA (protein kinases C and A, respectively). Additionally, the cargo-domain of MVI is a substrate *in vitro* for PKA (Karolczak et al., 2015a), which also interacts with receptor-stabilizing rapsyn (Li et al., 2018). Finally, the role of MVI has been investigated in the context of striated muscle. A

point mutation in the human homolog of *Myo6* was linked to familial hypertrophic cardiomyopathy (Mohiddin et al., 2004) and to left heart ventricle hypertrophy in *SV* mice (Hegan et al., 2015). In the past, our research group has described the expression and distribution pattern of MVI in rat skeletal muscle, where it was found predominantly in the periphery of fibers and within myonuclei. Further exploration revealed that peripheral MVI corresponds mostly to its localization at the sarcoplasmic component of the contractile machinery, and in the vicinity of the postsynaptic machinery *in vivo* and *in vitro* (Karolczak et al., 2013, 2014, 2015a). Interestingly, denervation of the skeletal muscle led to upregulation of *Myo6* gene and aberrations in protein localization (Karolczak et al., 2013). Moreover, neuromuscular accumulation of MVI was absent in a mouse model of amyotrophic lateral sclerosis (ALS), in which the human superoxide dismutase 1 gene (*SOD1*) with a G93A mutation was knocked-in (Karolczak et al., 2013). Alterations in MVI expression and localization have been also observed in patients with type 2 fiber atrophy, spinal muscular atrophy, bent spine disease, and myositis (Karolczak et al., 2014). Furthermore, MVI has been associated with neurodegenerative pathologies such as Alzheimer disease, Parkinson disease, and frontotemporal dementia (Kneussel & Wagner, 2013).

Notably, expression levels of MVI in C2C12 myoblasts gradually decrease in parallel with myogenic differentiation, and different isoforms of MVI are predominantly expressed depending on the differentiation state (Karolczak et al., 2015a). Similar to *in vivo* studies, MVI localizes to the cytoplasm of undifferentiated myoblasts and, in particular, to the vicinity of the SR and the Golgi apparatus, as well as adhesion-related machinery (e.g. vinculin), while it concentrates at the leading edge and cell periphery throughout the differentiation process (Karolczak et al., 2015a). Despite the fact that MVI downregulation does not affect myoblast growth nor proliferation, MVI-depleted myoblasts display morphological aberrations in the Golgi apparatus, the SR, the actin cytoskeleton stress fibers, and their overall cell morphology (Karolczak et al., 2015a). Moreover, adhesion complex formation, myoblast migration, and myotube formation were significantly impaired *in vitro* when *Myo6* expression was silenced (Karolczak et al., 2015a) and in primary myoblasts from *SV* mice (Lehka et al., 2020).

Altogether, the literature strongly supports the idea that MVI is involved in skeletal muscle differentiation and function, as well as postsynaptic machinery organization. Nevertheless, the underlying cellular mechanisms and, in particular, MVI role at the NMJ remain unclear.

"*If you know you are on the right track,*

if you have this inner knowledge,

then nobody can turn you off...

no matter what they say."

Barbara McClintock,

Nobel Prize laureate in Physiology or Medicine (1983)

CHAPTER 2: RESEARCH HYPOTHESES AND OBJECTIVES

Decades of studies have provided evidence of the important role of cytoskeletal regulators in the formation, development, maintenance, and remodeling of chemical synapses both at the central and peripheral nervous systems. Based on the literature, two candidates (namely drebrin and myosin VI) were selected to test the following hypotheses:

- Hypothesis 1: Drebrin is a synaptic component of neuromuscular junctions.
- Hypothesis 2: Drebrin mediates cytoskeleton-dependent regulation of the postsynaptic machinery through actin stabilization.
- Hypothesis 3: Myosin VI plays a role in the mobility of the postsynaptic machinery through endocytosis.

Therefore, the main goal of my PhD research was to investigate the role of actin-regulating proteins drebrin and myosin VI in the context of the murine neuromuscular junction structure and function. The detailed objectives are as follows:

- Aim 1: To study the localization of drebrin and myosin VI at the postsynaptic machinery *in vivo* and *in vitro*.
- Aim 2: To assess the specific mechanisms through which drebrin and myosin VI play a role at the postsynaptic machinery organization in cultured myotubes.
- Aim 3: To characterize the phenotype *in vivo* of drebrin and myosin VI knockout mice at the neuromuscular junction.

In order to support or refute my hypotheses, I performed a wide range of experimental procedures to assess the effects of drebrin and myosin VI on mice behavior, histology, and molecular pathways. Methods used included immunocyto- and immunohistochemical labelling, genetic manipulation of cell lines, *in vitro* muscle cell culture, *in vivo* exogenous expression of proteins of interest, optimized machine-learning-based analysis of 2D images, and co-immunoprecipitation assays.

"*I was taught that the way of progress was neither swift nor easy.*"

Maria Skłodowska-Curie,

Nobel Prize laureate in Physics (1903) and Chemistry (1911),

first woman to be awarded a Nobel Prize,

first person to be awarded two Nobel Prizes in different categories

CHAPTER 3: MATERIALS AND METHODS

3.1. Buffers

All buffers and reagents used for their preparation are listed in **Table 3.1**.

Table 3.1. List of homemade buffers used.

Name of the buffer	Reagents
Co-immunoprecipitation (co-IP) lysis buffer	50 mM Tris-HCL [pH = 8], 150 mM NaCl, 0.1-1% Igepal CA-630 (NP-40), 50 mM NaH_2PO_4, 10% glycerol, and 1 mM dithiothreitol (DTT), supplemented with cOmplete™ Protease Inhibitor cocktail (Roche, Indianapolis, IN, USA; cat. #11873580001)
Immunoassay blocking buffer	2% BSA, 2% Normal Goat Serum (NGS), 0.05% Triton X-100, 0.02% NaN_3, diluted in PBS 1X
Lysogeny broth (LB) medium	1% tryptone, 0.5% yeast extract, and 1% NaCl
Phosphate buffered saline (PBS)	137 mM NaCl, 2.7 mM KCl, 10mM Na_2HPO_4; 1.8 mM KH_2PO_4, pH = 7.4
Pull-down lysis buffer	100 mM HEPES [pH = 7.4], 150 mM NaCl, 5 mM NaF, 2 mM EDTA, 1 mM phenylmethylsulfonyl fluoride (PMSF), and 1% Igepal CA-360 (NP-40), supplemented with cOmplete™ Protease Inhibitor cocktail (Roche, Indianapolis, IN, USA; cat. #11873580001)
Pull-down washing buffer	100 mM HEPES [pH = 7.4], 150 mM NaCl, 1 mM phenylmethylsulfonyl fluoride (PMSF), and 0.5% Igepal CA-360 (NP-40), supplemented with cOmplete™ Protease Inhibitor cocktail (Roche, Indianapolis, IN, USA; cat. #11873580001)
Radioimmunoprecipitation assay (RIPA) buffer	50 mM Tris-HCl [pH = 8.0], 150 mM NaCl, 1% Igepal CA-630 (NP-40), 0.5% sodium deoxycholate, 0.1% SDS, and 1 mM DTT, supplemented with cOmplete™ Protease Inhibitor cocktail (Roche, Indianapolis, IN, USA; cat. #11873580001)
SDS-PAGE running buffer 10X	25 mM Tris-HCl [pH = 7.4], 192 mM glycine, 0.1 % SDS, pH = 8.3; diluted in distilled water before use to 1X concentration
Tris-acetate-EDTA buffer (TAE)	40 mM Tris [pH = 7.6], 20 mM acetic acid, 1 mM EDTA
Tris-buffered saline buffer 10X (TBS)	50 mM Tris-HCl [pH = 7.5], 200 mM NaCl; diluted before use to 1X concentration in distilled water
Tris-buffered saline with Tween buffer (TBST)	0.1% Tween-20 in 1X TBS buffer
Transfer buffer 5X	1.5 M glycine, 1.5 M Tris-Base, 0.15% SDS; diluted before use to 1X concentraction in proportions 1:3:1 (5X buffer : water : 100% ethanol)
Western blot (WB) blocking buffer	5-10% non-fat milk in TBST buffer

3.2. Commercial kits

All commercially available kits used throughout this thesis are listed in **Table 3.2**.

Table 3.2. List of commercial kits used.

Name	Description	Supplier and catalogue number
ExtractMe DNA Clean-Up & Gel-out kit	Kit for DNA purification after PCR, enzymatic reactions or from agarose gel	BLIRT, Gdańsk, Poland, cat. #EM26-250
GenElute™ HP Plasmid Midiprep Kit and GenElute™ HP Plasmid Maxiprep Kit	Kits for isolation of plasmid DNA from bacterial culture at medium and large scale	Sigma-Aldrich, Saint Louis, MO, USA; cat. #NA0200-1KT and #NA0310-1KT
GeneMATRIX PCR / DNA Clean-Up Purification Kit	Kit for DNA purification after PCR, enzymatic reactions or from agarose gel	EURx, Gdańsk, Poland, cat. #E3520
High-Capacity cDNA Reverse Transcription Kit	Kit for reverse transcription of mRNA into cDNA	Applied Biosystems, Waltham, MA, USA, cat. #4374966
RNeasy Plus Universal Mini Kit	Kit for RNA isolation	Qiagen, Hilden, Germany; cat. #73404
Skeletal Muscle Dissociation Kit	Kit for mouse and rat muscle tissue enzymatic dissociation into single-cell suspensions	MACS Miltenyi Biotec 130-098-305
SuperSignal™ West Femto Maximum Sensitivity Substrate	Kit for high-sensitivity chemiluminiscent-based detection of proteins in Western blotting	Thermo Fisher Scientific, Waltham, MA, USA, cat. #34096

3.3. Cell culture

Culture of mammalian cells was used throughout this PhD thesis as a methodological tool for exogenous protein expression (HEK293 and C2C12 cell lines) and for endogenous protein analysis (primary myogenic culture), or as an *in vitro* simplified model of the postsynaptic machinery (C2C12 cell line).

3.3.1. C2C12 cell line

C2C12 is an immortalized myoblast cell line subcloned from adult murine muscle, that can proliferate and differentiate into myotubes (Yaffe & Saxel, 1977).

C2C12 cells from normal adult C3H mouse hindlimb muscle (American Type Culture Collection, Manassas, VA, USA, cat. #CRL-1772) were cultured for up to seven passages in proliferation medium: Dulbecco's Modified Eagle's Medium (DMEM), containing 4.5 g/L glucose, and L-glutamine (Sigma-Aldrich, St. Louis, MO, USA; cat. #D6046), and supplemented with 20% fetal bovine serum (FBS) (EURx, Gdańsk, Poland, cat. #E5050-02), 1% penicillin and streptomycin (p/s) 10,000 U/mL (Gibco, ThermoFisher Scientific, Waltham, MA, USA; cat. #15140122), and 0.1% amphotericin B (Gibco, ThermoFisher Scientific, Waltham, MA, USA; cat. #15290018). They were maintained in an incubator at 37°C in a humidified atmosphere with 5% CO_2 and plated on plastic dishes coated with 0.2% gelatin (Sigma-Aldrich, St. Louis, MO, USA; cat. #G2500). Myoblasts were routinely passaged every 2-3 days and were not allowed to reach more than 60% confluence in order to prevent spontaneous myoblast fusion and differentiation into myotubes.

To induce differentiation of myoblasts into myotubes, cells were seeded at a density of 9 x 10^4-1,4 x 10^5 cells/cm^2 and incubated for 48 h in proliferation medium. Then, the medium was changed to fusion-inducing medium, containing DMEM, 1% p/s, 0.1% amphotericin B, and 2% horse serum (HS) (Gibco, ThermoFisher Scientific, Waltham, MA, USA; cat. #26050088), and cells were allowed to fuse for at least 72 hours.

To induce AChR cluster formation in C2C12 myotubes, two different protocols were used depending on the experimental design:

1) Neuron-derived agrin-mediated model: fusion of C2C12 cells cultured on a gelatin-coated surface was induced as described above. After 96 h, recombinant soluble rat agrin (R&D Systems, Minneapolis, MN, USA; cat. #550-AG-100/CF) was added at a concentration of 10 ng/mL. Then, cells were incubated for at least 24 hours in the agrin-enriched medium to allow AChR clusters to form.
2) Laminin-mediated model: Laminin-111 from Engelbreth-Holm-Swarm murine sarcoma basement membrane (Sigma-Aldrich, St. Louis, MO, USA; cat. #L2020) was added to uncoated plates at a concentration of 10 µg/mL in DMEM and incubated at 37°C for minimum 3 h. Then, C2C12 myoblasts were seeded and cultured in abovementioned fusion-inducing conditions.

3.3.2. HEK293 cell line

HEK293 (Human Embryonic Kidney) fibroblast cell line was generated from a single female fetus' kidney sample by Graham and Smiley (Graham et al., 1977). This cell line is

widely used for exogenous DNA expression due to its high efficiency of transfection (Thomas & Smart, 2005).

HEK-293 adherent cells (American Type Culture Collection, Manassas, VA, USA; cat. #CRL-1573) were cultured in proliferation medium: DMEM containing 4.5 g/L glucose and L-glutamine (Sigma-Aldrich, St. Louis, MO, USA; cat. #D6046), and supplemented with 10% FBS (EURx, Gdańsk, Poland, cat. #E5050-02), 1% p/s (Gibco, ThermoFisher Scientific, Waltham, MA, USA; cat. #15140122), and 0.1% amphotericin B (Gibco, ThermoFisher Scientific, Waltham, MA, USA; cat. #15290018). They were maintained in an incubator at 37°C in a humidified atmosphere with 5% CO_2 and plated on uncoated plastic dishes to be routinely subcultured every 3-4 days.

3.3.3. Primary myogenic culture

Primary myoblast cultures were obtained from three-month-old *SV* mice hindlimb muscles (*tibialis anterior*, *extensor digitorum longus*, *gastrocnemius* and *soleus*). Control muscles were obtained from WT littermates (*for more information, see section 3.11. Animal models*).

Muscles were dissected and rinsed in ice-cold DMEM containing 1 g/L glucose (Gibco, ThermoFisher Scientific, Waltham, MA, USA; cat. #21885025). Muscles were subsequently washed in sterile PBS (VMR International, Radnor, PA, USA; cat. #E504) with 1% p/s (Gibco, ThermoFisher Scientific, Waltham, MA, USA; cat. #15140122), Betadine™, and again PBS with 1% p/s. Then, all muscles were cut into 2-4 mm pieces and dissociated using the Skeletal Muscle Dissociation Kit (MACS Miltenyi Biotec 130-098-305) according to the manufacturer's instructions. Briefly, all muscle pieces from one animal were incubated in 2.5 mL of enzymatic mix at 37°C for 1 h, and dissociated in the gentleMACS™ Dissociator program "m_muscle_01" for 30 s. Then, the tissue was incubated again at 37°C for 30 min and gentleMACS™ Dissociator step was repeated. Finally, the cell suspension was filtered through a 40 µm-pore cell strainer and washed with 10 mL DMEM. Cells were spun at 300 RCF at room temperature (RT) for 20 min in a table top centrifuge (MPW Med. Instruments, Warsaw, Poland; cat. #10223e) and the pellet was resuspended in pre-plating medium, containing low-glucose DMEM supplemented with 10% HS (Gibco, ThermoFisher Scientific, Waltham, MA, USA; cat. #26050088), 1% p/s, and 0.5% chicken embryo extract (CCE) (MP Biomedicals, Irvine, CA, USA; cat. #092850145). The isolated cell mixture was first plated in 10 mL of pre-plating medium onto a 10 cm cell culture plate (Sarstedt, Newton, NC, USA; cat. #83.3902), and

incubated at 37°C overnight in an incubator with humidified atmosphere with 5% CO_2. During this time, undesired cell types (mainly fibroblasts and adipocytes) that were isolated together with muscle cells, attach to the plate surface, while satellite cells remain suspended in the medium. After 24 h, the satellite cell-containing medium was collected and spun at 300 RCF at RT for 20 min. The pellet was resuspended in growth medium containing low-glucose DMEM supplemented with 10% HS, 1% p/s, 0.5% CCE, and 20% FBS (Gibco, ThermoFisher Scientific, Waltham, MA, USA; cat. #10500064). Satellite cell-enriched suspensions were transferred into 6-cm cell tissue culture dishes (Sarstedt, Newton, NC, USA; cat. #83.3901) coated with 5% Matrigel (Corning, Corning, NY, USA; cat. #356230), maintining the same seeding density in both *SV* and WT-derived cultures (number of cells depended on isolation efficiency). Muscle cells were harvested at 5, 7, and 10 days *in vitro* (DIV) and processed for Western blot.

3.3.4. Plasmid transfection

Transient plasmid transfections of HEK293 cells were performed using TransIT®-LT1 Transfection Reagent (Mirus Bio, Madison, WI, USA; cat. #MIR 2304), according to the manufacturer's instructions. Briefly, around 18-24 h before transfection, cells were seeded on 6-well cell culture plates (VMR International, Radnor, PA, USA; cat. #10062-892) at a density of 0.8-3.0 x 10^5 cells/mL. Then, they were incubated at 37°C overnight until they reached approximately 80% confluency. For each well, 2.5 µg of plasmid DNA was mixed with 7.5 µL of TransIT®-LT1 Transfection Reagent and diluted in 250 µL of proliferation medium. After incubation at RT for 15-30 min, the transfection mix was added to the cells drop-wise. Cells were incubated at 37°C for 48-72 h and then harvested. The constructs used for transfection are listed in **Table 3.3**.

Table 3.3. Plasmids used for transfection of HEK293 cells.

Original vector	Source
pEGFP-C1-DbnE-WT	a generous gift from Prof. Hiroyuki Yamazaki
pEGFP-C1-DbnE-142A	a generous gift from Prof. Hiroyuki Yamazaki
pEGFP-N1-EB3	(Stepanova et al., 2003)
pShuttleCMV-Rapsyn-mCherry	a generous gift from Dr. Tomasz Prószyński

3.3.5. siRNA transfection

Transfection of GeneSolution siRNAs (Qiagen, Hilden, Germany; cat. #1027416) was performed with Lipofectamine RNAiMAX (ThermoFisher Scientific, Waltham, MA, USA;

cat. #13778075), according to the manufacturer's instructions. Briefly, siRNA-mediated knockdown of selected genes was performed in C2C12 myotubes 72 h after fusion (*see section 3.3.1. C2C12 cell line*). SiRNAs were mixed with Lipofectamine RNAiMAX and diluted in OptiMEM (Gibco, ThermoFisher Scientific, Waltham, MA, USA; cat. #11058-021), and the transfection mix was incubated at RT for 15 min. Then, siRNAs were added drop-wise to fusion media covering C2C12 myotubes at 37°C and incubated in the incubator for 48 h before further analyses.

Controls included were as follows: untransfected cells (vehicle Lipofectamine RNAiMAX only), negative control (non-targeting) siRNA (AllStars Negative Control, Qiagen, Hilden, Germany; cat. #1027280), and positive control (AChR cluster-inhibiting) MuSK-siRNA (Qiagen, Hilden, Germany; cat. #87435755). The sequences of specific targeted genes are listed in **Table 3.4**.

Table 3.4. List of siRNAs used in knock-down experiments *in vitro*.

Target gene	siRNA sequences used	Working concentration
Dbn1 [ID 56320]	siRNA1 [Mm_Dbn1_1, SI00974715, CCCGTTGGTAGTTGAAACAAT]	20 nM
	siRNA2 [Mm_Dbn1_2, SI00974722, CAGCAGAGTCTGGAAGCTGAA]	
	siRNA3 [Mm_Dbn1_3, SI00974729, CAGGAGGAAGAGTTCGCCCAA]	
	siRNA4 [Mm_Dbn1_4, SI00974736, ACCAATGGAGAGACCACTCAA]	
Myo6 [ID 17920]	siRNA1 [Mm_Myo6_1, SI01322251, CAGATAATTTCCGGTATTTAA]	20 nM
	siRNA2 [Mm_Myo6_2, SI01322258, AACCGAGATAATGAAATCTTA]	
	siRNA3 [Mm_Myo6_3, SI01322265, CAGCAGGAGATTGACATGAAA]	
	siRNA4 [Mm_Myo6_4, SI01322272, CAAGTTCAAGACACAATTAAA]	

3.3.6. BTP2-mediated pharmacological blockade of drebrin

The small-molecule compound BTP2 (N-[4-[3,5-bis(trifluoromethyl)pyrazol-1-yl]phenyl]-4-methylthiadiazole-5-caboxamide) is a pharmacological blocker of store-operated Ca^{2+} channels that binds directly to drebrin and inhibits drebrin-induced F-actin rearrangements (Mancini et al., 2011; Mercer et al., 2010). Inhibitor BTP2 (Santa Cruz Biotechnology, Dallas, TX, USA; cat. #sc-221441, lot. #G2815) was diluted in DMSO and added to fusion media covering C2C12 myotubes at a concentration of 5 µM 72 h after fusion, and incubated for 24 h without replenishing. Control cells were incubated with the same concentration of DMSO (vehicle) that experimental cells.

3.4. Stable cell line generation with SleepingBeauty system

Drebrin and EB3 inserts were amplified by PCR and subcloned into a vector (pSBbi-Pur) (**Fig. 3.1**). The resulting constructs were co-transfected with a second plasmid containing

the SleepingBeauty transposase system (pSB100) to generate C2C12 cell lines stably overexpressing GFP-fused drebrin variants or GFP-fused EB3.

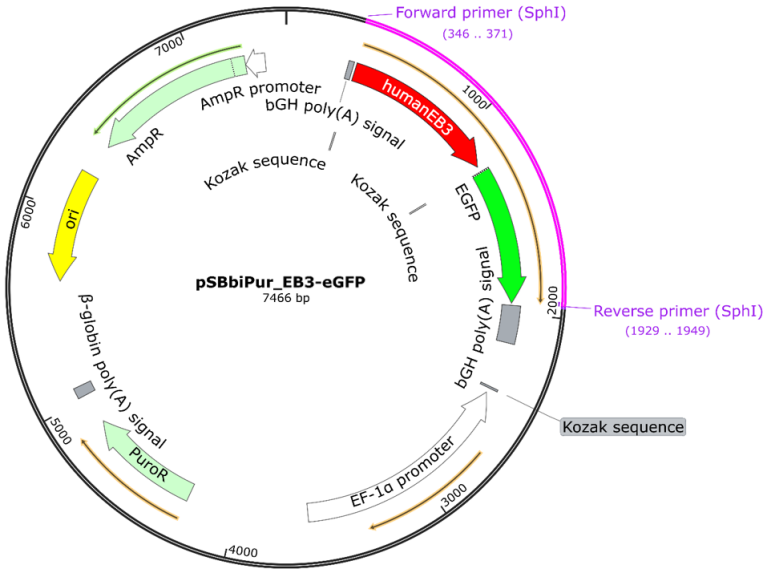

Figure 3.1. Representative map of a construct used for generation of stable C2C12 cell line overexpressing EB3-GFP. Generated in SnapGene® software (from Insightful Science; available at snapgene.com).

3.4.1. Insert amplification

The sequences of interest were amplified from the original vectors via PCR reaction, and the primers were designed to include flanking restriction sites (**Table 3.5**) (illustrated in **Fig. 3.2**). All restriction enzymes used were from New England BioLabs (Ipswich, MA, USA) (**Table 3.5**). To minimize the replication error rate, Q5 High-Fidelity DNA Polymerase (New England BioLabs, Ipswich, MA, USA; cat. #M0491) was used. The synthesis of primers was outsourced to the Laboratory of DNA Sequencing and Oligonucleotides Synthesis from the Institute of Biochemistry and Biophysics, Polish Academy of Sciences. PCR reactions were performed in a total volume of 50 µL in a 96-well T100 thermal cycler (Bio-Rad, Hercules, CA, USA, cat. #1861096) with the conditions described in **Table 3.6**.

Amplified PCR products were separated through 0.7-1.5% agarose gels containing 0.5 µg/mL ethidium bromide (Carl Roth, Karlsruhe, Germany; cat. #2218.2) in 1X TAE buffer (**Table 3.1**). Samples were mixed with 6X Loading Buffer GREEN (EURx, Gdańsk, Poland, cat. #E0262) at a final concentration of 1X and loaded on the gel with the DNA size marker GeneRuler 1kb DNA Ladder 250-10,000 bp (Thermo Fisher Scientific, Waltham,

MA, USA; cat. #SM0313). Electrophoresis was carried out at 100 mV and the results were visualized in the 3UV light benchtop transilluminator (UVP/Analytik Jena, Upland, CA, USA) at 254 nm wavelength. After confirmation of the expected insert size, amplicons were purified using GeneMATRIX PCR/DNA Clean-Up Purification Kit (**Table 3.2**), according to the manufacturer's instructions, and their DNA purity measured in NanoDrop 2000c Microvolume Spectrophotometer (Thermo Fisher Scientific, Waltham, MA, USA) (*see section 3.10. Measurement of DNA/RNA/protein concentration and purity*). The purified fragments of DNA were used for ligation with the target vector.

Table 3.5. List of plasmids used for generation of stable lines.

Original vector	Primers used for insert amplification	Resulting vector	Restriction enzymes
pEGFP-C1-DbnE-WT (a generous gift from Prof. Hiroyuki Yamazaki)	F: 5' ATTA**GGCC**TCTGA**GGCC**CACCATGGTGAGCAAGGGCGA 3' R: 5' ATTA**GGCC**TGACA**GGCC**CTAATCACCACCCTCGAAGC 3'	pSBbiPur-EGFP-C1-DbnE-WT	SfiI (#R0123S)
pEGFP-C1-DbnE-K270/271M (a generous gift from Prof. Hiroyuki Yamazaki)	F: 5' ATTAA**AGCTT**CACCATGGTGAGCAAGGGCGA 3' R: 5' ATTAT**CTAGA**CTAATCACCACCCTCGAAGC 3'	pSBbiPur-EGFP-C1-DbnE-K270/271M	F: HindIII (#R0104) R: XbaI (#R0145)
pEGFP-N1-EB3 (Stepanova et al., 2003)	F: 5' TATATA**GCATG**CGTCGACTGCCACCATGGCC 3' R: 5' TATATA**GCATG**CTTACTTGTACAGCTCGTCCAT 3'	pSBbiPur-EB3-EGFP	SphI-HF (#R3182)

Enzyme-specific restriction sites designed in primers are highlighted in red.

Table 3.6. PCR for insert amplification.

PCR reagents (V_T = 50 µL)	Volume added
Nuclease-free water	Up to 50 µL
5X Q5 Reaction Buffer	10 µL
10 mM dNTPs	1 µL
10 µM primers	5 µL
Template pDNA	10 ng
Q5 HF DNA Polymerase	0.5 µL

PCR step	Temperature	Time
Initial denaturation	98°C	30 s
Denaturation	98°C	10 s
Annealing	62°C	30 s
Extension	72°C	90-100 s
Final extension	72°C	120 s
Cooling	4°C	∞

PCR reaction mix (left) and conditions (right).

3.4.2. Digestion of insert and vector

The purified fragments of DNA and the pSBbi-Pur vector (a gift from Eric Kowarz, Addgene plasmid #60523, http://n2t.net/addgene:60523; RRID:Addgene_60523) (Kowarz et al., 2015) were digested using the appropriate restriction enzymes (**Table 3.5**) (illustrated in **Fig. 3.2**) (New England BioLabs, Ipswich, MA, USA). Briefly, 1 µg of

template DNA (vector or insert) was incubated with 0.5-1 µL of the restriction enzyme(s) at 37°C overnight (HindIII + XbaI, SphI) or 50°C (SfiI) in the suitable manufacturer buffer. Religation of the linearized plasmid was prevented by the addition of 0.5 µL of rSAP phosphatase (New England BioLabs, Ipswich, MA, USA; cat. #M0371) to the digestion mix.

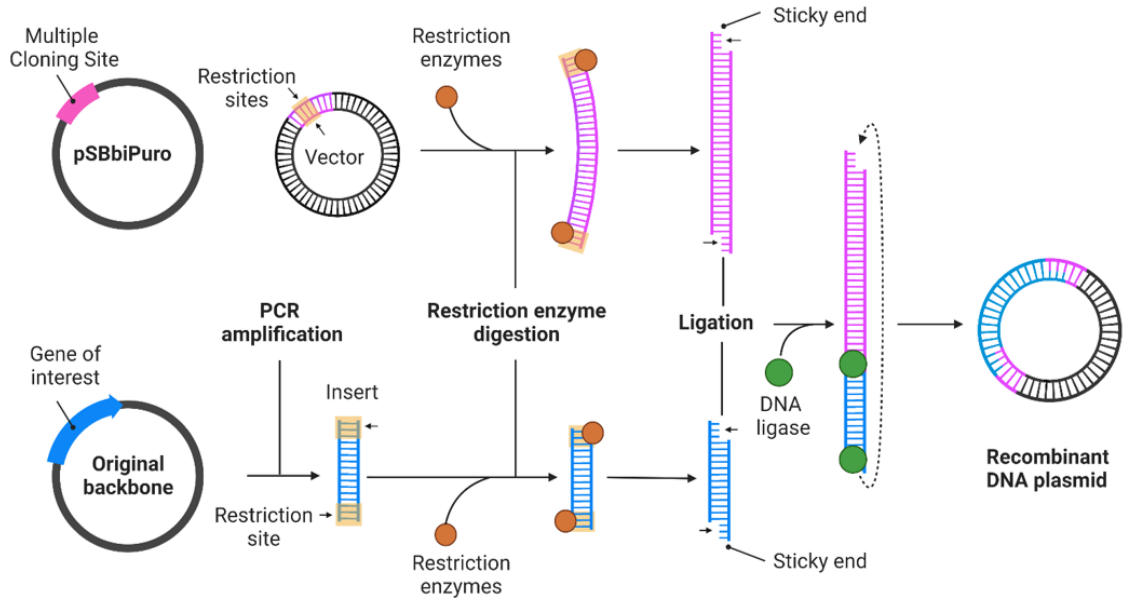

Figure 3.2. Schematic illustration of first steps of stable cell line generation. Insert amplification, insert and vector digestion, and insert and vector ligation are presented. Adapted from "Restriction Enzymes Cloning", by BioRender.com (2022). Retrieved from https://app.biorender.com/biorender-templates.

3.4.3. Ligation of insert into vector

After overnight digestion, enzymes were inactivated via incubation at 65°C for 10 min. The digested DNA inserts were purified with GeneMATRIX PCR/DNA Clean-Up Purification Kit (**Table 3.2**) according to the manufacturer's instructions. The digested vector was separated through a 0.7% agarose gel in the same conditions as described in section 3.4.1., and extracted with ExtractMe DNA/RNA extraction kit (**Table 3.2**) according to the manufacturer's instructions. The DNA purity was measured using NanoDrop.

The ligation reaction (illustrated in **Fig. 3.2**) was prepared for a total volume of 20 µL by mixing 1X T4 DNA Ligase Buffer and 1 µL T4 DNA Ligase (New England BioLabs, Ipswich, MA, USA; cat. #M0202S), 30 ng of the vector, and the desired insert. A ligation reaction control was included by incubating the digested vector alone with T4 DNA Ligase (no insert). The proportions of insert to vector DNA were calculated with the NEBio

Calculator for ligation (New England BioLabs, Ipswich, MA, USA) according to their size in base pairs. The PCR products were ligated with vectors in 7:1 and 5:1 molar ratios. The reaction was incubated at 16°C overnight.

3.4.4. Transformation of the ligated vector

After the overnight ligation, T4 DNA Ligase enzyme was inactivated via incubation at 65°C for 10 min. The ligation products were transformed into DH5α competent cells, generated as previously described (Inoue et al., 1990).

3.4.4.1. Transformation of competent bacteria

DH5α competent cells were transformed with the ligation products using the heat shock technique. Briefly, competent bacteria were thawed on ice and 10 µL of the ligation product or 1-10 ng of the original backbone vector were gently added to 100 µL of competent cells. After incubation on ice for 30 min, transformation was induced by a heat shock of 42°C for 45 s, followed by immediate incubation on ice for 2 min. Using an aseptic technique, bacteria were then diluted in 900 µL room-temperature LB medium and incubated at 37°C for 1 h with vigorous shaking (225 RPM) in a flask shaker. Then, grown bacteria cultures were spun at 6000 RCF for 3 min at RT in a microcentrifuge (VMR International, Radnor, PA, USA; cat. #521-1646P) and approximately 850 µL of the supernatants were discarded. The bacteria-containing pellets were resuspended in the remaining supernatant and seeded drop-wise in agar plates with the appropriate selection antibiotic (100 µg/µL ampicillin or 100 mg/µL kanamycin), then homogenously spread using sterile glass beads. The plates were incubated at 37°C overnight or at RT for 72 h.

3.4.4.2. Plasmid DNA isolation from bacteria culture

Successful ligations were confirmed with colony PCR of inserts by diluting half of each isolated colony in 3 µL water as a source of template DNA and mixing it with PCR Master Mix (EURx, Gdańsk, Poland; cat. #E2520) (**Table 3.7**) (illustrated in **Fig. 3.3_1**). After performing PCR, the products were separated through 0.7% agarose gels and visualized as described in section 3.4.1.

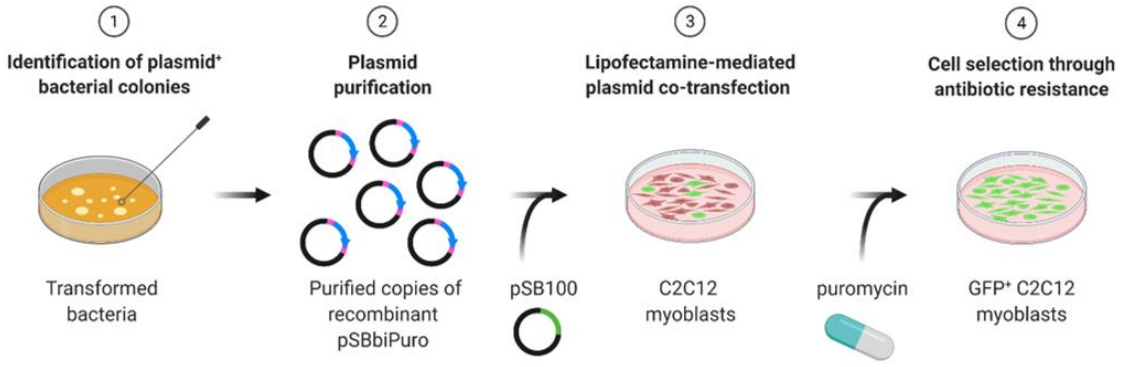

Figure 3.3. Schematic illustration of last steps of stable cell line generation. Plasmid DNA isolation from transformed bacteria (1, 2), cell co-transfection (3) and selection (4) are presented. Illustration created with BioRender.com.

Succesfully obtained constructs were isolated from the remaining half of the verified bacteria colonies, following the manufacturer's instructions of medium/large-scale commercial kits for plasmid isolation (**Table 3.2**) (illustrated in **Fig. 3.3_2**).

Table 3.7 Colony PCR reaction for ligation verification.

PCR reagents (V_T = 25 µL)	Original insert-containing vector (+ C)	Colonies
Nuclease-free water	Up to 25 µL	Up to 25 µL
PCR Master Mix 2X	12.5 µL	12.5 µL
10 µM primers	2.5 µL	2.5 µL
Template DNA	10 ng	colony diluted in 3 µL water

PCR step	Temperature	Time
Initial denaturation	98°C	30 s
Denaturation	98°C	10 s
Annealing	62°C	30 s
Extension	72°C	90-100 s
Final extension	72°C	120 s
Cooling	4°C	∞

PCR reaction mix (left) and conditions (right).

The purified plasmids were eluted in nuclease-free water and then concentrated overnight at -20°C in 0.7 volumes of isopropanol, 0.1 volumes of 3 M sodium acetate buffer and 1 µL glycogen diluted in water in 4:1 ratio (Invitrogen, ThermoFisher Scientific, Waltham, MA, USA; cat. #10814010). Then, the plasmids were spun at 20,000 RCF and 4°C for 30 min in a centrifuge (Eppendorf, Hamburg, Germany; cat. #5427R), and the resulting pellets were rinsed with 1.5 mL 70% ethanol, and spun again at 20,000 RCF and 4°C for 10 min. After discarding the supernatants, pellets were let to air-dry and resuspended in nuclease-free water before measuring their concentration and purity in NanoDrop. Finally, the appropriate size of obtained constructs was verified by digestion with specific restriction enzymes.

3.4.5. Transfection and selection of constructs in C2C12 myoblasts

C2C12 myoblasts were cultured as described in section 3.3.1. and kept undifferentiated throughout. Approximately 48 h before transfection, C2C12 were seeded at a density of 4.25 x 10^3 cells/cm^2 on 0.2% gelatin-coated, 6-well cell culture plates and incubated at 37°C. Immediately before transfection, cells were washed twice with Opti-MEM. Stable plasmid co-transfection of C2C12 myoblasts was performed using Lipofectamine 2000 (ThermoFisher Scientific, Waltham, MA, USA; cat. #11668030) according to the manufacturer's instructions (illustrated in **Fig. 3.3_3**). Briefly, 5 µL of Lipofectamine 2000 were diluted in 250 µL Opti-MEM, and 2000 ng of plasmid DNA (1800 ng of constructed vector and 200 ng of plasmid containing SleepingBeauty transposase system) (pCMV(CAT)T7-SB100, a gift from Zsuzsanna Izsvak, Addgene plasmid #34879, http://n2t.net/addgene:34879; RRID:Addgene_34879) (Mátés et al., 2009) were diluted in 250 µL Opti-MEM and then mixed together. To monitor the transfection efficiency, pSBbi-RP empty vector (a gift from Eric Kowarz, Addgene plasmid #60513, http://n2t.net/addgene:60513; RRID:Addgene_60513) (Kowarz et al., 2015) was used.

The transfection reaction mix was incubated at RT for 10 min and then added to cells in 1 mL Opti-MEM drop-wise. Finally, co-transfected C2C12 cells were incubated at 37°C for 12 h before selection. The selection of construct-containing cells was performed by adding puromycin at 10 µg/mL 12-72 h after transfection, since contruct-positive cells would be resistant to this antibiotic (illustrated in **Fig. 3.3_4**). Cells were seeded and propagated on 0.2% gelatin-coated 10 or 15 cm plates (Sarstedt, Newton, NC, USA; cat. #83.3902 or VMR International, Radnor, PA, USA; cat. #10062-882) in C2C12 proliferation medium for at least 72 h.

3.5. Protein co-immunoprecipitation

For co-immunoprecipitation (co-IP) of exogenous EB3 and endogenous drebrin, C2C12 myotubes stably overexpressing EB3-GFP (*see section 3.4. Stable cell line generation with SleepingBeauty system*) were harvested after five days of fusion (*see section 3.3.1. C2C12 cell line*). For co-IP of exogenous drebrin/rapsyn or EB3/rapsyn, transfected HEK293 cells were harvested 48 h after transfection (*see section 3.3.4. Plasmid transfection*). The constructs used for transfection are listed in **Table 3.3**.

Cells were scrapped from the plate surface in co-IP lysis buffer with 1% NP-40 (**Table 3.1**) and collected into microcentrifuge tubes to lyse them at 4°C for at least 60 min with

vigorous rotation and sterile glass beads, and then passed through a 25-gauge needle for further mechanical disruption. Lysates were then centrifuged at 10,000 RCF at 4°C for 10 min and supernatants were collected for protein concentration measurement with NanoDrop (*see section 3.10. Measurement of DNA/RNA/protein concentration and purity*).

For protein immunoprecipitation, a total volume of 25 µL Dynabeads™ Protein G (ThermoFisher Scientific, Waltham, MA, USA; cat. #10003D) were used for each sample. The separation of the magnetic beads from their solvent was performed using the 16-Tube SureBeads™ Magnetic Rack (Bio-Rad, Hercules, CA, USA, cat. #1614916). After washing the beads 4 times with 0.1% NP-40 diluted in PBS, 1 µg of anti-GFP antibody (GeneTex, Irvine, CA, USA, cat. #GTX26673) per co-IP reaction was incubated with the beads in 50 µL of 0.1% NP-40 diluted in PBS at RT with constant rotation for 60 min. In the control tube for non-specific immunoprecipitation, beads were incubated only with 50 µL of 0.1% NP-40 diluted in PBS, and no antibody was added. Once the bead-antibody bait was formed, unbound antibody residues were washed away by rinsing the beads 3 times with 200 µL of 0.1% NP-40 diluted in PBS per sample. Then, 80-200 µL of cell lysates were incubated with bead-antibody complexes at 4°C overnight with constant rotation. The variants of the experiment depended on the experimental design:

- EB3/Drebrin co-IP: for C2C12 myotubes overexpressing EB3-GFP, GFP was precipitated, while endogenous drebrin protein was co-immunoprecipitated. In this case, 200 µL of lysate from myotubes overexpressing EB3-GFP were incubated with beads.
- Drebrin/Rapsyn and EB3/Rapsyn co-IP: in transfected HEK293 cells, drebrin, EB3, or rapsyn were overexpressed separately and lysates containing exogenous proteins were mixed with each other at equal volumes and incubated together. Overexpressed DbnE-WT-GFP, DbnE-142A-GFP, or EB3-GFP were precipitated and Rapsyn-mCherry was co-immunoprecipitated.

After overnight incubation, flow-throughs were collected, and beads-antibody-protein complexes were washed four times with 200 µL co-IP lysis buffer per sample. Then, beads were resuspended in 30-40 µL 2X Laemmli Sample Buffer (Bio-Rad, Hercules, CA, USA; cat. #1610737) and boiled at 95°C for 10 min. Finally, protein-containing eluates were magnetically separated from the beads and further processed for SDS-PAGE and

Western blot analysis (*see section 3.9. Analysis of protein levels*). Antibodies used to detect immunoprecipitated proteins are listed in **Table 3.9**.

3.6. Cell surface delivery of AChRs

3.6.1. Immunofluorescence of surface and internal pools of AChRs

The cell surface delivery of AChRs upon drebrin downregulation was analyzed through immunofluorescence by using bungarotoxin (BTX) conjugated to different fluorophores (**Fig. 3.4**) (*see section 3.14. Immunofluorescence*). On the 5th day after fusion, live C2C12 myotubes were incubated with BTX conjugated to AlexaFluor™ 488 (ThermoFisher Scientific, Waltham, MA, USA; cat. #B13422) at 37°C for 15 min for labelling of surface AChRs, and then fixed with pure methanol at -20°C for 3 min. Cell membranes were permeabilized by incubation in immunoassay blocking buffer (**Table 3.1**) at RT for at least 30 min. Then, internal AChRs were labelled with BTX conjugated to AlexaFluor™ 555 (ThermoFisher Scientific, Waltham, MA, USA; cat. #B35451) by incubation at RT for 15 min.

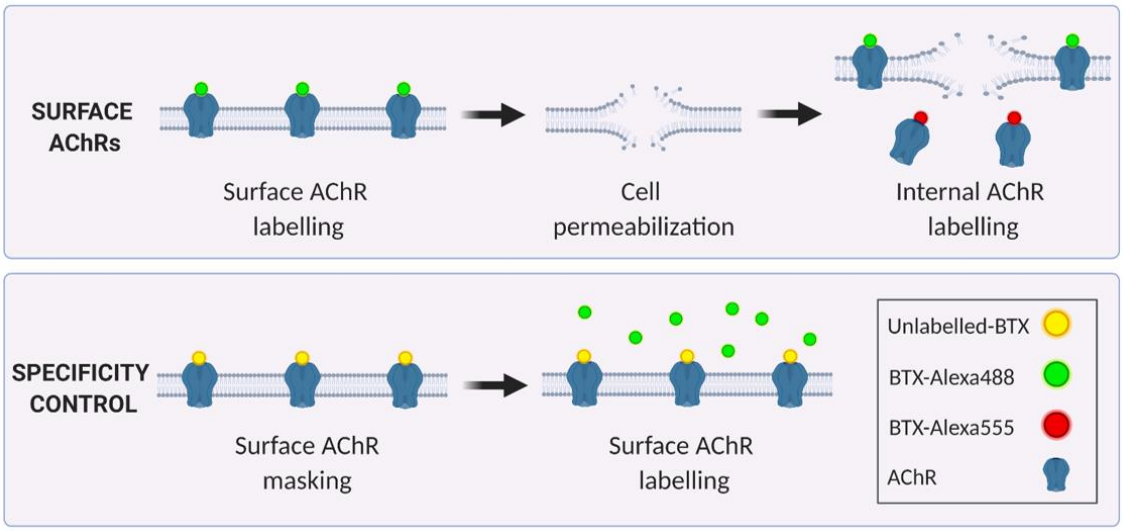

Figure 3.4. Schematic illustration of microscopy assay for assessment of cell surface delivery of AChRs. Illustration created with BioRender.com

To verify non-specific fluorescence and saturate surface AChRs, live control myotubes were incubated with BTX with no fluorescent conjugates (ThermoFisher Scientific, Waltham, MA, USA; cat. #B1601) at 37°C for 15 min. Then, cells were rinsed 3 times with warm sterile PBS (VMR International, Radnor, PA, USA; cat. #E504), further labelled with BTX conjugated to AlexaFluor™ 488, and fixed as the experimental cells described above.

3.6.2. Pull-down of total and surface AChR pools

Pull-down of total and surface AChRs upon drebrin downregulation was performed with BTX conjugated to biotin and NeutrAvidin beads (**Fig. 3.5**). On the 5th day after fusion, C2C12 myotubes were incubated live with BTX-Biotin (ThermoFisher Scientific, Waltham, MA, USA; cat. #B1196) at 37°C for 15 min in order to label the pool of surface AChRs. After thoroughly rinsing with sterile PBS, cells were lysed and harvested following the same procedure as for Co-IP experiments (*see section 3.5. Protein co-immunoprecipitation*), however using pull-down lysis buffer (**Table 3.1**). For pull-down of total AChRs, cells were first lysed and harvested, and the resulting lysates incubated with BTX-Biotin at RT for 15 min.

To control for non-specific signal and saturate the pool of surface AChRs, live control C2C12 myotubes were incubated at 37°C for 15 min with non-conjugated BTX (ThermoFisher Scientific, Waltham, MA, USA; cat. #B1601). Then, surface AChRs were labelled as described above. The concentration of BTX-Biotin was 2 µL of 1 mg/mL reagent per 250 µL lysate.

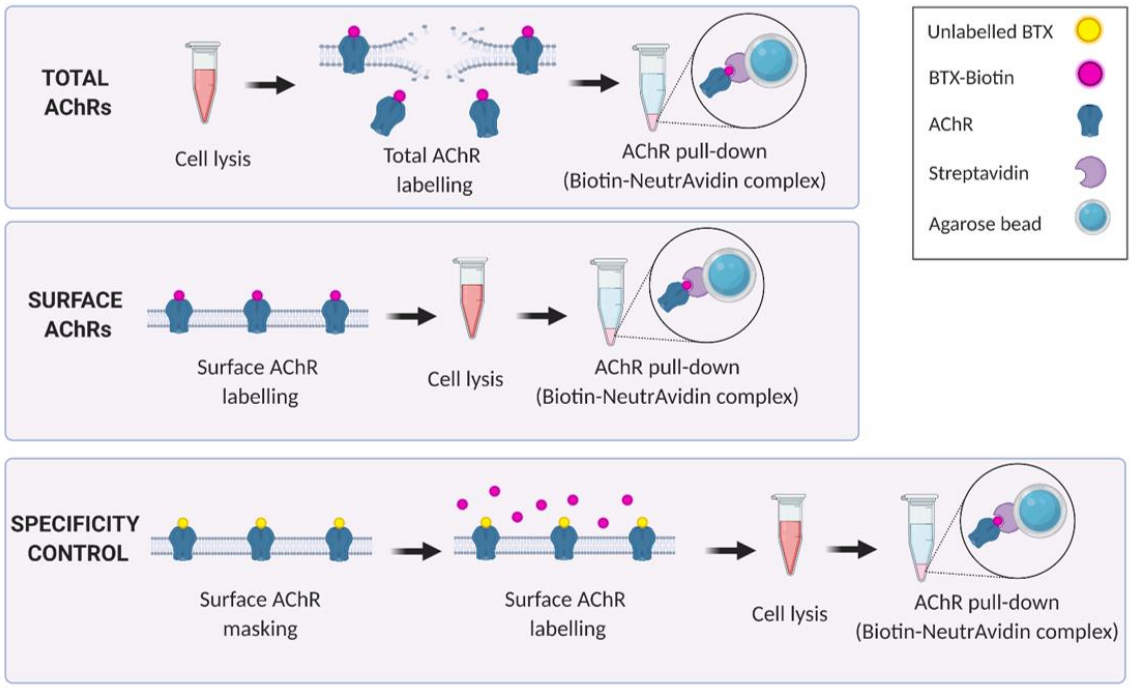

Figure 3.5. Schematic illustration of pull-down of surface or total AChRs for assessment of cell surface delivery of AChRs. Illustration created with BioRender.com

To pull-down surface and total AChR pools from the total protein content, lysates were incubated with constant rotation at 4°C overnight with Pierce™ NeutrAvidin™ Agarose

beads (ThermoFisher Scientific, Waltham, MA, USA; cat. #29201). After overnight incubation, AChR-BTX-Biotin-bound beads were separated from the solution by centrifugation at 2,500 RCF at RT for 2 min and the flow-throughs were collected. Then, beads were washed three times with pull-down washing buffer (**Table 3.1**), and resuspended in 45 µL 2X Laemmli Sample Buffer (Bio-Rad, Hercules, CA, USA; cat. #1610737) with 50 mM DTT and boiled at 95°C for 10 min. Finally, eluted AChR-containing supernatants were separated from the beads by centrifugation at 2,500 RCF at RT for 2 min, and further processed for SDS-PAGE and Western blot analysis (*see section 3.9. Analysis of protein levels*). Antibodies used to detect precipitated AChRs are listed in **Table 3.9**.

3.7. Immunofluorescence analysis of AChR turnover

To study the insertion of new AChRs to pre-existing clusters on the cell surface upon MVI knockdown, I performed fluorescence microscopy studies. First, C2C12 myoblasts were cultured on a laminin-coated surface as described in section 3.3.1. On the 5th day after fusion induction, old or newly incorporated surface AChRs were differentially labelled with BTX conjugated to different fluorophores (**Table 3.12**). Briefly, live myotubes were incubated at 37°C for 15 min with BTX-AlexaFluor™ 555 to label already incorporated AChRs. Then, cells were thoroughly washed with warm, sterile PBS, and incubated at 37°C for 6 h, in which new, unlabelled AChRs would be inserted between the previously incorporated, labelled AChRs. Then, myotubes were incubated with BTX-AlexaFluor™ 488 at 37°C for 15 min in order to label those newly incorporated AChRs, and then washed again thoroughly with warm, sterile PBS. Finally, cells were fixed in 4% paraformaldehyde (PFA) at RT for 10 min and mounted with DAPI diluted in Fluoromount™ Aqueous Mounting Medium (Sigma-Aldrich, St. Louis, MO, USA; cat. #F4680) to visualize cell nuclei, covered with coverslips, and sealed with nail polish.

3.8. Analysis of mRNA expression

3.8.1. RNA isolation

Total RNA was isolated from cell lysates by adding TRIsure reagent (Bioline, Taunton, MA, USA; cat. #BIO-38033) or from muscle tissue using RNeasy Plus Universal Mini Kit (Qiagen, Hilden, Germany; cat. #73404), according to the manufacturer's instructions. To remove residual genomic DNA, samples were incubated with 1 µL DNAase I, RNAase-free (ThermoFisher Scientific, Waltham, MA, USA; cat. #EN0521) per 1 µg RNA at 37°C for 60

min. The reaction was stopped by adding 1 µL EDTA per 10 µL reaction mix, followed by incubation at 65°C for 10 min.

Samples were measured with NanoDrop (*see section 3.10. Measurement of DNA/RNA/protein concentration and purity*) and stored temporarily at -20°C for further processing or immediately retrotranscribed into cDNA. Throughout the sample preparation procedure, a RNAase-free environment was kept through decontamination of the working area and equipment with RNaseAWAY solution (ThermoFisher Scientific, Waltham, MA, USA; cat. #21-236-21), and the use of gloves, certified RNAase-free reagents, and filtered pipette tips.

For reverse transcription, 1 µg of total RNA per reaction was used. cDNA was synthetized using High-Capacity cDNA Reverse Transcription Kit (Applied Biosystems, Waltham, MA, USA, cat. #4374966, #4368814) and following the manufacturer's instructions. The reverse transcription reaction was performed in a 96-well T100 thermal cycler.

3.8.2. Real-time quantitative PCR (RT-qPCR)

For each sample, a 20 µL-volume RT-qPCR reaction was performed in triplicates with StepOnePlus™ Real-Time PCR System (ThermoFisher Scientific, Waltham, MA, USA; cat. #4376600). The reaction was prepared using SYBR™ Green PCR Master Mix (ThermoFisher Scientific, Waltham, MA, USA; cat. #4385612). The synthesis of primers was outsourced to the Laboratory of DNA Sequencing and Oligonucleotides Synthesis from the Institute of Biochemistry and Biophysics, Polish Academy of Sciences. Primers used in RT-qPCR were tested for efficiency and specificity and only validated ones were used for experimental analysis. All primers used are listed in **Table 3.8**.

Table 3.8. Primers used for RT-qPCR.

Gene	Encoded protein	Primers used for cDNA amplification
Gapdh	Glyceraldehyde 3-phosphate dehydrogenase	F: 5'GGCCTTCCGTGTTCCTAC 3' R: 5' TGTCATCATACTTGGCAGGTT 3'
Dbn1	Drebrin	F: 5' GACCCAGGCCAGCGAAG 3' R: 5' CCCAGCAGGTGATGTCGATT 3'
Rpsn	Rapsyn	F: 5' CTTGGTAACAGCTCACTCGG 3' F: 5' CAGTATCAATCTGGACCACGG 3'
Myo6	Myosin VI	F: 5' GTGTGCTACGAGACAACCCA 3' R: 5' GTTTCCCACGCTGATGAAGC 3'
Macf1	Microtubule actin cross-linking factor 1	F: 5' GAAAACATTCACCAAGTGGGTCAAC 3' F: 5' TGTCCATCCCGAAGGTCTTCATAG 3'
Homer1	Homer1	F: 5' ACTGTTTATGGACTGGGATTCTC 3' F: 5' GTACTGGTCAGCTCCATCTTC 3'

The StepOnePlus™ Software v2.3 was used for data acquisition and the results were analyzed using the relative standard curve method. In order to standarize the samples, housekeeping gene *Gapdh* was used.

3.9. Analysis of protein levels

3.9.1. Total protein isolation

Cultured cells were lysed with ice-cold Co-IP lysis buffer with 0.1% NP-40 (**Table 3.1**) by placing the culture plate on ice and adding lysis buffer in a volume sufficient to cover the well surface (e.g. 200 µL buffer/0.9 cm^2). Cells were scrapped from the plate surface and collected into microcentrifuge tubes to lyse them at 4°C with vigorous rotation for at least 60 min with sterile glass beads, and then passed through a 25-gauge needle for further mechanical disruption. Immediately after isolation, muscles were lysed with ice-cold RIPA buffer (**Table 3.1**) in 1:10 ratio (100 µL buffer/10 mg tissue) and mechanically homogenized with Bio-Gen PRO200 Homogenizer (PRO Scientific, Oxford, CT, USA; cat. #01-01200). Cell lysates or tissue homogenates were then centrifuged at 10,000 RCF at 4°C for 10 min and supernatants were collected for protein concentration measurement with NanoDrop (*see section 3.10. Measurement of DNA/RNA/protein concentration and purity*) and stored at -20°C.

Before SDS-PAGE, samples were diluted in 2X Laemmli Sample Buffer (Bio-Rad, Hercules, CA, USA; cat. #1610737) (to a final concentration of 1X) and 50 mM DTT and boiled at 95°C for 10 min in order to denature proteins. The amount of protein diluted for SDS-PAGE was adjusted and optimized depending on the loading control (*see section 3.9.3. Western blot*).

3.9.2. SDS-PAGE

Proteins were separated by molecular weight with sodium dodecyl sulfate-polyacrylamide gel electrophoresis (SDS-PAGE). 1 mm-thick polyacrylamide gels were either homemade or purchased (4-15% Mini-PROTEAN® TGX™ Precast gels, BioRad, Hercules, CA, USA, cat. #4561083).

Gel homemade preparation and electrophoresis were performed using Mini-PROTEAN Tetra Cell system (BioRad, Hercules, CA, USA) and 3 µL Color Prestained Protein Standard Ladder (10–240 kDa) (New England BioLabs, Ipswich, MA, USA; cat. #P7712S or #P7719) was used as size reference of protein molecular weight. Equal concentrations of samples

were loaded onto the gel and the electrophoresis was performed in SDS-PAGE running buffer (**Table 3.1**) at 80-120 mV for 60-180 min.

3.9.3. Western blot

After SDS-PAGE, separated proteins were transferred to a BioTrace™ NT Nitrocellulose Transfer Membrane (Pall, Port Washington, NY, USA, cat. #66485) with Trans-Blot® Turbo™ Transfer System (Bio-Rad, Hercules, CA, USA; cat. #1704150), following the manufacturer's instructions. The transfer protocol used was the 7 min-long default protocol for mixed molecular weights and the blotting sandwich was soaked beforehand in Transfer buffer (**Table 3.1**). After transfer, membranes were rinsed in TBST buffer (**Table 3.1**) and incubated in 10% WB blocking buffer (**Table 3.1**) at RT for at least 30 min in order to prevent non-specific binding of antibodies. Then, membranes were incubated with primary antibodies diluted in 5% WB blocking buffer at 4°C overnight (**Table 3.9**). After washing away the residual primary antibodies with TBST three times at RT for 10 min, membranes were incubated with secondary antibodies conjugated to horseradish peroxidase (**Table 3.9**) diluted in 5% WB blocking buffer for at least 60 min at RT.

Table 3.9. List of antibodies used for immunoblotting.

Name	Dilution	Supplier and catalogue number
Primary antibodies		
anti-drebrin	1:1000	GeneTex, Irvine, CA, USA, cat. #GTX12350 Abcam, Cambridge, UK; cat. #ab60933
anti-myosin VI	1:500	Proteus BioSciences, Ramona, CA, USA; cat. #25-6791
anti-AChR α1, α3, α5	1:1000	BioLegend, San Diego, CA, USA; cat. #838301
anti-rapsyn	1:1000	Abcam, Cambridge, UK; cat. #ab156002
anti-GAPDH	1:1000	Santa Cruz Biotechnology, Dallas, TX, USA; cat. #sc-25778
anti-tubulin	1:10000	Abcam, Cambridge, UK; cat. #ab18251
anti-GFP	1:1000	GeneTex, Irvine, CA, USA; cat. #GTX26673
Secondary antibodies		
anti-mouse-HRP	1:5000	Cell Signaling Technologies, Danvers, MA, USA; cat. #7076
anti-rabbit-HRP	1:5000-20000	Jackson ImmunoResearch, West Grove, PA, USA; cat. #111-035-144
anti-goat-HRP	1:5000	Santa Cruz Biotechnology, Dallas, TX, USA; cat. #sc-2020
anti-rat-HRP	1:5000	Enzo Life Sciences, Farmingdale, NY, USA; cat. #ADI-SAB-200-J

Abbreviations: HRP = horseradish peroxidase.

Residual secondary antibodies were washed away with TBST at RT three times for 10 min. Finally, immunolabelled proteins were detected with Femto chemiluminiscent

substrate (Thermo Fisher Scientific, Waltham, MA, USA; cat. 34095) incubated with membranes at RT for 3-5 min. Membranes were developed for visualization in a dark room with Kodak® BioMax® MS films (Carestream, Rochester, NY, USA, cat. #771468) and a film processor (Fujifilm, Tokyo, Japan, cat. #FPM 800A). All incubations except the chemiluminiscent substrate were performed under gentle, constant rocking to allow even distribution of the reagents across the membranes.

For all immunoblotting experiments, a loading control was performed to ensure even amount of proteins in all samples within the same experiment. For that purpose, proteins encoded by housekeeping genes, tubulin or GAPDH, were detected.

3.10. Measurement of DNA/RNA/protein concentration and purity

The concentration and purity of DNA, RNA, or total protein were measured using NanoDrop 200c Microvolume Spectrophotometer (Thermo Fisher Scientific, Waltham, MA, USA) with pre-settings for DNA, RNA, or proteins. The measurement of absorbance at 260 nm (specific for nucleic acids), 280 nm (specific for proteins), and 230 nm (impurities) allows for the automatic calculation of 260/280 (to detect protein/nucleic acids contamination) and 260/230 (to detect other impurities) ratios and assessment of sample's purity. DNA was considered to be of sufficient quality and purity if the ratio 260/280 was between 1.7-2.0 and the 260/230 ratio was between 2.0-2.3. RNA was considered to be of sufficient quality and purity if the ratio 260/280 was between 1.9-2.1 and the 260/230 ratio was between 2.0-2.3. Protein content was considered to be of sufficient quality and purity if the ratio 260/280 was below 0.6 (minimal nucleic acid contamination).

3.11. Animal models

All procedures performed on mice (*Mus musculus*, house mouse) were approved by the First Warsaw Local Ethics Committee for Animal Experimentation (permissions 629/2018 and 1311/2022). *Snell's waltzer* (*SV*) and wild-type mice had a C57BL/6J genetic background and were maintained at the animal facility of the Nencki Institute of Experimental Biology, equipped with a selected pathogen free (SPF) barrier (standard).

Wild-type C57BL/6J mice (WT), the most widely used inbred mouse strain, were used for endogenous and exogenous protein colocalization and expression pattern studies. *Snell's waltzer* mice were a generous gift from Dr. Folma Buss (Cambridge Institute for Medical Research, United Kingdom) and they correspond to the strain C57BL/6J x STOCK $Tyr^{c\text{-}ch}$ $Bmp5^{se}$ +/+ $Myo6^{sv}$/J (stock #000578). Homozygous *SV* mice have a spontaneous 150-bp

deletion in the *Myo6* gene, resulting in the introduction of a stop codon in the sequence that produces a non-functional MVI protein. Therefore, these animals serve as natural MVI knockout mice (**Fig. 3.6B**). They are characterized by circling, head-tossing, deafness, and hyperactivity, behaviors that are recognizable by P7 (Avraham et al., 1995). These mice were used to assess the phenotype at the NMJ in the absence of MVI, as well as for primary myogenic culture. Heterozygous littermates were used as control animals for all experiments.

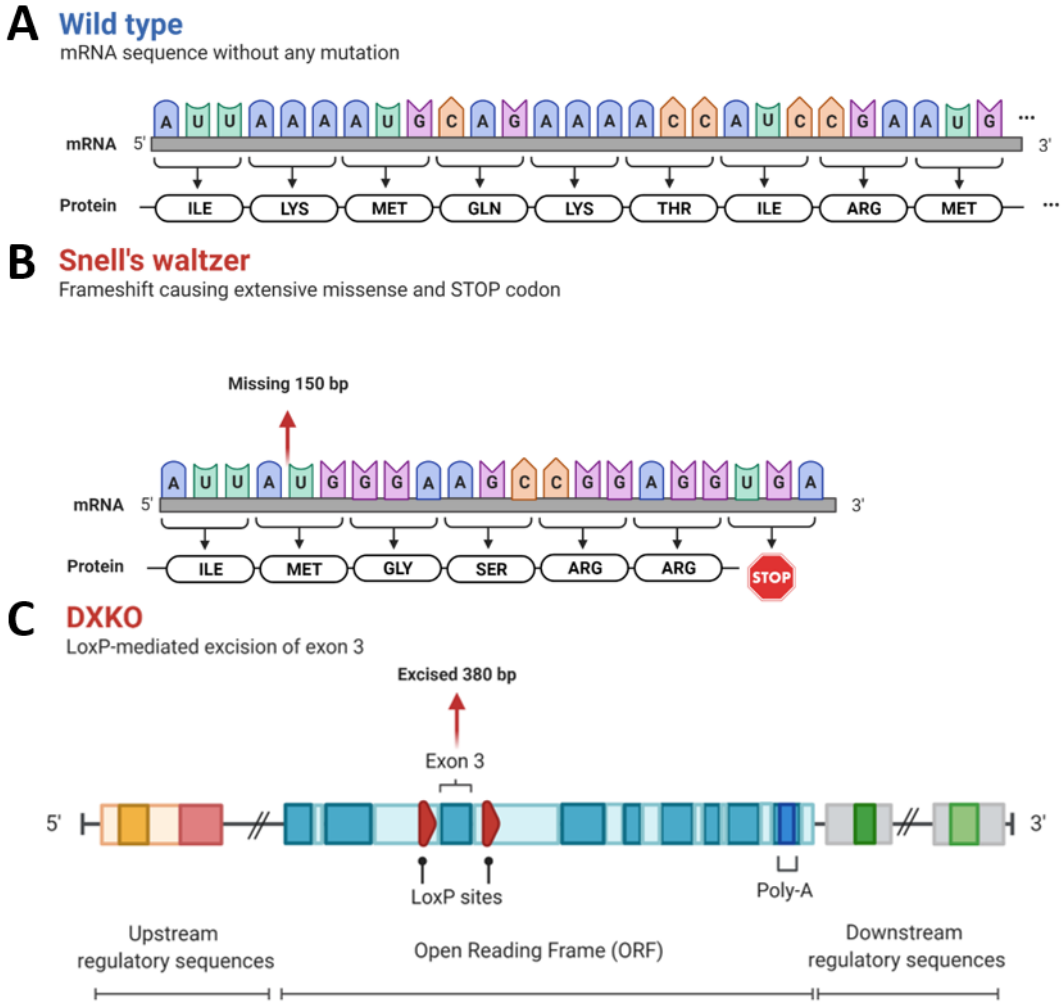

Figure 3.6. Mice strains. (A) Wild-type (C57BL/6J) *Myo6* gene, as a comparison to **(B)** *Snell's waltzer* (*SV*) mice generated as a consequence of a spontaneous deletion in the *Myo6* gene, resulting in a non-functional MVI protein. Adapted from "Frameshift Mutations", by BioRender.com (2022). Retrieved from https://app.biorender.com/biorender-templates. **(C)** DXKO mice generation via LoxP/CRE-mediated excision of exon 3 in *Dbn1* gene. Adapted from "Eukaryotic and Prokaryotic Gene Structure", by BioRender.com (2022). Retrieved from https://app.biorender.com/biorender-templates.

Muscle tissues from DXKO mice perfused with PFA were a generous gift from Dr. Hiroyuki Yamazaki (Gunma University, Japan). DXKO mice had a C57BL/6J genetic

background and were generated at the Gunma University, Japan by crossing of drebrin-flox mice and TLCN-Cre mice (Kajita et al., 2017). Homozygous DXKO mice have a deletion in exon 3 of both copies of the *Dbn1* gene, resulting in systemic absence of all drebrin isoforms (**Fig. 3.6C**). Received fixed muscles from homozygotes and WT littermates were used to assess the phenotype at the NMJ in the absence of drebrin protein.

Developmental time points were selected for the analysis of *in vivo* phenotypes based on age-associated changes to the murine NMJ, with morphological and functional aberrations appearing at 12-14 months old and worsening with age (Cheng et al., 2013).

3.11.1. Mice genotyping

All animals were routinely genotyped to identify and select the desired genotypes (**Fig. 3.7**). The genomic DNA was isolated from a 2-4 mm^2 piece of the mouse tail by incubating it for 20 min in a solution of 10% Chelex 100 resin (Sigma-Aldrich, St. Louis, MO, USA; cat. #C7901) at 95°C. Then, samples were spun at 13,000 RCF at RT for 5 min in a microcentrifuge and supernatants were collected for further PCR reactions. For the PCR reaction, PCR Master Mix (2X) was used in a final volume of 25 µL and PCR reactions were performed in a 96-well T100 thermal cycler, according to the manufacturer's instructions. Primers used for genotyping are summarized in **Table 3.10**, and PCR conditions are summarized in **Table 3.11**.

Table 3.10. Primers used for genotyping.

Gene	Encoded protein	Primers used for DNA amplification	Band size
Myo6	Myosin VI	SV1: 5'-CTGACCCTGATCACTTAGCAGAGTTG-3' SV2: 5'-CATTGGGCCAGGTCACAGAAGTAAGC-3' SV3: 5'-GGTCCTCTGAAAGAGTAACC-3'	SV mice = 318 bp Heterozygous = 318; 230 bp (WT) WT = 230 bp
Dbn1	Drebrin E	F: 5' GGGAACGGTAACCAAGGAAC 3' R: 5' TTCTGGAGAAACCAGGGAGA 3'	DXKO mice = 600 bp Heterozygous = 980; 600 bp (WT) WT = 980 bp

Table 3.11. PCR reaction for mice genotyping.

PCR reagents (V_T = 25 µL)	Volume added
Nuclease-free water	Up to 25 µL
Master Mix 2X	12.5 µL
10 µM primers	1-3 µL
Tail DNA	2.5 µL

PCR step	Temperature	Time
Initial denaturation	94°C	120 s
Denaturation	95°C	20 s
Annealing	54°C (*Myo6*) 55°C (*Dbn1*)	30 s
Extension	72°C	20 s (*Myo6*) 180 s (*Dbn1*)
Final extension	72°C	300 s

PCR reaction mix (left) and conditions (right).

DNA products from PCR reactions (amplicons) were visualized in agarose gels as described in section 3.4.1., and loaded with Perfect 100-1000 bp DNA Ladder (EURx, Gdańsk, Poland, cat. #E3141) as a size reference.

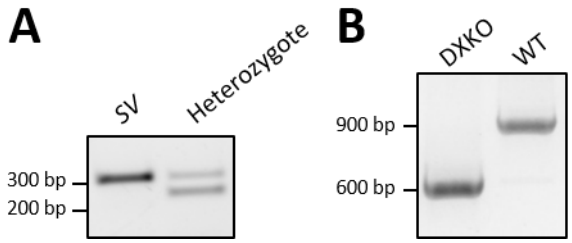

Figure 3.7. Mice genotyping results. (A) Genotyping results of *SV* and heterozygous WT mice from tail DNA. Myosin VI WT allele = 230 bp, MVI knockout allele = 318 bp. Heterozygote = 230 bp and 318 bp. **(B)** Genotyping results of DXKO and WT mice from tail DNA. Drebrin WT allele = 980 bp, drebrin knockout allele = 600 bp. Representative image by A. Nadel. **Abbreviations:** bp = base pairs; DXKO = drebrin global knockout mice; SV = MVI global knockout mice; WT = wild-type (control) mice.

3.12. Grip strength test

To assess muscle strength of MVI knockout mice, the non-invasive and stress-reduced method of grip strength testing was used. Behavioral experiments were outsourced to the Laboratory of Behavioral Methods, Nencki Institute of Experimental Biology, PAS. Test sessions took place around the same time of the light cycle (07:00-20:00) in the animal facility of the Nencki Institute of Experimental Biology. The apparatus used consists of an electronic strength test device (BIOSEB, Vitrolles, France, cat. #BIO-GS3) with a force gauge connected to a bar to which the mice were allowed to hold with either their forelimbs or both forelimbs and hindlimbs. In total, 20 mice at P365 of either WT (n = 4 females, 6 males) or *SV* genotype (n = 5 females, 5 males) were tested to account for sex-related differences in muscle strength during middle age (Dutta & Sengupta, 2016). Mice were tested in a randomized order for three consecutive trials on the same day, with one-minute inter-trial breaks, and the investigator performing the test was blind to their genotype. Each animal was allowed to grasp the bar, and the peak full force in grams (g) and Newtons (N) was recorded on a digital force transducer. Then, the gauge was reset to 0 g after stabilization and the mouse was gently pulled back from its tail by the investigator at a constant speed (slow enough for the mouse to build up resistance grip). When the mouse finally released its paws from the bar, the force was again measured and registered for data analysis as grip strength. The criteria for excluding trials from final data analysis included grasping the bar with only one paw,

only hindlimbs used, mouse turning around during the pull, or mouse not exerting any resistance to being pulled back.

Figure 3.8. Schematic illustration of vertical grip strength test. Black arrow indicates direction of pulling movement. Illustration created with BioRender.com

I chose a modified protocol that overcomes the main limitation of the conventional grip strength test (motivation to keep gripping the bar) by positioning the apparatus vertically (Takeshita et al., 2017). This way, the composite mouse muscle force (gravity on the mouse body and force exerted by the investigator) is completely conducted to the measuring device, providing high accuracy and low variability between measurements. Moreover, this protocol allows the detection of subtle differences, particularly in older animals. The variable analyzed was absolute grip strength measured in grams and it was not normalized by body weight, since it has been shown to be more sensible to detecting age-related impairments in skeletal muscle function (Takeshita et al., 2017).

3.13. Skeletal muscle electroporation

Plasmid DNA electroporation was performed on P30-45 WT mice under general anesthesia with intraperitoneal injection of ketamine/xylazine cocktail (150/10 mg/kg). After confirming heart beat presence and lack of reflexes, and shaving the hindlimb area to be electroporated, 25 µg DNA (1 µg/µl in sterile PBS) of pEGFP-C1-DbnE-WT or pEGFP-C1-DbnE-142A plasmid (**Table 3.3**) was injected into the *TA* muscle using a 702LT Hamilton syringe (Hamilton, Reno, NV, USA; cat. #24531). As a negative control, an empty pEGFP-C1 vector (Clontech, Mountain View, CA, USA; cat. #6084-1) was used. Immediately after injection, the electrodes of an ECM-830 electroporator (BTX Harvard Apparatus, Holliston, MA, USA; cat. #45-0052INT) were wetted with PBS and the muscle

was electroporated with 10 pulses of electrical current at 180 V/cm for 20 ms each with 1 s intervals. During the whole procedure, the animals' eyes were covered with hydrating Vidisic eye gel (Bausch+Lomb, Laval, Canada) to prevent them from drying, and the physiological body temperature was sustained throughout with a heat plate. The overall condition of the mice was monitored during and after the procedure. Immediately after the procedure, 2% lidocaine gel (Lignocainum Jelfa 20 mg, PharmaSwiss, Laval, Canada) was locally applied to the electroporated area and post-procedure analgesia was administered by subcutaneous injection of 1-5 mg/kg of butorphanol (Butomidor 10 mg/mL, Orion Pharma, Warsaw, Poland). Mice were sacrificed 7-10 days after the procedure.

3.14. Immunofluorescence

Proteins of interest were labelled with protein-specific antibodies and then stained with fluorescent dyes for microscopy visualization and analysis in either murine skeletal muscle tissue (immunohistochemistry) or in cultured cells (immunocytochemistry) (**Table 3.12**).

Table 3.12. List of antibodies and fluorescent markers used for immunofluorescence labelling.

Name	Dilution	Supplier and catalogue number
Primary antibodies		
anti-drebrin	1:300	ProteinTech, Rosemont, IL, USA; cat. #10260-1-AP ProteinTech, Rosemont, IL, USA; cat. #25770-1-AP
anti-phospho-drebrin	1:250	MilliporeSigma, Burlington, MA, USA; cat. #MABN833
anti-actinin	1:300	Santa Cruz Biotechnology, Dallas, TX, USA; cat. #sc-17829
anti-Ryr1	1:300	Abcam, Cambridge, UK; cat. #ab2868
anti-myosin heavy chain	1:300	DHSB, Iowa, IA, USA; cat. #AB_2147781
anti-LL5β	1:300	Homemade, a generous gift from Prof. Sanes (Kishi et al., 2005)
anti-2H3 neurofilament	1:350	DHSB, Iowa, IA, USA; cat. #AB_2314897
anti-synaptophysin	1:350	Synaptic Systems, Göttingen, Germany; cat. #101 004
anti-EB3	1:300	BD Biosciences, Franklin Lakes, NJ USA; cat. #612156
anti-myosin VI	1:250	Proteus BioSciences, Ramona, CA, USA; cat. #25-6791
Secondary antibodies/fluorescent markers		
BTX-AlexaFluor 488/555	1:500	ThermoFisher Scientific, Waltham, MA, USA; cat. #B13422/#B35451
Phalloidin-AlexaFluor 633	1:125	ThermoFisher Scientific, Waltham, MA, USA; cat. #A22284
anti-mouse-AlexaFluor 488/555/647	1:500-800	ThermoFisher Scientific, Waltham, MA, USA; cat. #A28175/#A-31570/#A-21236
anti-rabbit-AlexaFluor 555	1:500-800	ThermoFisher Scientific, Waltham, MA, USA; cat. #A-11004
anti-guinea pig-AlexaFluor 647	1:600	ThermoFisher Scientific, Waltham, MA, USA; cat. #A-21450
DAPI	1:1000	AppliChem, Darmstadt, Germany; cat. #A4099

Appropriate controls were performed in parallel to experimental samples to monitor the specificity of all primary antibodies. Briefly, control samples were subjected to all the steps of the immunostaining protocol except from the incubation with primary antibody. During microscopy imaging and analysis, it was confirmed that the signal observed in control samples (corresponding to the background noise of the secondary antibody fluorescence) was not specific and significantly reduced compared to experimental samples.

3.14.1. Skeletal muscle whole-mount fiber preparations

After confirming death of the animal, the skin and fasciae covering the muscle tissue of interest were carefully removed with surgical tools. The muscles excised are illustrated in **Fig. 3.9**.

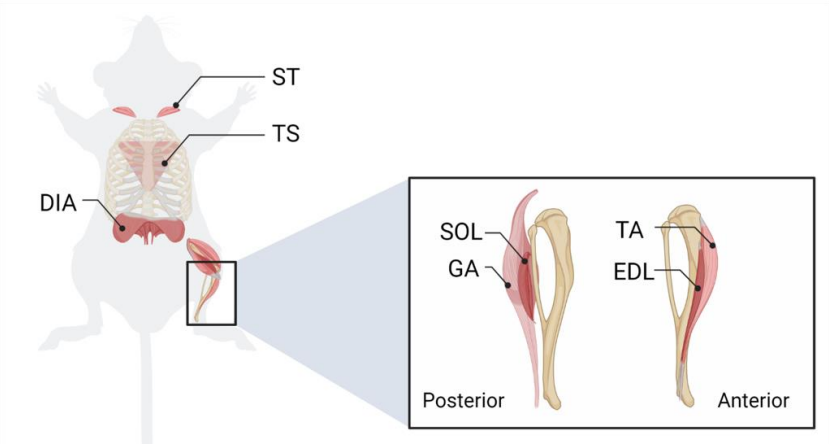

Figure 3.9. Schematic illustration of all skeletal muscles isolated. Abbreviations: DIA = diaphragm; EDL = extensor digitorum longus; GA = gastrocnemius; SOL = soleus; ST = sternomastoid; TA = tibialis anterior; TS = triangularis sterni. Illustration created with BioRender.com.

Different procedures were used for the excision of different muscles:

- *Tibialis anterior* (TA): The hindlimb was severed and a small incision in the ankle skin was enough to expose the underlying muscle. After removal of fasciae, the dissection forceps were placed under the first anterior tendon of the ankle and moved upwards to separate the muscle from the bone.
- *Gastrocnemius* (GA) and *soleus* (SOL): Similar to *TA* isolation, the dissection forceps were placed under the Achilles tendon and moved upwards. Then, the

tendon was cut and the calf muscle (*GA*) was gently separated from the *SOL* muscle with scissors.

- *Extensor digitorum longus* (EDL): After removal of *TA* and *GA*, the most lateral anterior muscle was exposed by placing forceps under the corresponding tendon of the ankle, and moving them upwards to isolate the muscle.
- *Diaphragm* (DIA): The skin around the torso was cut avoiding damage to any internal organ. The diaphragm is a very delicate and thin muscle limiting the ventral part of the ribcage, just above the liver, so after removing the lower body and internal organs below the ribcage, a small incision was made in the diaphragm membrane that allowed to cut the muscle along the ribcage bottom. Due to its close contact with internal organs, the diaphragm was rinsed off blood in PBS before fixation.
- *Triangularis sterni* (TS): The *TS*, also a delicate and thin muscle, covers a portion of the inner anterior wall of the ribcage, and its isolation requires the whole structure to be fixed. After removing heart and lungs from within the chest cavity, the whole ribcage was cutout and rinsed with PBS before fixation. Then, the ribcage was cut along the spinal cord, leaving the ribs attached to the sternum. The ribcage was then spread on a styrofoam platform with the inside of the chest cavity facing upwards. A thin needle was inserted into a blood vessel close to the sternum to slowly move outwards and separate the *TS* muscle from the ribs. The edges of the muscle were cut with a scalpel.
- *Sternomastoid* (ST): After removing skin, fat, and other tissues around the neck and throat area, the trachea and attached sternomastoid muscles were exposed. Both ends of the muscle were cut avoiding damage to blood vessels.

After isolation, muscles were fixed in 4% PFA at RT for 20-80 min, with the exception of the *TS* muscle, which was fixed with the whole ribcage in 100% methanol at -20°C for 3-5 min. The time of fixation depended on the age of the animal and the relative size of the muscle tissue: for reference, young and small muscles were fixed for 15-20 min, while big and aged muscles were fixed for 50-80 min. Muscles were stored at 4°C in PBS (**Table 3.1**) supplemented with 0.02% NaN_3 for better tissue preservation.

Approximately 10-30 single fibers from each muscle were isolated using fine surgical forceps. Incubation at RT for at least 30 min with immunoassay blocking buffer (**Table**

3.1) was used to both permeabilize the tissue and block non-specific antibody binding, in order to improve the sensitivity of the assay and reduce the background interference. Then, fibers were incubated at 4°C overnight with gentle shaking, with primary antibodies diluted in immunoassay blocking buffer. After washing fibers three times in PBS for 5 min, they were incubated with appropriate secondary antibodies diluted in the immunoassay blocking buffer. Finally, AChRs were labelled by incubating the fibers with bungarotoxin (BTX) at RT for 15 min, and rinsed once in PBS. Bungarotoxin binds with high affinity to the α subunit of AChRs and was coupled with green, red, or far-red fluorescence emiting-fluorophores depending on the experiment. Samples were mounted on glass slides with DAPI diluted in Fluoromount™ Aqueous Mounting Medium to visualize cell nuclei, covered with coverslips, and sealed with nail polish. All antibodies and fluorescently labelled markers are listed in **Table 3.12**.

3.14.2. C2C12 myotubes

C2C12 myoblasts for immunocytochemistry experiments were seeded on Permanox plastic Nunc™ Microscope slides (ThermoFisher Scientific, Waltham, MA, USA; cat. #160005) in 8-well flexiPERM® chambers (Sarstedt, Newton, NC, USA; cat. #94.6032.039) and differentiated into myotubes as described in section 3.4.1. On the 5^{th} day after fusion induction, the fusion-inducing medium was removed and cells were fixed by incubation with 4% PFA at RT for 10 min or 100% methanol at -20°C for 3 min, depending on the experiment. Then, remaining fixative solution was washed away with three rinses in PBS for 5 min each.

Similar to the immunohistochemistry procedure, fixed cells were incubated at RT for at least 30 min with immunoassay blocking buffer (**Table 3.1**) to permeabilize the cell membranes and improve signal-to-noise ratio. Then, cells were incubated at 4°C overnight with primary antibodies diluted in immunoassay blocking buffer. After washing the cells three times in PBS for 5 min, they were incubated with appropriate secondary antibodies diluted in the immunoassay blocking buffer. Finally, AChRs were labelled by incubating the cells with BTX at RT for 15 min, and rinsed once in PBS. Preparations were mounted with DAPI diluted in Fluoromount™ to visualize cell nuclei, covered with coverslips, and sealed with nail polish. All antibodies and fluorescently labelled markers are listed in **Table 3.12**.

3.15. Microscopy and image analysis

Microscope imaging was performed at the Laboratory of Imaging Tissue Structure and Function, Nencki Institute of Experimental Biology, PAS, with the use of CePT infrastructure financed by the European Union, The European Regional Development Fund within the Operational Programme "Innovative economy" for 2007–2013. Image acquisition was performed with Axio Observer Z.1 inverted microscope (Carl Zeiss AG, Oberkochen, Germany) equipped with CSU-X1 spinning disc unit (Yokogawa, Japan), Evolve 512 EMCCD camera (Photometrics, USA) and diode 405/488/561 and 639 nm lasers (Carl Zeiss AG, Oberkochen, Germany). The images were collected using ZEN 3.1 software (Carl Zeiss AG, Oberkochen, Germany) and processed with FijiJ distribution of ImageJ 1.51h software (Schindelin et al., 2012).

3.15.1. Quantification of fluorescence intensity of surface or internal AChRs

For the quantification of average fluorescence intensity of surface or internal AChR signal in control and drebrin-depleted C2C12 myotubes (*see section 3.6.1. Immunofluorescence of surface and internal pools of AChRs*), images were acquired in myotube areas without AChR clusters and of similar maturation state (overall fusion and width). The quantification of average fluorescence was performed with the contour (spline) tool in the ZEN software by manually selecting the area covered by the myotube. A small section of the background was also sampled for each image and substracted to the myotube fluorescence intensity. The data analyzed corresponded to the average fluorescence intensity of the surface or internal AChR signal divided by the area.

3.15.2. Quantification of EB3 foci

For the quantification of EB3 foci underneath AChR clusters, Z-stack images were acquired in AChR cluster-occupied areas of myotubes at 63X magnification with 0.5 µm interval between stack planes. Individual fluorescence channels for AChRs and EB3 labelling were acquired. The cluster surface was defined and measured with the contour (spline) tool in the ZEN software at the AChR channel as a region of interest. The Z plane selected for quantification of EB3 foci was at 0.5 µm below the plane with the highest fluorescence intensity detected for AChRs (corresponding to the cell membrane), based on the study showing that EB3 fluorescent signal peaks at 0.3-0.5 µm from the tip of dynamic microtubules in C2C12 cells (Roth et al., 2019). Within the defined AChR cluster

area, the events tool was used to manually count the number of EB3 foci, and contrast parameters were adjusted to improve visibility following the same method for each picture. To verify if the observed changes in EB3 foci number were specific to AChR clusters, the same analysis was performed for a myotube area outside of the AChR cluster. The results were calculated as number of EB3 foci per cluster area (#/μm^2).

Because the MT network is dense and its morphological characteristics are difficult to analyze manually, automated quantification was used for high throughput analysis and reduction in human bias. For the analysis of EB3 foci size and shape parameters, Ilastik 1.3.3.post3 (European Molecular Biology Laboratory, Heidelberg, Germany) (S. Berg et al., 2019) and CellProfiler 4.0.7 (Carpenter Lab, Broad Institute of Harvard and MIT, USA; www.cellprofiler.org) open-source softwares were used (**Fig. 3.10**).

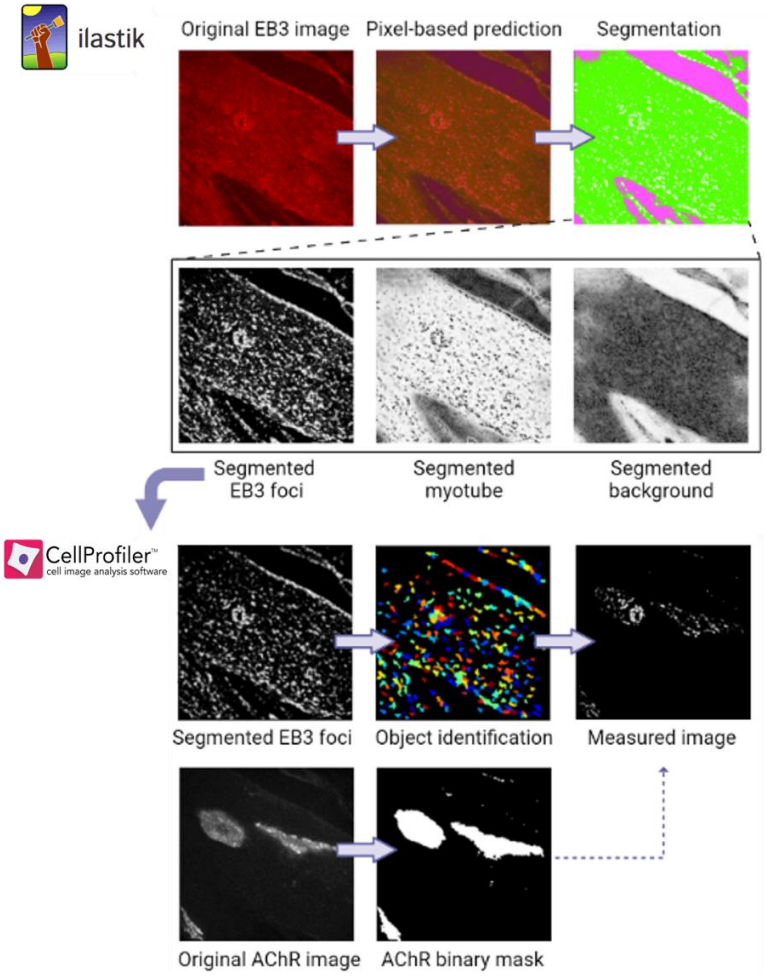

Figure 3.10. Schematic illustration of automated analysis of EB3 foci size and shape parameters. Illustration created with BioRender.com.

Ilastik's machine learning-based algorithm was used for pixel segmentation of the images into three categories: 5-10 pixels/image corresponding to "EB3 foci", "myotube", or "background" were manually selected in 5-10 images per group (BTP2 or DMSO) to train the algorithm to recognize which pixels of other images belong to each category. After training, the segmentation algorithm was applied to the whole image set (n = 30 images/group from at least 3 independent replicates). The images obtained were a binary version of the original microscopy images, containing only pixels classified as "EB3 foci". These binary images were imported into CellProfiler, where a customized pipeline was used for identification of foci as "objects" and subsequent measurement of size and shape parameters (surface, eccentricity, equivalent diameter, extent, form factor, maximum and minimum Feret diameter, perimeter, and solidity) (*see CellProfiler Manuals for detailed description of each parameter*: http://cellprofiler-manual.s3.amazonaws.com/CellProfiler-3.0.0/modules/measurement.html#measure objectsizeshape). Before the measurement, an extra step in the pipeline was added to apply a mask of the corresponding AChR cluster shape to the binary image, thus limiting the measurements of EB3 foci to the area of the AChR clusters.

To validate the automatic measurements obtained from CellProfiler, a manual quantification of EB3 foci surface was performed using ZEN's contour (spline) tool on a smaller image set (n = 15 foci/image, 10 images/group from at least 3 independent experiments). Finally, to validate the surface measurements obtained from the CellProfiler analysis, a smaller image set was used for manual quantification of EB3 foci surface. Then, a classification of single vs. coalescent EB3 foci was performed on the dataset obtained from manual quantification based on manual thresholding. For that purpose, the surfaces of 15 single (isolated) foci were averaged to use as the coalescence threshold (0.94 μm^2), and foci with smaller or equal surface than the threshold were classified as single, while foci with bigger surface than the threshold were classified as coalescent.

3.15.3. Morphological characterization of the NMJ in vivo

To characterize the morphology of the neuromuscular junction, Z-stack images of the BTX-labelled NMJs and neighboring myofibers with BTX^+ signal (AChR labelling) were acquired at 63X magnification with 0.5 µm interval between stack planes. Then, using an ImageJ macro (written by A. Wolny, Laboratory of Imaging Tissue Structure and Function, Nencki Institute of Experimental Biology, PAS), all images were batch-processed to

combine all Z planes and obtain orthogonal projections. Each image, containing only one NMJ, was individually processed to adjust the threshold for accurate segmentation of each NMJ. Finally, a second ImageJ macro was used to automatically segment the AChR signal into a mask that allowed for measurements of AChR-enriched area and perimeter, as well as endplate area, perimeter, and diameter (**Fig. 3.11**).

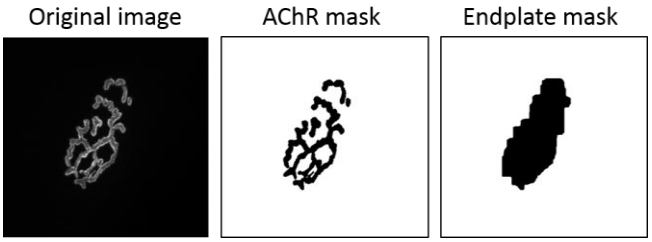

Figure 3.11. Representative image processing of single NMJs with ImageJ macro.

3.16. Statistical analysis

Statistical analyses were performed using IBM SPSS Statistics 22.0 (SPSS Inc., USA) and the data was graphically represented using SigmaPlot 8.0 (Systat, Richmond, USA) or with Interactive Dotplot data visualization tool (Weissgerber et al., 2017). Shapiro-Wilk normality test was used to test the null hypothesis of normal distribution required for parametric statistics and, when statistically significant ($P \leq .05$), an appropriate non-parametric test was used (independent samples Mann-Whitney's U or Kruskal-Wallis' U tests). Two-tailed independent Student's t-test was used to test differences between two experimental groups with continuous data that fulfilled assumptions for parametric tests. Chi-Square test was used to analyze nominal data that was manually divided in classes, in order to compare relative frequencies of each class in different experimental groups. Repeated measured two-way ANOVA, with 2 inter-subject independent variables (sex and genotype) and 1 intra-subject variable (trial), was used to analyze differences in the grip strength test of *SV* and WT mice. When *post-hoc* tests were necessary, a restrictive *post-hoc* test (Bonferroni correction) was used to limit the possibility of getting a statistically significant result when testing multiple hypotheses (control for type I error inflation).

Results from *in vitro* and molecular experiments were obtained from at least three independent experiments, unless stated otherwise. All manually measured variables were obtained in a blinded manner to reduce the introduction of human bias in data collection.

In the quantification of EB3 foci, upper or lower extreme values that fell outside 1.5 times the interquartile range between quartiles 1 and 3 of the data distribution (defined as outliers) were removed from the statistical analysis. The exclusion of these data points (1-3 values/group) did not alter the observed phenotype nor the statistical significance.

Results were considered statistically significant when $P \leq .05$, and represented as *, **, or *** when $P \leq .05$, $P \leq .01$, and $P \leq .001$, respectively. Specific tests used for statistical analyses and descriptive statistics used for graphical representation are described in each figure caption in the Results section. Chi-Square results are reported as X^2 (degrees of freedom, N = number of valid cases) = Pearson Chi-Square statistic value, P = p-value.

"*For a research worker, the unforgotten moments of her life*

are those rare ones which come after years of plodding work,

when the veil over nature's secret seems suddenly to lift

and when what was dark and chaotic

appears in a clear and beautiful light and pattern."

Gerty Cori,

first woman to be awarded the Nobel Prize in Physiology or Medicine (1947)

CHAPTER 4: RESULTS

4.1. Drebrin and myosin VI are present at the muscle postsynaptic machinery

4.1.1. Drebrin and myosin VI localize to the postsynaptic machinery *in vivo*

To study the localization of drebrin and MVI at the muscle postsynaptic machinery, I performed immunohistochemical analyses of whole-mount skeletal muscle fibers from WT mice. Controls of the specificity of antibodies were performed by omitting the primary antibody incubation (**Figs. 4.1A, 4.2A, bottom panels**). To observe their mutual localization, motoneuron cytoskeleton, presynaptic synaptic vesicles, and postsynaptic AChRs were co-stained.

Because NMJs undergo postnatal morphological remodeling (*see section 1.2.2.*), I decided to observe the distribution pattern of these proteins in relevant time points of NMJ development: maturation (P10), maintenance (P120), and age-related disruption of the NMJ (P365) (**Figs. 4.1A, 4.2A**). The image analysis showed that drebrin is concentrated both at pre- and postsynaptic NMJ compartments throughout the entire postnatal development (**Fig. 4.1A, panel P45**), while MVI is accumulated in the vicinity of the postsynaptic compartment, as it does not colocalize with the axon nor the synaptic axonal processes (**Fig. 4.2A, panel P120**). Therefore, drebrin and MVI differ in their local distribution at the NMJ. Drebrin colocalized with AChRs, which is particularly noticeable at the crest of junctional folds, where the fluorescence signal from AChRs is increased (**Fig. 4.1B**). On the other hand, MVI is accumulated in AChR-free areas at the periphery of AChR branches, as evidenced by the distinct peaks of AChR and MVI fluorescent signals (**Fig. 4.2B**).

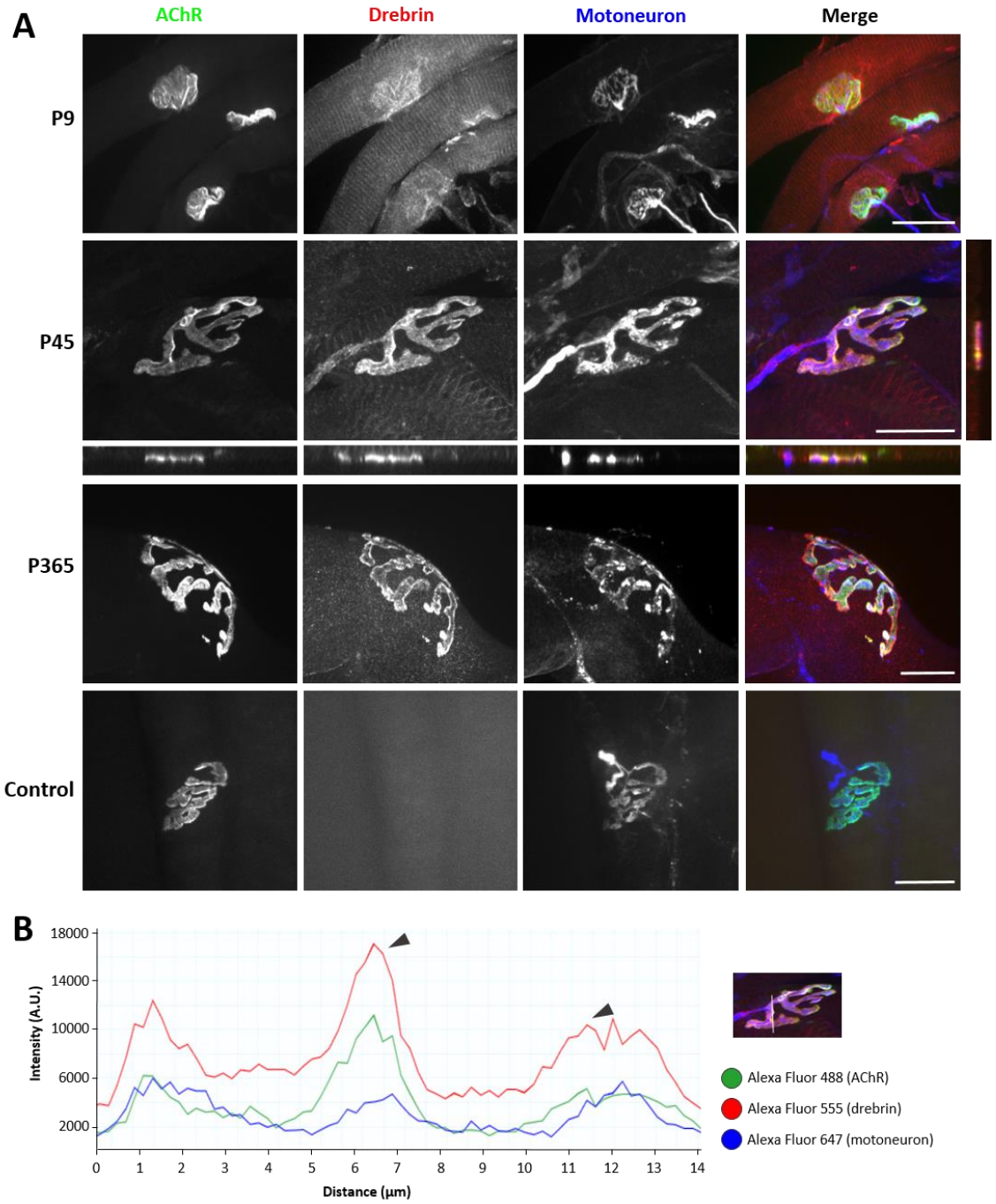

Figure 4.1. Drebrin localization at the pre- and postsynaptic compartments of the neuromuscular junction. (A) Colocalization of drebrin (red) with AChRs (labelled with BTX, green) and motoneuron (neurofilament + synaptophysin, blue) in the mouse *TS* muscle at different postnatal time points (P9, P45, P365). Panel for P45 shows orthogonal projections to visualize colocalization of drebrin and AChRs. Bottom panel corresponds to negative control of the secondary antibody. Scale bars = 20 µm. **(B)** Fluorescence intensity histogram obtained from a single plane of the optical cross-section (white line crossing the image). Fluorescence intensity corresponds to AChRs (green), drebrin (red), and motoneuron (blue) signals, respectively. Note how maximal fluorescence intensity for drebrin (black arrowheads) overlaps with peaks representing AChR signal.

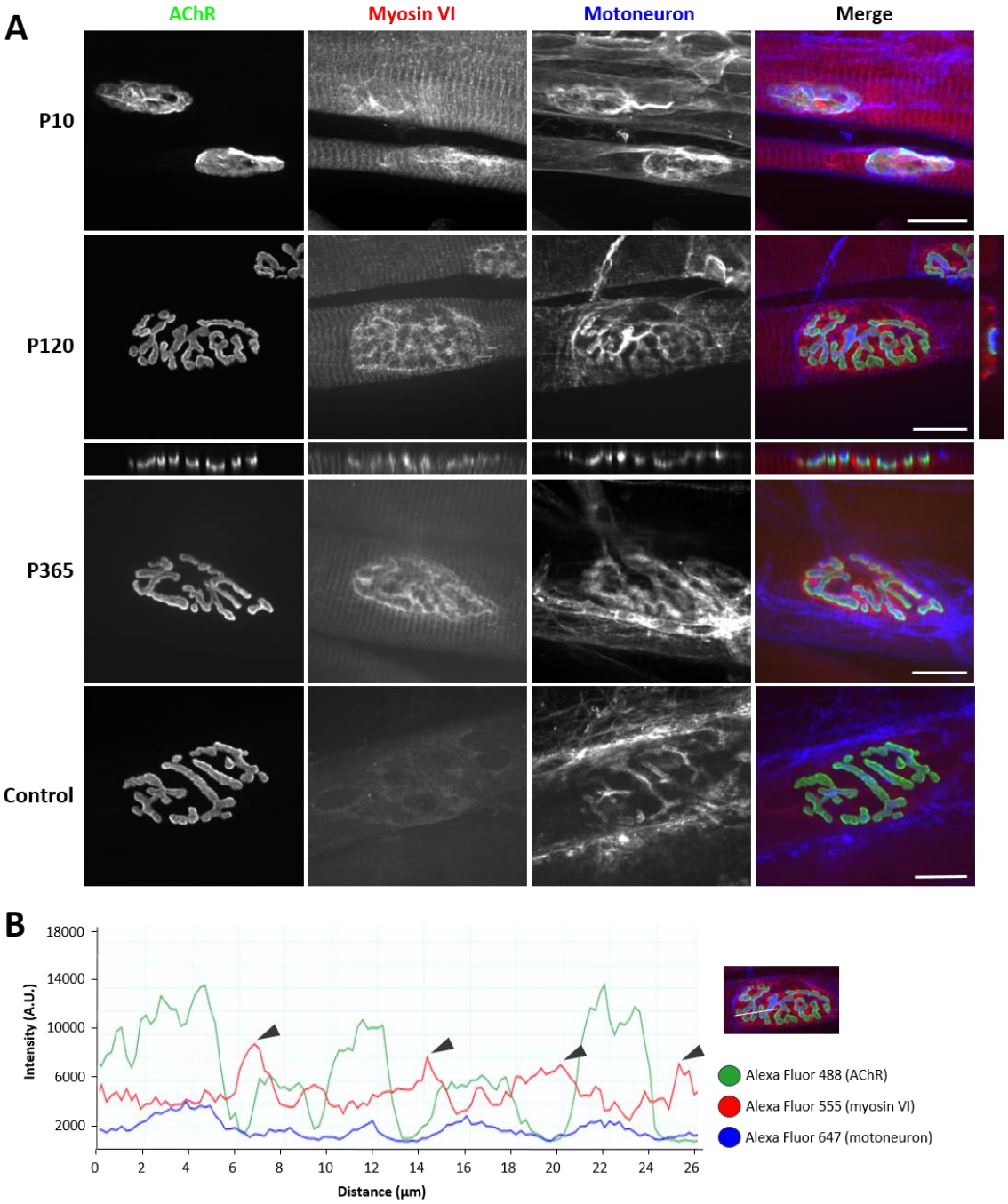

Figure 4.2. Myosin VI localization at the neuromuscular junction vicinity. (A) Localization of MVI (red) near AChRs (labelled with BTX, green) and motoneuron (neurofilament + synaptophysin, blue) in the mouse *TA* muscle at different postnatal time points (P10, P120, P365). Panel for P120 shows orthogonal projections to visualize MVI between AChRs. Bottom panel corresponds to negative control of the secondary antibody. Scale bars = 20 µm. **(B)** Fluorescence intensity histogram obtained from a single plane of the optical cross-section (white line crossing the image). Fluorescence intensity corresponds to AChRs (green), MVI (red), and motoneuron (blue) signals, respectively. Note how the maximal fluorescence intensity for MVI (black arrowheads) corresponds to the lowest levels in AChR signal.

The proportion of fiber types of each muscle determines the resistance to fatigue, the speed of contraction (fast- vs. slow-twitch) and the histochemical-metabolic properties (myosin ATPase and succinate dehydrogenase activity). Because several parameters of the neuromuscular transmission (muscle cytoskeleton structure or endplate area and morphology) depend on the fiber type (Schiaffino & Reggiani, 2011), I decided to compare the distribution pattern of drebrin and MVI across muscles with different functions and fiber composition: predominantly slow-twitch, type 1 fibers (*SOL*, *TS*), predominantly fast-twitch, type 2 fibers (*DIA*), and with a considerable proportion of intermediate fibers (*TA*) (Blank et al., 1988; Brust, 1976; Hodge et al., 1997) (*see section 1.2.1.*). As shown in **Fig. 4.3**, I found that drebrin and MVI localization at the NMJ is independent of the muscle type, since both proteins were enriched with similar patterns at the postsynaptic machinery of all muscles analyzed.

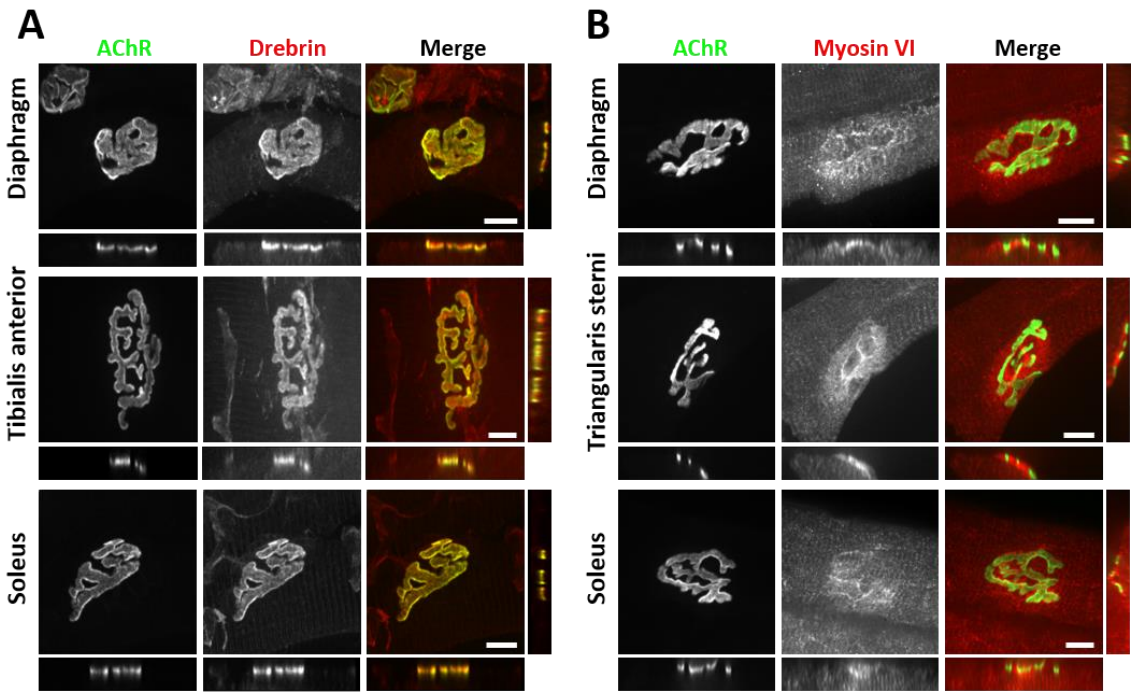

Figure 4.3. Drebrin and MVI localize to the postsynaptic machinery in different muscle types. **(A)** Colocalization of drebrin (red) with AChRs (labelled with BTX, green) in fast-twitch (*DIA*), intermediate (*TA*) and slow-twitch (*SOL*) muscles at P30-45. Representative image for *TA* by M. Gawor. **(B)** Localization of MVI (red) near AChRs (green) in fast-twitch (*DIA*) and slow-twitch (*TS*, *SOL*) muscles at P45. Bottom and right small panels of each image show orthogonal views. Scale bars = 10 µm.

4.1.2. Drebrin localizes to the postsynaptic machinery *in vitro*

I decided to confirm the *in vivo* localization of drebrin in the aneural *in vitro* model where I performed loss-of-function studies, in which the formation of complex

postsynaptic machinery resembles the process in myofibers (**Fig. 1.7**). To do so, I performed immunocytochemical analyses of C2C12 myotubes. The localization of drebrin was detected by immunolabelling with the same antibody used for the experiments described in the previous section, and confirmed with a second antibody. To observe drebrin localization in the context of the postsynaptic machinery, AChRs were labelled with BTX conjugated to a fluorophore.

As expected, drebrin distribution resembled the one at NMJs (**Fig. 4.4, top panel**). Additionally, drebrin was accumulated in AChR-free perforations in some clusters, with puncta-like scattering (**Fig. 4.4, bottom panel**), suggesting that drebrin might play a role in different postsynaptic compartments.

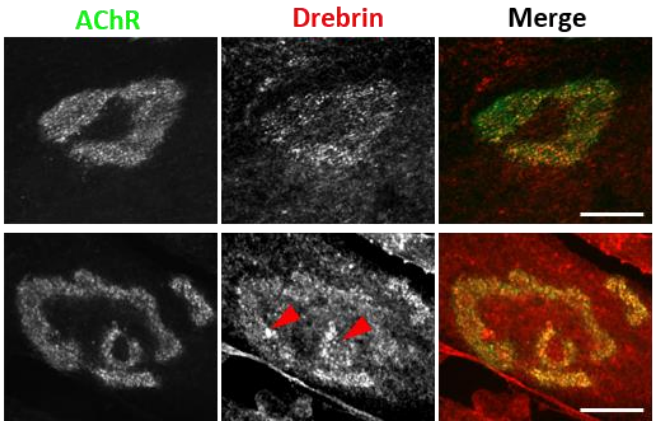

Figure 4.4. Drebrin localizes to the postsynaptic machinery *in vitro*. Colocalization of drebrin (red) with AChRs (labelled with BTX, green) in cultured C2C12 myotubes on the 5th day of fusion. Red arrowheads point at accumulation of drebrin in AChR-free areas. Scale bars = 20 µm.

Together with the previous section, these results support the conclusion that both drebrin and MVI are present at or in the vicinity of the postsynaptic machinery of skeletal muscle cells and could, potentially, play a role in its organization and/or maintenance.

4.1.3. Drebrin phosphorylation at Ser142 is dispensable for its localization at the NMJ

It has been previously proposed that drebrin post-translational phosphorylation by Cdk5 at the serine residue in position 142 (Ser142) is relevant for its cross-linking function between the actin cytoskeleton and the MT network (Worth et al., 2013). Since MT recruitment to the muscle postsynaptic machinery was shown to be crucial for AChR

organization at NMJs (Oury et al., 2019; Schmidt et al., 2012), I decided to study whether phosphorylation of drebrin affects its localization at the NMJ.

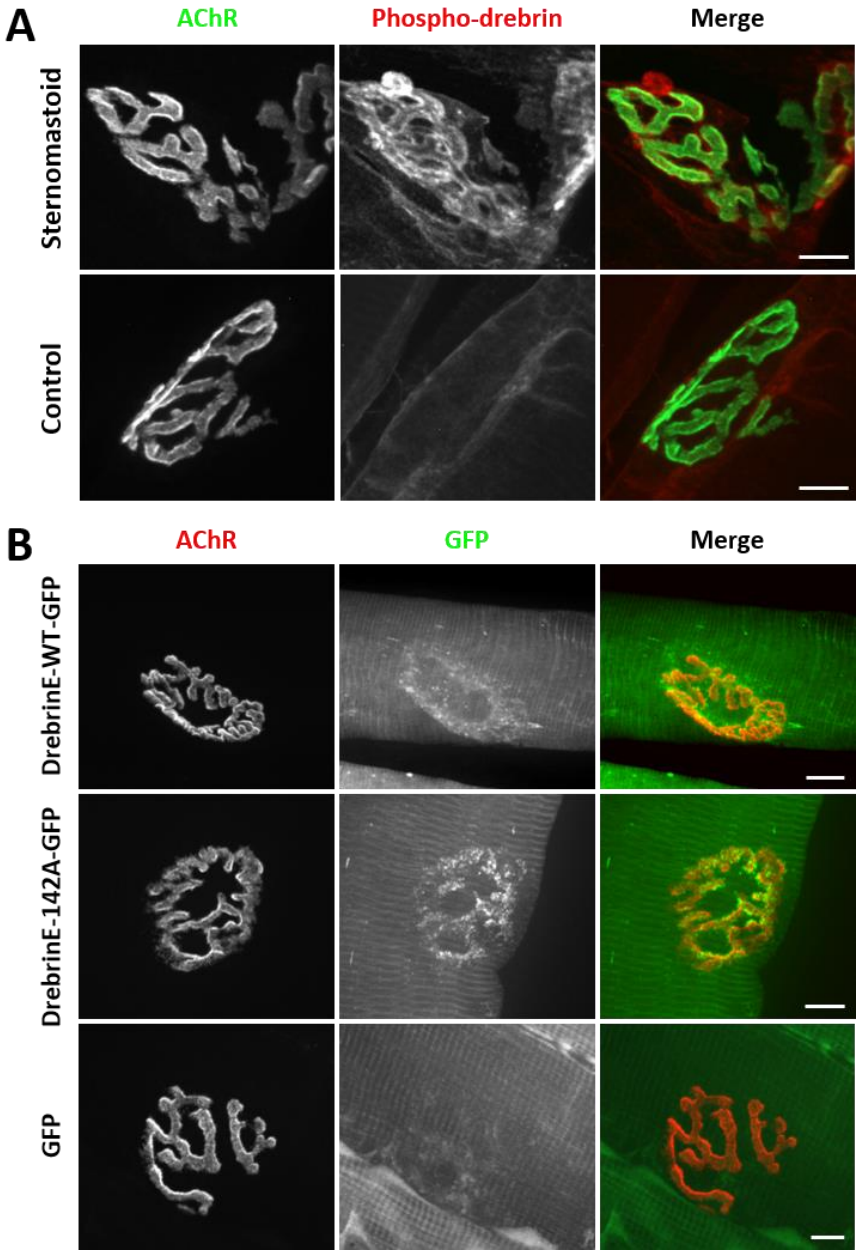

Figure 4.5. Drebrin E phosphorylation at Ser142 is not necessary for drebrin postsynaptic localization. (A) Colocalization of endogenous drebrin phosphorylated at Ser142 (red) with AChRs (green) in the mouse *ST* muscle at P45. **(B)** Colocalization of exogenous wild-type drebrin E (DrebrinE-WT-GFP, green) and Ser142 phospho-dead drebrin E mutant (DrebrinE-142A-GFP, green) with AChRs (labelled with BTX, red) in *TA* muscle after electroporation at P45. Bottom panel shows no accumulation of GFP protein at the NMJ when a vector encoding only GFP was overexpressed (negative control), representative image by A. Protasiuk-Filipunas. Scale bars = 10 µm.

First, I studied the localization of drebrin with an antibody specifically designed against phosphorylated drebrin at Ser142. As shown in **Fig. 4.5A**, phospho-drebrin colocalized with AChR distribution, similarly to the pattern observed with pan-drebrin antibodies showed in **Figs. 4.1A, 4.3A, and 4.4**. To test the hypothesis of whether only drebrin phosphorylated at Ser142 is recruited to the NMJ, I overexpressed two drebrin variants in the *TA* muscle (*see section 3.13.*): the most abundant drebrin isoform in myogenic cells, wild-type drebrin E, fused to GFP (DrebrinE-WT-GFP) (Mancini et al., 2011), and "phospho-dead" drebrin E, carrying a mutation at Ser142 that makes it unphosphorylatable by Cdk5, also fused to GFP (DrebrinE-142A-GFP). The localization of both WT and phospho-dead drebrin had similar degree of overlapping with AChRs (**Fig. 4.5B, top and central panels**), and resembled the localization of endogenous drebrin (**Figs. 4.1A, 4.3A**), thus confirming the observations described in sections 4.1.1. and 4.1.2. The specificity of drebrin localization at electroporated NMJs was confirmed by the lack of colocalization with AChRs of the control vector, encoding only GFP (**Fig. 4.5B, bottom panel**). Altogether, these results show that phospho-drebrin is recruited to the postsynaptic machinery, but phosphorylation at Ser142 is not necessary for this recruitment.

4.2. Drebrin is present at the contractile machinery in mice

During the localization analyses described in sections 4.1.1. and 4.1.3., I observed that drebrin not only accumulated at the NMJ, but also had a striated pattern throughout the skeletal muscle fiber that coincided with the pattern of the contractile machinery. The possible localization of drebrin at the contractile machinery was supported by previous studies in *C. elegans* (Butkevich et al., 2015), so I hypothesized that drebrin is present at the sarcomere in murine skeletal muscle. To further explore this idea, I performed colocalization studies of drebrin with several markers of different sarcomere or sarcoplasmic reticulum (SR) subcompartments.

As shown in **Fig. 4.6**, drebrin only colocalized with α-actinin, actin cross-linker and structural protein of the sarcomere Z-discs. Conversely, drebrin showed mutually exclusive distribution with both Ryr1, a Ca^{2+} channel receptor located at the SR membrane, and skeletal muscle myosin II, the major component of thick filaments that extends across the sarcomere A-bands. These results reveal drebrin as a novel component of sarcomeres in mammalian skeletal muscle.

It is noteworthy that MVI also displayed a striated pattern in muscle (**Fig. 4.2A**), however it was shown that this is a subcellular localization of MVI to the SR and not to the contractile apparatus (Karolczak et al., 2013).

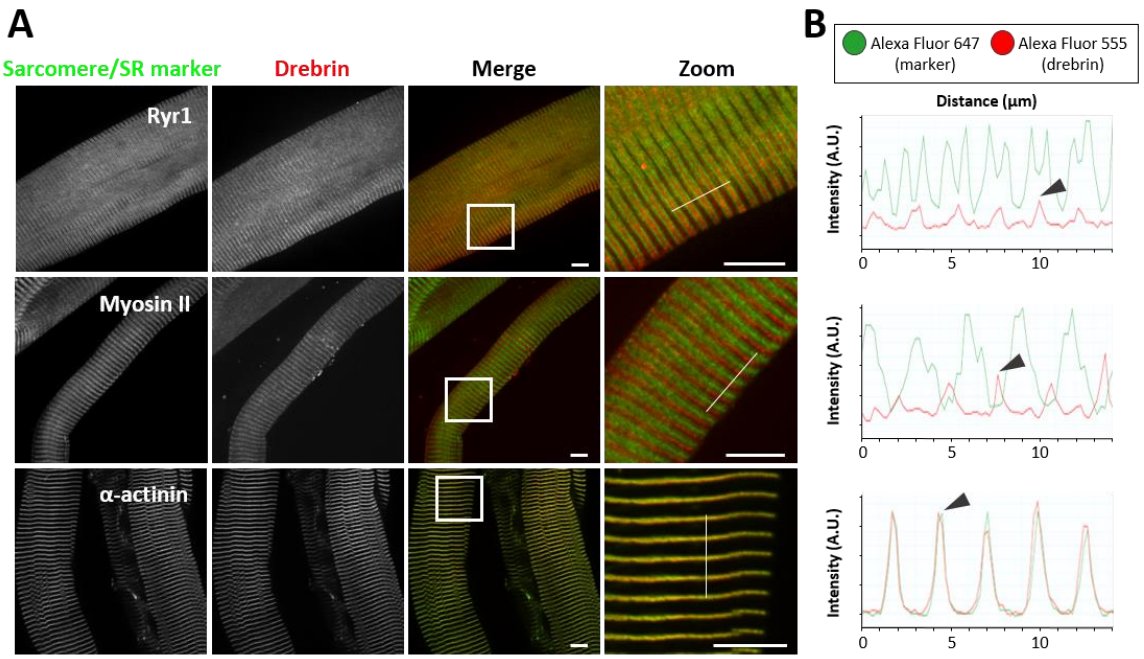

Figure 4.6. Drebrin localizes to the Z discs of sarcomeres. (A) Colocalization of drebrin (red) with different markers of the sarcomere or the sarcoplasmic reticulum (Ryr1, myosin II, α-actinin, green) in the mouse *TS* muscle at P45. White squares show the zoomed area. White lines in the zoomed area show the plane that histogram in B) was created from. Scale bars = 10 µm. **(B)** Fluorescence intensity histograms obtained from a single plane of the optical cross-section represented as a white line crossing the image in the zoomed panel in A). Intensities of Alexa Fluor fluorophores correspond to markers (green) and drebrin (red) signals, respectively. Note how maximal fluorescence intensity for drebrin (black arrowheads) overlaps with α-actinin but not with maximal fluorescence intensity for Ryr1 nor myosin II.

4.3. Drebrin is involved in the postsynaptic machinery organization *in vitro*

To explore the specific role of drebrin at the postsynaptic machinery, I performed loss-of-function studies and silenced drebrin expression with siRNA in C2C12 myotubes. The drop in drebrin expression was confirmed at both mRNA and protein levels in all four different siRNA tested in at least 3 independent biological replicates (**Fig. 4.7A-B**). The goal of these experiments was to examine whether the downregulation of drebrin expression will affect the postsynaptic machinery *in vitro*. Since drebrin plays a role in myoblast fusion and differentiation (Mancini et al., 2011), siRNAs were transfected to the cells 72 h after fusion induction, when myotubes were already formed and differentiated.

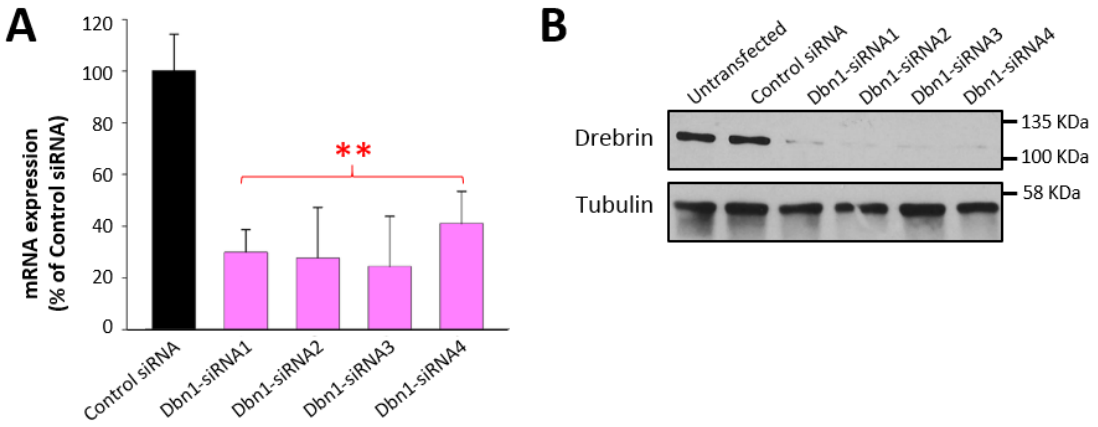

Figure 4.7. Validation of siRNA-mediated downregulation of drebrin. *Dbn1* knockdown validation in C2C12 myotubes on the 5th day of fusion at mRNA and protein levels with RT-qPCR **(A)** and Western blot **(B)**, respectively. Representative blot by M. Gawor. Student's t-test between Control siRNA and other experimental conditions, $P \leq .01$ (**). Error bars in A represent SD.

4.3.1. *Dbn1* knockdown impairs AChR organization in C2C12 myotubes

Due to the complexity of the NMJ, myotubes cultured *in vitro* are used as a simplified model of the postsynaptic machinery (*see section 1.2.3.*). I took advantage of the two most commonly used systems for inducing AChR cluster formation *in vitro*: soluble neural-derived agrin, which mimics the chemical signals of the motoneuron, and laminin-111, that also induces morphological remodeling resembling the one that takes place in *vivo* (**Fig. 1.7**).

In parallel with siRNA-treated myotubes, appropriate controls were included in all experiments (*see section 3.4.5.*). First, I confirmed that myotubes transfected with the *Control siRNA* (non-targeting) did not differ in terms of fusion efficiency (visually-assessed) nor number of AChR clusters formed when compared to untransfected cells. The *Musk-siRNA* (targeting MuSK, a receptor with a central role in NMJ formation and maintenance) is shown in **Figs. 4.8A and 4.9A** as an example of severely impaired AChR cluster formation (positive control). The total number of agrin-induced clusters was significantly reduced in three out of four *Dbn1*-siRNAs (siRNA2: $P = .001$, siRNA3: $P = .001$, siRNA4: $P = .007$) (**Fig. 4.8B**). Moreover, clusters of myotubes treated with those siRNAs most efficiently downregulating drebrin were characterized by a bigger proportion of short clusters (< 10 µm) in relation to the total number of clusters when compared to the *Control siRNA* (siRNA2: $P < .001$, siRNA3: $P < .001$) (**Fig. 4.8C**).

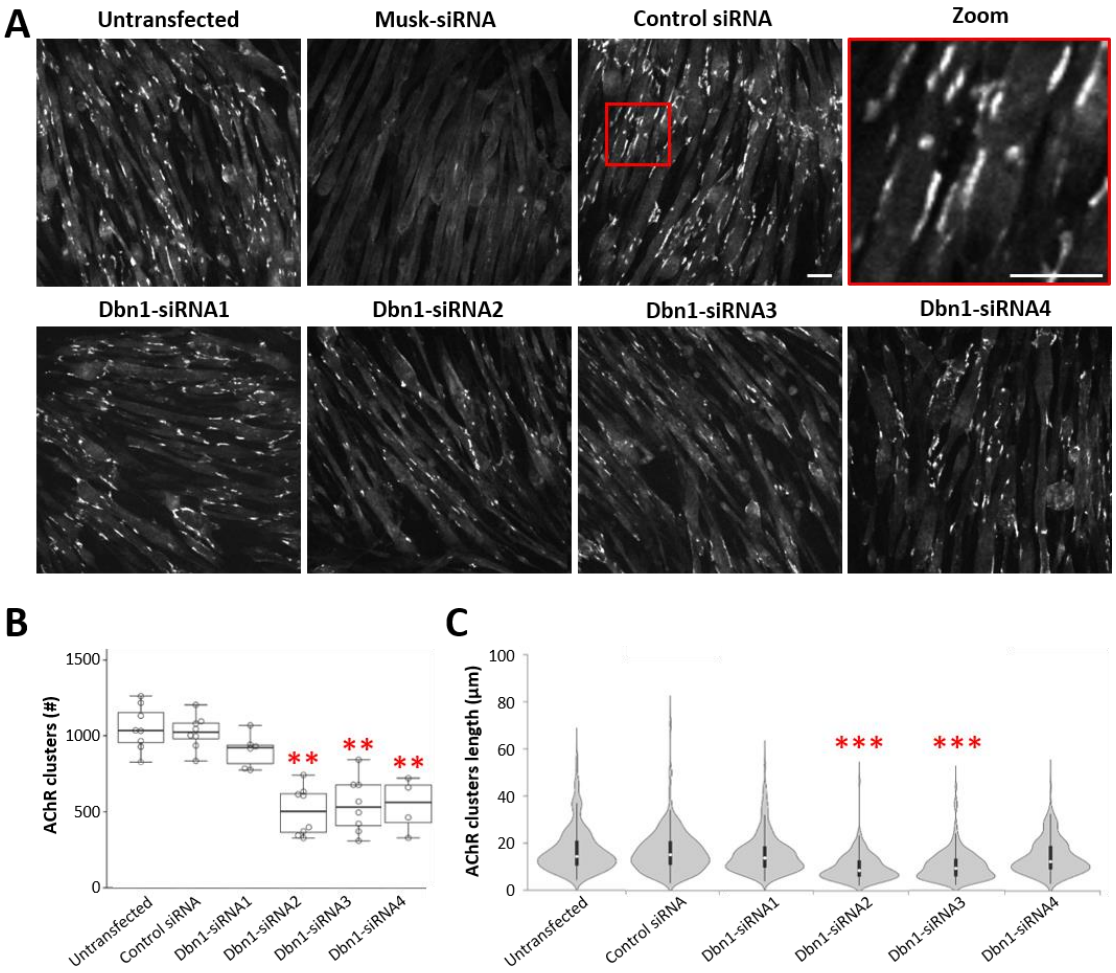

Figure 4.8. siRNA-mediated downregulation of drebrin affects agrin-dependent postsynaptic organization *in vitro*. (A) Representative images of C2C12 myotubes on the 5th day of fusion in different experimental conditions with agrin-induced AChR clusters labelled with BTX (white). Red square shows zoomed area of the Control siRNA. Scale bars = 50 µm. **(B)** Total number (#) of AChR clusters per field view upon drebrin downregulation. Kruskal-Wallis U test between Control siRNA and other experimental conditions, $P \leq .01$ (**). Datapoints (empty circles) represent quantifications of different fields of view from three independent experiments. Bold mid-line inside each box represents mean. Boxplot whiskers represent lower and upper extremes. **(C)** Length of AChR clusters upon drebrin downregulation. Chi-Square test, X^2 (14, N = 1354) = 177.535, $P \leq .001$ (***). Violin plot width (grey shape) represents frequency of values. Narrow boxplot inside each violin plot (black) represents mean (small white circle) ± lower and upper extremes (black lines).

Similar results were observed in the laminin-induced model (**Fig. 4.9A**), and the total number of AChR clusters was significantly reduced when the two most efficient siRNAs were used (siRNA2: $P < .001$, siRNA3: $P = .003$) (**Fig. 4.9B**). However, the surface covered by AChR clusters was similar in all groups (**Fig. 4.9C**). Notably, the wide range of values of AChR cluster area (38-1376 µm^2) in all experimental conditions most likely reflects the distinct maturation stages (i.e. simple clusters are smaller than complex clusters). On the

other hand, the frequency distribution of area values follows the expected Gaussian shape in both untransfected and control conditions, while its more irregular in *Dbn1*-siRNA groups. This tendency of Dbn1-siRNAs to alter the median of AChR clusters area resembles the one described for the length of agrin-induced clusters (**Fig. 4.8C**).

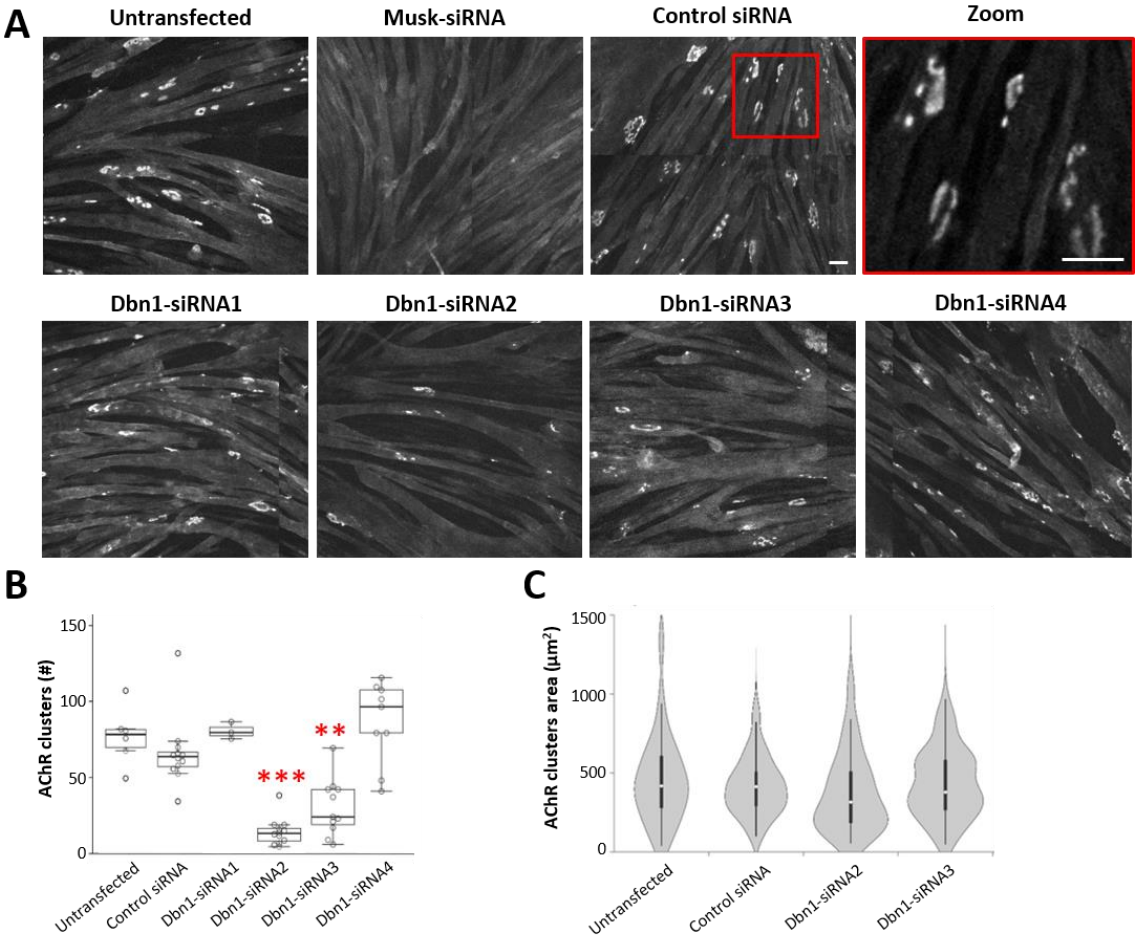

Figure 4.9. siRNA-mediated downregulation of drebrin affects laminin-111-dependent postsynaptic organization *in vitro*. (A) Representative images of C2C12 myotubes on the 5th day of fusion in different experimental conditions with laminin-induced AChR clusters (labelled with BTX, white). Red square shows zoomed area of the Control siRNA. Scale bars = 50 µm. **(B)** Total number (#) of AChR clusters upon drebrin downregulation. Kruskal-Wallis U test between Control siRNA and other experimental conditions, $P \leq .01$ (**), $P \leq .001$ (***). Datapoints (empty circles) represent quantifications of different fields of view from four independent experiments. Bold mid-line inside each box represents mean. Boxplot whiskers represent lower and upper extremes. **(C)** Area of AChR clusters upon drebrin downregulation. Student's t-test, not significant. Violin plot (grey shape) represents frequency of values. Narrow boxplot inside each violin plot (black) represents mean (small white circle) ± lower and upper extremes (black lines).

These results strongly suggest that drebrin is involved in AChR organization *in vitro*, in models that depend on either neuron-derived or muscle-derived signals and therefore, might play a significant role in NMJ formation.

4.3.2. The ability of drebrin to rearrange F-actin is indispensable for its role in AChR organization

To test the hypothesis that drebrin role in postsynaptic organization depends on its ability to remodel actin cytoskeleton, I used a drebrin antagonist, BTP2, that pharmacologically blocks such drebrin function (*see section 3.3.6.*) but does not affect its colocalization with actin (Mercer et al., 2010).

C2C12 myoblasts were allowed to fuse for 72 h on a laminin-coated surface before addition of BTP2. This particular time point was chosen for two reasons. First, to minimize negative effects of BTP2 on myoblast fusion and adhesion, which are observed within the first 60 h after fusion induction (Mancini et al., 2011). Second, to treat the cells at a similar differentiation stage that those in siRNA-mediated experiments from section 4.3.1.

Since BTP2 is a potent inhibitor and actin cytoskeleton plays a crucial role in myotube adhesion, fusion and differentiation, I first optimized BTP2 concentration (1, 5 and 10 µM). Control cells were treated with the same concentration of DMSO (vehicle) as 5 µM BTP2 experimental cells. As shown in **Fig. 4.10A-B**, 10 µM BTP2 significantly impairs myotube morphology, making them thinner and sparse, which is manifested by the reduced area covered by myotubes ($P = .05$). However, 1 µM and 5 µM BTP2, as well as DMSO (0.02% v/v), had no visible effects on myotube formation when compared to untreated cells. Importantly, 5 µM BTP2 had a more potent effect on AChR cluster formation and thus, this concentration was chosen for assessing the role of drebrin in the postsynaptic machinery organization, which is in accordance with a previous study in myoblasts (Mancini et al., 2011). Similarly to siRNA-mediated drebrin downregulation, BTP2-treated myotubes formed less than half of AChR clusters compared to control DMSO-treated myotubes ($P < .001$) (**Fig. 4.10C**).

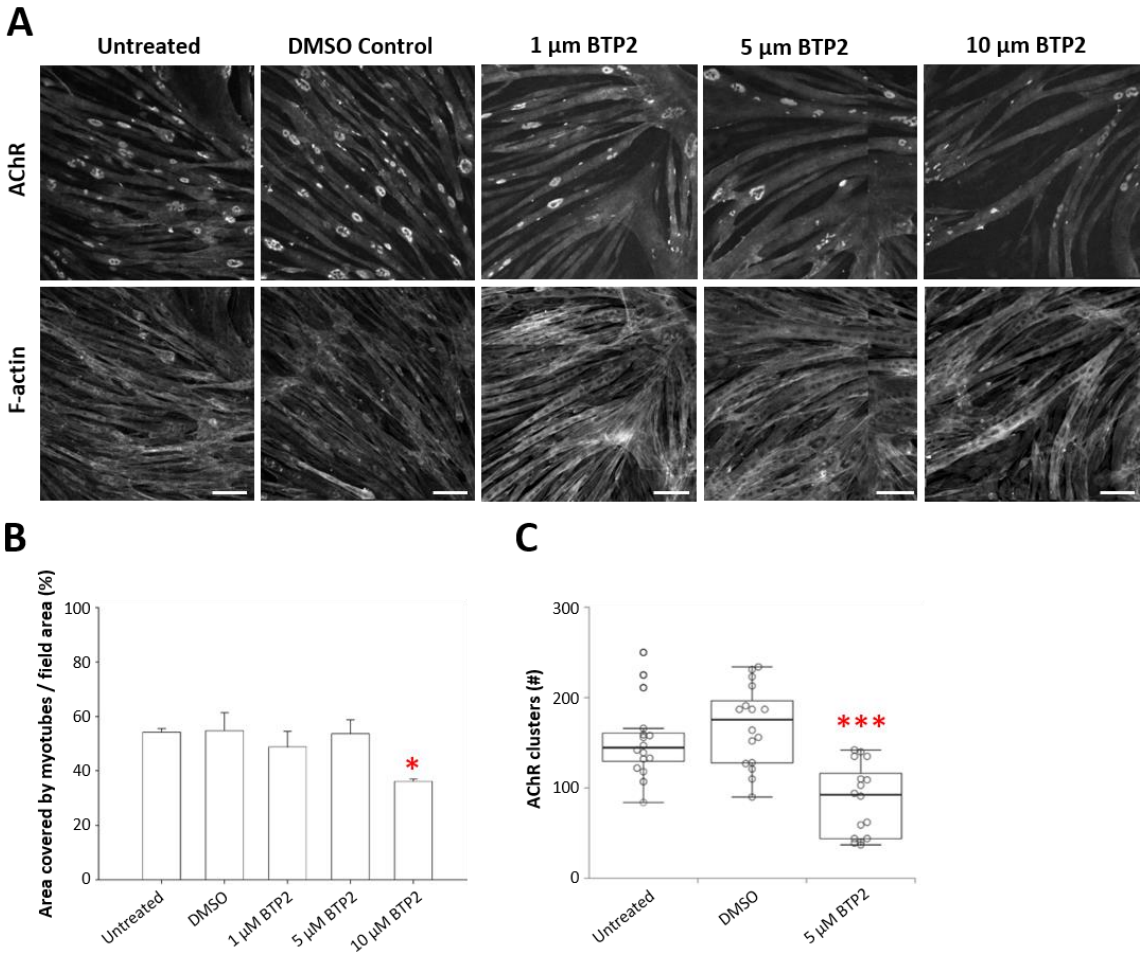

Figure 4.10. Drebrin-mediated F-actin rearrangements are indispensable for postsynaptic clustering *in vitro*. (A) Representative images of C2C12 myotubes on the 5th day of fusion in different experimental conditions, showing laminin-induced AChR clusters (labelled with BTX, top panel) and F-actin (labelled with phalloidin, bottom panel). Scale bars = 100 µm. **(B)** Area covered by myotubes (% of total field area) in control and BTP2-treated C2C12 myotubes. Kruskal-Wallis U test between DMSO and other experimental conditions, $P \leq .05$ (*). Error bars represent SD. **(C)** Total number (#) of AChR clusters upon BTP2 treatment. Mann-Whitney U test between DMSO and other experimental contidions, $P \leq .001$ (***). Datapoints (empty circles) represent quantifications of different fields of view from four independent experiments. Bold mid-line inside each box represents mean. Boxplot whiskers represent lower and upper extremes.

To further confirm the direct involvement of drebrin in AChR organization, I planned to perform rescue experiments of the phenotype in **Fig. 4.10**. To this end, I attempted to create a stable cell line of C2C12 myotubes constitutively expressing a mutated variant of drebrin E that does not bind to BTP2 (DrebrinE-K270/271M-GFP), and therefore, cannot be pharmacologically blocked by this compound, and a control stable line overexpressing wild-type drebrin E (DrebrinE-GFP) (**Fig. 4.11A**). Unfortunately, both stable lines had significant morphological impairments, and thus not enough GFP$^+$ myotubes could be imaged for statistically valid quantification of AChR clusters (**Fig.**

4.11B). One plausible explanation for this is that drebrin levels are tightly regulated to ensure proper function, so upregulation of *Dbn1* can have equally impairing results than downregulation. For example, it has been demonstrated that overexpression of wild-type drebrin in oculomotor neurons and subventricular zone-derived neuroblasts induces aberrant migration, possibly through affecting cell-cell adhesion (Sonego et al., 2015). Nevertheless, these results suggest that aberrations in drebrin expression have negative effects on the actin cytoskeleton.

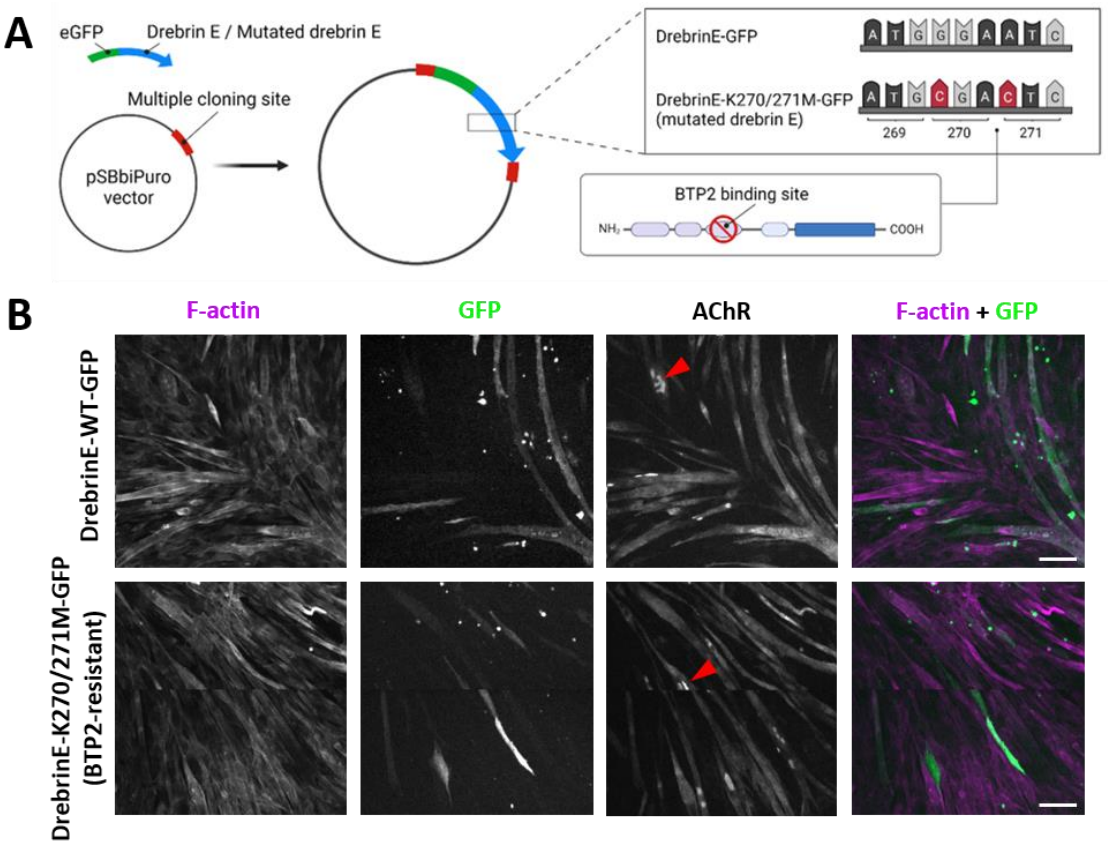

Figure 4.11. Stable line generation with wild-type and BTP2-resistant mutant of drebrin. (A) Illustrative explanation of drebrin variants used for the stable line generation. Illustration created with BioRender.com. **(B)** Representative images of C2C12 myotubes visualized with F-actin (labelled with phalloidin, purple), overexpressing wild-type drebrin E (DrebrinE-WT-GFP, green) or BTP2-resistant drebrin E (DrebrinE-K270-271M-GFP, green). Note the small number of GFP^+ myotubes and that they are devoid of mature AChR clusters (labelled with BTX), otherwise present in GFP^- myotubes (red arrowheads). Scale bars = 100 µm.

4.3.3. Drebrin is at the core of synaptic podosomes and regulates AChR cluster maturation

Drebrin could impact not only AChR cluster formation but also their maturation (**Fig. 4.12A**). This hypothesis was supported by the detection of drebrin in AChR-free areas

(**Fig. 4.4**), resembling the localization of synaptic podosomes, actin-rich structures involved in postsynaptic machinery maturation (Proszynski et al., 2009). Many cytoskeleton-regulating proteins have been identified at their core (Bernadzki et al., 2014), so I decided to co-label drebrin with synaptic podosome markers. Two different antibodies against drebrin showed that it colocalizes with the core podosome marker, F-actin (**Fig. 4.12B, top panel**), while it has a mutually exclusive localization with cortex podosome marker, LL5β (**Fig. 4.12B, bottom panel**). Moreover, an in-depth analysis of the optical cross-sections revealed that drebrin was present across the entire membrane-protruding structure (**Fig. 4.12B, lateral panels**), thus identifying drebrin as a novel protein at the core of synaptic podosomes.

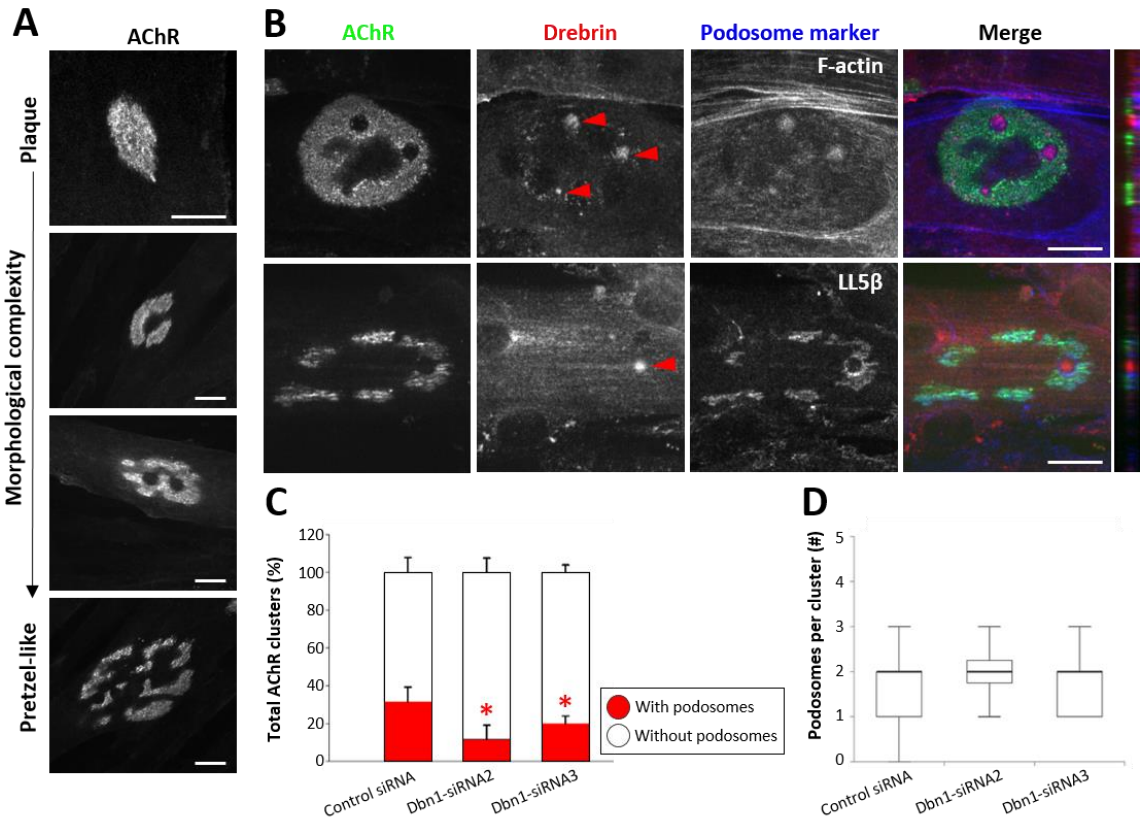

Figure 4.12. Drebrin is a novel component at the core of synaptic podosomes. (A) Representative images of postynaptic maturation in C2C12 myotubes with laminin-induced AChR clusters (labelled with BTX, white). Scale bars = 20 µm. **(B)** Colocalization of drebrin (red) with AChRs (labelled with BTX, green) and podosome markers F-actin (labelled with phalloidin, blue) and LL5β (blue). Drebrin was detected with two different antibodies. Red arrowheads point to active synaptic podosomes. Lateral panels show orthogonal projections, where protrusion of podosome core components is visible. Scale bars = 20 µm. **(C)** Percentage of AChR clusters with (red) and without (white) podosomes. Kruskal-Wallis U test between Control siRNA and other experimental conditions, $P \leq .05$ (*). Error bars represent SD. **(D)** Total number (#) of podosomes per AChR cluster among maturing clusters (clusters with at least one perforation). Bold mid-line inside each box represents mean. Boxplot whiskers represent lower and upper extremes. Kruskal-Wallis U test between Control siRNA and other experimental conditions, not significant.

Furthermore, the number of AChR clusters with podosomes was significantly reduced upon drebrin downregulation (siRNA2: *P* = .027, siRNA3: *P* = .021) (**Fig. 4.12C**), while the number of podosomes present per cluster was similar to *Control siRNA* (**Fig. 4.12D**). In the light of synaptic podosomes being considered a hallmark of AChR clusters morphological maturation *in vitro*, the impaired podosome formation suggests a role for this actin-binding protein in the developmental remodeling of the postsynaptic machinery.

4.3.4. Drebrin depletion does not impair cell surface delivery of AChRs

A possible explanation for the observed phenotype of reduced number of AChR clusters upon drebrin downregulation is that drebrin is involved in either the synthesis, delivery, or stability of AChR subunits at the cell membrane. To test these hypotheses, first I examined the total protein levels of AChRs in myotube lysates after siRNA-mediated knockdown of *Dbn1* gene. As depicted in **Fig. 4.13A**, a semi-quantitative analysis showed that there were no substantial differences in the total protein levels of AChRs between control and drebrin knockdown, however mild differences could not be excluded with this method. To address that, I performed a quantitative validation of this result through RT-qPCR analysis of the mRNA levels, but unfortunately it was not conclusive due to technical limitations (data not shown).

To overcome this limitation and test the second hypothesis, namely that the reduced number of AChR clusters is due to impairments in the intracellular transport of AChR subunits to the cell surface, I performed two types of experiments where I used either immunostaining or pull-down. In the first type of experiment, I differentially labelled internal and surface AChR with BTX conjugated to different fluorophores (red and green, respectively) two days after *Dbn1*-siRNA transfection (*for methodological details, refer to Fig. 3.4*). Specificity of the staining was controlled in a separate well by saturating surface AChRs ("masking") with non-fluorescent BTX (**Fig. 4.13B, top panel**). Fluorescent signal from AChRs was detected on the cell surface of both control and myotubes subjected to drebrin downregulation (**Fig. 4.13B**). This result refutes the hypothesis of severe impairment in cell surface delivery of AChRs as explanation for the phenotype described in section 4.3.1. Moreover, quantification of average fluorescence levels showed that neither surface nor internal AChR signals changed significantly upon *Dbn1* silencing, while the *Specificity control* showed the expected reduction in surface AChR signal (*P* < .001) (**Fig. 4.13C**). The *Specificity control* also showed a mild increase in the internal AChR signal compared to *Control siRNA* (*P* = .041). This latter result might be

explained by unknown effects of non-fluorescent BTX coupling to surface AChRs on AChR intracellular trafficking.

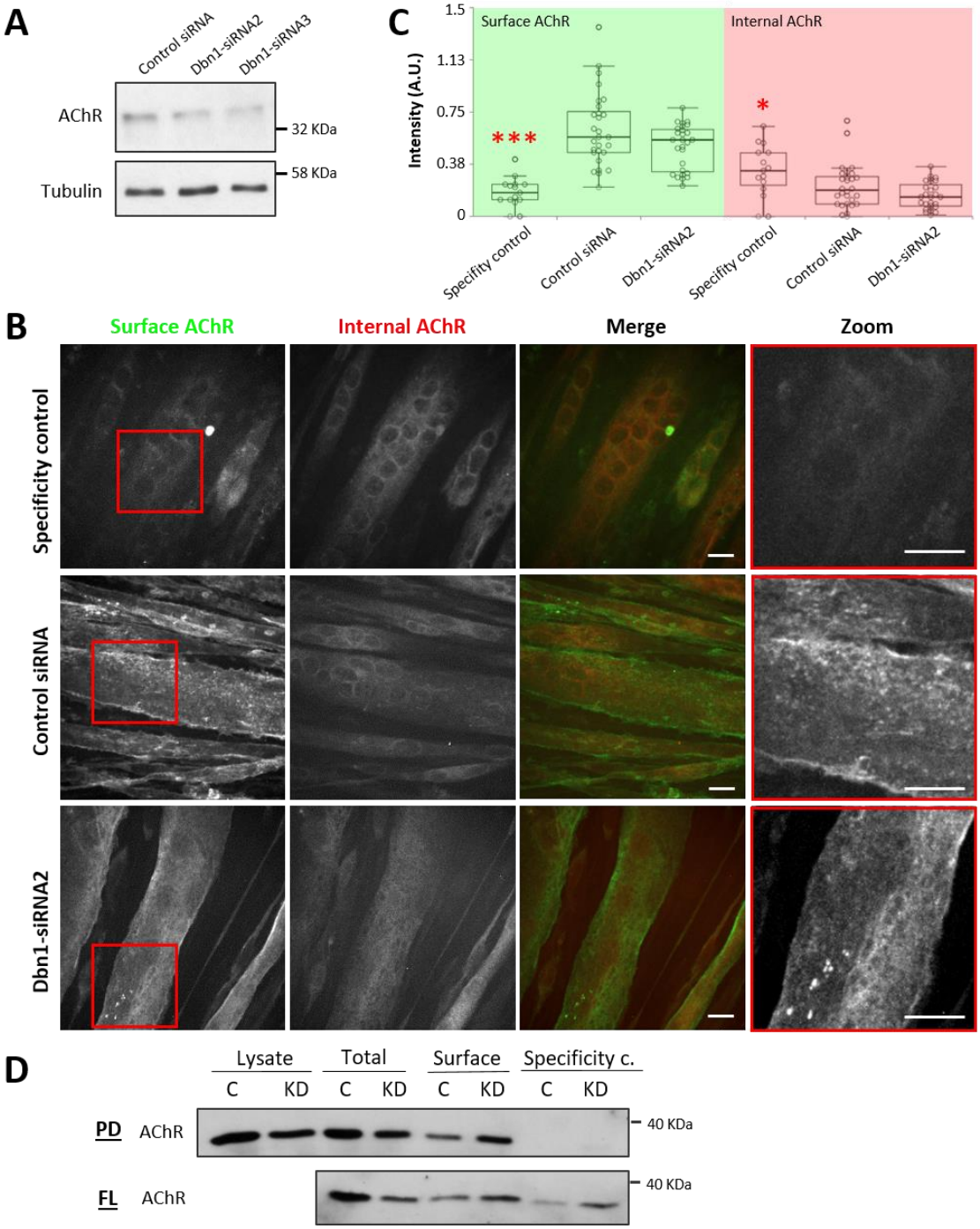

Figure 4.13. Drebrin is not crucial for neither synthesis nor cell surface delivery of AChRs *in vitro.* **(A)** AChR protein levels upon drebrin downregulation evaluated with Western blot. **(B)** Representative images of C2C12 myotubes with surface (green) and internal (red) AChRs (labelled with BTX). Red squares show zoomed area of surface AChRs. Scale bars = 20 µm. **(C)** Fluorescence intensity of surface (left, green) and internal (right, red) AChRs, measured in arbitrary units (A.U.) upon drebrin downregulation. Kruskal-Wallis U test between Control siRNA and other experimental conditions, $P \leq .05$ (*), $P \leq .001$ (***). Datapoints (empty circles) represent quantifications of single myotubes from three independent experiments. Bold mid-line

inside each box represents mean. Boxplot whiskers represent lower and upper extremes. **(D)** Pull-down assay of surface and total AChRs pools upon drebrin siRNA-mediated knockdown. **Abbreviations:** C = Control siRNA (non-targeting); FL = flow-through, supernatant eluted after AChR-BTX-Biotin-NeutrAvidin complex pull-down; KD = Dbn1-siRNA2; PD = pull-down, precipitation of AChRs with BTX-Biotin coupled to NeutrAvidin agarose beads.

To verify my results, the second type of experiment I performed was a biochemical assay to pull-down different pools of AChRs with BTX-Biotin (*for methodological details, refer to Fig. 3.5*) and compare their levels in control and drebrin-downregulated myotubes. I labelled surface AChRs with BTX-Biotin and then lysed the cells, thus isolating a pool of biotin-bound AChRs that could be pulled-down by incubation with avidin-conjugated beads (*see section 3.6.2.*). Separately, non-labelled myotubes were first lysed and then incubated with BTX-Biotin in order to isolate total AChRs. Similar to the microscopy-based approach, I controlled for specificity by saturating AChRs with non-conjugated BTX before incubation with BTX-Biotin. As shown in the two lanes on the very right of **Fig. 4.13D**, the specificity control had no detectable signal after blotting with an antibody specific for AChR α subunits 1, 3, and 5. Eluted supernatants after AChR pull-downs (flow-throughs) were used to control for pull-down efficiency. Total protein concentration and volumes were maintained equal throughout the assay.

Together with the fluorescence-based microscopy analysis, the pull-down of total and surface AChR pools showed that AChRs are delivered to the cell surface after drebrin downregulation (**Fig. 4.13D, central lanes**). Therefore, drebrin is not an indispensable protein for AChR synthesis nor surface delivery, and other explanations for the observed phenotype had to be assessed.

4.4. Drebrin regulates microtubule recruitment under AChR clusters *in vitro*

Actin-binding proteins guide MT plus-ends into a cortical actin mesh to generate actin-MT contraction or stabilize protein complexes, and MT insertion at the leading process promotes cytoskeleton-mediated remodeling in neurons (Shan et al., 2021). Moreover, it was demonstrated that MT recruitment to the NMJ postsynaptic machinery is important for AChR clustering and it depends on cytoskeletal regulators (Bernadzki et al., 2017; Oury et al., 2019; Schmidt et al., 2012). Since +TIP protein EB3 is an interactor of drebrin and MTs are involved in AChR cluster maintenance, I tested the hypothesis that reduction of AChR clusters upon drebrin downregulation was due to an impairment of the AChR-associated MT network.

4.4.1. Microtubule plus-end protein EB3 co-immunoprecipitates with drebrin in C2C12 myotubes

First, I decided to confirm whether EB3 and drebrin interact in C2C12 myotubes, the model that I used for postsynaptic machinery analysis, since this interaction was only reported before in non-muscle cells (Bazellières et al., 2012; Geraldo et al., 2008; Merriam et al., 2013). Because co-transfection of tagged recombinant proteins in C2C12 myotubes poses several technical difficulties, I created a stable line of C2C12 myoblasts that constitutively overexpressed GFP-tagged EB3 and could differentiate into myotubes (**Fig. 4.14A**) (*for methodological details, see section 3.4.*). This construct was shown to imitate the endogenous distribution of EB3 in epithelial Caco2 cells (Bazellières et al., 2012). In order to allow for EB3 and drebrin interaction, presumably cross-linking actin and MT networks to stabilize AChR clusters, I induced the formation of clusters by culturing the EB3-GFP^{+} myotubes on a laminin-coated surface. After EB3-GFP immunoprecipitation (*for methodological details, see section 3.5.*), I was able to detect endogenous drebrin that had co-immunoprecipitated with EB3-GFP (**Fig. 4.14B**). The specificity of the antibody used was verified with uncoated beads (described in figure caption).

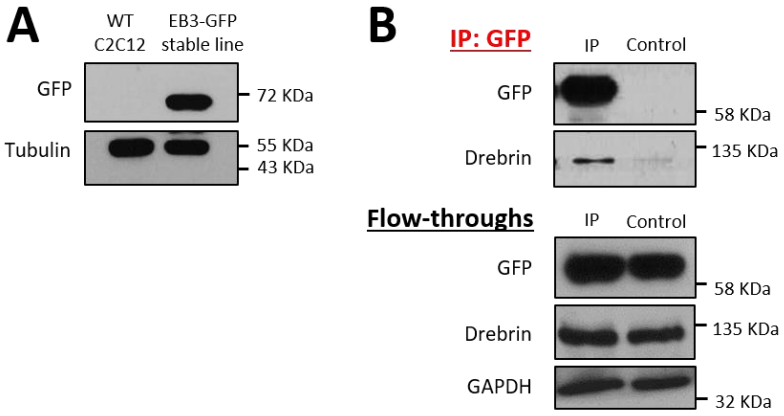

Figure 4.14. Drebrin interacts with microtubule +TIP protein EB3 in C2C12 mytoubes. (A) Validation of EB3-GFP^{+} stable cell line with Western blot. Note the lack of GFP signal in wild-type (WT) C2C12. **(B)** Co-immunoprecipitation of endogenous drebrin with EB3-GFP in lysates from C2C12 myotubes overexpressing EB3-GFP on the 7th day of fusion and cultured on a laminin-111-coated surface. Representative blot for flow-throughs by M. Gawor. **Abbreviations:** Control = eluate released during boiling from uncoated beads that were incubated with the lysate; Flow-throughs = supernatants eluted after incubation of the anti-GFP-coated beads with the lysate and protein-antibody-beads complex separation; IP = immunoprecipitation, eluate released during boiling from GFP-bound beads.

4.4.2. EB3 foci underneath AChR clusters are reduced upon *Dbn1* knockdown

It was reasonable to hypothesize that, if drebrin was depleted from cells, the recruitment of MTs via EB3-drebrin interaction would be reduced. To assess this, I performed immunofluorescent stainings of EB3 in C2C12 myotubes transfected with either *Control siRNA* (non-targeting) or *Dbn1*-targeting siRNA, and examined EB3 distribution at the postsynaptic machinery.

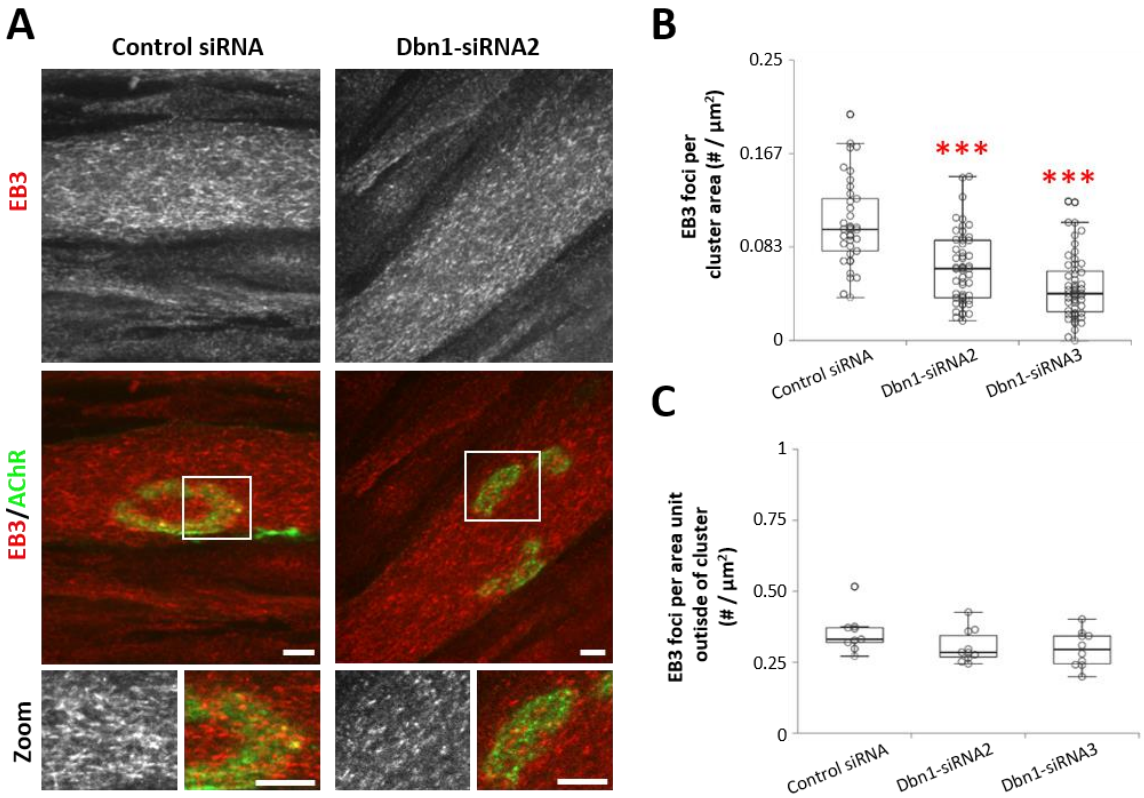

Figure 4.15. Drebrin downregulation impairs microtubule recruitment under the postsynaptic machinery *in vitro*. (A) Representative images of EB3 (red) distribution in C2C12 myotubes and its colocalization with AChRs (labelled with BTX, green) with and without siRNA-mediated drebrin knockdown (Dbn1-siRNA2 and Control siRNA, respectively). White squares show zoomed area. Scale bars = 10 µm. **(B)** Total number of EB3 foci per AChR cluster area (#/µm^2) upon drebrin downregulation. Mann-Whitney U test, $P \leq .001$ (***). Datapoints (empty circles) represent quantifications of foci number in single AChR clusters from three independent experiments. Bold mid-line inside each box represents mean. Boxplot whiskers represent lower and upper extremes. **(C)** Total number of EB3 foci per area unit outside of AChR cluster (#/µm^2) upon drebrin downregulation. Mann-Whitney U test, not significant. Datapoints (empty circles) represent quantifications of foci number in single myotubes from three independent experiments. Bold mid-line inside each box represents mean. Boxplot whiskers represent lower and upper extremes.

Since MTs form an intricate mesh through the entire intracellular space, and in order to focus on AChR-associated MT plus tips, I specifically chose a plane of analysis at 0.5 µm

below the level of highest fluorescence detected in the AChR signal, relying on the observation that EB3 fluorescent signal is mostly enriched at this distance from the tip of dynamic MTs (Roth et al., 2019). Then, I quantified the number of EB3 foci present within the area covered by the AChR clusters (*for methodological details, see section 3.15.2.*). I observed that downregulation of drebrin significantly reduced the number of EB3 foci underneath AChR clusters (siRNA2: $P < .001$, siRNA3: $P < .001$) (**Fig. 4.15A-B**), thus supporting the hypothesis that drebrin is involved in MT recruitment, crucial for AChR clustering. Importantly, the number of EB3 foci outside AChR clusters remained similar across all groups (**Fig. 4.15C**), which suggests that the observed effects of drebrin depletion are a result of impaired MT capture specifically at the postsynaptic machinery and not due to overall instability.

4.4.3. Drebrin interaction with F-actin regulates cortical microtubule organization

To test whether drebrin-mediated rearrangements of the actin cytoskeleton are necessary for MT recruitment, I quantified EB3 foci underneath AChRs on C2C12 myotubes after DMSO (vehicle) or BTP2 treatment (**Fig. 4.16A**). The number of EB3 foci outside AChR clusters in BTP2-treated cells remained similar to the vehicle (**Fig. 4.16C**) but, conversely to drebrin downregulation, the number of EB3 foci underneath AChR clusters was also unchanged upon BTP2 treatment (**Fig. 4.16B**). However, there was a noticeable difference in MT gross distribution pattern, with brighter and/or bigger EB3 foci in the control condition (**Fig. 4.16A, zoom panels**).

In order to thoroughly explore the organization and morphology of EB3 foci underneath AChR clusters, I used an automated method of quantification to increase the efficiency of the data collection and reduce human bias. This was combined with a machine learning-based tool that enabled a pre-processing of the images to reduce the background noise and make them suitable for the analysis (*for methodological details, see section 3.15.2.*). The automated analysis of size and shape parameters showed a reduction in surface, perimeter, and minimal and maximal Feret diameter of EB3 foci upon BTP2 treatment (**Fig. 4.16D**). I ruled out automated-derived inaccuracies in the detection of EB3 foci surface by manually measuring the area of isolated EB3 foci on a smaller dataset, which confirmed that BTP2 treatment resulted in the reduction of their surface (**Fig. 4.16E**).

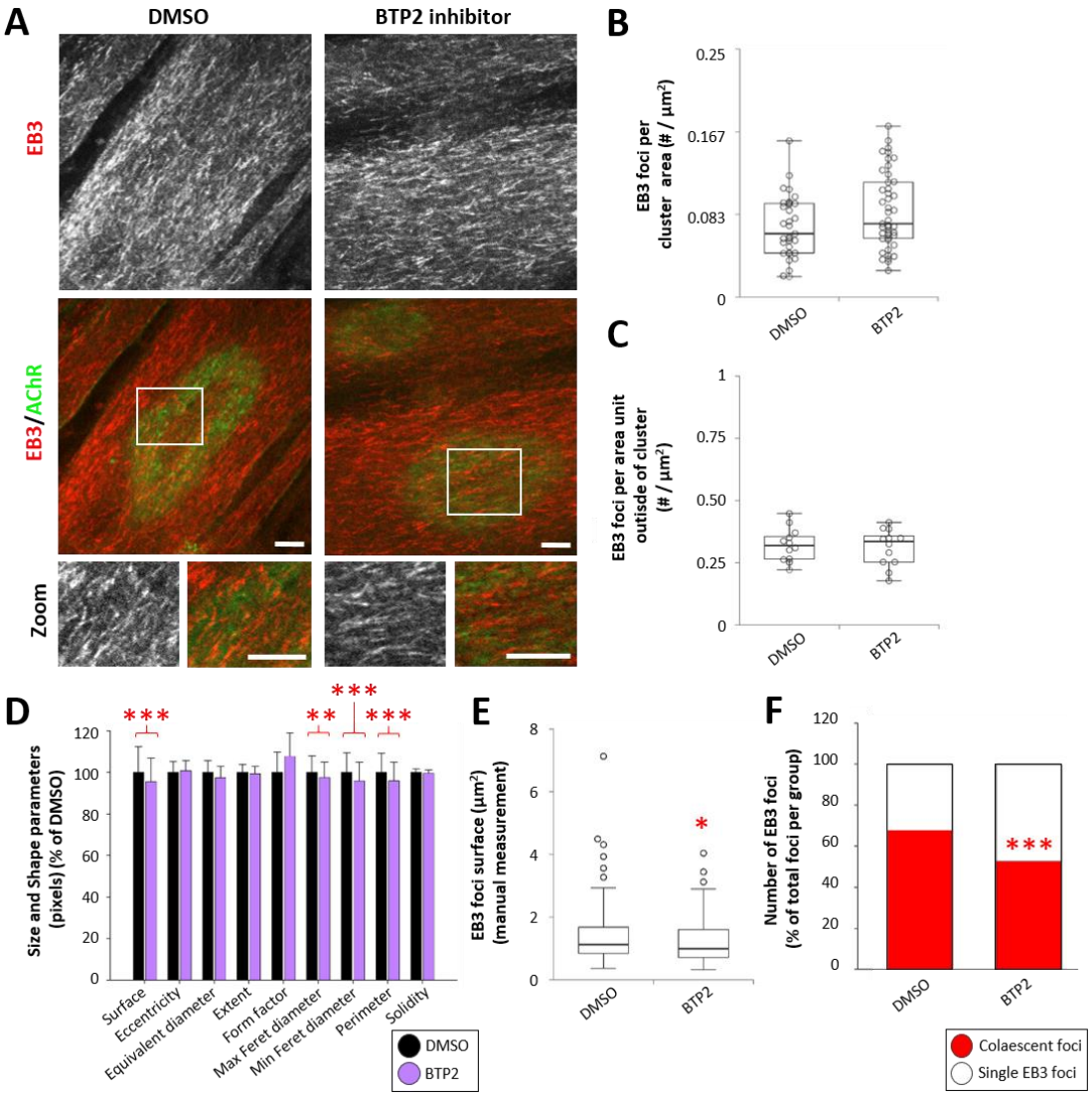

Figure 4.16. Drebrin-mediated remodeling of F-actin affects MT capture at the postsynaptic machinery *in vitro*. (A) Representative images of EB3 (red) distribution in C2C12 myotubes and its colocalization with AChRs (labelled with BTX, green) with and without BTP2 treatment. White squares show zoomed area. Scale bars = 10 µm. **(B)** Total number of EB3 foci per AChR cluster area (#/µm^2) upon BTP2 treatment. Mann-Whitney U test, not significant. Datapoints (empty circles) represent quantifications of foci number in single AChR clusters from three independent experiments. Bold mid-line inside each box represents mean. Boxplot whiskers represent lower and upper extremes. **(C)** Total number of EB3 foci per area unit outside of AChR cluster (#/µm^2) upon BTP2 treatment. Mann-Whitney U test, not significant. Datapoints (empty circles) represent quantifications of foci number in single myotubes from three independent experiments. Bold mid-line inside each box represents mean. Boxplot whiskers represent lower and upper extremes. **(D)** Size and shape parameters (surface, eccentricity, equivalent diameter, extent, form factor, maximal and minimal Feret diameter, perimeter, and solidity) measured with CellProfiler in C2C12 myotubes upon BTP2 treatment. Student's t-test, $P \leq .01$ (**), $P \leq .001$ (***). **(E)** Manual measurement of EB3 foci surface (µm^2) in C2C12 myotubes upon BTP2 treatment. Mann-Whitney U test, $P \leq .05$ (*). Datapoints (empty circles) represent quantifications of single EB3 foci surface within AChR clusters from two independent experiments. Bold mid-line inside each box represents mean. Boxplot whiskers represent lower and upper extremes. **(F)** Number of EB3 foci (% of total foci analyzed in each group) whose surface is above the "single

foci" threshold (colaescent foci, red) or below (single EB3 foci, white) upon BTP2 treatment. Chi-Square test, X^2 (4, N = 676) = 681.727, $P \leq .001$ (***).

However, it is unlikely that BTP2 affects the actual size of EB3. Considering drebrin EB3-binding and MT-recruiting functions, I hypothesized that the bigger EB3 foci surface observed in control myotubes was caused by either local assembly of multiple EB3-decorated MTs grouped together or multiple EB3 molecules recruited to the same MT, interpreted by the automated quantification software as single EB3 foci. In BTP2-treated myotubes, where drebrin-mediated rearrangements of F-actin were disturbed, recruited MTs or EB3s would not coalesce together when linked to F-actin bundles. Therefore, I manually measured the average size of individual, isolated EB3 foci from a control sample, set it as a threshold, and quantified the frequency of single (≤ threshold) and coalescent (> threshold) EB3 foci. Indeed, coalescent EB3 were less frequent upon BTP2 treatment (**Fig. 4.16F**), thus supporting the hypothesis that actin cytoskeleton remodeling is important for MT organization at the postsynaptic machinery.

4.4.4. Drebrin downregulation does not affect subsynaptic myonuclei number nor surface

Previous studies showed how cross-linking proteins that regulate MT recruitment to the postsynaptic machinery can also regulate the localization and morphology of subsynaptic and extrasynaptic myonuclei in skeletal muscle fibers (Bruusgaard et al., 2006; Ghasemizadeh et al., 2021). Moreover, drebrin itself was involved in actin-MT-mediated nuclear migration in cerebellar neurons (Trivedi et al., 2017). Based on my previous results regarding drebrin role in MT capture to the postsynaptic machinery, I decided to assess number and surface of subsynaptic myonuclei upon drebrin downregulation in C2C12 myotubes. Only nuclei with at least 50% of their surface within the AChR cluster area were considered subsynaptic and included in the analysis (**Fig. 4.17A**). Neither number of nuclei per cluster (**Fig. 4.17B**) nor surface of individual sybsynaptic myonuclei (**Fig. 4.17C**) were different between *Control siRNA* (non-targeting) and *Dbn1*-siRNA transfected cells. Therefore, my results do not support the hypothesis of drebrin involvement in synaptic nuclear positioning, although more in-depth analysis should be conducted to validate this conclusion.

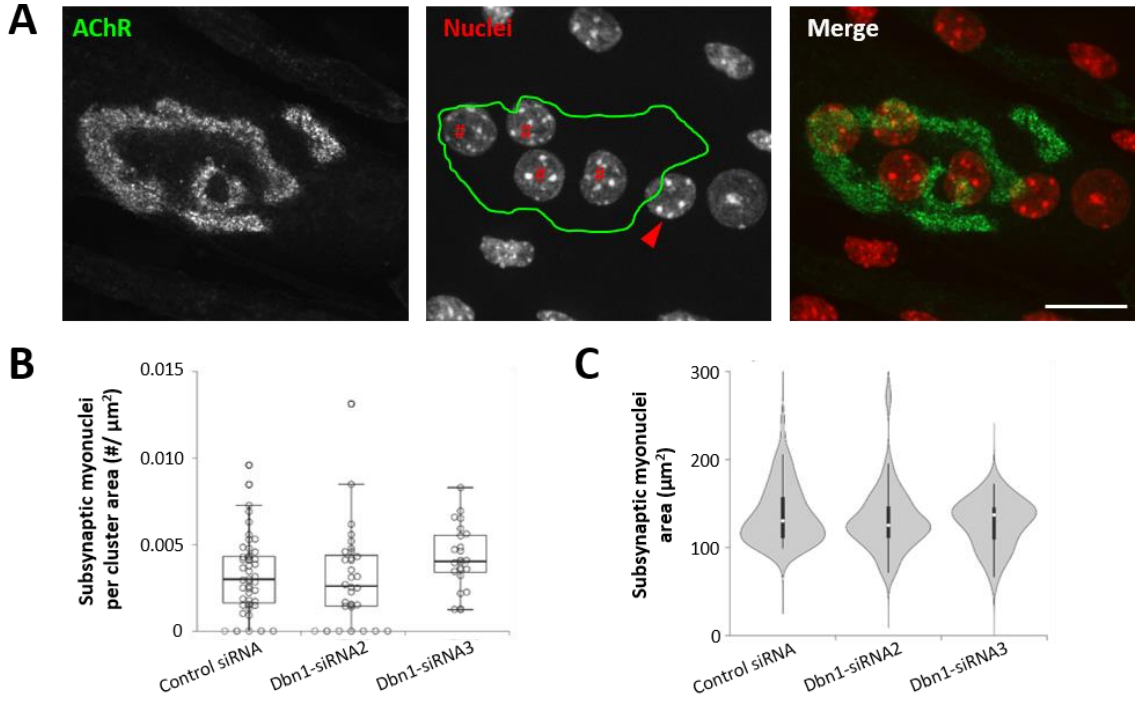

Figure 4.17. Drebrin downregulation does not affect subsynaptic myonuclei *in vitro.* (A) Illustrative image of laminin-induced AChR cluster (labelled with BTX, green) and myonuclei (labelled with DAPI, red) in C2C12 myotubes. Green outline in central image represents AChR cluster area. Red arrowhead points at myonucleus considered extrasynaptic, while red # indicate subsynaptic myonuclei. Scale bar = 20 µm. **(B)** Number of subsynaptic myonuclei per cluster area (#/µm^2) upon drebrin downregulation. Kruskal-Wallis U test between Control siRNA and other experimental conditions, not significant. Datapoints (empty circles) represent quantifications of myonuclei within AChR clusters from three independent experiments. Bold mid-line inside each box represents mean. Boxplot whiskers represent lower and upper extremes. **(C)** Synaptic myonuclei area (µm^2) upon drebrin downregulation. Kruskal-Wallis U test between Control siRNA and other experimental conditions, not significant. Violin plot (grey shape) represents frequency of values. Narrow boxplot inside each violin plot (black) represents mean (small white circle) ± lower and upper extremes (black lines).

4.4.5. Rapsyn co-immunoprecipitates with both drebrin and EB3

Next, I decided to explore the mechanism through which drebrin regulates MT-dependent AChR clustering, by studying proteins that had been previously involved in the dynamics of the postsynaptic machinery. Upon literature review, I selected several candidates based on 1) their similar role to drebrin in actin-MT cross-linking (MACF1), 2) their postsynaptic scaffolding properties and known interaction with cross-linkers at the NMJ (rapsyn), 3) their known interaction with drebrin at the postsynaptic density in the CNS (Homer1), and 4) their known role in neurotransmitter recycling and potential role in AChR maturation (MVI) (Banks et al., 2003; Oury et al., 2019; Shiraishi-Yamaguchi et al., 2009; Wagner et al., 2019).

First, I studied the expression pattern of genes encoding rapsyn, MACF1, Homer1, and MVI upon drebrin downregulation in C2C12 myotubes. The mRNA levels of all these postsynaptic-regulating proteins were not significantly affected by the drop in drebrin expression (**Fig. 4.18**), suggesting that drebrin is not a crucial regulator of their transcription.

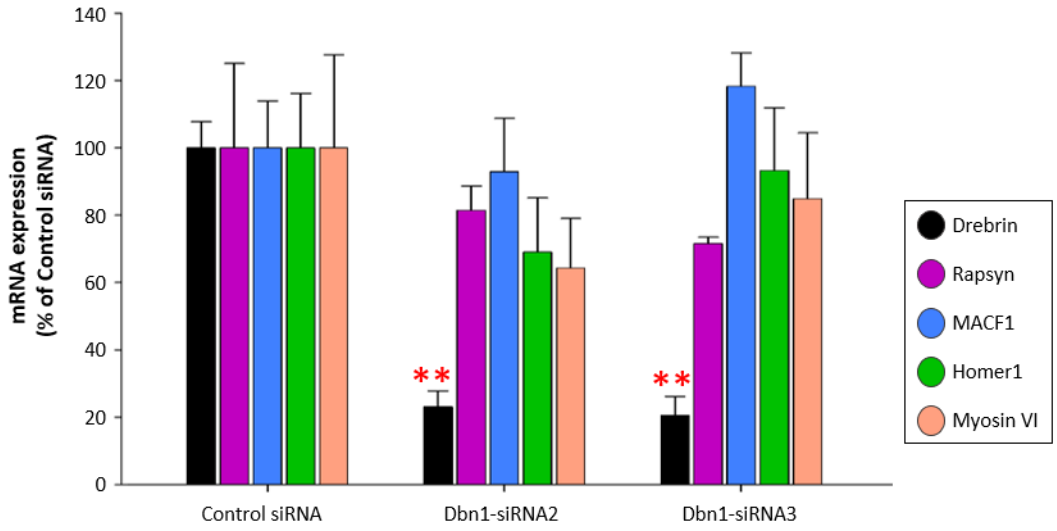

Figure 4.18. Drebrin downregulation does not significantly affect transcription of selected postsynaptic regulators. Student's t-test between Control siRNA and Dbn1-siRNAs for each gene did not reveal statistically significant differences in expression of postsynaptic regulators rapsyn, MACF1, Homer1, nor MVI upon drebrin downregulation, $P \leq .01$ (**). Error bars represent SD.

On the other hand, previous reports had shown how actin-MT cross-linkers, such as MACF1 and α-actinin, directly bind to rapsyn to participate in the maintenance of AChR clusters (Dobbins et al., 2008; Oury et al., 2019). Therefore, I decided to test whether rapsyn also interacted with actin- and MT-binding proteins drebrin and EB3. To this end, I performed transfection of HEK293 cells with plasmids encoding tagged rapsyn, drebrin E, or EB3, and lysed the cells for co-immunoprecipitation (*for methodological details, see section 3.5.*).

Rapsyn was successfully co-immunoprecipitated with drebrin E (DbnE-WT-GFP), the most abundant isoform of drebrin in the skeletal muscle (**Fig. 4.19A**), as well as with EB3 (EB3-GFP) (**Fig. 4.19B**). My previous results had shown that drebrin phosphorylation at Ser 142 was not necessary for its localization at the postsynaptic machinery (**Fig. 4.5**), where rapsyn is also accumulated and acts as a key regulator. Therefore, it seemed reasonable to hypothesize that this post-translational modification was not necessary for the

interaction between rapsyn and drebrin. Indeed, I successfully co-immunoprecipitated rapsyn with the "phospho-dead" mutant of drebrin (DbnE-142A-GFP) (**Fig. 4.19C**).

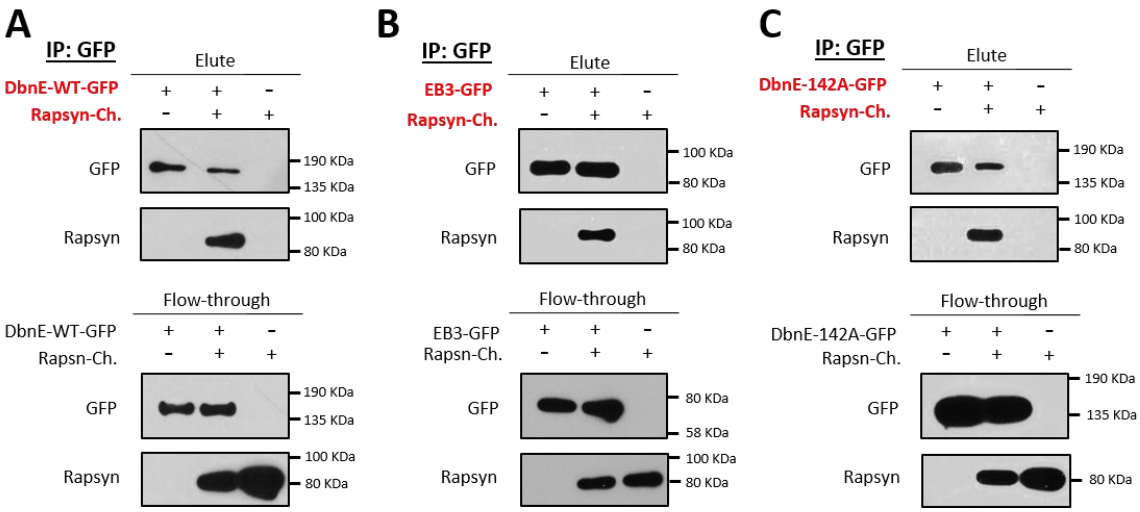

Figure 4.19. Clustering regulator rapsyn interacts with both drebrin and EB3. (A) Co-immunoprecipitation of overexpressed wild-type drebrin E (DbnE-WT-GFP) and rapsyn (Rapsyn-Ch) from lysates of transfected HEK293 cells. **(B)** Co-immunoprecipitation of overexpressed EB3 (EB3-GFP) and rapsyn (Rapsyn-Ch) from lysates of transfected HEK293 cells. **(C)** Co-immunoprecipitation of overexpressed phospho-dead drebrin E (DbnE-142A-GFP) and rapsyn (Rapsyn-Ch) from lysates of transfected HEK293 cells.

Altogether, these results suggest that rapsyn could be involved in drebrin-mediated regulation of AChR clustering and MT capture at the postsynaptic machinery, and that drebrin phosphorylation at Ser142 is not necessary for this function.

4.5. Drebrin loss mildly impairs postsynaptic machinery organization *in vivo*

To assess whether the phenotype *in vitro* was translated into a physiological dysfunction *in vivo*, I characterized the NMJs of drebrin global knockout mice (DXKO), which lack all drebrin isoforms (*see section 3.11.*), and compared NMJ morphology, fragmentation, and maturation stage to their WT littermates. The genotyping of animals was performed by prof. Hiroyuki Yamazaki (provider of the fixed samples) and confirmed in our laboratory later on following the protocol as previously described (Kajita et al., 2017). The validation of drebrin absence in muscle tissue was not possible due to technical problems with protein samples received, however its full elimination in brain tissue has been confirmed by our collaborators (Kajita et al., 2017) and in skeletal muscle by J. Stiber's research group (unpublished data, reported as a poster (Xu et al., 2012)).

For this analysis, I performed immunohistochemical stainings of different types of muscle obtained from 5 male animals per group after intravascular perfusion with 4%

PFA. To assess whether morphological differences were muscle type-dependent, I compared the parameters of the *TA* (predominantly fast-twitch, hybrid type 2A, 2B, and 2X fibers), *DIA* (predominantly pure fast-twitch, type 2X fibers), and *ST* muscles (predominantly fast-twitch, hybrid type 2B/2X fibers) from adult WT and DXKO mice (5-10 months of age, P150-300) to evaluate NMJ maintenance. To assess NMJ morphology in early development, I also decided to look at the *TA* muscle of mice undergoing postnatal NMJ maturation (15 days of age, P15).

4.5.1. Drebrin knockout mildly affects AChR and endplate surface of NMJs throughout lifespan

In order to compare the NMJ size and shape of DXKO mice with their WT littermates, I used an automated ImageJ script that measures surface covered by the postsynaptic machinery (AChRs) and its corresponding perimeter, as well as the surface, perimeter and diameter of the whole endplate (**Fig. 3.11**). I analyzed 5 to 43 NMJs/mouse (n = 5 mice/group) in male adults (P150-300), and 6 to 25 NMJs/mouse (n = 5 mice/group) in juvenile males (P15). The variability in number of NMJs analyzed per animal attends to manually filtering out images that were not suitable for automatic analysis.

During postnatal development (P15), *TA* muscle of DXKO mice showed a significantly decreased surface covered by AChRs (P = .013) and whole endplate perimeter when compared to their WT counterparts (P = .021) (**Fig. 4.20A**). These differences are exacerbated in adulthood and early middle age (P150-300), when DXKO mice have significantly smaller NMJs than their WT counterparts in almost all morphological parameters analyzed in *TA* (AChR surface: P = .001; AChR perimeter: P = .001; Endplate surface: P = .002; Endplate perimeter: P = .038) (**Fig. 4.20B**) and *DIA* muscles (AChR surface: P = .001; AChR perimeter: P = .017; Endplate surface: P = .011; Endplate diameter: P = .014) (**Fig. 4.20C**). Surprisingly, opposite results were obtained from the analysis of *ST* muscle (**Fig. 4.20D**), in which the postsynaptic surface in DXKO mice was bigger than in their WT counterparts (AChR surface: P < .001; AChR perimeter: P = .046; Endplate diameter: P = .024).

In summary, drebrin absence mildly affects the size of NMJs in various muscle types.

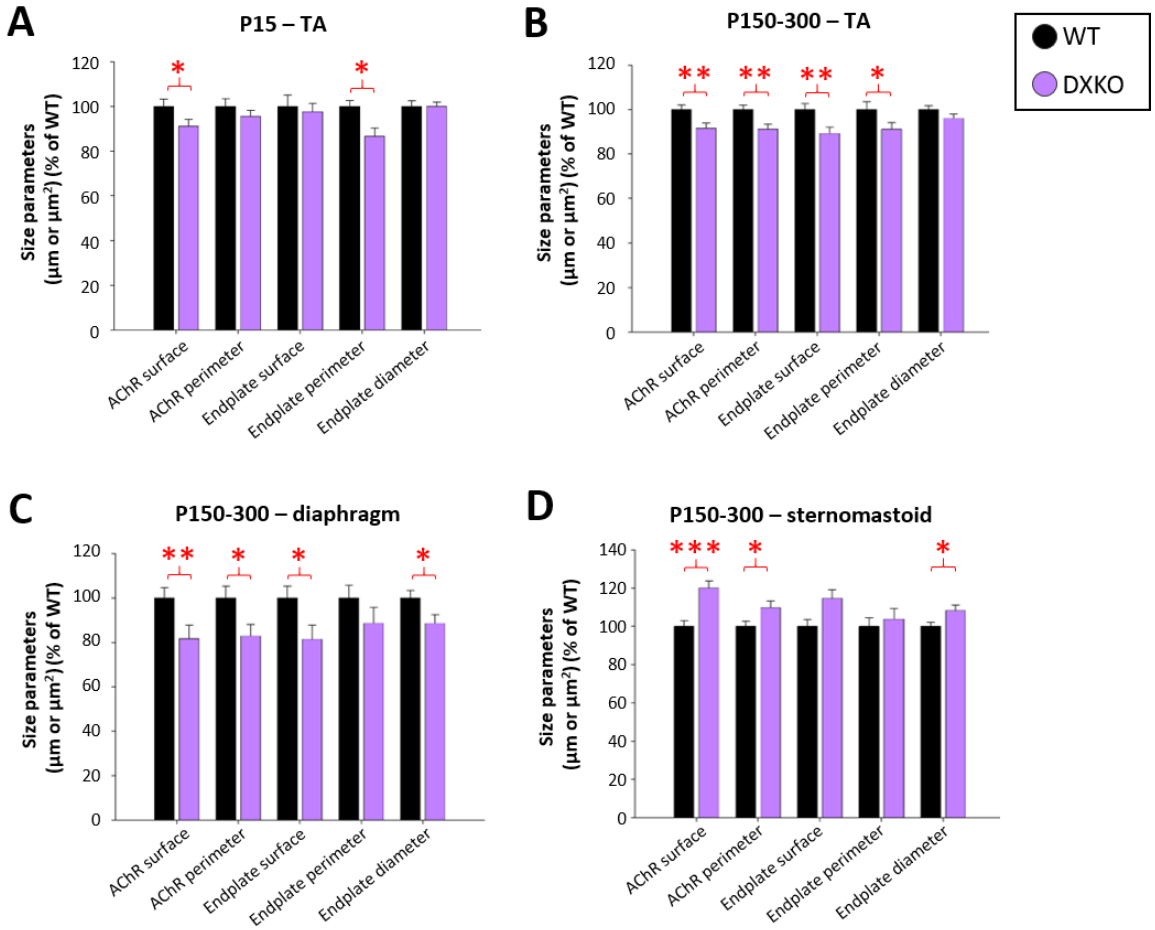

Figure 4.20. Drebrin knockout mildly affects NMJ size at different ages. Size parameters (AChR surface, AChR perimeter, Endplate surface, Endplate perimeter, Endplate diameter) expressed as percentage of WT for each parameter, in NMJs from *TA* muscle at P15 **(A)** and at P150-300 **(B)**, as well as NMJs from *DIA* **(C)** and *ST* **(D)** muscles at P150-300. Mann-Whitney U test, $P \leq .05$ (*), $P \leq .01$ (**), $P \leq .001$ (***). Bars represent mean and error bars represent SEM. **Abbreviations:** DXKO = drebrin global knockout mice; WT = wild-type (control) mice.

4.5.2. Drebrin knockout does not affect NMJ postnatal maturation

Based on previous results where drebrin was associated with AChR maturation-driving structures called synaptic podosomes (**Fig. 4.12**), I decided to assess whether this phenotype translated into defects of NMJ development *in vivo*. To this end, I classified 15-25 NMJs/mouse (n = 5 mice/group) into one of three different maturation stages typically found at 15 days of age: plaque (0 perforations), perforated (plaques with ≥ 1 perforations), and mature (perforated and with pretzel-like branches) (**Fig. 4.21A**). In each NMJ, I also quantified the number of perforations per NMJ. Neither of the maturation parameters analyzed were different between DXKO and WT mice (**Fig. 4.21B-C**), which suggests that drebrin role in postnatal NMJ remodeling is dispensable or, at least, its absence could be compensated by other proteins with similar functions.

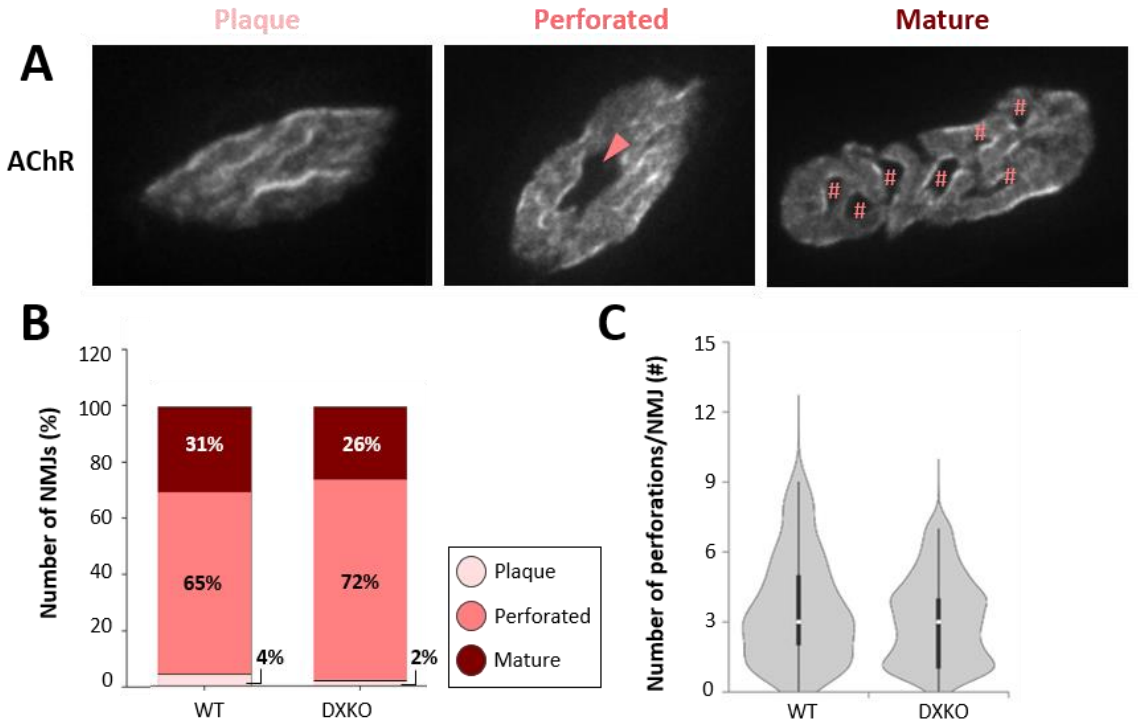

Figure 4.21. Drebrin knockout does not impair NMJ maturation. (A) Representative images of neuromuscular maturation stages quantified at P15 based on AChR morphology (labelled with BTX, white). Pink arrowhead points at perforation. Pink # show the number of perforations. **(B)** Number of NMJs (% of total NMJs measured for each group) that classify as plaque, perforated, or mature in *TA* muscle from control and drebrin knockout mice. Chi-Square test, not significant. **(C)** Number of perforations per NMJ (#) in *TA* muscle from control and drebrin knockout mice. Kruskal-Wallis U test, not significant. Violin plot's width (grey shape) represents frequency of values. Narrow boxplot inside each violin plot (black) represents mean (small white circle) ± lower and upper extremes (black lines). **Abbreviations:** DXKO = drebrin global knockout mice; WT = wild-type (control) mice.

4.5.3. Drebrin knockout does not disrupt adult NMJ integrity

In non-pathological conditions, aging NMJs are characterized by increasing fragmentation or disruption of the branches (Faulkner et al., 2007). To further explore whether drebrin absence induces early onset of age-induced NMJ fragmentation in male adult and middle-aged mice (5-10 months), I manually quantified the number of fragments of each NMJ (10-25 NMJs/mouse, n = 5 mice/group) and classified the NMJs depending on their fragmentation level into four classes (**Fig. 4.22A**): 1-2 fragments (Class 1), 3-4 fragments (Class 2), 5-6 fragments (Class 3), 7 or more fragments (Class 4). As shown in **Fig. 4.22**, DXKO mice do not exhibit NMJ fragmentation measured as fragmentation class (**Fig. 4.22D-E**) or number of fragments per NMJ (**Fig. 4.22D-E**) when compared to their WT counterparts, in neither *TA* nor *DIA* muscles.

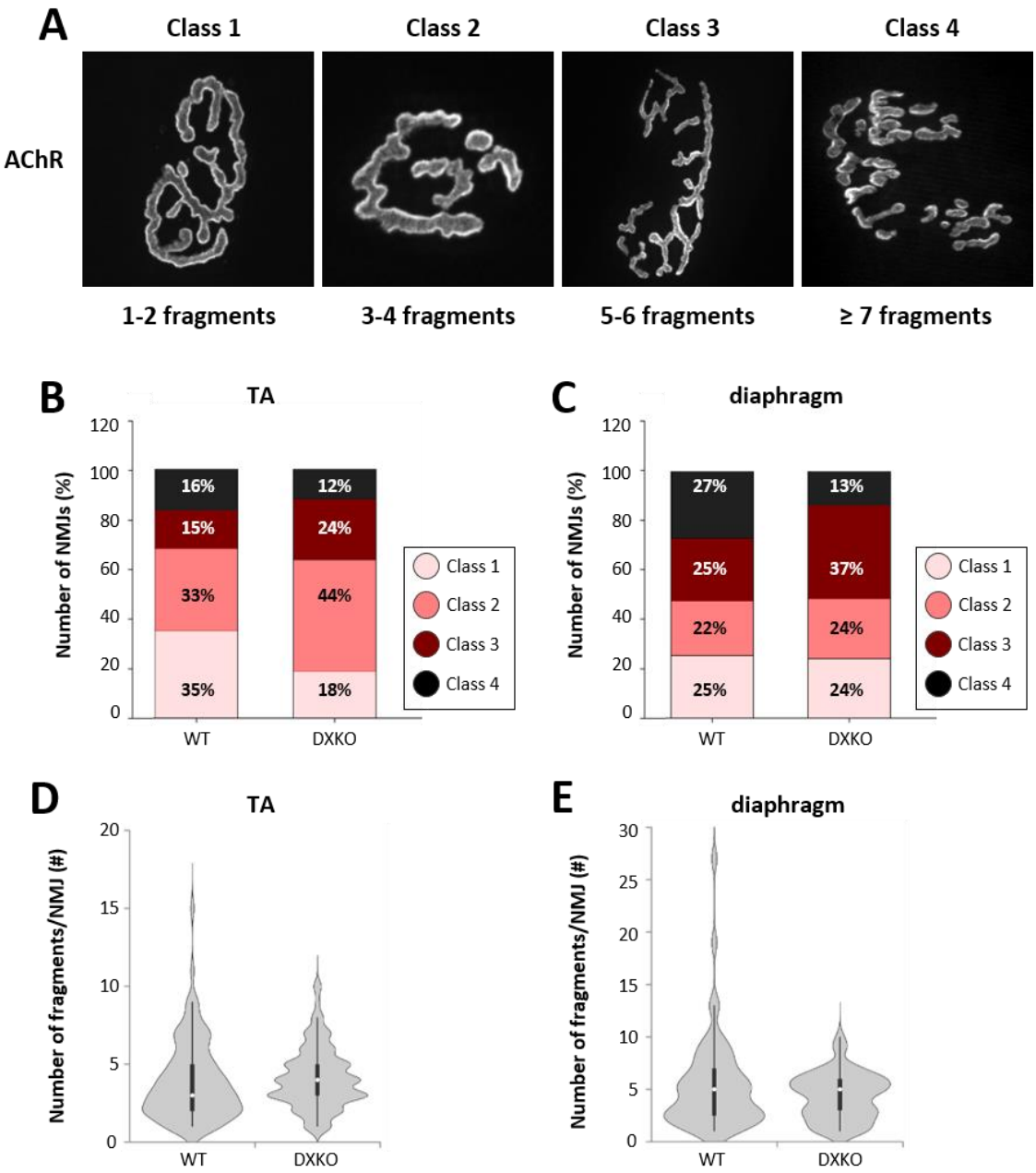

Figure 4.22. Drebrin knockout does not impact NMJ fragmentation in adult mice. (A) Representative images of neuromuscular fragmentation classes assessed at P150-300 based on AChR morphology (labelled with BTX, white). **(B-C)** Number of NMJs (% of total NMJs measured for each group) that classify as class 1, 2, 3, or 4, in *TA* (B) and *DIA* (C) muscles from control and drebrin knockout mice. Chi-Square test, not significant. **(D-E)** Number of fragments per NMJ (#) in *TA* (D) and *DIA* (E) muscles from control and drebrin knockout mice. Kruskal-Wallis U test, not significant. Violin plot's width (grey shape) represents frequency of values. Narrow boxplot inside each violin plot (black) represents mean (small white circle) ± lower and upper extremes (black lines). **Abbreviations:** DXKO = drebrin global knockout mice; WT = wild-type (control) mice.

Moreover, I assessed the integrity of NMJ branches by measuring the number of AChR-free "holes" within branches (Schmidt et al., 2011) and the presence or absence of dispersed AChR in the edges of branches (**Fig. 4.23A**) (10-24 NMJs/mouse, n = 5

mice/group). Neither number of perforated NMJs (**Fig. 4.23B-C**), number of NMJs displaying AChR dispersion (**Fig. 4.23D-E**), nor number of perforations per NMJ (data not shown) were different in the *TA* or *DIA* muscles of DXKO mice when compared to their WT counterparts.

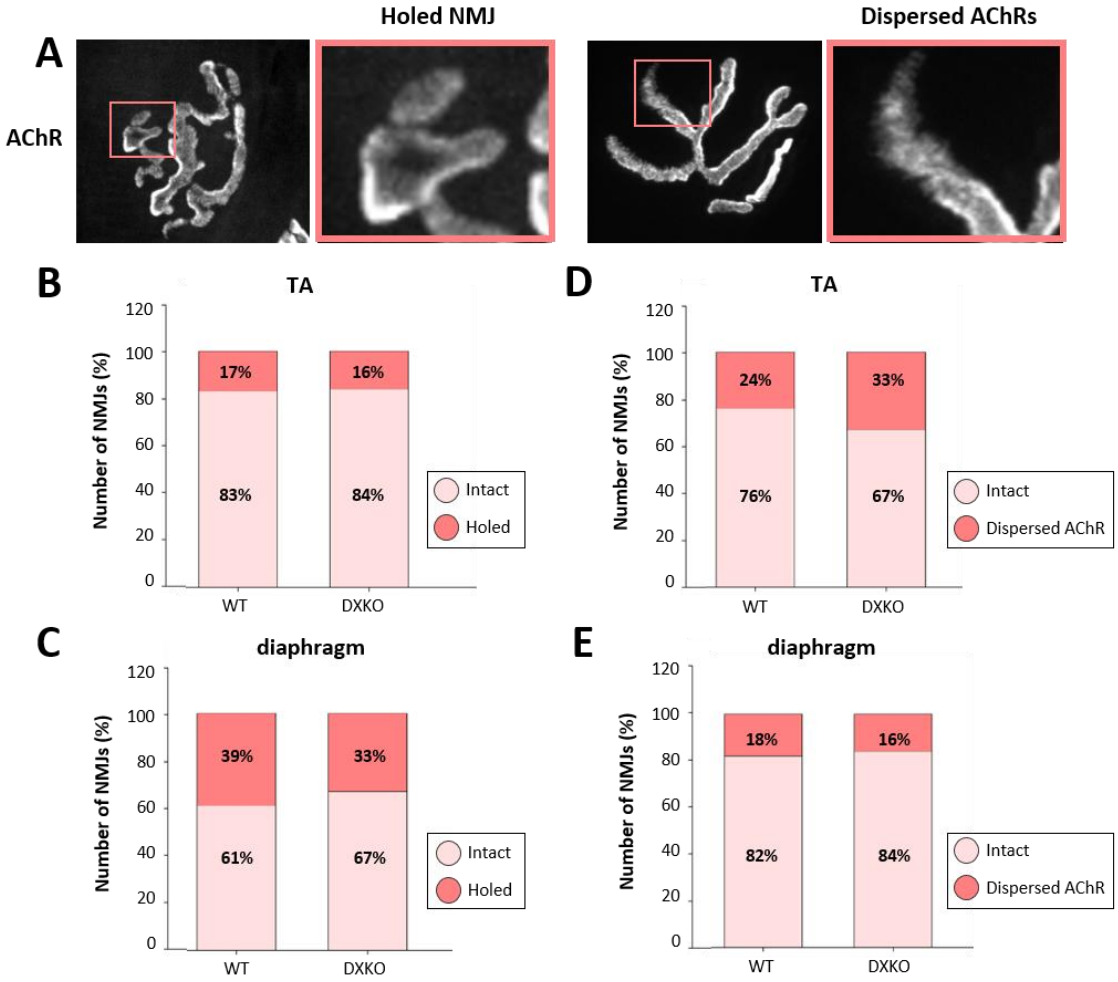

Figure 4.23. Drebrin knockout does not impair adult NMJ integrity. (A) Representative images of disrupted AChR clusters (labelled with BTX, white) with holes within the branches (left panel) or dispersed AChR in the edges (right panel). Pink squares show zoomed area. **(B-C)** Number of NMJs (% of total NMJs measured for each group) that classify as intact or with perforations within AChR branches in the *TA* (B) and *DIA* (C) muscles of WT and drebrin knockout mice. Chi-Square test, not significant. **(D-E)** Number of NMJs (% of total NMJs measured for each group) that classify as intact or with dispersed AChRs in the edges of branches in the *TA* (D) and *DIA* (E) muscles of wild-type and drebrin knockout mice. Chi-Square test, not significant. **Abbreviations:** DXKO = drebrin global knockout mice; WT = wild-type (control) mice.

Based on the morphological studies performed, the data suggest that drebrin absence does not affect NMJ integrity in adult and middle-aged male mice.

4.6. Drebrin is upregulated in primary myotubes lacking MVI

Studies performed by our research group showed that MVI is involved in myoblasts adhesion and fusion into myotubes (Karolczak et al., 2015a; Lehka et al., 2020). As part of these studies, the expression levels of several proteins involved in myoblasts differentiation were evaluated. Since previous reports provided evidence for both drebrin and MVI involvement in cell-cell adhesion processes (Krauss, 2017; Maddugoda et al., 2007; Rehm et al., 2013), I examined whether their relative expression levels would impact one another. I found that primary myoblasts obtained from *SV* mice lacking functional MVI (*for methodological details, see section 3.3.3.*) have increased levels of drebrin after 7 days of *in vitro* culture (**Fig. 4.24**), as well as the MyoD transcription factor, that regulates the expression of drebrin during myoblast differentiation (data not shown). On the other hand, *Myo6* expression in C2C12 myotubes upon drebrin downregulation was not significantly impacted when compared to the control (**Fig. 4.18**).

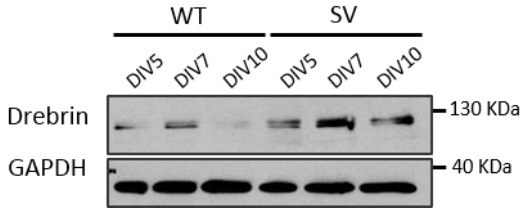

Figure 4.24. Myosin VI absence enhances drebrin expression in primary myotubes. Representative blot by D. Wojton. **Abbreviations:** SV = MVI global knockout mice; WT = wild-type (control) mice.

Taken together, these results suggest that MVI and drebrin might be involved in the same molecular cues regulating myoblast differentiation.

4.7. Myosin VI loss does not severely impair postsynaptic machinery organization *in vitro*

Similar to the functional analyses described in section 4.3. for drebrin, I performed preliminary loss-of-function studies in which MVI was downregulated in C2C12 myotubes with specific siRNA encoding murine MVI (*Myo6*). Because it was previously demonstrated that MVI plays a crucial role in myoblast fusion and adhesion (Lehka et al., 2020), siRNAs were transfected 72 h after fusion induction, when myotubes were already

formed and differentiated. The drop in MVI expression was confirmed at mRNA level in all four siRNAs and at protein level in two out of four different siRNA tested (**Fig. 4.25**).

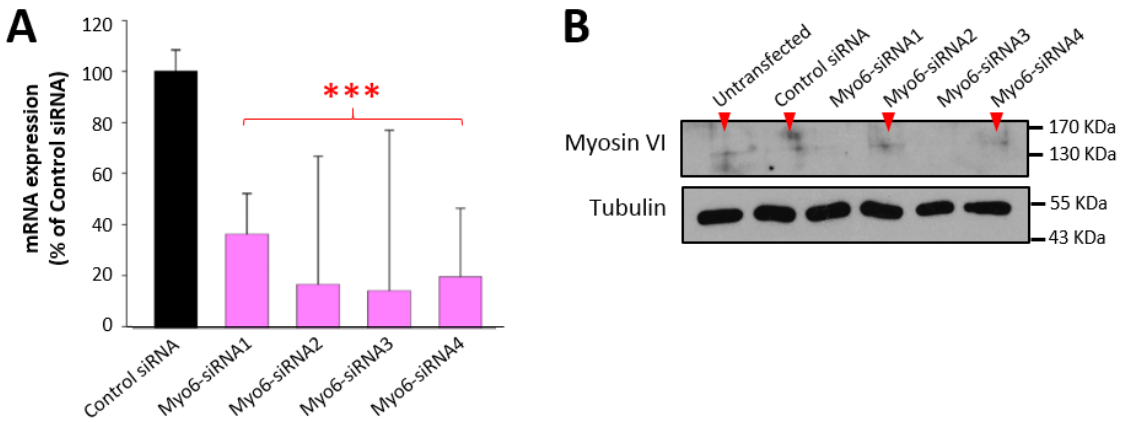

Figure 4.25. Validation of siRNA-mediated downregulation of MVI. *Myo6* knockdown validation in C2C12 myotubes on the 5th day of fusion at mRNA and protein levels with RT-qPCR **(A)** and Western blot **(B)**, respectively. Representative blot by M. Gawor. Student's t-test between Control siRNA and other experimental conditions, $P \leq .001$ (***), from a single independent experiment. Error bars in A represent SD. Red arrowheads in B indicate bands corresponding to detected MVI protein.

4.7.1. AChR cluster formation *in vitro* is not substantially affected upon MVI knockdown

As previously described, I used two models for induction of postsynaptic machinery in C2C12 myotubes, namely agrin-based (neuron-dependent induction) (**Fig. 4.26A**) and laminin-based (muscle-dependent induction) (**Fig. 4.27A**). Then, I downregulated the expression of MVI and confirmed that myotubes transfected with *Control siRNA* did not differ in terms of fusion efficiency (visually-assessed) nor number of AChR clusters formed when compared to untransfected cells. *Musk-siRNA* was used as a positive control and, as expected, it severely impaired AChR cluster formation. The total number of agrin-induced clusters was not significantly changed, with the exception of one out of four *Myo6*-siRNAs (siRNA1: $P = .01$) (**Fig. 4.26B**) previously confirmed to considerably downregulate MVI (**Fig. 4.25**). On the other hand, two different *Myo6*-siRNAs induced differences in the proportions of very long (> 50 µm, siRNA4) and short (< 10 µm, siRNA2) agrin-induced clusters when compared to *Control siRNA* (siRNA2: $P < .001$, siRNA4: $P < .001$) (**Fig. 4.26C**).

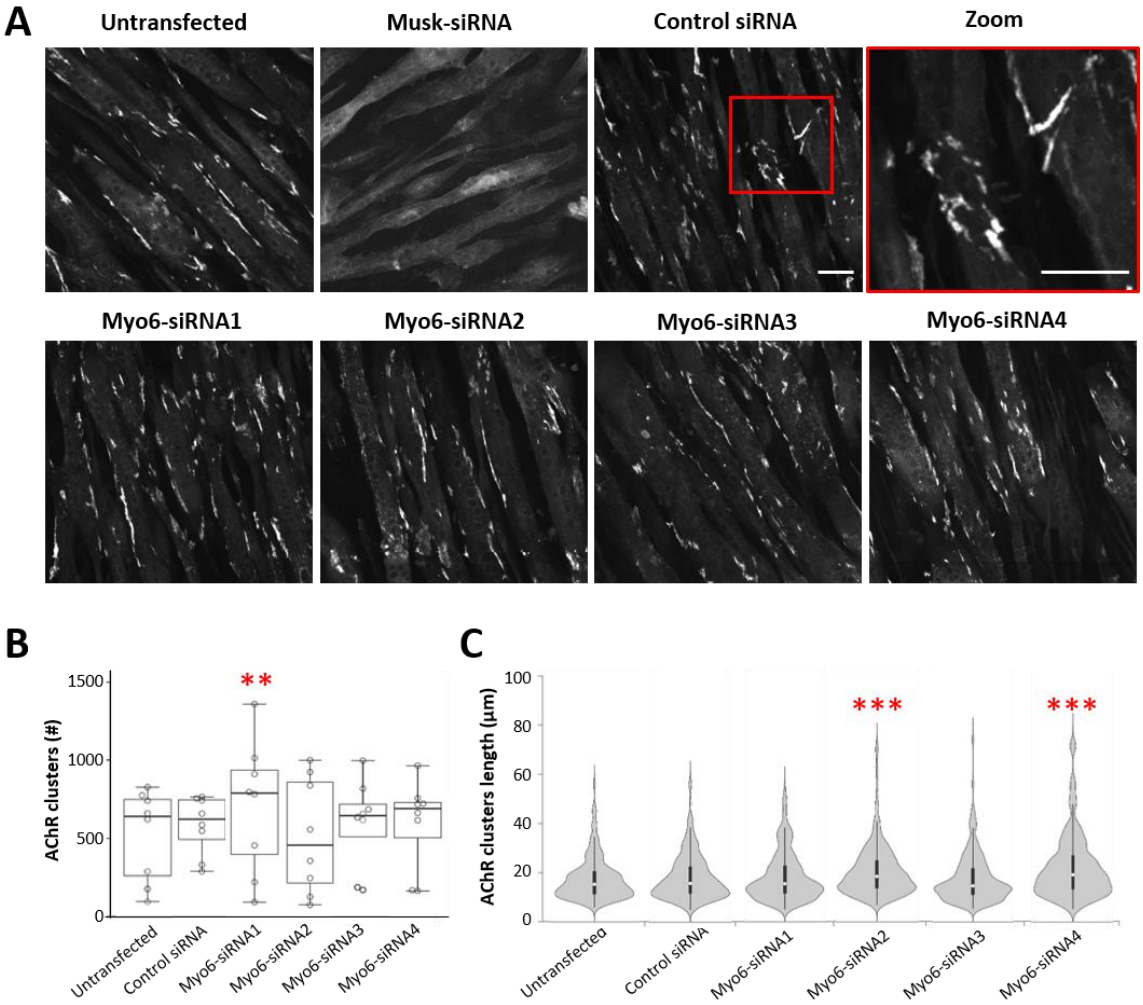

Figure 4.26. siRNA-mediated downregulation of MVI does not affect agrin-dependent postsynaptic organization *in vitro*. (A) Representative images of C2C12 myotubes on the 5th day of fusion in different experimental conditions with agrin-induced AChR clusters labelled with BTX (white). Red square shows zoomed area of the Control siRNA. Scale bars = 50 µm. **(B)** Total number (#) of AChR clusters upon MVI downregulation. Mann-Whitney U test between Control siRNA and other experimental conditions, $P \leq .01$ (**). Datapoints (empty circles) represent quantifications of different fields of view from three independent experiments. Bold mid-line inside each box represents mean. Boxplot whiskers represent lower and upper extremes. **(C)** Length (µm) of AChR clusters upon MVI downregulation. Chi-Square test, X^2 (25, N = 1200) = 57.714, $P \leq .001$ (***). Violin plot's width (grey shape) represents frequency of values. Narrow boxplot inside each violin plot (black) represents mean (small white circle) ± lower and upper extremes (black lines).

The number of laminin-induced AChR clusters remained similar upon MVI downregulation (**Fig. 4.27B**). Even though some *Myo6*-siRNA-treated myotubes displayed aberrantly expanded or fragmented clusters (**Fig. 4.27A, zoom panel**), there was no significant increase in the number of such clusters when compared to *Control siRNA* (**Fig.**

4.27C). Instead, one out of four *Myo6*-siRNAs displayed a reduced number of dispersed AChR clusters (siRNA4: *P* = .035).

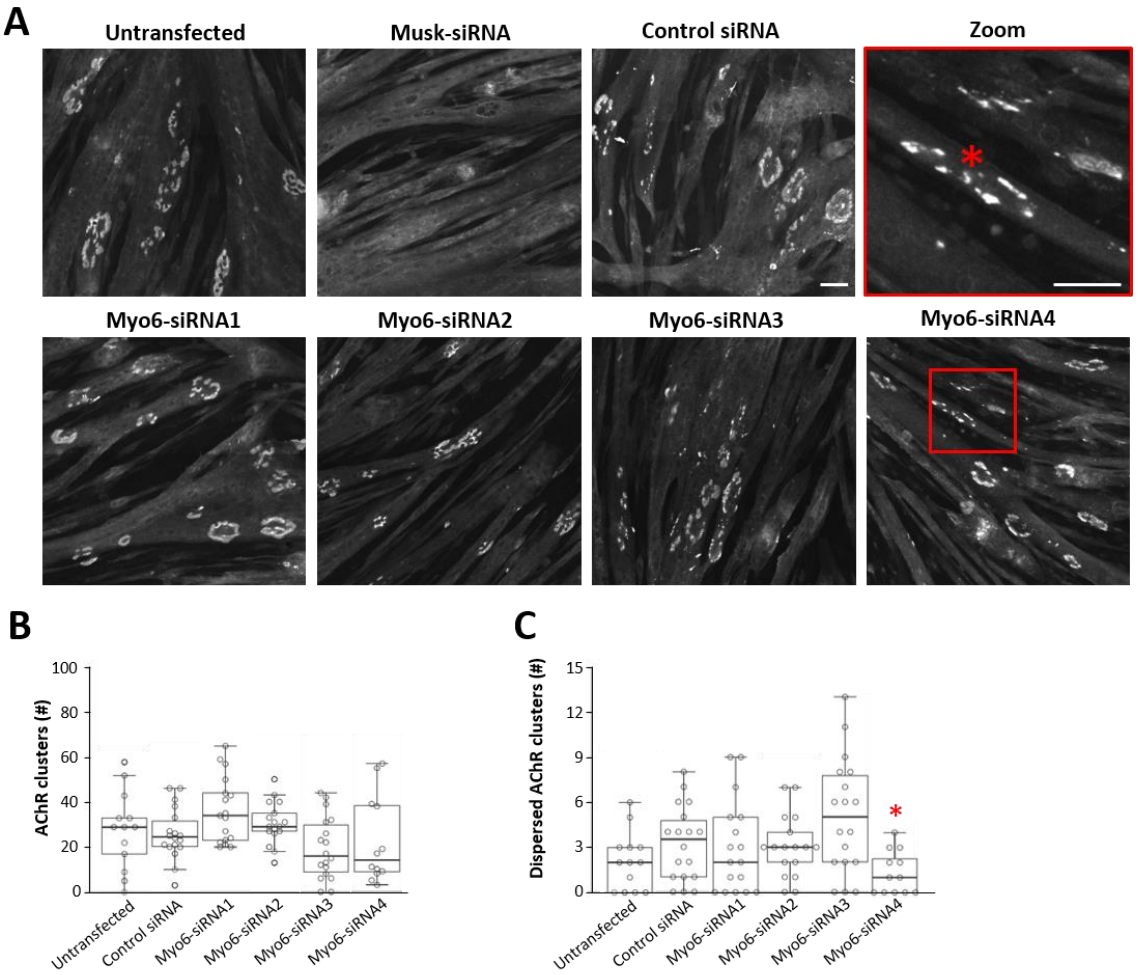

Figure 4.27. siRNA-mediated downregulation of MVI does not affect laminin-dependent postsynaptic organization *in vitro*. (A) Representative images of C2C12 myotubes on the 5th day of fusion in different experimental conditions with laminin-induced AChR clusters (labelled with BTX, white). Red square shows zoomed area of the Myo6-siRNA4, * indicates disrupted cluster. Scale bars = 50 µm. **(B)** Total number (#) of AChR clusters upon MVI downregulation. Kruskal-Wallis U test between Control siRNA and other experimental conditions, not significant. Datapoints (empty circles) represent quantifications of different fields of view from four independent experiments. Bold mid-line inside each box represents mean. Boxplot whiskers represent lower and upper extremes. **(C)** Total number (#) of dispersed AChR clusters upon MVI downregulation. Mann-Whitney U test between Control siRNA and other experimental conditions, $P \leq .05$ (*). Datapoints (empty circles) represent quantifications of different fields of view from four independent experiments. Bold mid-line inside each box represents mean. Boxplot whiskers represent lower and upper extremes.

Due to the large variability between experiments, manifested by large differences in AChR cluster formation in control conditions, namely *Untransfected* and *Control siRNA*, the role of MVI in postsynaptic organization *in vitro* requires further thorough analyses.

4.7.2. Myosin VI downregulation does not abolish AChR turnover

Relying on the results obtained *in vivo* (**Fig. 4.2B**) and *in vitro* (Karolczak et al., 2015a), I wanted to explore the functional mechanisms underlying MVI accumulation around and in AChR-free areas of the postsynaptic machinery *in vitro.* As a minus-oriented actin-based motor, MVI was involved in endocytic processes in different mammalian cell types, including the internalization of surface receptors in kidney epithelial cells (Naccache et al., 2006) (*see section 1.3.4.*). Similarly, I hypothesized that if MVI was promoting trafficking of NMJ components, it would be in their vicinity (**Fig. 4.2B**) and its downregulation would significantly affect the turnover of postsynaptic proteins.

To this end, I performed microscopy studies of old vs. newly incorporated AChRs into laminin-induced clusters (*for methodological details*, *see section 3.7.*) in *Control siRNA* and *Myo6*-siRNA conditions and observed whether old AChRs were abnormally retained at the surface upon MVI downregulation. As shown in **Fig. 4.28**, insertion of new AChRs and internalization of old AChRs took place regardless of MVI expression levels, thus refuting the hypothesis of severe MVI-dependent impairments in receptor recycling. Due to technical difficulties encountered, an in-depth analysis of AChR turnover was not possible, however further characterization (surface covered and fluorescence intensity of old vs. new AChRs) in a different model could be an interesting follow-up to this experiment.

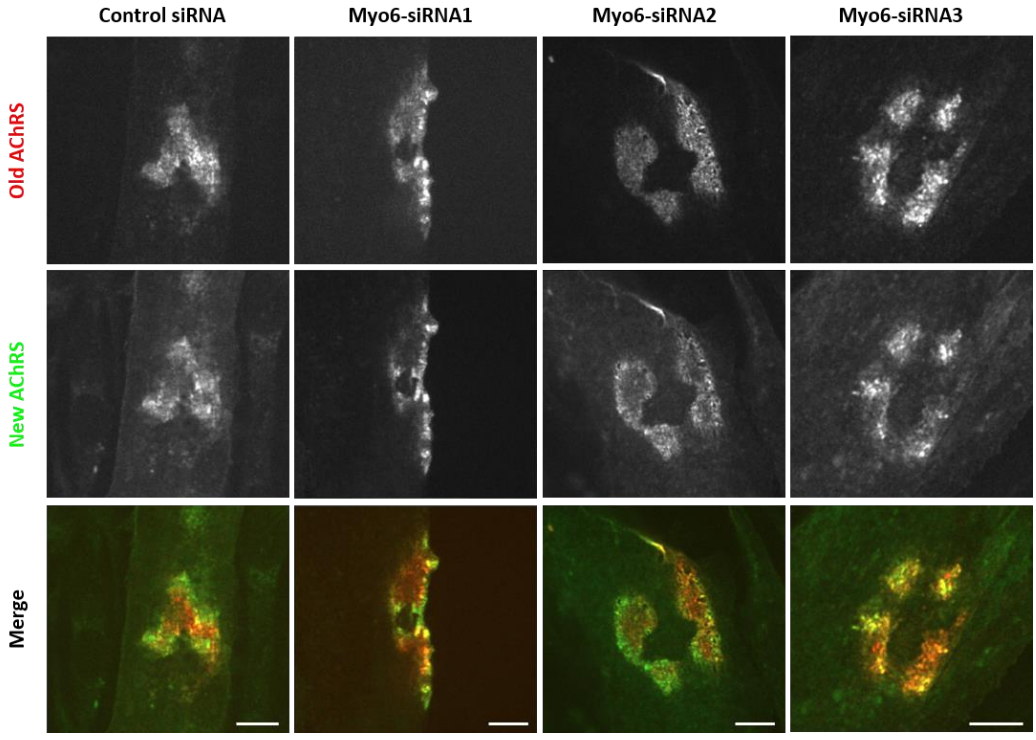

Figure 4.28. AChR turnover is not abolished upon siRNA-mediated downregulation of MVI. Representative images of C2C12 myotubes on the 5th day of fusion in different experimental

conditions with laminin-induced AChR clusters with old vs. newly incorporated AChRs (labelled with BTX, red and green, respectively). Scale bars = 10 µm.

4.8. Myosin VI is involved in the postsynaptic machinery organization *in vivo*

Because *in vitro* experiments did not provide enough evidence to support the hypothesis of MVI being involved in the postsynaptic organization of AChR clusters, I decided to characterize NMJs of MVI knockout mice (*SV*) and their WT counterparts (*see section 3.11.*) in terms of NMJ morphology, fragmentation, and maturation stage. The validation of MVI absence in homozygous *SV* mice is shown in **Fig. 4.29**.

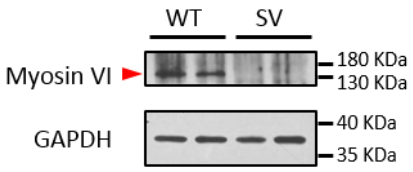

Figure 4.29. Validation of MVI knockout with Western blot. Representative blot by L. Lehka on homogenates of hindlimb muscles from P0 mice. **Abbreviations:** SV = MVI global knockout mice; WT = wild-type (control) mice. Red arrowhead indicates bands corresponding to detected MVI protein.

For studying NMJ morphology, I performed immunohistochemical stainings of different muscles obtained from 5-6 animals per group after fixation of the tissue. Similar to the characterization of DXKO mice, I decided to study relevant time points in the development of NMJs: P10 (postnatal remodeling), P120 (maintenance), and P365 (age-related remodeling) (Cheng et al., 2013). I also explored whether these animals displayed grip strength or motor impairments besides their constant circling behavior (Lee et al., 2002).

4.8.1. Neuromuscular junctions of juvenile MVI knockout mice are smaller and their morphological maturation is delayed

First, I characterized the NMJ morphology of *SV* mice during postnatal maturation. To this end, I used the automated ImageJ script that measures surface covered by the postsynaptic machinery (AChRs) and its corresponding perimeter, as well as the surface, perimeter and diameter of the whole endplate (**Fig. 3.11**). I measured 20-27 NMJs/mouse (n = 4 mice/group) of animals from both sexes at P10.

All parameters analyzed were significantly decreased in the *SOL* muscle of *SV* mice (AChR surface: $P < .001$; AChR perimeter: $P < .001$; Endplate surface: $P < .001$; Endplate perimeter: $P < .001$; Endplate diameter: $P < .001$) (**Fig. 4.30A**), while only the Endplate diameter of NMJs from *TA* muscle was slightly reduced upon MVI knockout ($P = .041$) (**Fig. 4.30B**).

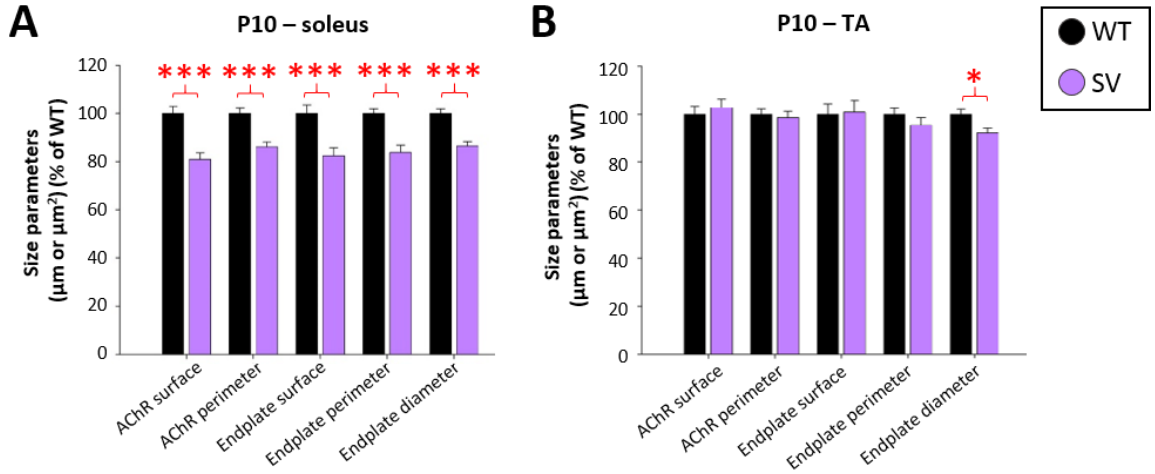

Figure 4.30. Myosin VI knockout reduces the size of maturing NMJs in the slow-twitch *soleus* muscle. Size parameters (AChR surface, AChR perimeter, Endplate surface, Endplate perimeter, Endplate diameter) represented as percentage of WT for each parameter, in NMJs from *SOL* **(A)** and *TA* **(B)** muscles of control and MVI knockout male and female mice at P10. Mann-Whitney U test, $P \leq .05$ (*), $P \leq .001$ (***). Bars represent mean and error bars represent SEM. **Abbreviations:** SV = MVI global knockout mice; WT = wild-type (control) mice.

Moreover, when I classified NMJs according to their maturation stage (plaque or already perforated) (**Fig. 4.31A**), both *TA* and *SOL* muscles from *SV* mice had a significantly increased percentage of plaque-shaped, unperforated NMJs ($P = .007$ and $P < .001$, respectively) (**Fig. 4.31B-C**). The number of perforations in NMJs that had already started the transition from plaque to pretzel remained similar regardless of the muscle type or the genotype (**Fig. 4.31D-E**).

Altogether, these results suggest that MVI absence differentially affects juvenile NMJs of different muscle types by reducing their overall size and delaying their plaque-to-pretzel transition.

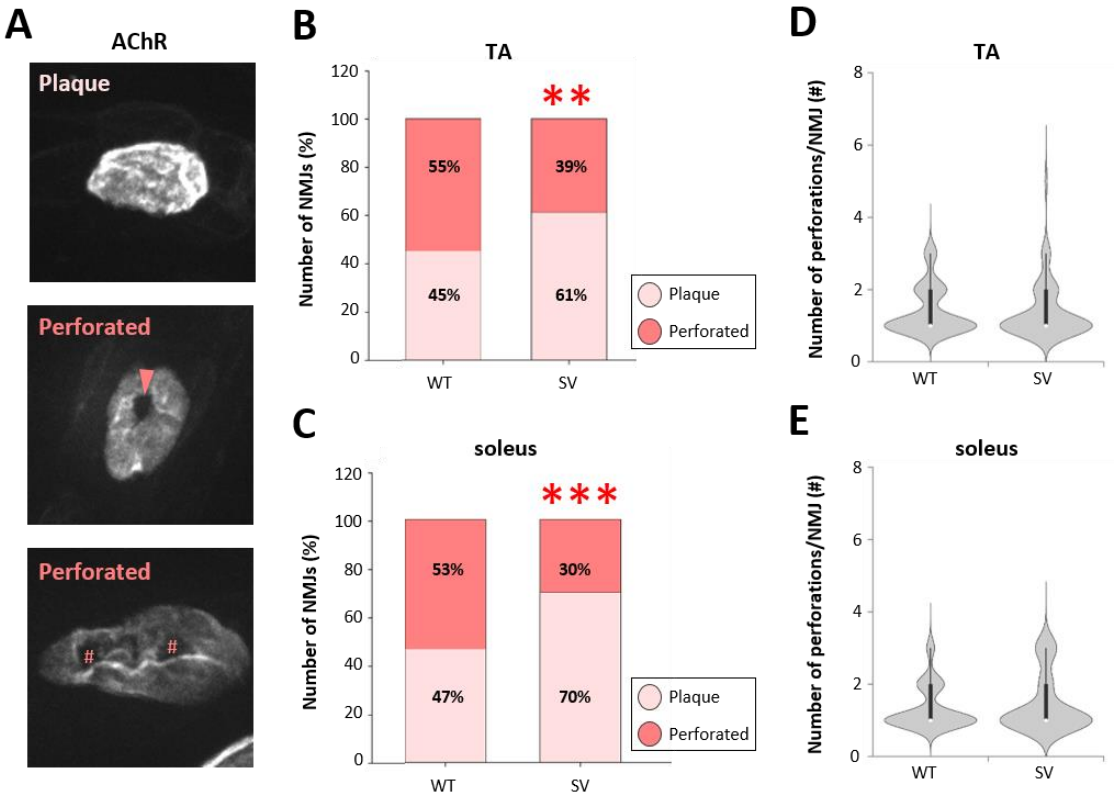

Figure 4.31. Myosin VI knockout impairs NMJ maturation. (A) Representative images of NMJ maturation stages assessed at P10. Pink arrowhead points at single perforation. Pink # indicate multiple perforations. **(B-C)** Number of NMJs (% of total NMJs measured for each group) that classify as plaque or perforated in the *TA* (B) and *SOL* (C) muscles of control wild-type and MVI knockout mice. Chi-Square test, *TA*: X^2 (1, N = 286) = 7.261, $P \leq .01$ (**); *SOL*: X^2 (1, N = 240) = 13.440, $P \leq .001$ (***). **(D-E)** Number of perforations per NMJ (#) in the *TA* (D) and *SOL* (E) muscles of control wild-type and MVI knockout mice. Kruskal-Wallis U test, not significant. Violin plot's width (grey shape) represents frequency of values. Narrow boxplot inside each violin plot (black) represents mean (small white circle) ± lower and upper extremes (black lines). **Abbreviations:** SV = MVI global knockout mice; WT = wild-type (control) mice.

4.8.2. Grip strength impairments in middle-aged MVI knockout mice are sexually dimorphic

The grip strength test allows for *in vivo* gross assessment of neuromuscular functionality through measuring muscle strength in a non-invasive, stress-reduced way. The protocol chosen is particularly sensitive to sex-related differences and mild phenotypes, especially in aged individuals (Takeshita et al., 2017). One-year-old animals (n = 10 mice/group) were analyzed from either *SV* (n = 5 females and 5 males) or WT (n = 4 females and 6 males) genotypes. Because each test was performed in 3 consecutive trials on each animal, intra-subject variability was assessed in the statistical analysis.

First, trial number (1, 2, 3) was not statistically significant neither as a single factor, nor in combination with genotype, sex, nor both. Therefore, all animals, regardless of sex and genotype, behave similarly throughout the 3 trials of their session (**Fig. 4.32**).

Second, the inter-subject analysis showed differences in grip strength between animals of different genotypes when segregated by sex (P = .013), which means that differences observed in *SV* mice when compared to WT depended on the sex of the animals. To know whether both or only one sex displayed these genotype-dependent differences, males and females were analyzed separately. Interestingly, *SV* females (P = .004) but not males (P = .906) displayed grip strength impairments in their limb musculature (**Fig. 4.32A**). These impairments were specific to the hindlimb muscles, since the evaluation of forelimbs alone did not yield any significant results for either male (P = .178) nor female mice (P = .263) (**Fig. 4.32B**). These results suggest that the reduced muscle strength observed in middle-aged MVI knockout mice is both sex- and muscle-dependent.

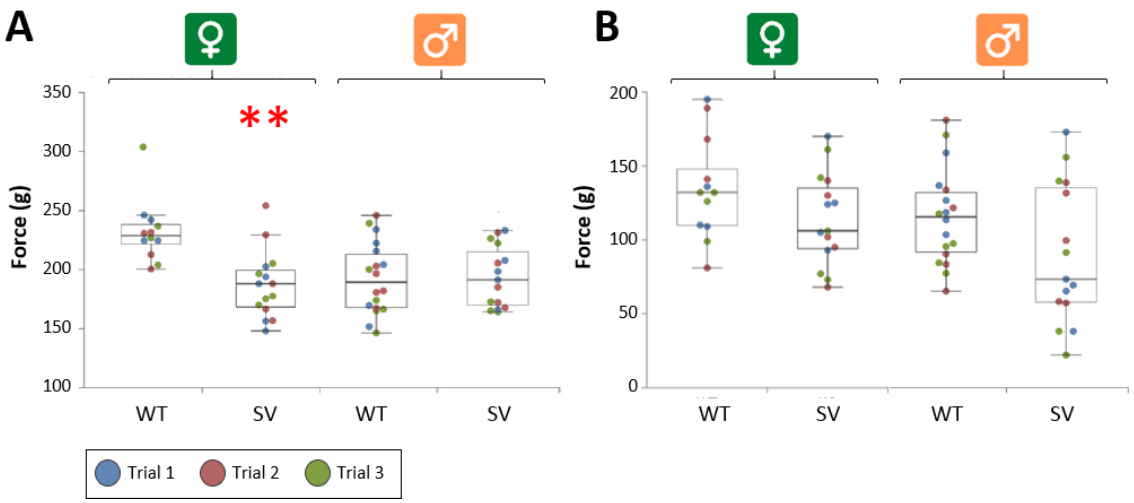

Figure 4.32. Myosin VI knockout impairs grip strength in middle-aged female mice. (A-B) Grip strength in forelimbs+hindlimbs (A) or only forelimbs (B) of female (green ♀) and male (orange ♂) mice at P365. Datapoints (coloured circles) represent grip strength measurements of each animal in Trial 1 (blue), 2 (red), or 3 (green). Bold mid-line inside each box represents mean. Boxplot whiskers represent lower and upper extremes. Repeated measures two-way ANOVA, $P \leq .01$ (**). **Abbreviations:** SV = MVI global knockout mice; WT = wild-type (control) mice.

4.8.3. Neuromuscular junctions of middle-aged MVI knockout mice are smaller in fast-twitch TA muscle

Based on the results of the grip strength test (**Fig. 4.32**), I decided to study the morphological parameters of NMJs of middle-age female mice lacking MVI in *TA*

(predominantly fast-twitch fibers) and *SOL* (predominantly slow-twitch fibers) muscles (10 NMJs/mouse, n = 5-6 female mice/group).

Only NMJs from *TA* muscles were significantly different in female *SV* mice. Specifically, *SV* mice had decreased AChR area (P = .016) and Endplate area (P = .033), but increased AChR perimeter (P = .003), which suggests the development of more elongated or intricate NMJs (**Fig. 4.33A**). On the other hand, slow-twitch *SOL* muscle displayed no significant differences in size when comparing *SV* and WT female mice at P365 (**Fig. 4.33C**). When the same parameters were analyzed in younger adults (P120), only a mild reduction in Endplate diameter (P = .037) was observed in the *TA* but not in *SOL* muscles of *SV* mice, indicating a more pronounced phenotype in older mice.

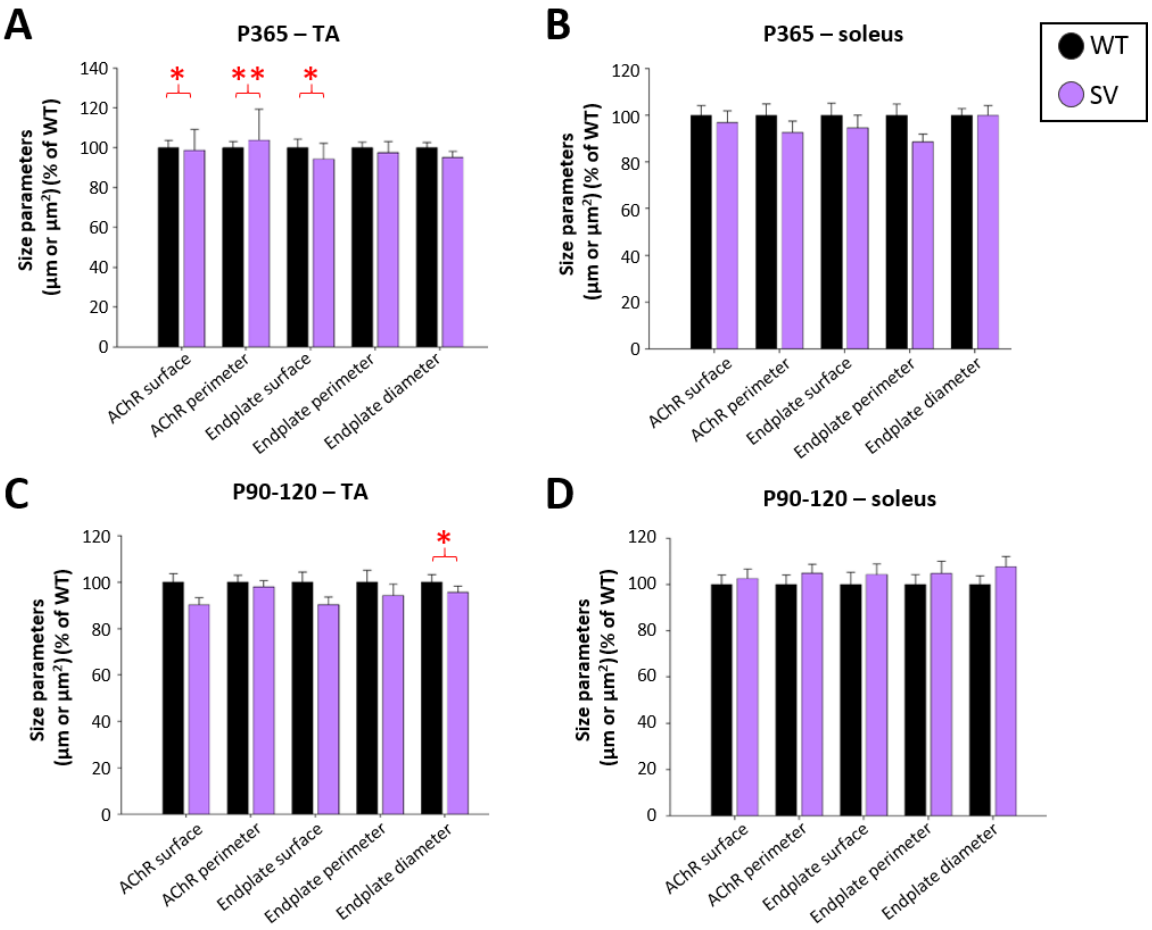

Figure 4.33. Myosin VI knockout mildly reduces NMJ size at P365 in fast-twitch TA muscle. Size parameters (AChR surface, AChR perimeter, Endplate surface, Endplate perimeter, Endplate diameter) represented as a percentage of WT for each parameter, in NMJs in *TA* **(A, C)** and *SOL* muscles (**B, D)** obtained from P365 (A-B) or P90-120 (C-D) female mice. Mann-Whitney U test, $P \leq .05$ (*), $P \leq .01$ (**). Bars represent mean and error bars represent SEM. **Abbreviations:** SV = MVI global knockout mice; WT = wild-type (control) mice.

4.8.4. Aging-related disruption of NMJs is mildly enhanced in MVI knockout mice

Finally, I decided to explore other hallmarks of neuromuscular aging by manually assessing the level of postsynaptic fragmentation and disruption of integrity. To this end, I quantified the number of fragments of each NMJ at P365 (10 NMJs/mouse, n = 6 female mice/group) and classified the NMJs depending on their fragmentation level into 4 classes: 1-2 fragments (Class 1), 3-4 fragments (Class 2), 5-6 fragments (Class 3), 7 or more fragments (Class 4) (**Fig. 4.34A**). Middle-aged *SV* female mice did not exhibit increased NMJ fragmentation measured as number of NMJs within each fragmentation class (**Fig. 4.34B-C**) when compared to their WT counterparts, in neither *TA* nor *SOL* muscles. On the other hand, a minor reduction was found in the number of fragments per NMJ in *SOL* (P = .023) but not in *TA* muscles of *SV* mice (**Fig. 4.34D-E**).

Interestingly, the integrity of NMJ branches, measured as the number of AChR-devoid "holes" within each NMJ (Schmidt et al., 2011) and the presence or absence of dispersion of AChRs in the edges of pretzel branches (**Fig. 4.35A**), showed muscle type-dependent differences (10 NMJs/mouse, n = 5-6 female mice/group). In the absence of MVI, NMJs from *TA* but not from *SOL* muscles were characterized by: 1) increased number of NMJs with "holes" within AChR branches (P = .031) (**Fig. 4.35B**), 2) increased number of holes per NMJ in those NMJs that are perforated (P = .025) (**Fig. 4.35F)**, and 3) increased number of NMJs with dispersed AChR in the edges of NMJ branches (P = .019) (**Fig. 4.35D**).

Altogether, the results described in sections 4.8.3. and 4.8.4. show that MVI knockout in middle-age female mice impairs NMJ morphology and integrity in fast-twitch *TA* muscles. However, the relationship of the observed morphological differences and the muscle strength of *SV* mice requires further investigation.

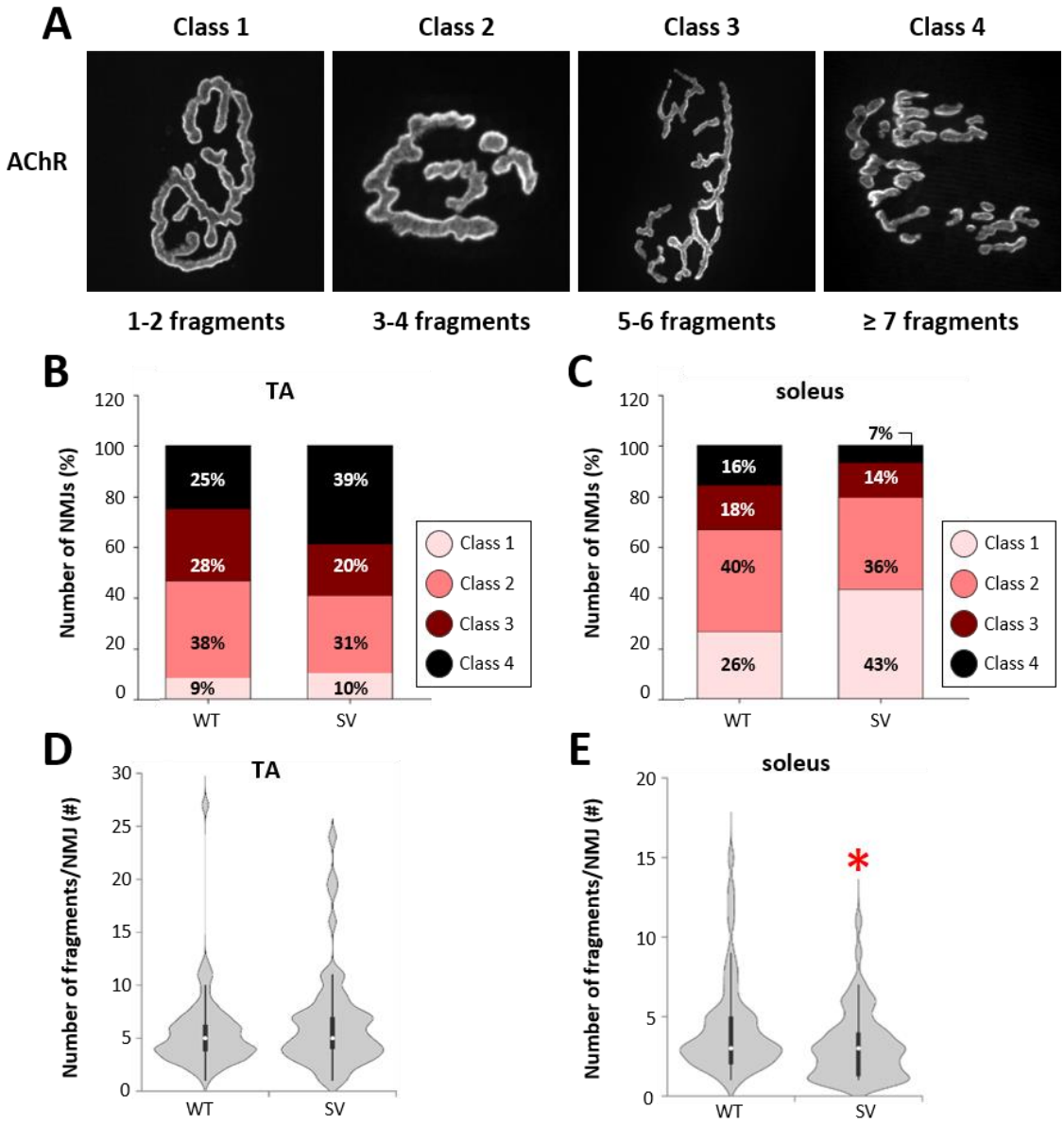

Figure 4.34. Myosin VI knockout does not promote NMJ fragmentation. (A) Representative images of neuromuscular fragmentation classes assessed at P365 based on AChR morphology (labelled with BTX, white). **(B-C)** Number of NMJs (% of total NMJs measured for each group) that classify as class 1, 2, 3, or 4, in *TA* (B) and *SOL* (C) muscles from control wild-type and MVI knockout mice. Chi-Square test, not significant. **(C-D)** Number of fragments per NMJ (#) in *TA* (D) and *SOL* (E) muscles from control wild-type and MVI knockout mice. Kruskal-Wallis U test, $P \leq .05$ (*). Violin plot (grey shape) represents frequency of values. Narrow boxplot inside each violin plot (black) represents mean (small white circle) ± lower and upper extremes (black lines). **Abbreviations:** SV = MVI global knockout mice; WT = wild-type (control) mice.

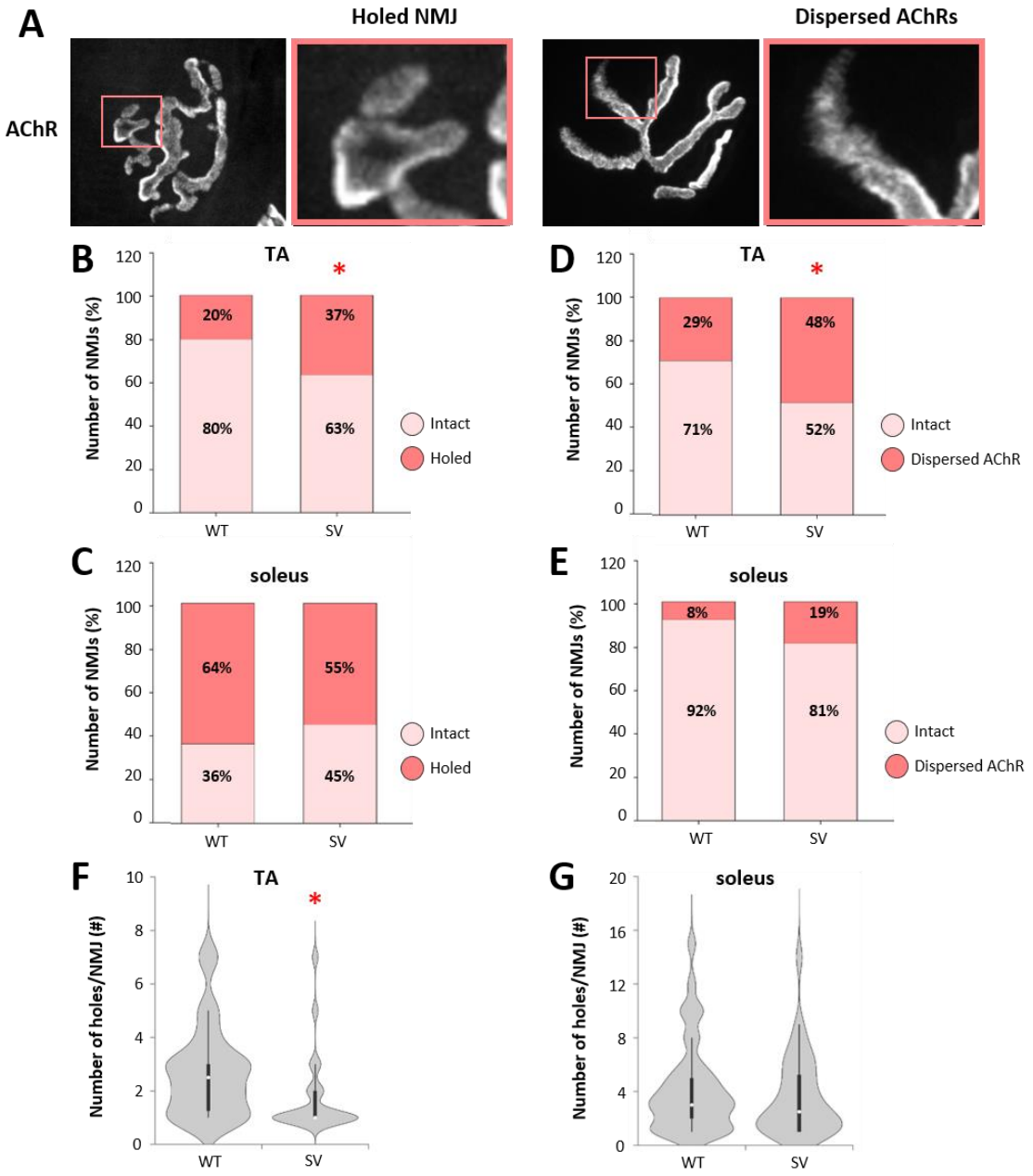

Figure 4.35. Myosin VI knockout impairs NMJ integrity. (A) Representative images of disrupted AChR clusters (labelled with BTX, white) assessed at P365, showing holes within the branches (left panel) or dispersed AChR on the edges (right panel). Pink squares show zoomed area. **(B-C)** Number of NMJs (% of total NMJs measured for each group) that classify as intact or with holes within AChR branches in the *TA* (B) or *SOL* (C) muscles of control wild-type and MVI knockout mice. Chi-Square test, *TA:* X^2 (1, N = 129) = 4.278, $P \leq .05$ (*); *SOL:* X^2 (1, N = 119) = 0.948, $P > .05$ (not significant). **(D-E)** Number of NMJs (% of total NMJs measured for each group) that classify as intact or with dispersed AChRs in the branches edges in the *TA* (D) or *SOL* (E) muscles of control wild-type and MVI knockout mice. Chi-Square test, $P \leq .05$ (*). **(F-G)** Number of holes per NMJ (#) in *TA* (F) and *SOL* (G) muscles from control wild-type and MVI knockout mice. Kruskal-Wallis U test, $P \leq .05$ (*). Violin plot (grey shape) represents frequency of values. Narrow boxplot inside each violin plot (black) represents mean (small white circle) ± lower and upper extremes (black lines). **Abbreviations:** SV = MVI global knockout mice; WT = wild-type (control) mice.

"*Sciences provide an understanding of a universal experience,*

arts are a universal understanding of a personal experience.

they are both a part of us and a manifestation of the same thing,

the arts and sciences are avatars of human creativity."

Mae Jemison,

first African-American female astronaut in space (1992)

CHAPTER 5: DISCUSSION

The intimate contact between motoneurons, muscle fibers, and perisynaptic Schwann cells at the NMJ reflects a mutual regulation throughout development that is tightly controlled by a multitude of intracellular signaling pathways (Alvarez-Suarez et al., 2020; Tintignac et al., 2015). This holds true to the extent that morphological or functional aberrations in these regulatory processes often lead to neuromuscular disorders, whose pathological manifestations include muscle wasting and fatigue, and even premature death (Li et al., 2018; Verschuuren et al., 2016). Moreover, the development and function of pre- and postsynaptic subcellular compartments depend on highly dynamic cytoskeletal components, and impairments of actin, MTs, and/or cytoskeleton-regulating proteins can lead to neurological disorders and myopathies, including Duchenne's muscular dystrophy (DMD), amyotrophic lateral sclerosis (ALS), and nemaline myopathy (NM) (Jungbluth et al., 2018; Khairallah et al., 2013; Kounakis & Tavernarakis, 2019; Lasser et al., 2018). Nevertheless, the molecular mechanisms underlying the etiopathology of these disorders are still poorly understood. Elucidating the regulation of healthy neuromuscular function can provide meaningful information for the cause and pathogenesis of neuromuscular disorders.

In an attempt to investigate some of these mechanisms, my research focused on a rather specific aspect of the highly complex structures that NMJs constitute: the development and maintenance of the postsynaptic machinery. I identified two cytoskeletal-interacting proteins, drebrin and myosin VI, that could play a relevant role in this context. Drebrin, as a stabilizer of actin filaments, was previously shown to actively regulate postsynaptic morphology and function of dendritic spines (Aoki et al., 2005; Hayashi et al., 1996; Honkura et al., 2008), as well as muscle adhesion, fusion, and differentiation (Mancini et al., 2011). However, to my knowledge, the role of drebrin at the vertebrate NMJ had not been studied so far. On the other hand, previous research of our group and others showed that unconventional actin-based motor myosin VI not only is involved in recycling of postsynaptic elements at the CNS (Wagner et al., 2019) and in skeletal muscle differentiation (Karolczak et al., 2015a; Lehka et al., 2020), but that it also localizes to the synaptic compartment of muscle cells in both invertebrates, such as *Drosophila* (Kisiel et al., 2011), and vertebrates (rodents and humans) (Karolczak et al., 2013, 2014, 2015a).

After exploring some of the functions that these proteins may play using *in vitro* models of the muscle postsynaptic machinery, I performed preliminary assessment of their function *in vivo* by taking advantage of mice lacking either drebrin or myosin VI.

5.1. Drebrin as a novel component of the muscle postsynaptic and contractile machineries

In the first part of my doctoral research, I identified drebrin as a novel protein localized at the neuromuscular postsynaptic machinery throughout development (Fig. 4.1). I confirmed these findings in different muscles (Fig. 4.3) and with various methodological approaches (Figs. 4.4, 4.5). These results are in line with the postsynaptic accumulation of drebrin in dendritic spines of neurons from chicken (Shirao et al., 1987), rat (Hayashi et al., 1996), human (Harigaya et al., 1996), and mouse brains (Kobayashi et al., 2007).

Drebrin localization in the muscle was not limited to the postsynaptic machinery, but also presented a striated pattern across the entire myofiber that resembled that of the typical sarcomeric structures in skeletal muscle. Indeed, due to its colocalization with α-actinin, I identified sarcomere Z-discs as the second cellular compartment to which drebrin is targeted in skeletal muscle fibers (Fig. 4.6). A previous report about drebrin ortholog in *C. elegans*, DBN-1, showed that DBN-1 reversibly and rapidly translocates between actin I-bands and myosin M-lines within muscle contraction cycles (Butkevich et al., 2015). Strikingly, when functional DBN-1 is lost, the distribution of actin and other actin-binding proteins of the sarcomere is affected: F-actin appears disorganized and α-actinin loses its compact appearance at dense bodies (Z-disc analogues in nematode muscles that anchor cortical actin to the ECM). One explanation proposed for these phenomena is that DBN-1 protects actin filaments from depolymerization at dense bodies and in proximal actin zones in the contracted state of the sarcomere (Butkevich et al., 2016). In vertebrates, drebrin purified from brains of rat embryos competes with α-actinin and tropomyosin for binding to actin, and it inhibits the cross-linking activity of α-actinin (Ishikawa et al., 1994). Moreover, both drebrin and tropomyosin inhibit the actin-activated ATPase activity of myosin II (Hayashi et al., 1996), suggesting that drebrin may play a direct role in muscle contraction. Importantly, many congenital myopathies are caused by mutations in genes encoding contractile components, such as titin, skeletal α-actin, and β heavy chain of slow-twitch muscle myosin. Nemaline myopathies, in particular, are characterized by the presence of so-called nemaline rods, which are believed to be derived from Z-discs but have unknown ethiology (Jungbluth et al., 2018).

Interestingly, drebrin and DBNL are overexpressed in mitochondrial encefalomyopathy (GSE1462 accession number in database for gene expression profiling Gene Expression Omnibus, http://www.ncbi.nlm.nih.gov/geo/) and sporadic late-onset nemaline myopathy (Naddaf et al., 2022), respectively.

The intimate relationship between drebrin and other contractile components suggests a promising line of research. These preliminary data have set the foundation for potential follow-up experiments, such as evaluation of the sarcomere structure and function in drebrin knockout mice, in order to better explore the role of drebrin at the contractile compartment of vertebrate skeletal muscle.

5.2. Role of drebrin in postsynaptic neurotransmitter receptor clustering

Aiming to assess whether drebrin plays a role in postsynaptic formation, organization, and/or maintenance, I downregulated *Dbn1* expression in the simplified model of aneurally cultured C2C12 myotubes. I found severe impairments in the formation of AChR clusters in both agrin-dependent (Fig. 4.8) and laminin-dependent (Fig. 4.9) models. Moreover, I specifically identified postsynaptic F-actin rearrangements as a crucial function of drebrin in this process – pharmacological blockade of the ability of drebrin to remodel F-actin similarly inhibited AChR cluster formation (Fig. 4.10). Other groups have observed that siRNA-mediated downregulation of drebrin has comparable effects to BTP2 treatment when studied in the context of myoblast differentiation (Mancini et al., 2011) and prostate cancer cell invasion (Dart et al., 2017). Therefore, drebrin-mediated F-actin rearrangements are a common core mechanism for both postsynaptic organization and myoblast differentiation.

To further explore the underlying mechanistic pathway of this phenotype, I assessed drebrin function as F-actin and MT cross-linker. Based on previous studies describing drebrin-EB3 interaction at the core of drebrin main functions (Bazellières et al., 2012; Dart et al., 2017; Poobalasingam et al., 2021; Worth et al., 2013), I determined whether drebrin depletion would impact EB3 distribution and, therefore, organization of dynamic MTs. First, I verified the interaction between drebrin and EB3 in postsynaptic machinery-forming myotubes (Fig. 4.14). This interaction was not studied before in this model of skeletal muscle cells, but it was previously reported for neurons (Geraldo et al., 2008), COS-7 cells (Worth et al., 2013), and colon epithelial cells (Bazellières et al., 2012). Second, I found that drebrin downregulation reduced the number of EB3-decorated MTs specifically under the postsynaptic machinery but not in other areas of the cell (Fig.

4.15). These results indicate impairments in synaptic MT capture but not in whole-cell stability of the MT network, reinforcing the idea that the drebrin-EB3 interplay is locally activated in regions of cytoskeletal dynamic remodeling. Consistently, other groups have found Cdk5-drebrin-EB3 pathway to be essential for the development of certain morphological features necessary for cell function, such as apico-basal elongation for cell polarity of intestinal epithelial cells (Bazellières et al., 2012), stabilization of filopodia for cancer invasive activity in luminal epithelial cells of malignant prostate glands (Dart et al., 2017), neuritogenesis in embryonic cortical neurons (Poobalasingam et al., 2021), and dendritic spine maturation in mature neurons undergoing LTP (Gordon-Weeks, 2016).

On the other hand, pharmacological blockade of drebrin-mediated rearrangements of actin filaments reduced $EB3^{+}$ surface under AChR clusters but not EB3 foci number, possibly impacting MTs ability to coalesce (Fig. 4.16). The difference between the effect of drebrin knockdown and its pharmacological inhibition could be explained by broader and more profound alterations on cytoskeleton dynamics upon drebrin depletion at mRNA and protein levels, than the localized effects of BTP2 preventing drebrin from inducing F-actin rearrangements (Mercer et al., 2010). On the contrary, a recent work showed how BTP2 treatment reduces the number of EB1 puncta that colocalize with drebrin at the cortical actin mesh of migrating neurons (Shan et al., 2021). However, the versatility of drebrin that allows for different cellular functions, such as migration-associated actin reorganization, actin-MT cross-linking, or interaction with postsynaptic proteins, could account for the differences I observed in BTP2 and siRNA effects on MT organization compared to other studies. As a potential model based on my results, postsynaptic drebrin would cross-link F-actin bundles and MTs and further stabilize them by coalescing multiple MTs, which have been recruited to the postsynaptic compartment (**Fig. 5.1**).

Other postsynaptic proteins and drebrin-interacting partners are likely to mediate drebrin cross-linking function. It is noteworthy that BTP2 inhibits NFAT (nuclear factor of activated T cell) nuclear translocation in T cells through blockade of store-operated CRAC (Ca^{2+} release-activated Ca^{2+}) channels (Ishikawa et al., 2003; Trevillyan et al., 2001). Calcium-mediated nuclear translocation of NFAT is indispensable for gene transcription leading to hypertrophy of cardiomyocytes, including cell growth and increased protein synthesis transcription programs (Molkentin et al., 1998). Interestingly, scaffolding protein Homer, known interactor of drebrin in dendritic spines (Shiraishi-Yamaguchi et

al., 2009), enhances NFAT-dependent signaling in differentiating myotubes by increasing the release of Ca^{2+} from intracellular stores (Stiber et al., 2005). Not only Homer binds to drebrin, but its tetrameric conformation is required for efficient drebrin-mediated bundling of F-actin (Hayashi, 2019; Li et al., 2019). Additionally, Homer family has been shown to regulate postsynaptic machinery interactions at the CNS (Ehrengruber et al., 2004) and Homer1/2 isoforms are both enriched postsynaptically at the human NMJ (Salanova et al., 2011). On the other hand, transcription levels of Homer1 remained similar to the control when drebrin was depleted in C2C12 myotubes (Fig. 4.18), suggesting that drebrin-Homer crosstalk does not rely on the regulation of gene transcription. Remarkably, both Homer1 and CRAC channel subunits, Orai1 and Stim1, have been described in the literature as correlates of aberrant Ca^{2+} homeostasis in the context of congenital myopathy and DMD (Jungbluth et al., 2018; Stiber et al., 2008; Zhao et al., 2012), indicating that skeletal muscle health depends on proper CRAC channel function. Finally, drebrin seems to regulate F-actin depolymerization and repolymerization following depletion of intracellular Ca^{2+} stores, which is needed to activate CRAC channels (Mercer et al., 2010). It has been proposed that modulation of actin dynamics could be triggered by interaction of drebrin with Homer and IP_3R (inositol triphosphate receptor), controlling the release of intracellular Ca^{2+} stores from the SR (Mercer et al., 2010). Furthermore, EB3 binds to IP_3Rs in endothelial cells to promote their clustering and thus, organizes IP_3-evoked Ca^{2+} signals (Geyer et al., 2015).

The specific mechanism through which drebrin is involved in molecular pathways regulating intracellular Ca^{2+} levels and how it may affect neuromuscular transmission remains largely unexplored. Nevertheless, my observations strongly indicate that drebrin could play an important role in the clustering of the muscle postsynaptic machinery via Ca^{2+}-modulated rearrangements of actin and MT cytoskeletal networks.

5.3. Role of drebrin in postsynaptic stability

In previous research, MTs were shown to play a key role in AChR turnover rather than cluster formation (Basu et al., 2015; Bernadzki et al., 2017), however their involvement in maintenance of cluster stability remains poorly understood. Microtubule-based transport is critical for RNA and protein distribution in skeletal myofibers, and the synaptic-specific arrangement of the MT network restricts mobility of RNAs produced by synaptic myonuclei (Denes et al., 2021). Some of the mechanisms for recruitment of MTs to the NMJ require the interaction between +TIP protein CLASP2, actin, and LL5β (Basu et al., 2015; Lansbergen et al., 2006), as well as binding of scaffold protein liprin-α-1 to

the synaptic anchor DGC (Bernadzki et al., 2017). Disruption of any of these two nerve-dependent mechanisms impaired AChR clustering and, in the case of CLASP2, also reduced subsynaptic myonuclei number (Bernadzki et al., 2017; Schmidt et al., 2012). In accordance with these studies, *in vitro* experiments described in this thesis also showed impairments in nerve-dependent postsynaptic organization in an agrin-induced model of AChR cluster formation (Fig. 4.8). Moreover, I also demonstrated that these impairments are associated with deficient MT capture and organization under AChR clusters in a muscle-dependent mechanism (laminin-induced model) (Fig. 4.9), suggesting independent pathways in drebrin-, CLASP2-, and liprin-mediated regulation of postsynaptic stability through MT organization.

Scaffolding protein MACF1 is another synaptic organizer of MT-associated proteins, such as EB1 and MAP1b, actin-associated protein vinculin, and AChR-stabilizing protein rapsyn, and it regulates maintenance rather than formation of the postsynaptic machinery (Oury et al., 2019). Furthermore, it has been recently demonstrated that MACF1 regulates NMJ stability through controlling MT organization around myonuclei (Ghasemizadeh et al., 2021), which highlights the importance of synaptic myonuclei distribution for proper MT-mediated NMJ formation and function. Based on this, together with reports on the role of drebrin in nuclear migration (Trivedi et al., 2017), I screened for major alterations in the pool of synaptic nuclei in drebrin-depleted C2C12 myotubes and found no significant differences (Fig. 4.17). Likewise, in the search for postsynaptic proteins regulated by drebrin, neither rapsyn nor rapsyn-binding MACF1 gene expression was significantly affected by *Dbn1* downregulation (Fig. 4.18). Since rapsyn and AChRs are co-transported to the postsynaptic membrane inside the same exocytic vesicles (Marchand et al., 2000), it seemed reasonable that unaffected synthesis and delivery of AChRs (Fig. 4.13) would be accompanied by unchanged rapsyn levels. Accordingly, MACF1 loss does not affect rapsyn expression nor it recapitulates rapsyn loss, however the presence of rapsyn was found to be essential for MACF1 association with AChRs (Oury et al., 2019). Similarly, I found that rapsyn interacts with both EB3 and drebrin, independently of the phosphorylation at Ser142 residue of the latter (Fig. 4.19). Moreover, I showed that overall drebrin recruitment to the postsynaptic machinery is independent of its phosphorylation state at Ser142 (Fig. 4.4). In a previous report, it was proposed that Cdk5-mediated phosphorylation of drebrin at this particular residue is important but not essential for its actin-bundling activity and interaction with EB3 (Worth et al., 2013), and the results obtained in this thesis do not contradict this idea.

Several interpretations can be extracted from the abovementioned combination of results and literature review. First, drebrin probably regulates MT capture in a non-

redundant pathway from those previously described for CLASP2-LL5β and DGC-liprin-α-1. Second, it is unlikely that the role of drebrin in MT organization includes effects on myonuclei distribution and morphology, which would suggest separate regulatory mechanisms from those mediated by MACF1. These would be in line with the model proposed by Sanes and Lichtman for synapse formation, in which agrin-MuSK signaling activates two pathways: a rapsyn-dependent pathway for AChR clustering and a rapsyn-independent pathway for localized transcription (Sanes & Lichtman, 2001). Third, drebrin could serve as a hub for cross-linking actin bundles and MTs to the postsynaptic machinery by forming a complex with rapsyn and EB3 (**Fig. 5.1**). Finally, Cdk5-mediated phosphorylation of Ser142 is not necessary for drebrin recruitment to the synaptic compartment nor its interaction with rapsyn. However, because it enhances EB3-drebrin interaction and drebrin-mediated F-actin bundling, this phosphorylation site could be relevant for the formation of the complex composed of drebrin, rapsyn, EB3 and associated cytoskeletal filaments at the postsynaptic compartment.

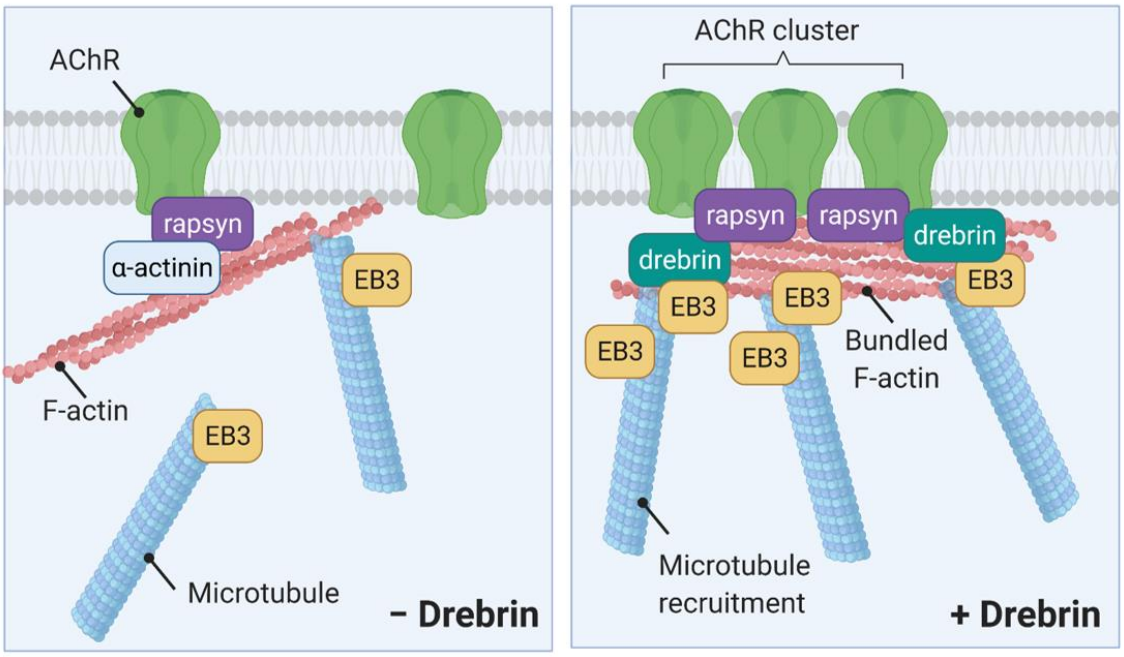

Figure 5.1. Proposed model of drebrin mechanism of action at the skeletal muscle postsynaptic machinery. In drebrin-depleted myofibers (left), other mechanisms for AChR clustering and stabilization, such as α-actinin cross-linking of F-actin and its interaction with rapsyn might mediate postsynaptic machinery organization. When drebrin is present (right), α-actinin could be displaced from F-actin, however drebrin would stabilize AChR clusters by both bundling actin filaments and cross-linking them to MTs via EB3-rapsyn complex formation. Illustration created with BioRender.com.

Additionally, drebrin loss could affect the interaction between rapsyn and α-actinin, which form a ternary complex with AChRs (Dobbins et al., 2008). Moreover, not only α-

actinin depletion inhibits AChR clustering, but it was proposed that it binds to rapsyn upon Cdk5 phosphorylation (Dobbins et al., 2008). This Cdk5-independent ability of drebrin to bind to rapsyn could be a separate pathway to guarantee F-actin mediated stabilization of AChR clusters in myopathy-associated loss of normal α-actinin function (North & Beggs, 1996; Schultheiss et al., 1992) or in drebrin-induced α-actinin displacement (Ishikawa et al., 1994) (**Fig. 5.1**). Drebrin colocalization with α-actinin in Z-discs (Fig. 4.6) supports their shared actin-associated functions, however the relationship between these two proteins in skeletal muscle and, specifically at the NMJ, requires further research. Altogether, my data suggest that drebrin regulates postsynaptic stability through subsynaptic actin and MTs, and potentially by linking these cytoskeletal networks to rapsyn. Furthermore, this model is in accordance with the role of MT recruitment in AChR cluster stability proposed by other groups (Basu et al., 2014, 2015; Schmidt et al., 2012). More research is necessary to further explore the crosstalk between drebrin, rapsyn, and MT-associated proteins, as well as their specific role in postsynaptic maintenance and stability.

5.4. Role of drebrin in postsynaptic maturation

Morphological remodeling of the postsynaptic machinery from plaque to pretzel, where AChRs are reorganized in perfect apposition to presynaptic nerve terminals, is a hallmark of mature, healthy NMJs (Tintignac et al., 2015). At the molecular level, postnatal maturation also includes the replacement in pentameric AChR channels of γ for ε subunits, which provide faster recovery rates from desensitization, higher Ca^{2+} permeability, and increased half-life of AChRs (Medina-Moreno & Henríquez, 2021). Altogether, these developmental changes lead to stable and more efficient neuromuscular transmission than that observed in embryonic or pathological contexts. Actin-rich structures with the ability to remodel the ECM and reorganize membrane proteins, namely synaptic podosomes (Bernadzki et al., 2014; Veillat et al., 2015), were proposed to underlie the structural changes of AChR clusters *in vitro* (Proszynski et al., 2009). However, most of the molecular signaling pathways and cytoskeletal proteins underlying maturation of the postsynaptic machinery remain largely unknown.

In my assessment of the role of drebrin at the postsynaptic machinery *in vitro*, I noticed that the synaptic localization of the protein appeared in different subcompartments: some clusters were characterized by a dominant colocalization of AChRs and drebrin, while others also presented puncta-like accumulation of drebrin in AChR-free areas that

correspond to the domain occupied by synaptic podosomes (Fig. 4.5). Because drebrin is an F-actin-binding protein, it was reasonable to expect that it colocalized with the core of these structures, but not with their cortex, which I confirmed through immunofluorescence (Fig. 4.12). Similarly, MACF1 colocalized with AChRs *in vivo* but also to synaptic podosomes *in vitro* (Oury et al., 2019). Moreover, actin-binding and scaffolding protein, Tks5, that also localizes to the core of synaptic podosomes (Proszynski et al., 2009), localizes to AChR-devoid areas of the NMJ in early developmental stages but colocalizes with AChR-rich branches in adulthood (Pęziński et al., 2021). In order to explore whether drebrin localization had any functional significance, I analyzed podosome formation in drebrin-depleted C2C12 myotubes. I found that drebrin downregulation led to a reduction of up to 50% of clusters with podosomes when compared to the control, but did not affect the number of podosomes per cluster (Fig. 4.12). This suggests a role for drebrin in pathways regulating the formation of podosomes, and therefore, the topological remodeling of the postsynaptic machinery.

Accordingly, previous work from our research group demonstrated that other actin-regulating proteins colocalize with the core of synaptic podosomes and are crucial for laminin-induced cluster maturation *in vitro*. For instance, depletion of Amotl2 results in a dramatic enlargement of synaptic podosomes and alters the localization of other podosome components (Proszynski & Sanes, 2013). Moreover, Amotl2 synthesis is upregulated *in vivo* during the second and third postnatal weeks, when NMJ morphological maturation takes place, and its postsynaptic distribution is confined to AChR-free areas throughout the entire development (Proszynski & Sanes, 2013). Opposite to Amotl2, Tks5 downregulation leads to almost complete loss of synaptic podosomes in C2C12 myotubes, which form unstable, immature AChR clusters (Pęziński et al., 2021). Most importantly, Tks5 downregulation results in reduced interactions between actin and rapsyn but no major alterations in rapsyn distribution under AChR clusters of C2C12 myotubes (Pęziński et al., 2021). To further assess the parallelisms between drebrin and Tks5 or Amotl2, it would be interesting to explore whether EB3-rapsyn interaction and podosome morphology are impaired by drebrin loss.

Some of the molecular players of synaptic podosome formation were elucidated in recent years. After triggering of actin polymerization, podosomes mature due to the recruitment of Tks5 and mechano-GTPase dynamin-2. Specifically, phosphorylated dynamin-2 forms a stabilizing belt-shaped structure at the actin core of podosomes, and

its disappearance is followed by podosome disassembly (Lin et al., 2020). Simultaneously, ECM remodeling by MT1-MMP disrupts the stabilization mechanisms of AChR clusters, thus resulting in higher turnover rates of AChRs (Chan et al., 2020). In a yet unclear mechanism, dynamin-2 downregulation impairs local ECM degradation and reduces podosome size and lifespan (Lin et al., 2020). Similar to my results for drebrin (Fig. 4.12), dynamin-2 depletion impairs podosome formation without affecting their number per cluster (Lin et al., 2020). Notably, loss of dynamin-2 was associated with deficient NMJ function in *Drosophila,* and loss of ECM-remodeling MT1-MMP was associated with impairments in NMJ maturation in mice (Chan et al., 2020; Lin et al., 2020). Dynamin-2 actin-bundling activity depends on Src-mediated phosphorylation of residue Y597, which also regulates its targeting to synaptic podosomes (Lin et al., 2020). It would be interesting to explore whether drebrin phosphorylation state impacts synaptic podosomes and AChR cluster maturation. Importantly, drebrin inhibits dynamin-2 function by interacting with actin-regulating cortactin, and loss of drebrin in HEK293 cells leads to enhanced endocytosis of dynamin-dependent cargo (Li et al., 2017). Cortactin is also found at the core of synaptic podosomes (Proszynski et al., 2009), and it has been involved in early and late stages of synaptic and non-synaptic podosome formation in skeletal and vascular smooth muscle cells (Lin et al., 2020; Webb et al., 2006). Interestingly, mutations in *DNM2* (human gene encoding dynamin-2) have been associated with centronuclear myopathy of skeletal fibers, and alterations in muscle Ca^{2+} homeostasis and excitation-contraction coupling were described in mouse models of dynamin-2-related myopathy (Jungbluth et al., 2018). Given the potential role of drebrin in CRAC channel function in skeletal muscle, it would be interesting to evaluate whether the interplay between drebrin and dynamin-2 extends beyond synaptic podosome formation. Finally, overexpression of a *DNM2* mutant with high actin-bundling activity lead to reduced surface covered by AChRs (Lin et al., 2020). Similarly, I observed reduced AChR surface in drebrin knockout mice (Fig. 4.20), however not in C2C12 myotubes (Fig. 4.9C). Other actin-modulating proteins have similar discrepancies between *in vivo* and *in vitro* models. For instance, Arhgef5 is relevant for podosome formation in MCDK (kidney cells) and NIH/3T3 cells (fibroblasts) (Kuroiwa et al., 2011) and binds to phosphorylated α-dystrobrevin-1, whose loss significantly impairs AChR cluster maturation in C2C12 mytoubes (Bernadzki et al., 2020; Pawlikowski & Maimone, 2009). Opposite to my results for drebrin, Arhgef5 depletion does not inhibit the formation of complex AChR clusters

nor the presence of synaptic podosomes in C2C12 myotubes, however it leads to increased NMJ fragmentation in adult muscle (Bernadzki et al., 2020).

Altogether, it is tempting to speculate that the role of drebrin in podosome formation is to keep dynamin-2 activity under control through interaction with cortactin. If this model held true, larger and/or longer-lived podosomes should be observed in drebrin-depleted myotubes, parameters that were not evaluated in this thesis but constitute an interesting follow-up. However, participation of other actin-organizing proteins increases the complexity of podosome formation mechanisms involving actin remodeling. For instance, ephexin1 was proven crucial in regulating AChR stability and topological maturation through downstream RhoA-dependent reorganization of F-actin (Shi et al., 2010). Specifically, ephexin1 signaling contributes to dispersion of AChR in synaptic podosomes, probably by weakening of the interaction between AChRs and the stabilizing actin cytoskeleton (Shi et al., 2010). Notably, ephexin1 and drebrin could share regulatory pathways: upstream ephexin1 regulators interact with cortactin (Lai et al., 2001) and ephexin1-mediated activation of RhoA pathway is enhanced when phosphorylated by Cdk5 (Fu & Ip, 2007). Therefore, upstream regulators and post-translational modifications of drebrin should be addressed in future studies that explore its role in synaptic podosome formation.

Participation of drebrin in morphological maturation of the postsynaptic machinery was extensively studied in the CNS, specifically in morphogenesis and maturation of dendritic spines of hippocampal excitatory synapses (Takahashi et al., 2003). In this context, activity-induced drebrin clustering is necessary for proper arrangement of components of the postsynaptic density, such as PSD-95 and F-actin (Takahashi et al., 2009). Furthermore, drebrin was proposed as the trigger for cell remodeling processes in neurons, glia, and other non-neuronal cell types, and it has been associated with non-synaptic podosomes and podosome-like structures in primary endothelial cell lines, fibroblast-like cell cultures and HUVEC cells, but never in myotubes (Asada et al., 1994; Majoul et al., 2007; Peitsch et al., 1999). In summary, my results support the existing literature on the role of drebrin in postsynaptic maturation through rearrangements of the cortical F-actin cytoskeleton, and reveal a novel cell type in which this phenomenon takes place, namely skeletal muscle cells.

5.5. Concluding remarks on drebrin as a cytoskeletal organizer of the postsynaptic machinery

The multiple subcellular localizations of drebrin and its ability to translocate between subcompartments within both sarcomeres and the postsynaptic machinery reflect the multifaceted role of this actin-binding protein in cellular processes of skeletal muscle. The versatility of drebrin distribution is an important molecular mechanism underlying neuronal migration processes and organization of structures modulated by F-actin remodeling, such as the base of filopodia in leading processes, the transitional zone of axonal growth cones, and axonal actin patches in collateral axon branching (Hanamura, 2017). Disruption of developmental and plasticity processes mediated by drebrin was shown to contribute to the development of synaptic dysfunction, certain neurological disorders, and subsequent cognitive impairments (Kojima & Shirao, 2007). Consistent with the existing literature, I have demonstrated that drebrin can be targeted to different cytoskeletal components of the postsynaptic machinery, where it can interact with both actin and +TIP protein EB3 and act as both cross-linker and MT organizer and/or recruiter. Drebrin interacts with rapsyn, a major regulator of AChR clusters and, possibily, contributes to postsynaptic machinery stabilization. Additionally, drebrin is recruited *in vitro* to synaptic podosomes, where it could interact with cortactin and dynamin-2 to regulate postsynaptic topological remodeling. In the same way, MACF1 was proposed to transition from binding to MTs to attachment to rapsyn during NMJ maturation (Oury et al., 2019). In future studies, exploring the molecular interconnections mediating drebrin and rapsyn interaction, as well as their role in the organization of the postsynaptic machinery, would be extremely valuable to better understand the function of drebrin at the NMJ.

5.6. Myosin VI as a dispensable organizer of muscle postsynaptic machinery

In the second part of my doctoral research, I attempted to elucidate the role of myosin VI (MVI) in the organization of the postsynaptic machinery in skeletal muscle cells. Based on previous reports from our and other research groups on the synaptic involvement of MVI, I further confirmed its localization *in vivo* across different ages (Fig. 4.2) and muscle types (Fig. 4.3), which was similar to its distribution pattern *in vitro* (Karolczak et al., 2015a). A possible role of MVI arose from its localization to AChR-free areas *in vitro*, which suggested involvement in redistribution and mobility of membrane proteins. Of note, MVI has been proven crucial for the integrity of cell adhesion contacts through

interaction with E-cadherin and vinculin (Maddugoda et al., 2007), the latter being a component of synaptic (Proszynski et al., 2009) and non-synaptic podosomes (Linder & Aepfelbacher, 2003).

In order to further explore the specific role of MVI in synapse formation, maturation or maintenance, I downregulated *Myo6* expression in C2C12 myotubes in the same experimental settings as drebrin loss-of-function experiments (Fig. 4.25). Regrettably, technical issues regarding replicability and cell line behavior limited my ability to extract any conclusions from these experiments other than the loss of MVI does not seem to severely impair AChR cluster formation (Figs. 4.26, 4.27), receptor turnover (Fig. 4.28), nor synaptic podosome formation (data not shown). As alternative methods to overcome C2C12 misbehavior, other systems of cultured myotubes should be explored in the future, such as primary myotubes derived from WT and *SV* mice. Another crucial limitation in my phenotypic characterization of C2C12 upon MVI downregulation is that protein synthesis was not confirmed to be consistently and strongly depleted throughout several independent experiments (Fig. 4.25), which could explain the lack of alterations detected and the inconsistent phenotype *in vitro*.

Based on MVI similarity in functional domains and mechanoenzymatic properties to myosin V, the most probable from all roles explored for MVI is internalization of AChRs, however not as a crucial regulator of this process. It is noteworthy that myosin V and MVI move in opposite directions along actin filaments (Wells et al., 1999), thus providing the means for bidirectional movement in processes such as intracellular transport. Mice lacking myosin V, which is normally enriched at the NMJ, display severe morphological aberrations as early as two weeks of age (Röder et al., 2008). Moreover, myosin Va interacts with AChRs and its overexpression increases the number of rapsyn-containing vesicles around myonuclei (Röder et al., 2008), suggesting a central role in intracellular transport of synaptic components. Importantly, downregulation of myosin Va not only induces fragmentation of NMJs, but also reduces the time AChRs remain inserted into the postsynaptic membrane, indicating myosin Va involvement in recycling internalized AChRs back to the postsynaptic membrane (Röder et al., 2008). In line with a less central role for MVI than myosin Va in AChR turnover, I found that NMJ fragmentation and integrity are only mildly affected in middle-aged *SV* mice (Figs. 4.34, 4.35), and morphological remodeling of the postsynaptic machinery during the second week of life is delayed in both males and females lacking MVI, but not severely impaired (Fig. 4.33). However, the fact that MVI loss increases the number of aberrations in AChR density

(more NMJs with holes in AChR branches or dispersed branch edges), and reduces AChR and endplate surface, suggests a moderate impact on AChR stability, which is in accordance with MVI function in targeted membrane transport. Importantly, *TA* (fast-twitch, type II fibers) but not *SOL* (slow-twitch, type I fibers) muscles of *SV* mice displayed such aberrations (Figs. 4.33, 4.34, and 4.35). Abundance of type II fibers correlates with strength and muscle performance in humans (Serrano et al., 2019), indicating that fast-twitch muscles contribute more than slow-twitch muscles to strength. Indeed, *SV* mice at P365 exhibited reduced grip strength of their hindlimbs (Fig. 4.32), which could be explained by impaired functionality of fast-twitch muscles, such as *TA*, whose neurotransmission efficiency might be compromised by structural defects.

Stimulation of PKC or inhibition of PKA accelerates the removal of synaptic AChRs and depresses AChR recycling (Martinez-Pena y Valenzuela et al., 2013). The underlying mechanism of myosin Va role in maintaining size, integrity, and turnover rate of the postsynaptic machinery involves AKAP-dependent cooperation with PKA and requires an intact actin cytoskeleton (Röder et al., 2010). Importantly, AKAP depletion *in vivo* impairs NMJ structure and reduces AChR density (Martinez-Pena y Valenzuela et al., 2015), which depends on AKAP-mediated inhibition of receptor ubiquitination and subsequent degradation (Mouslim et al., 2012). It is noteworthy that AKAP9 links MVI to PKA signaling in myogenic cells (Karolczak et al., 2015b). Moreover, rapsyn anchors PKA to the subsynaptic compartment both *in vivo* and *in vitro* (Choi et al., 2012). Notably, unpublished data from our research group indicates that total AChR levels remain unchanged in newborn, 3-month-old, and 1-year-old mice lacking MVI when compared to WT littermates, supporting the idea that MVI regulates redistribution rather than synthesis of AChR subunits. However, AChR turnover was not severely impaired by *Myo6* downregulation (Fig. 4.28). Therefore, as suggested in section 4.7.2., AChR recycling in MVI-depleted cultured myotubes requires in-depth studies, including the expression profile and distribution of AKAP, PKA, PKC, and rapsyn, in order to detect subtler phenotypes resulting from MVI knockdown. Similarly, these postsynaptic proteins, as well as presynaptic elements, could be analyzed in *SV* mice.

Altogether, my preliminary studies on the role of MVI at the postsynaptic machinery have laid the path for multiple follow-up experiments that might be insightful in the context of MVI involvement in NMJ structure and function.

5.7. Functional significance of drebrin and MVI *in vivo*

Based on the similar distribution pattern of drebrin found across different skeletal muscle types and ages, one could expect comparable results between drebrin knockout murine muscles (DXKO mice) with different fiber type composition and at different ages (Fig. 4.20). On the other hand, despite the important role of drebrin in postsynaptic machinery assembly and maintenance demonstrated *in vitro*, I found that NMJs are normally formed in the absence of drebrin and do not seem particularly vulnerable to age-related changes (Figs. 4.22, 4.23). Knockout mice of another actin cross-linker, α-actinin-3, had no significant differences in sarcomeric stability and structure, but displayed different metabolic properties in their fast-twitch muscles, that adapt into a more slow-twitch, oxidative-based contraction (Chan et al., 2008). Such changes were not addressed in DXKO mice and constitute and interesting research path, especially considering that all muscles analyzed, except for *ST* muscle, had similar reductions in AChR surface throughout lifespan (Fig. 4.20). These similarities between slow- and fast-twitch muscles could indicate a transformation of drebrin-free fast-twitch fibers to resemble the metabolic properties of slow-twitch fibers, presumably as a consequence of altered neuromuscular activity (Pette & Vrbová, 2017). Accordingly, data from the International Mouse Phenotyping Consortium (www.mousephenotype.org) revealed that heterozygote mouse mutants for the $Dbn1^{tm1b(KOMP)Wtsi}$ allele display reduced grip strength (Dickinson et al., 2016). Finally, the potential involvement in postsynaptic maturation *in vitro,* that I found as a result of drebrin role in synaptic podosome formation, does not translate into postnatal maturation defects in young DXKO mice (Fig. 4.21). On the other hand, the effect of drebrin loss can be particularly masked in juvenile NMJs, since their morphological variability is much higher than in adults (Mech et al., 2020). Another important limitation of my *in vivo* studies was the nature of fixed samples obtained and no access to living animals, which limited the variety of analyses available.

Perhaps more detailed characterization of drebrin knockout animals is necessary in order to detect subtler changes in neuromuscular transmission, such as density of AChRs, which is also reduced during aging (Valdez et al., 2010), and whether it results in electrophysiological and grip strength impairments. Drebrin loss has been previously associated with subtle phenotypes in other tissues. For example, even though brain morphometric data showed no gross changes in drebrin knockout mice (Shan et al.,

2021; Willmes et al., 2017), the degree of drebrin loss in dendritic spines from Alzheimer patients and individuals with Down's Syndrome correlates with the severity of cognitive impairment and reduction in dendritic spine plasticity (Gordon-Weeks, 2016; Harigaya et al., 1996). On the other hand, functional redundancy of homologs and signaling pathways displayed in the absence of one synaptic component often mask its relevance when studied *in vivo* (Fowler et al., 2017; Lijam et al., 1997; Wong et al., 2018), which protects synapses from becoming dysfunctional. Moreover, activation of compensatory mechanisms that safeguard cytoskeleton dynamics at the synapse was previously proposed for the lack of phenotype in the brains of drebrin-deficient mice (Willmes et al., 2017). Furthermore, the mildly reduced size of NMJs observed upon drebrin depletion could be compensated by the common strategy of increasing junctional folding of the postsynaptic membrane (Slater, 2017), a paremeter that was not evaluated in this thesis. It is noteworthy that synthesis and delivery of AChRs to the cell surface does not seem to be significantly affected by drebrin depletion (Fig. 4.13), and NMJs of DXKO mice are formed and mature normally (Fig. 4.21). These results, together with the fact that surface covered by AChRs is significantly smaller in DXKO mice across all ages, suggests that the least redundant role of drebrin in skeletal muscle is maintenance of NMJ stability rather than formation or maturation. In summary, drebrin could play a role in driving early synaptic development, that in the aneural *in vitro* system of C2C12 myotubes would be visible due to a lack of compensational mechanisms from motoneurons and PSCs, which are present *in vivo*. On the other hand, it could have a stabilizing function in later stages, when functional redundancy of muscle-dependent mechanisms of AChR stabilization would make it difficult to detect. Similarly, drebrin drives early developmental morphogenesis of dendritic spines and maintains homeostatic plasticity of NMDAR (Aoki et al., 2010; Takahashi et al., 2003, 2006), while it later plays a stabilizing role in synaptic plasticity processes of mature spines, such as LTP and LTD (long-term depression) (Merriam et al., 2013; Mizui et al., 2014).

Myosin VI knockout resulted in altered morphology of the murine NMJ throughout lifespan, however with different effects depending on the age and muscle type. Whereas it significantly reduced NMJ size in slow-twitch muscles and delayed maturation at P10 (Figs. 4.30, 4.31), it also mildly affected NMJ morphology of *SV* muscles with predominantly fast-twitch fibers in adult and middle-aged mice (Figs. 4.33, 4.34, and 4.35). A potential factor underlying age differences in the muscle type affected is that *SV* mice are characterized by hyperactivity and constant circling movements (Self et al.,

1999). Muscle plasticity upon long-term endurance training contributes to changes in fiber type composition and metabolism from glycolitic to more oxidative-based (Plotkin et al., 2021), thus explaining why NMJs from either slow- or fast-twitch muscles are altered by MVI loss in early or later developmental stages, respectively. Moreover, the overall size of *SV* mice is smaller, however the muscle/body weight ratio is bigger than in WT mice (Lehka et al., 2022). This alteration seems to be due to MVI loss-induced muscle hyperplasia (formation of new, but small myofibers) rather than hypertrophy (growth of existing myofibers), particularly in slow-twitch muscles (Lehka et al., 2022). Furthermore, unpublished data from our research group seems to indicate that MVI impacts metabolism of slow- but not fast-twitch fibers in males. In summary, structural NMJ defects in juvenile *SV* mice are probably due to the impact of MVI on oxidative metabolism, which could be propagated to fast-twitch muscles later in life due to exercise-induced metabolic changes.

Nevertheless, these morphological changes seemed to be sufficient to induce functional impairments in the lower body grip strength of middle-aged *SV* females but not males (Fig. 4.32). Therefore, although mild, defects in the structure of NMJs or changes in fiber type composition as a consequence of MVI loss seem to reduce the efficiency of muscle contraction. Interestingly, differences in muscle mass and strength have been observed during aging in men but not in women (Oh et al., 2018). As age progresses, a stronger negative correlation between muscle myosin heavy chain (MHC) isoforms and muscle strength appears in men, presumably due to higher proportion of MHC I and lower proportion of MHC IIA and MHC IIX in aged individuals (Oh et al., 2018). This could be partially explained by the general trend in reduced expression of MHC isoforms IIA and IIX, but not isoform I, in humans from young to middle age and, more dramatically, from middle to old age (Balagopal et al., 2001). On the other hand, predominantly fast-twitch *supraspinatus* muscle in women, and more markedly in older women, tends to upregulate MHC II isoforms and downregulate MHC I (Potau et al., 2012). Moreover, *SOL* muscles from male rats have a considerable expression of MHC IIA that is almost entirely absent in females (Drzymala-Celichowska et al., 2012). Since nuclear MVI was recently proven to play a crucial role in spatial regulation of gene expression (Hari-Gupta et al., 2022), one could speculate that MVI absence affects gene transcription of MHC isoforms in a way that would alter normal sex dimorphisms in fiber type in favour of males, rather than direct effects on NMJ function. Accordingly, our group showed that slow and fast

MHC isoforms change their protein expression profile as MVI levels change during myoblast differentiation (Karolczak et al., 2015a).

In conclusion, the functional relevance of drebrin and MVI in skeletal muscle tissue requires further investigation, but the results collected in this thesis support their participation in postsynaptic organization at the NMJ.

CHAPTER 6: SUMMARY AND CONCLUSIONS

In my PhD thesis, I aimed at unveiling new molecular components and mechanisms underlying the formation and maintenance of the muscle postsynaptic machinery. As a result, I identified and characterized two main actin-interacting candidates, namely drebrin and myosin VI, in models of the muscle postsynaptic machinery lacking either of these proteins.

Key findings of my research include:

1. Drebrin is a novel component of the murine postsynaptic machinery *in vitro* and *in vivo,* as well as of synaptic podosomes in cultured C2C12 myotubes, and of sarcomeres in skeletal muscle.
2. Drebrin participates in stability and maturation of AChRs *in vitro* through regulation of actin cytoskeleton rearrangements.
3. Drebrin binds to AChR-anchoring protein rapsyn and microtubule +TIP protein EB3 in order to stabilize the postsynaptic machinery through the recruitment of microtubules and their anchorage to the synaptic membrane.
4. Myosin VI contributes to muscle contraction efficiency *in vivo*.
5. Myosin VI loss impairs neuromuscular junction maturation and maintenance.

In conclusion, drebrin is a novel postsynaptic machinery regulator that cross-links two major cytoskeletal components involved in the stabilization of neurotransmitter receptors, EB3-decorated microtubules and cortical F-actin. Myosin VI is an important regulator of proper neuromuscular function, potentially in a sex- and muscle type-dependent manner.

"I hadn't been aware that there were doors closed to me
until I started knocking on them."
Gertrude B. Elion,
Nobel Prize laureate in Physiology or Medicine (1988)

CHAPTER 7: REFERENCES

1. Aittaleb, M., Martinez-Pena y Valenzuela, I., & Akaaboune, M. (2017). Spatial distribution and molecular dynamics of dystrophin glycoprotein components at the neuromuscular junction in vivo. *Journal of Cell Science*, 130(10), 1752–1759. doi: 10.1242/jcs.198358
2. Akhmanova, A., & Hoogenraad, C. C. (2005). Microtubule plus-end-tracking proteins: mechanisms and functions. *Current Opinion in Cell Biology*, 17, 47–54. doi: 10.1016/j.ceb.2004.11.001
3. Alberts, B., Johnson, A., Lewis, J., Raff, M., Roberts, K., & Walte, P. (Eds.). (2007) *Molecular Biology of The Cell*, 5th edition. New York: Garland Science. doi: 10.1002/bmb.20192
4. Alvarez-Suarez, P., Gawor, M., & Prószyński, T. J. (2020). Perisynaptic schwann cells - The multitasking cells at the developing neuromuscular junctions. *Seminars in Cell and Developmental Biology*, 104(December 2019), 31–38. doi: 10.1016/j.semcdb.2020.02.011
5. Anderson, M. J., & Cohen, M. W. (1977). Nerve-induced and spontaneous redistribution of acetylcholine receptors on cultured muscle cells. *Journal of Physiology*, 268, 757–773. doi: 10.1113/jphysiol.1977.sp011880
6. Antolik, C., Catino, D. H., O'Neill, A. M., Resneck, W. G., Ursitti, J. A., & Bloch, R. J. (2007). The actin binding domain of ACF7 binds directly to the tetratricopeptide repeat domains of rapsyn. *Neuroscience*, 145(1), 56–65. doi: 10.1016/j.neuroscience.2006.11.047
7. Aoki, C., Kojima, N., Sabaliauskas, N., Shah, L., H, T., Oakford, J., Ahmed, T., Yamazaki, H., Hanamura, K., & Shirao, T. (2010). Drebrin A Knockout Eliminates the Rapid Form of Homeostatic Synaptic Plasticity at Excitatory Synapses of Intact Adult Cerebral Cortex Chiye. *Journal of Comparative Neurology*, 517(1), 105–121. doi: 10.1002/cne.22137.Drebrin
8. Aoki, C., Sekino, Y., Hanamura, K., & Fujisawa, S. H. O. (2005). Drebrin A Is a Postsynaptic Protein That Localizes In Vivo to the Submembranous Surface of Dendritic Sites Forming Excitatory Synapses. *Journal of Comparative Neurology*, 402, 383–402. doi: 10.1002/cne.20449
9. Apel, E. D., Roberds, S. L., Campbell, K. P., & Merlie, J. P. (1995). Rapsyn may function as a link between the acetylcholine receptor and the agrin-binding dystrophin-associated glycoprotein complex. *Neuron*, 15(1), 115–126. doi: 10.1016/0896-6273(95)90069-1
10. Araque, A., Parpura, V., Sanzgiri, R. P., & Haydon, P. G. (1999). Tripartite synapses: glia, the unacknowledged partner. *Trends in Neurosciences*, 22(5), 208–215. doi: 10.1016/S0166-2236(98)01349-6
11. Arendt, D., Denes, A. S., Jekely, G., & Tessmar-Raible, K. (2008). The evolution of nervous system centralization. *Philosophical Transactions of the Royal Society B: Biological Sciences*, 363(January), 1523–1528. doi: 10.1098/rstb.2007.2242
12. Asada, H., Uyemura, K., & Shirao, T. (1994). Actin-Binding protein, drebrin, accumulates in submembranous regions in parallel with neuronal differentiation. *Journal of Neuroscience Research*, 38(2), 149–159. doi: 10.1002/jnr.490380205
13. Aschenbrenner, L., Lee, T., & Hasson, T. (2003). Myo6 Facilitates the Translocation of Endocytic Vesicles from Cell Peripheries. *Molecular Biology of the Cell*, 14(July), 2728–2743. doi: 10.1091/mbc.E02–11–0767.
14. Avraham, K. B., Hasson, T., Steel, K. P., Kingsley, D. M., Russell, L. B., Mooseker, M. S., Copeland, N. G., & Jenkins, N. A. (1995). The mouse snell's waltzer deafness gene

encodes an unconventional myosin required for structural integrity of inner ear hair cells. *Nature Genetics*, 11(4), 369–375. doi: 10.1038/ng1295-369

15. Balagopal, P., Schimke, J. C., Ades, P., Adey, D., & Nair, K. S. (2001). Age effect on transcript levels and synthesis rate of muscle MHC and response to resistance exercise. *American Journal of Physiology - Endocrinology and Metabolism*, 280(2 43-2), 203–208. doi: 10.1152/ajpendo.2001.280.2.e203

16. Balice-Gordon, R. J., & Lichtman, J. W. (1993). In vivo observations of pre- and postsynaptic changes during the transition from multiple to single innervation at developing neuromuscular junctions. *Journal of Neuroscience*, 13(2), 834–855. doi: 10.1523/jneurosci.13-02-00834.1993

17. Banks, G. B., Fuhrer, C., Adams, M. E., & Froehner, S. C. (2003). The postsynaptic submembrane machinery at the neuromuscular junction: Requirement for rapsyn and the utrophin/dystrophin-associated complex. *Journal of Neurocytology*, 32(5–8), 709–726. doi: 10.1023/B:NEUR.0000020619.24681.2b

18. Barik, A., Li, L., Sathyamurthy, A., Xiong, W. C., & Mei, L. (2016). Schwann Cells in Neuromuscular Junction Formation and Maintenance. *Journal of Neuroscience*, 36(38), 9770–9781. doi: 10.1523/JNEUROSCI.0174-16.2016

19. Barik, A., Lu, Y., Sathyamurthy, A., Bowman, A., Shen, C., Li, L., Xiong, W. C., & Mei, L. (2014). LRP4 is critical for neuromuscular junction maintenance. *Journal of Neuroscience*, 34(42), 13892–13905. doi: 10.1523/JNEUROSCI.1733-14.2014

20. Barik, A., Zhang, B., Sohal, G. S., Xiong, W. C., & Mei, L. (2014). Crosstalk between Agrin and Wnt signaling pathways in development of vertebrate neuromuscular junction. *Developmental Neurobiology*, 74(8), 828–838. doi: 10.1002/dneu.22190

21. Basu, S., Sladecek, S., Martinez de la Peña y Valenzuela, I., Akaaboune, M., Smal, I., Martin, K., Galjart, N., & Brenner, H. R. (2015). CLASP2-dependent microtubule capture at the neuromuscular junction membrane requires LL5β and actin for focal delivery of acetylcholine receptor vesicles. *Molecular Biology of the Cell*, 26(5), 938–951. doi: 10.1091/mbc.E14-06-1158

22. Basu, S., Sladecek, S., Pemble, H., Wittmann, T., Slotman, J. A., Van Cappellen, W., Brenner, H. R., & Galjart, N. (2014). Acetylcholine receptor (AChR) clustering is regulated both by glycogen synthase kinase 3β (GSK3β)-dependent Phosphorylation and the level of CLIP-associated protein 2 (CLASP2) mediating the capture of microtubule plus-ends. *Journal of Biological Chemistry*, 289(44), 30857–30867. doi: 10.1074/jbc.M114.589457

23. Bazellières, E., Massey-Harroche, D., Barthélémy-Requin, M., Richard, F., Arsanto, J. P., & Le Bivic, A. (2012). Apico-basal elongation requires a drebrin-E-EB3 complex in columnar human epithelial cells. *Journal of Cell Science*, 125(4), 919–931. doi: 10.1242/jcs.092676

24. Beffert, U., Dillon, G. M., Sullivan, J. M., Stuart, C. E., Gilbert, J. P., Kambouris, J. A., & Ho, A. (2012). Microtubule plus-end tracking protein CLASP2 regulates neuronal polarity and synaptic function. *Journal of Neuroscience*, 32(40), 13906–13916. doi: 10.1523/JNEUROSCI.2108-12.2012

25. Bellmann, J., Goswami, R. Y., Girardo, S., Rein, N., Hosseinzadeh, Z., Hicks, M. R., Busskamp, V., Pyle, A. D., Werner, C., & Sterneckert, J. (2019). A customizable microfluidic platform for medium-throughput modeling of neuromuscular circuits. *Biomaterials*, 225(April), 119537. doi: 10.1016/j.biomaterials.2019.119537

26. Benashski, S. E., Harrison, A., Patel-King, R. S., & King, S. M. (1997). Dimerization of the highly conserved light chain shared by dynein and myosin V. *Journal of Biological Chemistry*, 272(33), 20929–20935. doi: 10.1074/jbc.272.33.20929

27. Berg, J. S., Powell, B. C., & Cheney, R. E. (2001). A Millennial Myosin Census. *Molecular Biology of the Cell*, 12(4), 780–794. doi: 10.1091/mbc.12.4.780

28. Berg, S., Kutra, D., Kroeger, T., Straehle, C. N., Kausler, B. X., Haubold, C., Schiegg, M., Ales, J., Beier, T., Rudy, M., Eren, K., Cervantes, J. I., Xu, B., Beuttenmueller, F., Wolny, A., Zhang, C., Koethe, U., Hamprecht, F. A., & Kreshuk, A. (2019). Ilastik: Interactive Machine Learning for (Bio)Image Analysis. *Nature Methods*, 16(12), 1226–1232. doi: 10.1038/s41592-019-0582-9

29. Bergamin, E., Hallock, P. T., Burden, S. J., & Hubbard, S. R. (2010). The Cytoplasmic Adapter-Protein Dok7 Activates the Receptor Tyrosine Kinase MuSK via Dimerization. *Molecular Cell*, 39(1), 100–109. doi: 10.1016/j.molcel.2010.06.007.

30. Bernadzki, K. M., Daszczuk, P., Rojek, K. O., Pęziński, M., Gawor, M., Pradhan, B. S., de Cicco, T., Bijata, M., Bijata, K., Włodarczyk, J., Prószyński, T. J., & Niewiadomski, P. (2020). Arhgef5 Binds α-Dystrobrevin 1 and Regulates Neuromuscular Junction Integrity. *Frontiers in Molecular Neuroscience*, 13(June), 1–13. doi: 10.3389/fnmol.2020.00104

31. Bernadzki, K. M., Gawor, M., Pęziński, M., Mazurek, P., Rędowicz, M. J., & Prószyński, T. J. (2017). Liprin-α-1 is a novel component of the murine neuromuscular junction and is involved in the organization of the postsynaptic machinery. *Scientific Reports*, 7(9116), 1–12. doi: 10.1038/s41598-017-09590-7

32. Bernadzki, K. M., Rojek, K. O., & Prószyński, T. J. (2014). Podosomes in muscle cells and their role in the remodeling of neuromuscular postsynaptic machinery. *European Journal of Cell Biology*, 93(10–12), 478–485. doi: 10.1016/j.ejcb.2014.06.002

33. Blanchoin, L., Boujemaa-Paterski, R., Sykes, C., & Plastino, J. (2014). Actin dynamics, architecture, and mechanics in cell motility. *Physiological Reviews*, 94(1), 235–263. doi: 10.1152/physrev.00018.2013

34. Blank, S., Chen, V., Hamilton, N., Salerno, T. A., & Ianuzzo, C. D. (1988). Biochemical characteristics of mammalian myocardia. *Respiration Physiology*, 74(1), 115–126. doi: 10.1016/0034-5687(88)90145-4

35. Bodaleo, F. J., & Gonzalez-Billault, C. (2016). The Presynaptic Microtubule Cytoskeleton in Physiological and Pathological Conditions: Lessons from Drosophila Fragile X Syndrome and Hereditary Spastic Paraplegias. *Frontiers in Molecular Neuroscience*, 9(July), 1–16. doi: 10.3389/fnmol.2016.00060

36. Boehm, I., Alhindi, A., Leite, A. S., Logie, C., Gibbs, A., Murray, O., Farrukh, R., Pirie, R., Proudfoot, C., Clutton, R., Wishart, T. M., Jones, R. A., & Gillingwater, T. H. (2020). Comparative anatomy of the mammalian neuromuscular junction. *Journal of Anatomy*, 237(5), 827–836. doi: 10.1111/joa.13260

37. Borodinsky, L. N., & Spitzer, N. C. (2006). Activity-dependent neurotransmitter-receptor matching at the neuromuscular junction. *PNAS*, 104(1), 335–340. doi: 10.1073/pnas.0607450104

38. Bruneau, E. G., Esteban, J. A., & Akaaboune, M. (2009). Receptor-associated proteins and synaptic plasticity. *The FASEB Journal*, 23(3), 679–688. doi: 10.1096/fj.08-107946

39. Brust, M. (1976). Fatigue and caffeine effects in fast-twitch and slow-twitch muscles of the mouse. *Pflügers Archiv: European Journal of Physiology*, 367(2), 189–200. doi: 10.1007/BF00585157

40. Bruusgaard, J. C., Liestø, K., & Gundersen, K. (2006). Distribution of myonuclei and microtubules in live muscle fibers of young, middle-aged, and old mice. *Journal of Applied Physiology*, 100(6), 2024–2030. doi: 10.1152/japplphysiol.00913.2005

41. Buchthal, F., & Schmalbruch, H. (1980). Motor Unit of Mammalian Muscle. *Physiological Reviews*, 60(1), 91-142. doi: 10.1152/physrev.1980.60.1.90.

42. Burgess, R. W., Nguyen, Q. T., Young-Jin, S., Lichtman, J. W., & Sanes, J. R. (1999). Alternatively spliced isoforms of nerve- and muscle-derived agrin: Their roles at the neuromuscular junction. *Neuron*, 23(1), 33–44. doi: 10.1016/S0896-6273(00)80751-5

43. Buss, F., Arden, S. D., Lindsay, M., Luzio, J. P., & Kendrick-Jones, J. (2001). Myosin VI isoform localized to clathrin-coated vesicles with a role in clathrin-mediated endocytosis. *EMBO Journal*, 20(14), 3676–3684. doi: 10.1093/emboj/20.14.3676

44. Buss, F., Spudich, G., & Kendrick-Jones, J. (2004). Myosin VI: Cellular functions and motor properties. *Annual Review of Cell and Developmental Biology*, 20, 649–676. doi: 10.1146/annurev.cellbio.20.012103.094243

45. Butkevich, E., Bodensiek, K., Fakhri, N., Von Roden, K., Schaap, I. A. T., Majoul, I., Schmidt, C. F., & Klopfenstein, D. R. (2015). Drebrin-like protein DBN-1 is a sarcomere component that stabilizes actin filaments during muscle contraction. *Nature Communications*, 6(May), 1–12. doi: 10.1038/ncomms8523

46. Butkevich, E., Hu, S., Wenzel, D., Shirao, T., Duden, R., & Majoul, I. (2004). Drebrin Is a Novel Connexin-43 Binding Partner that Links Gap Junctions to the Submembrane Cytoskeleton. *Current Biology*, 14, 650–658. doi: 10.1016/j.cub.2004.03.063

47. Butkevich, E., Klopfenstein, D. R., & Schmidt, C. F. (2016). Game of Zones: how actin-binding proteins organize muscle contraction. *Worm*, 5(2), e1161880. doi: 10.1080/21624054.2016.1161880

48. Caillol, G., Vacher, H., Musarella, M., Bellouze, S., Dargent, B., & Autillo-Touati, A. (2012). Motor endplate disease affects neuromuscular junction maturation. *European Journal of Neuroscience*, 36(4), 2400–2408. doi: 10.1111/j.1460-9568.2012.08164.x

49. Chal, J., & Pourquié, O. (2017). Making muscle: Skeletal myogenesis in vivo and in vitro. *Development*, 144(12), 2104–2122. doi: 10.1242/dev.151035

50. Chan, S., Seto, J. T., MacArthur, D. G., Yang, N., North, K. N., & Head, S. I. (2008). A gene for speed: Contractile properties of isolated whole EDL muscle from an α-actinin-3 knockout mouse. *American Journal of Physiology - Cell Physiology*, 295(4), 897–904. doi: 10.1152/ajpcell.00179.2008

51. Chan, Z. C. K., Kwan, H. L. R., Wong, Y. S., Jiang, Z., Zhou, Z., Tam, K. W., Chan, Y. S., Chan, C. B., & Lee, C. W. (2020). Site-directed MT1-MMP trafficking and surface insertion regulate achr clustering and remodeling at developing NMJS. *ELife*, 9, 1–33. doi: 10.7554/eLife.54379

52. Chazeau, A., Mehidi, A., Nair, D., Gautier, J. J., Leduc, C., Chamma, I., Kage, F., Kechkar, A., Thoumine, O., Rottner, K., Choquet, D., Gautreau, A., Sibarita, J., & Giannone, G. (2014). Nanoscale segregation of actin nucleation and elongation factors determines dendritic spine protrusion. *EMBO Journal*, 33(23), 2745–2764. doi: 10.15252/embj.201488837

53. Chen, H., Li, M. W. M., Cheng, C. Y., & Council, P. (2017). Drebrin and Spermatogenesis. *Advances in Experimental Medicine and Biology*, 1006(1), 291–312. doi: 10.1007/978-4-431-56550-5_17.

54. Cheng, A., Morsch, M., Murata, Y., Ghazanfari, N., Reddel, S. W., & Phillips, W. D. (2013). Sequence of Age-Associated Changes to the Mouse Neuromuscular Junction and the Protective Effects of Voluntary Exercise. *PLoS ONE*, 8(7), e67970. doi: 10.1371/journal.pone.0067970

55. Choi, H. Y., Liu, Y., Tennert, C., Sugiura, Y., Karakatsani, A., Kröger, S., Johnson, E. B., Hammer, R. E., Lin, W., & Herz, J. (2013). APP interacts with LRP4 and agrin to coordinate the development of the neuromuscular junction in mice. *ELife*, 2, e00220. doi: 10.7554/eLife.00220

56. Choi, K. R., Berrera, M., Reischl, M., Strack, S., Albrizio, M., Röder, I. V., Wagner, A., Petersen, Y., Hafner, M., Zaccolo, M., & Rudolf, R. (2012). Rapsyn mediates subsynaptic anchoring of PKA type I and stabilisation of acetylcholine receptor in vivo. *Journal of Cell Science*, 125(3), 714–723. doi: 10.1242/jcs.092361

57. Dai, Z., Luo, X., Xie, H., & Peng, H. B. (2000). The actin-driven movement and formation of acetylcholine receptor clusters. *Journal of Cell Biology*, 150(6), 1321–1334. doi: 10.1083/jcb.150.6.1321

58. Dart, A. E., Worth, D. C., Muir, G., Chandra, A., Morris, J. D., McKee, C., Verrill, C., Bryant, R. J., & Gordon-Weeks, P. R. (2017). The drebrin/EB3 pathway drives invasive activity in prostate cancer. *Oncogene*, 36(29), 4111–4123. doi: 10.1038/onc.2017.45

59. Das, M., Rumsey, J. W., Gregory, C. A., Bhargava, N., Kang, J. F., Molnar, P., Riedel, L., Guo, X., & Hickman, J. J. (2007). Embryonic motoneuron-skeletal muscle co-culture in a defined system. *Neuroscience*, 146(2), 481–488. doi: 10.1016/j.neuroscience.2007.01.068

60. De la Cruz, E. M., Ostap, E. M., & Sweeney, H. L. (2001). Kinetic Mechanism and Regulation of Myosin VI. *Journal of Biological Chemistry*, 276(34), 32373–32381. doi: 10.1074/jbc.M104136200

61. De La Cruz, E. M., Wells, A. L., Rosenfeld, S. S., Ostap, E. M., & Sweeney, H. L. (1999). The kinetic mechanism of myosin V. *Proceedings of the National Academy of Sciences of the United States of America*, 96(24), 13726–13731. doi: 10.1073/pnas.96.24.13726

62. Dempsey, C. E., Bigotti, M. G., Adams, J. C., & Brancaccio, A. (2019). Analysis of α-dystroglycan/LG domain binding modes: Investigating protein motifs that regulate the affinity of isolated LG domains. *Frontiers in Molecular Biosciences*, 6(MAR). doi: 10.3389/fmolb.2019.00018

63. Denes, L. T., Kelley, C. P., & Wang, E. T. (2021). Microtubule-based transport is essential to distribute RNA and nascent protein in skeletal muscle. *Nature Communications*, 12(1). doi: 10.1038/s41467-021-26383-9

64. Desai, A., & Mitchison, T. (1997). Microtubule Polymerization. *Annual Review of Cell and Developmental Biology*, 13, 83–117.

65. Desaki, J., & Uehara, Y. (1981). The overall morphology of neuromuscular junctions as revealed by scanning electron microscopy. *Journal of Neurocytology*, 10, 101–110. doi: 10.1007/bf01181747

66. Deschenes, M. R., Covault, J., Kraemer, W. J., & Maresh, C. M. (1994). The Neuromuscular Junction: Muscle Fibre Type Differences, Plasticity and Adaptability to Increased and Decreased Activity. *Sports Medicine: Evaluations of Research in Exercise Science and Sports Medicine*, 17(6), 358–372. doi: 10.2165/00007256-199417060-00003

67. Deschenes, M. R., Hurst, T. E., Ramser, A. E., & Sherman, E. G. (2013). Presynaptic to postsynaptic relationships of the neuromuscular junction are held constant across age and muscle fiber type. *Developmental Neurobiology*, 73(10), 744–753. doi: 10.1002/dneu.22095

68. Dickinson, M. E., Flenniken, A. M., Ji, X., Teboul, L., Wong, M. D., White, J. K., Meehan, T. F., Weninger, W. J., Westerberg, H., Adissu, H., Baker, C. N., Bower, L., Brown, J. M., Brianna Caddle, L., Chiani, F., Clary, D., Cleak, J., Daly, M. J., Denegre, J. M., … Murakami, A. (2016). High-throughput discovery of novel developmental phenotypes. *Nature*, 537(7621), 508–514. doi: 10.1038/nature19356

69. Dobbins, G. C., Luo, S., Yang, Z., Xiong, W. C., & Mei, L. (2008). alpha-Actinin interacts with rapsyn in agrin-stimulated AChR clustering. *Molecular Brain*, 1(18). doi: 10.1186/1756-6606-1-18

70. Dogterom, M., & Koenderink, G. H. (2019). Actin–microtubule crosstalk in cell biology. *Nature Reviews Molecular Cell Biology*, 20(1), 38–54. doi: 10.1038/s41580-018-0067-1

71. Donaudy, F., Ferrara, A., Esposito, L., Hertzano, R., Ben-David, O., Bell, R. F., Melchionda, S., Zelante, L., Avraham, K. B., & Gasparini, P. (2003). Multiple mutations of MYO1A, a

cochlear-expressed gene, in sensorineural hearing loss. *American Journal of Human Genetics*, 72(6), 1571–1577. doi: 10.1086/375654

72. Drzymala-Celichowska, H., Karolczak, J., Redowicz, M. J., & Bukowska, D. (2012). The Content of Myosin Heavy Chains in Hindlimb Muscles of Female and Male Rats. *Journal of Physiology and Pharmacology*, 63(2), 187–193.

73. Dutta, S., & Sengupta, P. (2016). Men and mice: Relating their ages. *Life Sciences*, 152, 244–248. doi: 10.1016/j.lfs.2015.10.025

74. Edström, L., & Kugelberg, E. (1968). Histochemical composition, distribution of fibres and fatiguability of single motor units. Anterior tibial muscle of the rat. *Journal of Neurology, Neurosurgery, and Psychiatry,* 31(5), 424–433. doi: 10.1136/jnnp.31.5.424

75. Eguchi, T., Tezuka, T., Miyoshi, S., & Yamanashi, Y. (2016). Postnatal knockdown of dok-7 gene expression in mice causes structural defects in neuromuscular synapses and myasthenic pathology. *Genes to Cells*, 21(6), 670–676. doi: 10.1111/gtc.12370

76. Ehrengruber, M. U., Kato, A., Inokuchi, K., & Hennou, S. (2004). Homer/Vesl proteins and their roles in CNS neurons. *Molecular Neurobiology*, 29(3), 213–227. doi: 10.1385/MN:29:3:213

77. Evans, D., Baillie, H., Caswell, A., & Wigmore, P. (1994). During fetal muscle development, clones of cells contribute to both primary and secondary fibers. *Developmental Biology*, 162, 348–353. doi: 10.1006/dbio.1994.1092

78. Faulkner, J. A., Larkin, L. M., Claflin, D. R., & Brooks, S. V. (2007). Age-related changes in the structure and function of skeletal muscles. *Clinical and Experimental Pharmacology and Physiology*, 34(11), 1091–1096. doi: 10.1111/j.1440-1681.2007.04752.x

79. Faustino Martins, J. M., Fischer, C., Urzi, A., Vidal, R., Kunz, S., Ruffault, P. L., Kabuss, L., Hube, I., Gazzerro, E., Birchmeier, C., Spuler, S., Sauer, S., & Gouti, M. (2020). Self-Organizing 3D Human Trunk Neuromuscular Organoids. *Cell Stem Cell*, 26(2), 172-186.e6. doi: 10.1016/j.stem.2019.12.007

80. Feng, Z., & Ko, C. P. (2008). The role of glial cells in the formation and maintenance of the neuromuscular junction. *Annals of the New York Academy of Sciences*, 1132, 19–28. doi: 10.1196/annals.1405.016

81. Finan, D., Hartman, M. A., & Spudich, J. A. (2011). Proteomics approach to study the functions of Drosophila myosin VI through identification of multiple cargo-binding proteins. *Proceedings of the National Academy of Sciences of the United States of America*, 108(14), 5566–5571. doi: 10.1073/pnas.1101415108

82. Fisher, L. W., McBride, O. W., Filpula, D., Ibaraki, K., & Young, M. F. (1994). Human drebrin: cDNA sequence, mRNA tissue distribution and chromosomal localization. *Neuroscience Research Communications*, 14, 35–42.

83. Flanagan-Steet, H., Fox, M. A., Meyer, D., & Sanes, J. R. (2005). Neuromuscular synapses can form in vivo by incorporation of initially aneural postsynaptic specializations. *Development*, 132(20), 4471–4481. doi: 10.1242/dev.02044

84. Fowler, D. K., Peters, J. H., Williams, C., & Washbourne, P. (2017). Redundant Postsynaptic Functions of SynCAMs 1 – 3 during Synapse Formation. *Frontiers in Molecular Neuroscience*, 10(24). doi: 10.3389/fnmol.2017.00024

85. Fralish, Z., Lotz, E. M., Chavez, T., Khodabukus, A., & Bursac, N. (2021). Neuromuscular Development and Disease: Learning From in vitro and in vivo Models. *Frontiers in Cell and Developmental Biology*, 9(October), 1–35. doi: 10.3389/fcell.2021.764732

86. Fu, A. K. Y., & Ip, N. Y. (2007). Cyclin-dependent kinase 5 links extracellular cues to actin cytoskeleton during dendritic spine development. *Cell Adhesion & Migration*, 1(2), 110–112. doi: 10.4161/cam.1.2.4617

87. Fucini, R. V, Navarrete, A., Vadakkan, C., Lacomis, L., Erdjument-bromage, H., Tempst, P., & Stamnes, M. (2000). Activated ADP-ribosylation Factor Assembles Distinct Pools of Actin on Golgi Membranes. *Journal of Biological Chemistry*, 275(25), 18824–18829. doi: 10.1074/jbc.M000024200

88. Fürst, D. O., Osborn, M., & Weber, K. (1989). Myogenesis in the Mouse Embryo: Differential Onset of Expression of Myogenic Proteins and the Involvement of Titin in Myofibril Assembly. *Journal of Cell Biology*, 109(August), 517–527. doi: 10.1083/jcb.109.2.517

89. Gardner, L. A., Naren, A. P., & Bahouth, S. W. (2007). Assembly of an SAP97-AKAP79-cAMP-dependent protein kinase scaffold at the type 1 PSD-95/DLG/ZO1 motif of the human β1-adrenergic receptor generates a receptosome involved in receptor recycling and networking. *Journal of Biological Chemistry*, 282(7), 5085–5099. doi: 10.1074/jbc.M608871200

90. Gautam, M., Noakes, P. G., Moscoso, L., Rupp, F., Scheller, R. H., Merlie, J. P., & Sanes, J. R. (1996). Defective neuromuscular synaptogenesis in agrin-deficient mutant mice. *Cell*, 85(4), 525–535. doi: 10.1016/S0092-8674(00)81253-2

91. Gautam, M., Noakes, P. G., Mudd, J., Nichol, M., Chu, G. C., Sanes, J. R., & Merlie, J. P. (1995). Failure of postsynaptic specialization to develop at neuromuscular junctions of rapsyn-deficient mice. *Nature*, 377(6546), 232–236). doi: 10.1038/377232a0.

92. Gawor, M., & Prószyński, T. J. (2018). The molecular cross talk of the dystrophin–glycoprotein complex. *Annals of the New York Academy of Sciences*, 1412(1), 62–72. doi: 10.1111/nyas.13500

93. Gentile, J. E., Carrizales, M. G., & Koleske, A. J. (2022). Control of Synapse Structure and Function by Actin and Its Regulators. *Cells*, 11(603), 1–20. doi: 10.3390/ cells11040603

94. Geraldo, S., Khanzada, U. K., Parsons, M., Chilton, J. K., & Gordon-Weeks, P. R. (2008). Targeting of the F-actin-binding protein drebrin by the microtubule plus-tip protein EB3 is required for neuritogenesis. *Nature Cell Biology*, 10(10), 1181–1189. doi: 10.1038/ncb1778

95. Geyer, M., Huang, F., Sun, Y., Vogel, S. M., Malik, A. B., Taylor, C. W., & Komarova, Y. A. (2015). Microtubule-Associated Protein EB3 Regulates IP3 Receptor Clustering and Ca2+ Signaling in Endothelial Cells. *Cell Reports*, 12(1), 79–89. doi: 10.1016/j.celrep.2015.06.001

96. Ghasemizadeh, A., Christin, E., Guiraud, A., Couturier, N., Abitbol, M., Risson, V., Girard, E., Jagla, C., Soler, C., Laddada, L., Sanchez, C., Jaque, F., Jacquemond, V., Thomas, J. L., Lanfranchi, M., Courchet, J., Gondin, J., Schaeffer, L., & Gache, V. (2021). MACF1 controls skeletal muscle function through the microtubule-dependent localization of extra-synaptic myonuclei and mitochondria biogenesis. *ELife*, 10, 1–32. doi: 10.7554/eLife.70490

97. Gingras, J., Gawor, M., Bernadzki, K. M., Grady, R. M., Hallock, P., Glass, D. J., Sanes, J. R., & Proszynski, T. J. (2016). α-Dystrobrevin-1 recruits Grb2 and α-catulin to organize neurotransmitter receptors at the neuromuscular junction. *Journal of Cell Science*, 129(5), 898–911. doi: 10.1242/jcs.181180

98. Glass, D. J., Bowen, D. C., Stitt, T. N., Radziejewski, C., Bruno, J. A., Ryan, T. E., Gies, D. R., Shah, S., Mattsson, K., Burden, S. J., DiStefano, P. S., Valenzuela, D. M., DeChiara, T. M., & Yancopoulos, G. D. (1996). Agrin acts via a MuSK receptor complex. *Cell*, 85(4), 513–523. doi: 10.1016/S0092-8674(00)81252-0

99. Godena, V. K., Romano, G., Romano, M., Appocher, C., Klima, R., Buratti, E., Baralle, F. E., & Feiguin, F. (2011). TDP-43 regulates drosophila neuromuscular junctions growth by modulating futsch/MAP1B levels and synaptic microtubules organization. *PLoS ONE*, 6(3). doi: 10.1371/journal.pone.0017808

100. Gordón-Alonso, M., Rocha-Perugini, V., Álvarez, S., Ursa, Á., Izquierdo-Useros, N., Martinez-Picado, J., Muñoz-Fernández, M. A., & Sánchez-Madrid, F. (2013). Actin-binding Protein Drebrin Regulates HIV-1-triggered Actin Polymerization and Viral Infection. *Journal of Biological Chemistry*, 288(39), 28382–28397. doi: 10.1074/jbc.M113.494906

101. Gordon-Weeks, P. R. (2016). The role of the drebrin/EB3/Cdk5 pathway in dendritic spine plasticity, implications for Alzheimer's disease. *Brain Research Bulletin*, 126, 293–299. doi: 10.1016/j.brainresbull.2016.06.015

102. Gould, T. W., Dominguez, B., De Winter, F., Yeo, G. W., Liu, P., Sundararaman, B., Stark, T., Vu, A., Degen, J. L., Lin, W., & Lee, K. F. (2019). Glial cells maintain synapses by inhibiting an activity-dependent retrograde protease signal. *PLoS Genetics*, 15(3), 1–26. doi: 10.1371/journal.pgen.1007948

103. Grady, R. M., Akaaboune, M., Cohen, A. L., Maimone, M. M., Lichtman, J. W., & Sanes, J. R. (2003). Tyrosine-phosphorylated and nonphosphorylated isoforms of α-dystrobrevin: Roles in skeletal muscle and its neuromuscular and myotendinous junctions. *Journal of Cell Biology*, 160(5), 741–752. doi: 10.1083/jcb.200209045

104. Graham, F. L., Smiley, J., Russell, W. C., & Nairn, R. (1977). Characteristics of a human cell line transformed by DNA from human adenovirus type 5. *Journal of General Virology*, 36(1), 59–72. doi: 10.1099/0022-1317-36-1-59

105. Griffin, C. A., Apponi, L. H., Long, K. K., & Pavlath, G. K. (2010). Chemokine expression and control of muscle cell migration during myogenesis. *Journal of Cell Science*, 123, 3052–3060. doi: 10.1242/jcs.066241

106. Gu, J., Firestein, B. L., & Zheng, J. Q. (2008). Microtubules in Dendritic Spine *Development*. 28(46), 12120–12124. doi: 10.1523/JNEUROSCI.2509-08.2008

107. Hanamura, K. (2017). Drebrin in neuronal migration and axonal growth. In T. Shirao & Y. Sekino (Eds.), *Drebrin - From Structure and Function to Physiological and Pathological Roles* (pp. 141–155). Springer Japan KK. doi: 10.1007/978-4-431-56550-5_9

108. Hari-Gupta, Y., Fili, N., dos Santos, Á., Cook, A. W., Gough, R. E., Reed, H. C. W., Wang, L., Aaron, J., Venit, T., Wait, E., Grosse-Berkenbusch, A., Gebhardt, J. C. M., Percipalle, P., Chew, T. L., Martin-Fernandez, M., & Toseland, C. P. (2022). Myosin VI regulates the spatial organisation of mammalian transcription initiation. *Nature Communications*, 13(1), 1–18. doi: 10.1038/s41467-022-28962-w

109. Harigaya, Y., Shoji, M., Shirao, T., & Hirai, S. (1996). Disappearance of Actin-Binding Protein, Drebrin, From Hippocampal Synapses in Alzheimer's Disease. *Journal of Neuroscience Research*, 43, 87–92. doi: 10.1002/jnr.490430111

110. Hasson, T., Gillespie, P. G., Garcia, J. A., MacDonald, R. B., Zhao, Y. D., Yee, A. G., Mooseker, M. S., & Corey, D. P. (1997). Unconventional myosins in inner-ear sensory epithelia. *Journal of Cell Biology*, 137(6), 1287–1307. doi: 10.1083/jcb.137.6.1287

111. Hatanpaa, K., Isaacs, K. R., Shirao, T., Brady, D. R., & Rapoport, S. I. (1999). Loss of Proteins Regulating Synaptic Plasticity in Normal Aging of the Human Brain and in Alzheimer Disease. *Journal of Neuropathology and Experimental Neurology*, 58(6), 637–643. doi: 10.1097/00005072-199906000-00008

112. Hayashi, K., Ishikawa, R., Kawai-Hirai, R., Takagi, T., Taketomi, A., & Shirao, T. (1999). Domain analysis of the actin-binding and actin-remodeling activities of drebrin. *Experimental Cell Research*, 253(2), 673–680. doi: 10.1006/excr.1999.4663

113. Hayashi, K., Ishikawa, R., Ye, L. H., He, X. L., Takata, K., Kohama, K., & Shirao, T. (1996). Modulatory role of drebrin on the cytoskeleton within dendritic spines in the rat cerebral cortex. *Journal of Neuroscience*, 16(22), 7161–7170. doi: 10.1523/jneurosci.16-22-07161.1996

114. Hayashi, Y. (2019). Drebrin-Homer Interaction at An Atomic Scale. *Structure*, 27(1), 3–5. doi: 10.1016/j.str.2018.12.008

115. Hegan, P. S., Lanahan, A. A., Simons, M., & Mooseker, M. S. (2015). Myosin VI and cardiomyopathy: Left ventricular hypertrophy, fibrosis, and both cardiac and pulmonary vascular endothelial cell defects in the Snell's waltzer mouse. *Cytoskeleton*, 72(8), 373–387. doi: 10.1002/cm.21236.

116. Henriquez, J. P., Webb, A., Bence, M., Bildsoe, H., Sahores, M., Hughes, S. M., & Salinas, P. C. (2008). Wnt signaling promotes AChR aggregation at the neuromuscular synapse in collaboration with agrin. *Proceedings of the National Academy of Sciences of the United States of America*, 105(48), 18812–18817. doi: 10.1073/pnas.0806300105

117. Hering, H., & Sheng, M. (2001). Dentritic spines: structure, dynamics and regulation. *Nature Reviews Neuroscience*, 2(12), 880–888. doi: 10.1038/35104061

118. Hicks, J. L., Deng, W. M., Rogat, A. D., Miller, K. G., & Bownes, M. (1999). Class VI unconventional myosin is required for spermatogenesis in Drosophila. *Molecular Biology of the Cell*, 10(12), 4341–4353. doi: 10.1091/mbc.10.12.4341

119. Hodge, K., Powers, S. K., Coombes, J., Fletcher, L., Demirel, H. A., Dodd, S. L., & Martin, D. (1997). Bioenergetic characteristics of the costal and crural diaphragm in mammals. *Respiration Physiology*, 109(2), 149–154. doi: 10.1016/S0034-5687(97)00051-0

120. Homma, K., & Ikebe, M. (2005). Myosin X is a high duty ratio motor. *Journal of Biological Chemistry*, 280(32), 29381–29391. doi: 10.1074/jbc.M504779200

121. Honkura, N., Matsuzaki, M., Noguchi, J., Ellis-Davies, G. C. R., & Kasai, H. (2008). The Subspine Organization of Actin Fibers Regulates the Structure and Plasticity of Dendritic Spines. *Neuron*, 57, 719–729. doi: 10.1016/j.neuron.2008.01.013

122. Horio, T., & Murata, T. (2014). The role of dynamic instability in microtubule organization. *Frontiers in Plant Science*, 5(OCT), 1–11. doi: 10.3389/fpls.2014.00511

123. Hörner, S. J., Couturier, N., Bruch, R., Koch, P., Hafner, M., & Rudolf, R. (2021). hiPSC-Derived Schwann Cells Influence Myogenic Differentiation in Neuromuscular Cocultures. *Cells*, 10(12), 1–25. doi: 10.3390/cells10123292

124. Hu, X., Viesselmann, C., Nam, S., Merriam, E., & Dent, E. W. (2008). Activity-dependent dynamic microtubule invasion of dendritic spines. *Journal of Neuroscience*, 28(49), 13094–13105. doi: 10.1523/JNEUROSCI.3074-08.2008

125. Huxley, A. F., & Simmons, R. M. (1971). Proposed mechanism of force generation in striated muscle. *Nature*, 233(5321), 533–538. doi: 10.1038/233533a0

126. Inoue, A., Setoguchi, K., Matsubara, Y., Okada, K., Sato, N., Iwakura, Y., Higuchi, O., & Yamanashi, Y. (2009). Dok-7 Activates the Muscle Receptor Kinase MuSK and Shapes Synapse Formation. *Science Signaling*, 2(59), 1–9. doi: 10.1126/scisignal.2000113

127. Inoue, H., Nojima, H., & Okayama, H. (1990). High efficiency transformation of Escherichia coli with plasmids. *Gene*, 96(1), 23–28. doi: 10.1016/0378-1119(90)90336-P

128. Ionescu, A., Zahavi, E. E., Gradus, T., Ben-Yaakov, K., & Perlson, E. (2016). Compartmental microfluidic system for studying muscle-neuron communication and neuromuscular junction maintenance. *European Journal of Cell Biology*, 95(2), 69–88. doi: 10.1016/j.ejcb.2015.11.004

129. Isaji, M., Lenartowska, M., Noguchi, T., Frank, D. J., & Miller, K. G. (2011). Myosin VI regulates actin structure specialization through conserved cargo-binding domain sites. *PLoS ONE*, 6(8). doi: 10.1371/journal.pone.0022755

130. Ishikawa, J., Ohga, K., Yoshino, T., Takezawa, R., Ichikawa, A., Kubota, H., & Yamada, T. (2003). A Pyrazole Derivative, YM-58483, Potently Inhibits Store-Operated

Sustained Ca^{2+} Influx and IL-2 Production in T Lymphocytes. *Journal of Immunology*, 170(9), 4441–4449. doi: 10.4049/jimmunol.170.9.4441

131. Ishikawa, R., Hayashi, K., Shirao, T., Xue, Y., Takagi, T., Sasaki, Y., & Kohama, K. (1994). Drebrin, a Development-associated Brain Protein from Rat Embryo, Causes the Dissociation of Tropomyosin from Actin Filaments. *Journal of Biological Chemistry*, 269(47), 29928–29933. doi: 10.1016/s0021-9258(18)43970-1

132. Jing, L., Lefebvre, J. L., Gordon, L. R., & Granato, M. (2009). Wnt signals organize synaptic prepattern and axon guidance through the zebrafish unplugged/MuSK receptor. *Neuron*, 61(5), 721–733. doi: 10.1016/j.neuron.2008.12.025. Wnt

133. Juanes, M. A., Fees, C. P., Hoeprich, G. J., Jaiswal, R., & Goode, B. L. (2020). EB1 Directly Regulates APC-Mediated Actin Nucleation. *Current Biology*, 30(23), 4763-4772.e8. doi: 10.1016/j.cub.2020.08.094

134. Jungbluth, H., Treves, S., Zorzato, F., Sarkozy, A., Ochala, J., Sewry, C., Phadke, R., Gautel, M., & Muntoni, F. (2018). Congenital myopathies: Disorders of excitation-contraction coupling and muscle contraction. *Nature Reviews Neurology*, 14(3), 151–167. doi: 10.1038/nrneurol.2017.191

135. Kajita, Y., Kojima, N., Koganezawa, N., Yamazaki, H., Sakimura, K., & Shirao, T. (2017). Drebrin E regulates neuroblast proliferation and chain migration in the adult brain_Supplementary material. *European Journal of Neuroscience*, 46(6), 2214–2228.

136. Karolczak, J., Pavlyk, I., Majewski, Ł., Sobczak, M., Niewiadomski, P., Rzhepetskyy, Y., Sikorska, A., Nowak, N., Pomorski, P., Prószyński, T., Ehler, E., & Rędowicz, M. J. (2015a). Involvement of unconventional myosin VI in myoblast function and myotube formation. *Histochemistry and Cell Biology*, 144(1), 21–38. doi: 10.1007/s00418-015-1322-6

137. Karolczak, J., Sobczak, M., Majewski, Ł., Yeghiazaryan, M., Jakubiec-Puka, A., Ehler, E., Sławińska, U., Wilczyński, G. M., & Rędowicz, M. J. (2013). Myosin VI in skeletal muscle: Its localization in the sarcoplasmic reticulum, neuromuscular junction and muscle nuclei. *Histochemistry and Cell Biology*, 139(6), 873–885. doi: 10.1007/s00418-012-1070-9

138. Karolczak, J., Sobczak, M., Skowronek, K., & Rędowicz, M. J. (2015b). A kinase anchoring protein 9 is a novel myosin VI binding partner that links myosin VI with the PKA pathway in myogenic cells. *BioMed Research International*, 2015. doi: 10.1155/2015/816019

139. Karolczak, J., Weis, S., Ehler, E., Kierdaszuk, B., Berdyński, M., Zekanowski, C., Kamińska, A. M., & Redowicz, M. J. (2014). Myosin VI localization and expression in striated muscle pathology. *Anatomical Record*, 297(9), 1706–1713. doi: 10.1002/ar.22967

140. Kassar-Duchossoy, L., Giacone, E., Gayraud-morel, B., Jory, A., Gomès, D., & Tajbakhsh, S. (2005). Pax3/Pax7 mark a novel population of primitive myogenic cells during development, Kassar-Duchossoy, Giacone, Gayraud-Morel, Jory, Gomès, Tajbakhsh.pdf. *Genes & Development*, 19(12), 1426–1431. doi: 10.1101/gad.345505

141. Khairallah, R. J., Shi, G., Sbrana, F., Prosser, B. L., Mazaitis, M. J., Hoffman, E. P., Mahurkar, A., Sachs, F., Chen, Y., Raiteri, R., Lederer, W. J., Dorsey, S. G., & Ward, C. W. (2013). Microtubules Underlie Dysfunction in Duchenne Muscular Dystrophy. *Sci Signal*, 5(236). doi: 10.1126/scisignal.2002829.Microtubules

142. Kim, N., Stiegler, A. L., Cameron, T. O., Hallock, P. T., Gomez, A. M., Huang, J. H., Hubbard, S. R., Dustin, M. L., & Burden, S. J. (2008). Lrp4 is a Receptor for Agrin and Forms a Complex with MuSK. *Cell*, 135(2), 334–342. doi: 10.1016/j.cell.2008.10.002

143. Kishi, M., Kummer, T. T., Eglen, S. J., & Sanes, J. R. (2005). LL5β: A regulator of postsynaptic differentiation identified in a screen for synaptically enriched transcripts at

the neuromuscular junction. *Journal of Cell Biology*, 169(2), 355–366. doi: 10.1083/jcb.200411012

144. Kisiel, M., Majumdar, D., Campbell, S., & Stewart, B. A. (2011). Myosin VI contributes to synaptic transmission and development at the Drosophila neuromuscular junction. *BMC Neuroscience*, 12. doi: 10.1186/1471-2202-12-65

145. Kitanishi, T., Sakai, J., Kojima, S., Saitoh, Y., Inokuchi, K., Fukaya, M., Watanabe, M., Matsuki, N., & Yamada, M. K. (2010). Activity-dependent localization in spines of the F-actin capping protein CapZ screened in a rat model of dementia. *Genes to Cells*, 15(7), 737–747. doi: 10.1111/j.1365-2443.2010.01411.x

146. Kneussel, M., & Wagner, W. (2013). Myosin motors at neuronal synapses: Drivers of membrane transport and actin dynamics. *Nature Reviews Neuroscience*, 14(4), 233–247. doi: 10.1038/nrn3445

147. Kobayashi, C., Aoki, C., Kojima, N., Yamazaki, H., & Shirao, T. (2007). Drebrin A content correlates with spine head size in the adult mouse cerebral cortex. *Journal of Comparative Neurology*, 503(5), 618–626. doi: 10.1002/cne.21408

148. Koch, N., Kobler, O., Thomas, U., Qualmann, B., & Kessels, M. M. (2014). Terminal Axonal Arborization and Synaptic Bouton Formation Critically Rely on Abp1 and the Arp2/3 Complex. *PLoS ONE*, 9(5). doi: 10.1371/journal.pone.0097692

149. Koganezawa, N., Hanamura, K., Sekino, Y., & Shirao, T. (2017). The role of drebrin in dendritic spines. *Molecular and Cellular Neuroscience*, 84, 85–92. doi: 10.1016/j.mcn.2017.01.004

150. Kojima, N., & Shirao, T. (2007). Synaptic dysfunction and disruption of postsynaptic drebrin-actin complex: A study of neurological disorders accompanied by cognitive deficits. *Neuroscience Research*, 58(1), 1–5. doi: 10.1016/j.neures.2007.02.003

151. Kong, X. C., Barzaghi, P., & Ruegg, M. A. (2004). Inhibition of synapse assembly in mammalian muscle in vivo by RNA interference. *EMBO Reports*, 5(2), 183–188. doi: 10.1038/sj.embor.7400065

152. Kounakis, K., & Tavernarakis, N. (2019). The Cytoskeleton as a Modulator of Aging and Neurodegeneration. *Advances in Experimental Medicine and Biology*, 1178, 227–245. doi: 10.1007/978-3-030-25650-0_12

153. Kowarz, E., Löscher, D., & Marschalek, R. (2015). Optimized Sleeping Beauty transposons rapidly generate stable transgenic cell lines. *Biotechnology Journal*, 10(4), 647–653. doi: 10.1002/biot.201400821

154. Krauss, R. S. (2017). Regulation of Skeletal Myoblast Differentiation by Drebrin. *Advances in Experimental Medicine and Biology,* 1006, 361–373. doi: 10.1007/978-4-431-56550-5

155. Kreis, P., Hendricusdottir, R., Kay, L., Papageorgiou, I. E., van Diepen, M., Mack, T., Ryves, J., Harwood, A., Leslie, N. R., Kann, O., Parsons, M., & Eickholt, B. J. (2013). Phosphorylation of the Actin Binding Protein Drebrin at S647 Is Regulated by Neuronal Activity and PTEN. *PLoS ONE*, 8(8), 1–12. doi: 10.1371/journal.pone.0071957

156. Krendel, M., & Mooseker, M. S. (2005). Myosins: Tails (and Heads) of Functional Diversity. *Physiology*, 20(20), 239–251. doi: 10.1152/physiol.00014.2005

157. Kühne, W. (1864). Untersuchungen über das Protoplasma und die Contractilität (Engelmann, Leipzig). doi: 10.5962/bhl.title.46515

158. Kummer, T. T., Misgeld, T., Lichtman, J. W., & Sanes, J. R. (2004). Nerve-independent formation of a topologically complex postsynaptic apparatus. *Journal of Cell Biology*, 164(7), 1077–1087. doi: 10.1083/jcb.200401115

159. Kuroiwa, M., Oneyama, C., Nada, S., & Okada, M. (2011). The guanine nucleotide exchange factor Arhgef5 plays crucial roles in Src-induced podosome formation. *Journal of Cell Science*, 124(10), 1726–1738. doi: 10.1242/jcs.080291

160. Lai, K. O., Ip, F. C. F., Cheung, J., Fu, A. K. Y., & Ip, N. Y. (2001). Expression of Eph receptors in skeletal muscle and their localization at the neuromuscular junction. *Molecular and Cellular Neuroscience*, 17(6), 1034–1047. doi: 10.1006/mcne.2001.0997

161. Langford, G. M. (1995). Actin- and microtubule-dependent organelle motors: interrelationships between the two motility systems. *Current Opinion in Cell Biology*, 7(1), 82–88. doi: 10.1016/0955-0674(95)80048-4

162. Lansbergen, G., Grigoriev, I., Mimori-Kiyosue, Y., Ohtsuka, T., Higa, S., Kitajima, I., Demmers, J., Galjart, N., Houtsmuller, A. B., Grosveld, F., & Akhmanova, A. (2006). CLASPs Attach Microtubule Plus Ends to the Cell Cortex through a Complex with LL5β. *Developmental Cell*, 11(1), 21–32. doi: 10.1016/j.devcel.2006.05.012

163. Lapidos, K. A., Kakkar, R., & McNally, E. M. (2004). The Dystrophin Glycoprotein Complex: Signaling Strength and Integrity for the Sarcolemma. *Circulation Research*, 94(8), 1023–1031. doi: 10.1161/01.RES.0000126574.61061.25

164. Lasser, M., Tiber, J., & Lowery, L. A. (2018). The role of the microtubule cytoskeleton in neurodevelopmental disorders. *Frontiers in Cellular Neuroscience*, 12(June), 1–18. doi: 10.3389/fncel.2018.00165

165. Lee, Y. il. (2019). Differences in the constituent fiber types contribute to the intermuscular variation in the timing of the developmental synapse elimination. *Scientific Reports*, 9(8694). doi: 10.1038/s41598-019-45090-6

166. Lee, Y. il, Mikesh, M., Smith, I., Rimer, M., & Thompson, W. (2011). Muscles in a mouse model of spinal muscular atrophy show profound defects in neuromuscular development even in the absence of failure in neuromuscular transmission or loss of motor neurons. *Developmental Biology*, 356(2), 432–444. doi: 10.1016/j.dcn.2011.01.002.

167. Lee, Y. il, Thompson, W. J., & Harlow, M. L. (2017). Schwann cells participate in synapse elimination at the developing neuromuscular junction. *Current Opinion in Neurobiology*, 47, 176–181. doi: 10.1016/j.conb.2017.10.010

168. Lee, J. W., Ryoo, Z. Y., Lee, E. J., Hong, S. H., Chung, W. H., Lee, H. T., Chung, K. S., Kim, T. Y., Oh, Y. S., & Suh, J. G. (2002). Circling mouse, a spontaneous mutant in the inner ear. *Experimental animals*, 51(2), 167–171.

169. Lee, M., Paik, S. K., Lee, M. J., Kim, Y. J., Kim, S., Nahm, M., Oh, S. J., Kim, H. M., Yim, J., Lee, C. J., Bae, Y. C., & Lee, S. (2009). Drosophila Atlastin regulates the stability of muscle microtubules and is required for synapse development. *Developmental Biology*, 330(2), 250–262. doi: 10.1016/j.ydbio.2009.03.019

170. Lehka, L., Topolewska, M., Wojton, D., Karatsai, O., Alvarez-Suarez, P., Pomorski, P., & Rędowicz, M. J. (2020). Formation of Aberrant Myotubes by Myoblasts Lacking Myosin VI Is Associated with Alterations in the Cytoskeleton Organization, Myoblast Adhesion and Fusion. *Cells*, 9(1673), 1–15. doi: 10.3390/cells9071673

171. Lehka, L., Wojton, D., Topolewska, M., Chumak, V., Majewski, Ł., & Rędowicz, M. J. (2022). Loss of Unconventional Myosin VI Affects cAMP/PKA Signaling in Hindlimb Skeletal Muscle in an Age-Dependent Manner. *Frontiers in Physiology* [in press]. doi: 10.3389/fphys.2022.933963

172. Li, B., Ding, S., Fenga, N., Mooney, N., Ooia, Y. S., Ren, L., Diep, J., Kelly, M. R., Yasukawa, L. L., Patton, J. T., Yamazaki, H., Shirao, T., Jackson, P. K., & Greenberg, H. B. (2017). Drebrin restricts rotavirus entry by inhibiting dynamin-mediated endocytosis. *Proceedings of the National Academy of Sciences of the United States of America*, 114(18), E3642–E3651. doi: 10.1073/pnas.1619266114

173. Li, L., Cao, Y., Wu, H., Ye, X., Zhu, Z., Xing, G., Shen, C., Barik, A., Zhang, B., Xie, X., Zhi, W., Gan, L., Su, H., Xiong, W.-C., & Mei, L. (2016). Enzymatic Activity of the Scaffold Protein Rapsyn for Synapse Formation. *Neuron*, 92(5), 1007–1019. doi: 10.1016/j.neuron.2016.10.023

174. Li, L., Xiong, W.-C., & Mei, L. (2018). Neuromuscular Junction Formation, Aging, and Disorders. *Annual Review of Physiology*, 8014(November 2017), 1–30. doi: 10.1146/annurev-physiol-022516

175. Li, M. W. M., Xiao, X., Mruk, D. D., Lam, Y., Lee, W. M., Lui, W.-Y., Bonanomi, M., Silvestrini, B., & Cheng, C. Y. (2011). Actin-binding protein drebrin E is involved in junction dynamics during spermatogenesis. *Spermatogenesis*, 1(2), 123–136. doi: 10.4161/spmg.1.2.16393

176. Li, X., Dong, X., Luo, S., Zhang, B., Lee, D., Ting, A., Neiswender, H., Kim, C.-H., Carpenter-Hyland, E., Gao, T.-M., Xiong, W.-C., & Mei, L. (2008). Retrograde regulation of motoneuron differentiation by muscle beta-catenin. *Nature Neuroscience*, 11(3), 262–268. doi: doi: 10.1038/nn2053

177. Li, Z., Liu, H., Li, J., Yang, Q., Feng, Z., Li, Y., Yang, H., Yu, C., Wan, J., Liu, W., & Zhang, M. (2019). Homer Tetramer Promotes Actin Bundling Activity of Drebrin. *Structure*, 27(1), 27-38.e4. doi: 10.1016/j.str.2018.10.011

178. Lieber, R. L., Roberts, T. J., Blemker, S. S., Lee, S. S. M., & Herzog, W. (2017). Skeletal muscle mechanics, energetics and plasticity Daniel P Ferris. *Journal of NeuroEngineering and Rehabilitation*, 14(1), 1–16. doi: 10.1186/s12984-017-0318-y

179. Liebl, F. L. W., Chen, K., Karr, J., Sheng, Q., & Featherstone, D. E. (2005). Increased synaptic microtubules and altered synapse development in Drosophila sec8 mutants. *BMC Biology*, 3, 1–20. doi: 10.1186/1741-7007-3-27

180. Lijam, N., Paylor, R., Mcdonald, M. P., Crawley, J. N., Deng, C., Herrup, K., Stevens, K. E., Maccaferri, G., Mcbain, C. J., Sussman, D. J., & Wynshaw-Boris, A. (1997). Social Interaction and Sensorimotor Gating Abnormalities in Mice Lacking Dvl1. *Cell*, 90, 895–905. doi: 10.1016/s0092-8674(00)80354-2.

181. Lin, S., Hsieh, T., Liou, G., Li, T., Lin, H., & Chang, C. (2020). Dynamin-2 Regulates Postsynaptic Cytoskeleton Organization and Neuromuscular Junction Development. *Cell Reports*, 33(4), 108310. doi: 10.1016/j.celrep.2020.108310

182. Lin, W., Burgess, R. W., Dominguez, B., Pfaff, S. L., Sanes, J. R., & Lee, K. F. (2001). Distinct roles of nerve and muscle in postsynaptic differentiation of the neuromuscular synapse. *Nature*, 410(6832), 1057–1064. doi: 10.1038/35074025

183. Linder, S., & Aepfelbacher, M. (2003). Podosomes: Adhesion hot-spots of invasive cells. *Trends in Cell Biology*, 13(7), 376–385. doi: 10.1016/S0962-8924(03)00128-4

184. Liu, X.-Z., Walsh, J., Mburu, P., Kendrick-Jones, J., Cope, M. J. T. V., Steel, K. P., & Brown, S. D. M. (1997). Mutations in the myosin VIIA gene causes non-syndromic recessive deafness. *Nature Genetics*, 16(June), 188–190. doi: 10.1038/ng0697-188

185. Luther, P. K. (2009). The vertebrate muscle Z-disc: Sarcomere anchor for structure and signalling. *Journal of Muscle Research and Cell Motility*, 30(5–6), 171–185. doi: 10.1007/s10974-009-9189-6

186. Maddugoda, M. P., Crampton, M. S., Shewan, A. M., & Yap, A. S. (2007). Myosin VI and vinculin cooperate during the morphogenesis of cadherin cell-cell contacts in mammalian epithelial cells. *Journal of Cell Biology*, 178(3), 529–540. doi: 10.1083/jcb.200612042

187. Majoul, I., Shirao, T., Sekino, Y., & Duden, R. (2007). Many faces of drebrin: From building dendritic spines and stabilizing gap junctions to shaping neurite-like cell

processes. *Histochemistry and Cell Biology*, 127(4), 355–361. doi: 10.1007/s00418-007-0273-y

188. Mammoto, A., Sasaki, T., Asakura, T., Hotta, I., Imamura, H., Takahashi, K., Matsuura, Y., Shirao, T., & Takai, Y. (1998). Interactions of Drebrin and Gephyrin with Profilin 1. *Biochemical and Biophysical Research Communications*, 243, 86–89. doi: 10.1006/bbrc.1997.8068

189. Mancini, A., Sirabella, D., Zhang, W., Yamazaki, H., Shirao, T., & Krauss, R. S. (2011). Regulation of myotube formation by the actin-binding factor drebrin. *Skeletal Muscle*, 1(1), 36. doi: 10.1186/2044-5040-1-36

190. Mao, C.-X., Xiong, Y., Xiong, Z., Wang, Q., Zhang, Y. Q., & Jin, S. (2014). Microtubule-severing protein Katanin regulates neuromuscular junction development and dendritic elaboration in Drosophila. *Development*, 141(5), 1064–1074. doi: 10.1242/dev.097774

191. Marchand, S., Bignami, F., Stetzkowski-Marden, F., & Cartaud, J. (2000). The myristoylated protein rapsyn is cotargeted with the nicotinic acetylcholine receptor to the postsynaptic membrane via the exocytic pathway. *Journal of Neuroscience*, 20(2), 521–528. doi: 10.1523/jneurosci.20-02-00521.2000

192. Marques, M. J., Conchello, J. A., & Lichtman, J. W. (2000). From plaque to pretzel: Fold formation and acetylcholine receptor loss at the developing neuromuscular junction. *Journal of Neuroscience*, 20(10), 3663–3675. doi: 10.1523/jneurosci.20-10-03663.2000

193. Martinez-Pena y Valenzuela, I., Aittaleb, M., Chen, P.-J., & Akaaboune, M. (2015). The Knockdown of αkap Alters the Postsynaptic Apparatus of Neuromuscular Junctions in Living Mice. *Journal of Neuroscience*, 35(13), 5118–5127. doi: 10.1523/JNEUROSCI.3951-14.2015

194. Martinez-Pena y Valenzuela, Isabel, Pires-Oliveira, M., & Akaaboune, M. (2013). PKC and PKA regulate AChR dynamics at the neuromuscular junction of living mice. *PLoS ONE*, 8(11), e81311. doi: 10.1371/journal.pone.0081311

195. Mátés, L., Chuah, M. K. L., Belay, E., Jerchow, B., Manoj, N., Acosta-Sanchez, A., Grzela, D. P., Schmitt, A., Becker, K., Matrai, J., Ma, L., Samara-Kuko, E., Gysemans, C., Pryputniewicz, D., Miskey, C., Fletcher, B., Vandendriessche, T., Ivics, Z., & Izsvák, Z. (2009). Molecular evolution of a novel hyperactive Sleeping Beauty transposase enables robust stable gene transfer in vertebrates. *Nature Genetics*, 41(6), 753–761. doi: 10.1038/ng.343

196. Mazhar, S., & Herbst, R. (2012). The formation of complex acetylcholine receptor clusters requires MuSK kinase activity and structural information from the MuSK extracellular domain. *Molecular and Cellular Neuroscience*, 49(4), 475–486. doi: 10.1016/j.mcn.2011.12.007

197. Mech, A. M., Brown, A. L., Schiavo, G., & Sleigh, J. N. (2020). Morphological variability is greater at developing than mature mouse neuromuscular junctions. *Journal of Anatomy*, 237(4), 603–617. doi: 10.1111/joa.13228

198. Medina-Moreno, A., & Henríquez, J. P. (2021). Maturation of a postsynaptic domain: Role of small Rho GTPases in organising nicotinic acetylcholine receptor aggregates at the vertebrate neuromuscular junction. *Journal of Anatomy*, July, 1–9. doi: 10.1111/joa.13526

199. Menna, E., Zambetti, S., Morini, R., Donzelli, A., Disanza, A., Calvigioni, D., Braida, D., Nicolini, C., Orlando, M., Fossati, G., Cristina Regondi, M., Pattini, L., Frassoni, C., Francolini, M., Scita, G., Sala, M., Fahnestock, M., & Matteoli, M. (2013). Eps8 controls dendritic spine density and synaptic plasticity through its actin-capping activity. *EMBO Journal*, 32(12), 1730–1744. doi: 10.1038/emboj.2013.107

200. Mercer, J. C., Qi, Q., Mottram, L. F., Law, M., Bruce, D., Iyer, A., Morales, J. L., Yamazaki, H., Shirao, T., R, B., & August, A. (2010). Chemico-Genetic Identification of Drebrin as a Regulator of Calcium Responses. *International Journal of Biochemistry*, 42(2), 337–345. doi: 10.1016/j.biocel.2009.11.019.Chemico-Genetic

201. Mermall, V., & Miller, K. G. (1995). The 95F unconventional myosin is required for proper organization of the Drosophila syncytial blastoderm. *Journal of Cell Biology*, 129(6), 1575–1588. doi: 10.1083/jcb.129.6.1575

202. Merriam, E. B., Millette, M., Lumbard, D. C., Saengsawang, W., Fothergill, T., Hu, X., Ferhat, L., & Dent, E. W. (2013). Synaptic Regulation of Microtubule Dynamics in Dendritic Spines by Calcium, F-Actin, and Drebrin. *Journal of Neuroscience*, 33(42), 16471–16482. doi: 10.1523/JNEUROSCI.0661-13.2013

203. Mizui, T., Kojima, N., Yamazaki, H., Katayama, M., Hanamura, K., & Shirao, T. (2009). Drebrin E is involved in the regulation of axonal growth through actin-myosin interactions. *Journal of Neurochemistry*, 109, 611–622. doi: 10.1111/j.1471-4159.2009.05993.x

204. Mizui, T., Sekino, Y., Yamazaki, H., Ishizuka, Y., & Takahashi, H. (2014). Myosin II ATPase Activity Mediates the Long-Term Potentiation-Induced Exodus of Stable F-Actin Bound by Drebrin A from Dendritic Spines. *PLoS ONE*, 9(1), e85367. doi: 10.1371/journal.pone.0085367

205. Mohamed, A. S., & Swope, S. L. (1999). Phosphorylation and Cytoskeletal Anchoring of the Acetylcholine Receptor by Src Class Protein-tyrosine Kinases: Activation by Rapsyn. *Journal of Biological Chemistry*, 274(29), 20529–20539. doi: 10.1074/jbc.274.29.20529

206. Mohiddin, S. A., Ahmed, Z. M., Griffith, A. J., Tripodi, D., Friedman, T. B., Fananapazir, L., & Morell, R. J. (2004). Novel association of hypertrophic cardiomyopathy, sensorineural deafness, and a mutation in unconventional myosin VI (MYO6). *Journal of Medical Genetics*, 41(4), 309–314. doi: 10.1136/jmg.2003.011973

207. Molkentin, J. D., Lu, J.-R., Antos, C. L., Markham, B., Richardson, J., Robbins, J., Grant, S. R., & Olson, E. N. (1998). A calcineurin-dependent transcriptional pathway for cardiac hypertrophy. *Cell*, 93(2), 215–228. doi: 10.1016/s0092-8674(00)81573-1.

208. Moransard, M., Borges, L. S., Willmann, R., Marangi, P. A., Brenner, H. R., Ferns, M. J., & Fuhrer, C. (2003). Agrin regulates rapsyn interaction with surface acetylcholine receptors, and this underlies cytoskeletal anchoring and clustering. *Journal of Biological Chemistry*, 278(9), 7350–7359. doi: 10.1074/jbc.M210865200

209. Mouslim, C., Aittaleb, M., Hume, R. I., & Akaaboune, M. (2012). A role for the calmodulin kinase II-related anchoring protein (αkap) in maintaining the stability of nicotinic acetylcholine receptors. *Journal of Neuroscience*, 32(15), 5177–5185. doi: 10.1523/JNEUROSCI.6477-11.2012

210. Mukherjea, M., Llinas, P., Kim, H., Travaglia, M., Safer, D., Me, J., Franzini-armstrong, C., Selvin, P. R., Houdusse, A., & Sweeney, H. L. (2009). Myosin VI Dimerization Triggers an Unfolding of a Three-Helix Bundle in Order to Extend Its Reach. *Molecular Cell*, 35, 305–315. doi: 10.1016/j.molcel.2009.07.010

211. Naccache, S. N., Hasson, T., & Horowitz, A. (2006). Binding of internalized receptors to the PDZ domain of GIPC/synectin recruits myosin VI to endocytic vesicles. *Proceedings of the National Academy of Sciences of the United States of America*, 103(34), 12735–12740. doi: 10.1073/pnas.0605317103

212. Naddaf, E., Dasari, S., Selcen, D., Charlesworth, M. C., Johnson, K. L., Mauermann, M. L., & Kourelis, T. (2022). Proteomic profiling of sporadic late-onset nemaline myopathy. *Annals of Clinical and Translational Neurology*, 9(3), 391–402. doi: 10.1002/acn3.51527

213. Nager, A. R., Goldstein, J. S., Ye, F., Garcia-verdugo, J. M., Nachury, M. V, Portran, D., & Ye, F. (2017). An Actin Network Dispatches Ciliary GPCRs into Extracellular Vesicles to Modulate Signaling Article An Actin Network Dispatches Ciliary GPCRs into Extracellular Vesicles to Modulate Signaling. *Cell*, 168, 1–12. doi: 10.1016/j.cell.2016.11.036

214. Nakamura, M., Zhou, X. Z., & Lu, K. P. (2001). Critical role for the EB1 and APC interaction in the regulation of microtubule polymerization. *Current Biology*, 11(13), 1062–1067. doi: 10.1016/S0960-9822(01)00297-4

215. Nash, J. E., Appleby, V. J., Corrêa, S. A. L., Wu, H., Fitzjohn, S. M., Garner, C. C., Collingridge, G. L., & Molnár, E. (2010). Disruption of the interaction between myosin VI and SAP97 is associated with a reduction in the number of AMPARs at hippocampal synapses. *Journal of Neurochemistry*, 112(3), 677–690. doi: 10.1111/j.1471-4159.2009.06480.x

216. Needham, D. M. (1926). Red and white muscle. *Physiological Reviews*, 6(1), 1–27. doi:10.1152/physrev.1926.6.1.1

217. Nelson, J. C., Stavoe, A. K. H., Colón-ramos, D. A., Nelson, J. C., Stavoe, A. K. H., Colón-ramos, D. A., Nelson, J. C., Stavoe, A. K. H., & Colón-ramos, D. A. (2013). The actin cytoskeleton in presynaptic assembly. *Cell Adhesion & Migration*, 7(4), 379–387. doi: 10.4161/cam.24803

218. Noakes, P. G., Gautam, M., Mudd, J., Sanes, J. R., & Merlie, J. P. (1995). Aberrant differentiation of neuromuscular junctions in mice lacking s-laminin/laminin β2. *Nature*, 374(6519), 258–262). doi: 10.1038/374258a0

219. North, K. N., & Beggs, A. H. (1996). Deficiency of a skeletal muscle isoform of α-actinin (α-actinin-3) in merosin-positive congenital muscular dystrophy. *Neuromuscular Disorders*, 6(4), 229–235. doi: 10.1016/0960-8966(96)00361-6

220. Odronitz, F., & Kollmar, M. (2007). Drawing the tree of eukaryotic life based on the analysis of 2,269 manually annotated myosins from 328 species. *Genome Biology*, 8(9), 1–23. doi: 10.1186/gb-2007-8-9-r196

221. Oh, S.L., Yoon, S. H., & Lim, J.Y. (2018). Age- and sex-related differences in myosin heavy chain isoforms and muscle strength, function, and quality: a cross sectional study. *Journal of Exercise Nutrition & Biochemistry*, 22(2), 43–50. doi: 10.20463/jenb.2018.0016

222. Ohno, K., Engel, A. G., Shen, X. M., Selcen, D., Brengman, J., Harper, C. M., Tsujino, A., & Milone, M. (2002). Rapsyn mutations in humans cause endplate acetylcholine-receptor deficiency and myasthenic syndrome. *American Journal of Human Genetics*, 70(4), 875–885. doi: 10.1086/339465

223. Okada, K., Inoue, A., Okada, M., Murata, Y., Kakuta, S., Jigami, T., Kubo, S., Shiraishi, H., Eguchi, K., Motomura, M., Akiyama, T., Iwakura, Y., Higuchi, O., & Yamanashi, Y. (2006). The Muscle Protein Dok-7 Is Essential for Neuromuscular Synaptogenesis. *Science*, 312(June), 1802–1806. doi: 10.1126/science.1127142

224. Osterweil, E., Wells, D. G., & Mooseker, M. S. (2005). A role for myosin VI in postsynaptic structure and glutamate receptor endocytosis. *Journal of Cell Biology*, 168(2), 329–338. doi: 10.1083/jcb.200410091

225. Oury, J., Liu, Y., Töpf, A., Todorovic, S., Hoedt, E., Preethish-Kumar, V., Neubert, T. A., Lin, W., Lochmüller, H., & Burden, S. J. (2019). MACF1 links Rapsyn to microtubule- and actin-binding proteins to maintain neuromuscular synapses. *Journal of Cell Biology*, 218(5), 1686–1705. doi: 10.1083/jcb.201810023

226. Patton, B. L. (2003). Basal lamina and the organization of neuromuscular synapses. *Journal of Neurocytology*, 32(5–8), 883–903. doi: 10.1023/B:NEUR.0000020630.74955.19

227. Patton, B. L., Cunningham, J. M., Thyboll, J., Kortesmaa, J., Westerblad, H., Edström, L., Tryggvason, K., & Sanes, J. R. (2001). Properly formed but improperly localized synaptic specializations in the absence of laminin α4. *Nature Neuroscience*, 4(6), 597–604. doi: 10.1038/88414

228. Pawlikowski, B. T., & Maimone, M. M. (2009). Formation of complex AChR aggregates in vitro requires α-Dystrobrevin. *Developmental Neurobiology*, 69(5), 326–338. doi: 10.1002/dneu.20703

229. Peitsch, W. K., Bulkescher, J., Spring, H., Hofmann, I., Goerdt, S., & Franke, W. W. (2006). Dynamics of the actin-binding protein drebrin in motile cells and definition of a juxtanuclear drebrin-enriched zone. *Experimental Cell Research*, 2, 2605–2618. doi: 10.1016/j.yexcr.2006.04.017

230. Peitsch, W. K., Grund, C., Kuhn, C., Schnölzer, M., Spring, H., Schmelz, M., & Franke, W. W. (1999). Drebrin is a widespread actin-associating protein enriched at junctional plaques, defining a specific microfilament anchorage system in polar epithelial cells. *European Journal of Cell Biology*, 78(11), 767–778. doi: 10.1016/S0171-9335(99)80027-2

231. Pereira, J. D., DuBreuil, D. M., Devlin, A. C., Held, A., Sapir, Y., Berezovski, E., Hawrot, J., Dorfman, K., Chander, V., & Wainger, B. J. (2021). Human sensorimotor organoids derived from healthy and amyotrophic lateral sclerosis stem cells form neuromuscular junctions. *Nature Communications*, 12(1). doi: 10.1038/s41467-021-24776-4

232. Pérez-Martínez, M., Gordón-Alonso, M., Cabrero, J. R., Barrero-Villar, M., Rey, M., Mittelbrunn, M., Lamana, A., Morlino, G., Calabia, C., Yamazaki, H., Shirao, T., Vázquez, J., González-Amaro, R., Veiga, E., & Sánchez-Madrid, F. (2010). F-actin-binding protein drebrin regulates CXCR4 recruitment to the immune synapse. *Journal of Cell Science*, 1(123), 1160–1170. doi: 10.1242/jcs.064238

233. Peter, J. B., Barnard, R. J., Edgerton, V. R., Gillespie, C. A., & Stempel, K. E. (1972). Metabolic Profiles of Three Fiber Types of Skeletal Muscle in Guinea Pigs and Rabbits. *Biochemistry*, 11(14), 2627–2633.

234. Pette, D., & Vrbová, G. (2017). The Contribution of Neuromuscular Stimulation in Elucidating Muscle Plasticity Revisited. *European Journal of Translational Myology*, 27(1), 33–39.

235. Pęziński, M., Daszczuk, P., Pradhan, B. S., Lochmüller, H., & Prószyński, T. J. (2020). An improved method for culturing myotubes on laminins for the robust clustering of postsynaptic machinery. *Scientific Reports*, 10(1), 1–13. doi: 10.1038/s41598-020-61347-x

236. Pęziński, M., Maliszewska-Olejniczak, K., Daszczuk, P., Mazurek, P., Niewiadomski, P., & Rędowicz, M. J. (2021). Tks5 regulates synaptic podosome formation and stabilization of the postsynaptic machinery at the neuromuscular junction. International *Journal of Molecular Sciences*, 22(21). doi: 10.3390/ijms222112051

237. Pielage, J., Cheng, L., Fetter, R. D., Carlton, P. M., Sedat, J. W., & Davis, G. W. (2008). A Presynaptic Giant Ankyrin Stabilizes the NMJ through Regulation of Presynaptic Microtubules and Transsynaptic Cell Adhesion. *Neuron*, 58(2), 195–209. doi: 10.1016/j.neuron.2008.02.017

238. Pilpel, Y., & Segal, M. (2005). Rapid WAVE dynamics in dendritic spines of cultured hippocampal neurons is mediated by actin polymerization. *Journal of Neurochemistry*, 95(5), 1401–1410. doi: 10.1111/j.1471-4159.2005.03467.x

239. Plotkin, D. L., Roberts, M. D., Haun, C. T., & Schoenfeld, B. J. (2021). Muscle fiber type transitions with exercise training: Shifting perspectives. *Sports*, 9(9), 1–11. doi: 10.3390/SPORTS9090127

240. Pollard, T. D., & Cooper, J. A. (2009). Actin, a Central Player in Cell Shape and Movement. *Science*, 326(5957), 1208–1212. doi: 10.1126/science.1175862.

241. Poobalasingam, T., Bianco, F., Oozeer, F., & Gordon-Weeks, P. R. (2021). The drebrin/EB3 pathway regulates cytoskeletal dynamics to drive neuritogenesis in embryonic cortical neurons. *Journal of Neurochemistry*, 160(2), 185–202. doi: 10.1111/jnc.15502

242. Potau, J. M., Artells, R., Muoz, C., Daz, T., Bello-Hellegouarch, G., Arias-Martorell, J., Prez-Prez, A., & Monz, M. (2012). Expression of myosin heavy chain isoforms in the human supraspinatus muscle: Variations related to age and sex. *Cells Tissues Organs*, 196(5), 456–462. doi: 10.1159/000336680

243. Pratt, S. J. P., Shah, S. B., Ward, C. W., Kerr, J. P., Stains, J. P., & Lovering, R. M. (2014). Recovery of altered neuromuscular junction morphology and muscle function in mdx mice after injury. *Cellular and Molecular Life Sciences*, 72(1), 153–164. doi: 10.1007/s00018-014-1663-7

244. Proszynski, T. J., Gingras, J., Valdez, G., Krzewski, K., & Sanes, J. R. (2009). Podosomes are present in a postsynaptic apparatus and participate in its maturation. *Proceedings of the National Academy of Sciences of the United States of America*, 106(43), 18373–18378. doi: 10.1073/pnas.0910391106

245. Proszynski, T. J., & Sanes, J. R. (2013). Amotl2 interacts with LL5β, localizes to podosomes and regulates postsynaptic differentiation in muscle. *Journal of Cell Science*, 126(10), 2225–2235. doi: 10.1242/jcs.121327

246. Purves, D., Augustine, G. J., White, D. F., Hall, W. C., LaMantia, A.-S., Mooney, R. D., Platt, M. L., & E.White, L. (Eds.). (2018). *Neuroscience* (6th ed.). Oxford University Press USA. doi: 10.2307/j.ctvw1d7fz.6

247. Racz, B., & Weinberg, R. J. (2006). Spatial organization of cofilin in dendritic spines. *Neuroscience*, 138(2), 447–456. doi: 10.1016/j.neuroscience.2005.11.025

248. Rafuse, V. F., Polo-Parada, L., & Landmesser, L. T. (2000). Structural and functional alterations of neuromuscular junctions in NCAM-deficient mice. *Journal of Neuroscience*, 20(17), 6529–6539.

249. Rahimov, F., & Kunkel, L. M. (2013). Cellular and molecular mechanisms underlying muscular dystrophy. *Journal of Cell Biology*, 201(4), 499–510. doi: 10.1083/jcb.201212142

250. Ratliff, W. A., Saykally, J. N., Kane, M. J., & Citron, B. A. (2018). Neuromuscular Junction Morphology and Gene Dysregulation in the Wobbler Model of Spinal Neurodegeneration. *Journal of Molecular Neuroscience*, 66(1), 114–120. doi: 10.1007/s12031-018-1153-8.

251. Reddy, L. V., Koirala, S., Sugiura, Y., Herrera, A. A., & Ko, C.-P. (2003). Glial Cells Maintain Synaptic Structure and Function and Promote Development of the Neuromuscular Junction In Vivo. *Neuron*, 40, 563–580. doi: 10.1016/s0896-6273(03)00682-2

252. Redfern, P. A. (1970). Neuromuscular transmission in new-born rats. *Journal of Physiology*, 209, 701–709. doi: 10.1113/jphysiol.1970.sp009187

253. Redowicz, M. J. (2007). Unconventional myosins in muscle. *European Journal of Cell Biology*, 86(9), 549–558. doi: 10.1016/j.ejcb.2007.05.007

254. Rehm, K., Panzer, L., van Vliet, V., Genot, E., & Linder, S. (2013). Drebrin preserves endothelial integrity by stabilizing nectin at adherens junctions. *Journal of Cell Science*, 126(16), 3756–3769. doi: 10.1242/jcs.129437

255. Röder, I. V., Petersen, Y., Choi, K. R., Witzemann, V., Hammer, J. A., & Rudolf, R. (2008). Role of myosin Va in the plasticity of the vertebrate neuromuscular junction in vivo. *PLoS ONE*, 3(12). doi: 10.1371/journal.pone.0003871

256. Röder, I. V., Choi, K. R., Reischl, M., Petersen, Y., Diefenbacher, M. E., Zaccolo, M., Pozzan, T., & Rudolf, R. (2010). Myosin Va cooperates with PKA RIα to mediate maintenance of the endplate in vivo. *Proceedings of the National Academy of Sciences of the United States of America*, 107(5), 2031–2036. doi: 10.1073/pnas.0914087107

257. Rogat, A. D., & Miller, K. G. (2002). A role for myosin VI in actin dynamics at sites of membrane remodeling during Drosophila spermatogenesis. *Journal of Cell Science*, 115(24), 4855–4865. doi: 10.1242/jcs.00149

258. Roostalu, J., Thomas, C., Cade, N. I., Kunzelmann, S., Taylor, I. A., & Surrey, T. (2020). The speed of GTP hydrolysis determines GTP cap size and controls microtubule stability. *ELife*, 9, 1–22. doi: 10.7554/eLife.51992

259. Roth, D., Fitton, B. P., Chmel, N. P., Wasiluk, N., & Straube, A. (2019). Spatial positioning of EB family proteins at microtubule tips involves distinct nucleotide-dependent binding properties. *Journal of Cell Science*, 132(4). doi: 10.1242/jcs.219550

260. Salanova, M., Bortoloso, E., Schiffl, G., Gutsmann, M., Belavy, D. L., Felsenberg, D., Furlan, S., Volpe, P., & Blottner, D. (2011). Expression and regulation of Homer in human skeletal muscle during neuromuscular junction adaptation to disuse and exercise. *The FASEB Journal*, 25(12), 4312–4325. doi: 10.1096/fj.11-186049

261. Samuel, M. A., Valdez, G., Tapia, J. C., Lichtman, J. W., & Sanes, J. R. (2012). Agrin and Synaptic Laminin Are Required to Maintain Adult Neuromuscular Junctions. *PLoS ONE*, 7(10). doi: 10.1371/journal.pone.0046663

262. Sanes, J. R., & Lichtman, J. W. (2001). Induction, assembly, maturation and maintenance of a postsynaptic apparatus. Nature Reviews. *Neuroscience*, 2(11), 791–805. doi: 10.1038/35097557\r35097557 [pii]

263. Sanes, J. R., & Lichtman, J. W. (1999). Development of the vertebrate neuromuscular junction. *Annual Review of Neuroscience*, 22, 389–442. doi: 10.1007/978-0-387-92708-4_3

264. Sanghvi-Shah, R., & Weber, G. F. (2017). Intermediate filaments at the junction of mechanotransduction, migration, and development. *Frontiers in Cell and Developmental Biology*, 5(SEP), 1–19. doi: 10.3389/fcell.2017.00081

265. Schätzle, P., Esteves da Silva, M., Tas, R. P., Katrukha, E. A., Hu, H. Y., Wierenga, C. J., Kapitein, L. C., & Hoogenraad, C. C. (2018). Activity-Dependent Actin Remodeling at the Base of Dendritic Spines Promotes Microtubule Entry Article Activity-Dependent Actin Remodeling at the Base of Dendritic Spines Promotes Microtubule Entry. *Current Biology*, 28(13), 2081–2093. doi: 10.1016/j.cub.2018.05.004

266. Schiaffino, S., & Reggiani, C. (2011). Fiber types in Mammalian skeletal muscles. *Physiological Reviews*, 91(4), 1447–1531. doi: 10.1152/physrev.00031.2010

267. Schindelin, J., Arganda-Carreras, I., Frise, E., Kaynig, V., Longair, M., Pietzsch, T., Preibisch, S., Rueden, C., Saalfeld, S., Schmid, B., Tinevez, J.-Y., White, D. J., Hartenstein, V., Eliceiri, K., Tomancak, P., & Cardona, A. (2012). Fiji: an open-source platform for biological-image analysis. *Nature Methods*, 9, 676–682. doi: 10.1038/nmeth.2019

268. Schmidt, N., Akaaboune, M., Gajendran, N., Martinez-Pena y Valenzuela, I., Wakefield, S., Thurnheer, R., & Brenner, H. R. (2011). Neuregulin/ErbB regulate neuromuscular junction development by phosphorylation of α-dystrobrevin. *Journal of Cell Biology*, 195(7), 1171–1184. doi: 10.1083/jcb.201107083

269. Schmidt, N., Basu, S., Sladecek, S., Gatti, S., van Haren, J., Treves, S., Pielage, J., Galjart, N., & Brenner, H. R. (2012). Agrin regulates CLASP2-mediated capture of

microtubules at the neuromuscular junction synaptic membrane. *Journal of Cell Biology*, 198(3), 421–437. doi: 10.1083/jcb.201111130

270. Schultheiss, T., Choi, J., Lin, Z. X., DiLullo, C., Cohen-Gould, L., Fischman, D., & Holtzer, H. (1992). A sarcomeric α-actinin truncated at the carboxyl end induces the breakdown of stress fibers in PtK2 cells and the formation of nemaline-like bodies and breakdown of myofibrils in myotubes. *Proceedings of the National Academy of Sciences of the United States of America*, 89(19), 9282–9286. doi: 10.1073/pnas.89.19.9282

271. Seene, T., Umnova, M., & Kaasik, P. (2017). NMJ among different fiber types and endurance exercise training Morphological peculiarities of neuromuscular junctions among different fiber types: Effect of exercise. *European Journal of Translational Myology*, 27(3), 139–146. doi: 10.4081/ejtm.2017.6708

272. Self, T., Sobe, T., Copeland, N. G., Jenkins, N. A., Avraham, K. B., & Steel, K. P. (1999). Role of myosin VI in the differentiation of cochlear hair cells. *Developmental Biology*, 214(2), 331–341. doi: 10.1006/dbio.1999.9424

273. Serrano, N., Colenso-semple, L. M., Lazauskus, K. K., Siu, J. W., Id, J. R. B., Lockie, R. G., Costa, P. B., & Id, A. J. G. (2019). Extraordinary fast-twitch fiber abundance in elite weightlifters. *PLoS ONE*, 14(3), e0207975. doi: 10.1371/journal.pone.0207975

274. Shan, Y., Farmer, S. M., & Wray, S. (2021). Drebrin regulates cytoskeleton dynamics in migrating neurons through interaction with CXCR4. *Proceedings of the National Academy of Sciences of the United States of America*, 118(3), 1–12. doi: 10.1073/pnas.2009493118

275. Sharma, S., Grintsevich, E. E., Phillips, M. L., Reisler, E., & Gimzewski, J. K. (2011). Atomic Force Microscopy Reveals Drebrin Induced Remodeling of F-Actin with Subnanometer Resolution. *Nano Letters*, 11(2), 825–827. doi: 10.1021/nl104159v.

276. Shen, C., Li, L., Zhao, K., Bai, L., Wang, A., Shu, X., Xiao, Y., Zhang, J., Zhang, K., Hui, T., Chen, W., Zhang, B., Hsu, W., Xiong, W. C., & Mei, L. (2018). Motoneuron Wnts regulate neuromuscular junction development. *ELife*, 7, 1–18. doi: 10.7554/eLife.34625

277. Shi, L., Butt, B., Ip, F. C. F., Dai, Y., Jiang, L., Yung, W. H., Greenberg, M. E., Fu, A. K. Y., & Ip, N. Y. (2010). Ephexin1 Is Required for Structural Maturation and Neurotransmission at the Neuromuscular Junction. *Neuron*, 65(2), 204–216. doi: 10.1016/j.neuron.2010.01.012

278. Shiraishi-Yamaguchi, Y., Sato, Y., Sakai, R., Mizutani, A., Knöpfel, T., Mori, N., Mikoshiba, K., & Furuichi, T. (2009). Interaction of Cupidin/Homer2 with two actin cytoskeletal regulators, Cdc42 small GTPase and Drebrin, in dendritic spines. *BMC Neuroscience*, 10, 1–14. doi: 10.1186/1471-2202-10-25

279. Shiraishi, Y., Mizutani, A., Bito, H., Fujisawa, K., Narumiya, S., Mikoshiba, K., & Furuichi, T. (1999). Cupidin, an Isoform of Homer/Vesl, Interacts with the Actin Cytoskeleton and Activated Rho Family Small GTPases and Is Expressed in Developing Mouse Cerebellar Granule Cells. *Journal of Neuroscience*, 19(19), 8389–8400. doi: 10.1523/JNEUROSCI.19-19-08389.1999

280. Shirao, T., Inoue, H. K., Kano, Y., & Obata, K. (1987). Localization of a developmentally regulated neuron-specific protein $ 54 in dendrites as revealed by immunoelectron microscopy. Brain Research, 413, 374–378. doi: 10.1016/0006-8993(87)91032-8

281. Shirao, T., Kojima, N., Terada, S., & Obata, K. (1990). Expression of three drebrin isoforms in the developing nervous system. *Neuroscience Research,* 13, S106–111.

282. Shirao, T., & Obata, K. (1986). Immunochemical Homology of 3 Developmentally Regulated Brain Proteins and Their Developmental Change in Neuronal Distribution. *Developmental Brain Research*, 29, 233–244. doi: 10.1016/0165-3806(86)90099-4

283. Shirao, T., & Sekino, Y. (2017). *Drebrin - From Structure and Function to Physiological and Pathological Roles*. Springer Japan KK. doi: 10.1007/978-4-431-56550-5

284. Sivaramakrishnan, S., & Spudich, J. A. (2009). Coupled myosin VI motors facilitate unidirectional movement on an F-actin network. *Journal of Cell Biology*, 187(1), 53–60. doi: 10.1083/jcb.200906133

285. Slater, C. (2017). The Structure of Human Neuromuscular Junctions: Some Unanswered Molecular Questions. *International Journal of Molecular Sciences*, 18(10), 2183. doi: 10.3390/ijms18102183

286. Slater, C. R. (2008). Structural Factors Influencing the Efficacy of Neuromuscular Transmission. *Annals of the New York Academy of Sciences*, 1132, 1–12. doi: 10.1196/annals.1405.003

287. Sobczak, M., Chumak, V., Pomorski, P., Wojtera, E., Majewski, Ł., Nowak, J., Yamauchi, J., & Redowicz, M. J. (2016). Interaction of myosin VI and its binding partner DOCK7 plays an important role in NGF-stimulated protrusion formation in PC12 cells. *Biochimica et Biophysica Acta - Molecular Cell Research*, 1863(7), 1589–1600. doi: 10.1016/j.bbamcr.2016.03.020

288. Soldati, T., & Schliwa, M. (2006). Powering membrane traffic in endocytosis and recycling. *Nature Reviews Molecular Cell Biology*, 7(December), 897–908. doi: 10.1038/nrm1960

289. Sonego, M., Oberoi, M., Stoddart, J., Gajendra, S., Hendricusdottir, R., Oozeer, F., Worth, D. C., Hobbs, C., Eickholt, B. J., Gordon-Weeks, P. R., Doherty, P., & Lalli, G. (2015). Drebrin regulates neuroblast migration in the postnatal mammalian brain. *PLoS ONE*, 10(5), 1–26. doi: 10.1371/journal.pone.0126478

290. Song, M., Kojima, N., Hanamura, K., Sekino, Y., Inoue, H. K., Mikuni, M., & Shirao, T. (2008). Expression of Drebrin E in Migrating Neuronblasts in Adult Rat Brain: Coincidence Between Drebrin E Dissappearance from Cell Body and Cessation of Migration. *Neuroscience*, 152, 670–682. doi: 10.1016/j.neuroscience.2007.10.068

291. Spence, E. F., & Soderling, S. H. (2015). Actin out: Regulation of the synaptic cytoskeleton. *Journal of Biological Chemistry*, 290(48), 28613–28622. doi: 10.1074/jbc.R115.655118

292. Spink, B. J., Sivaramakrishnan, S., Lipfert, J., Doniach, S., & Spudich, J. A. (2008). Long single α-helical tail domains bridge the gap between structure and function of myosin VI. *Nature Structural & Molecular Biology*, 15(6), 591–597. doi: 10.1038/nsmb.1429

293. Spudich, J. A., & Sivaramakrishnan, S. (2010). Myosin VI: an innovative motor that challenged the swinging lever arm hypothesis. *Nature Reviews Molecular Cell Biology*, 11(2), 128–137. doi: 10.1038/nrm2833

294. Squire, J. M. (1997). Architecture and function in the muscle sarcomere. *Current Opinion in Structural Biology*, 7(2), 247–257. doi: 10.1016/S0959-440X(97)80033-4

295. Stepanova, T., Slemmer, J., Hoogenraad, C. C., Lansbergen, G., Dortland, B., De Zeeuw, C. I., Grosveld, F., Van Cappellen, G., Akhmanova, A., & Galjart, N. (2003). Visualization of Microtubule Growth in Cultured Neurons via the Use of EB3-GFP (End-Binding Protein 3-Green Fluorescent Protein). *Journal of Neuroscience*, 23(7), 2655–2664. doi: 10.1523/jneurosci.23-07-02655.2003

296. Stiber, J. A., Zhang, Z.-S., Burch, J., Eu, J. P., Zhang, S., Truskey, G. A., Seth, M., Yamaguchi, N., Meissner, G., Shah, R., Worley, P. F., Williams, R. S., & Rosenberg, P. B. (2008). Mice Lacking Homer 1 Exhibit a Skeletal Myopathy Characterized by Abnormal Transient Receptor Potential Channel Activity. *Molecular and Cellular Biology*, 28(8), 2637–2647. doi: 10.1128/MCB.01601-07

297. Stiber, Jonathan A, Tabatabaei, N., Hawkins, A. F., Hawke, T., Worley, P. F., Williams, R. S., & Rosenberg, P. (2005). Homer modulates NFAT-dependent signaling during muscle differentiation. *Developmental Biology*, 287, 213–224. doi: 10.1016/j.ydbio.2005.06.030

298. Straube, A., & Merdes, A. (2007). EB3 Regulates Microtubule Dynamics at the Cell Cortex and Is Required for Myoblast Elongation and Fusion. *Current Biology*, 17(15), 1318–1325. doi: 10.1016/j.cub.2007.06.058

299. Sweeney, H. L., & Hammers, D. W. (2018). Muscle contraction. *Perspectives in Biology*, 10(2), a023200. doi: 10.1101/cshperspect.a023200

300. Takahashi, H., Mizui, T., & Shirao, T. (2006). Down-regulation of drebrin A expression suppresses synaptic targeting of NMDA receptors in developing hippocampal neurones. *Journal of Neurochemistry*, 97(1), 110–115. doi: 10.1111/j.1471-4159.2005.03536.x

301. Takahashi, H., Sekino, Y., Tanaka, S., Mizui, T., Kishi, S., & Shirao, T. (2003). Drebrin-dependent actin clustering in dendritic filopodia governs synaptic targeting of postsynaptic density-95 and dendritic spine morphogenesis. *Journal of Neuroscience*, 23(16), 6586–6595. doi: 10.1523/jneurosci.23-16-06586.2003

302. Takahashi, H., Yamazaki, H., Hanamura, K., Sekino, Y., & Shirao, T. (2009). Activity of the AMPA receptor regulates drebrin stabilization in dendritic spine morphogenesis. *Journal of Cell Science*, 122, 1211–1219. doi: 10.1242/jcs.043729

303. Takeshita, H., Yamamoto, K., Nozato, S., Inagaki, T., Tsuchimochi, H., Shirai, M., Yamamoto, R., Imaizumi, Y., Hongyo, K., Yokoyama, S., Takeda, M., Oguro, R., Takami, Y., Itoh, N., Takeya, Y., Sugimoto, K., Fukada, S. I., & Rakugi, H. (2017). Modified forelimb grip strength test detects aging-associated physiological decline in skeletal muscle function in male mice. *Scientific Reports*, 7(February), 1–9. doi: 10.1038/srep42323

304. Takikawa, K., & Nishimune, H. (2022). Similarity and Diversity of Presynaptic Molecules at Neuromuscular Junctions and Central Synapses. *Biomolecules*, 12(2), 179. doi: 10.3390/biom12020179

305. Tanabe, K., Yamazaki, H., Inaguma, Y., Asada, A., Kimura, T., Takahashi, J., Taoka, M., Ohshima, T., Furuichi, T., Isobe, T., Nagata, K. I., Shirao, T., & Hisanaga, S. I. (2014). Phosphorylation of Drebrin by Cyclin-dependent Kinase 5 and Its role in neuronal migration. *PLoS ONE*, 9(3). doi: 10.1371/journal.pone.0092291

306. Thomas, P., & Smart, T. G. (2005). HEK293 cell line: A vehicle for the expression of recombinant proteins. *Journal of Pharmacological and Toxicological Methods*, 51(3 SPEC. ISS.), 187–200. doi: 10.1016/j.vascn.2004.08.014

307. Thompson, R. F., & Langford, G. M. (2002). Myosin superfamily evolutionary history. *Anatomical Record*, 268(3), 276–289. doi: 10.1002/ar.10160

308. Tintignac, L. A., Brenner, H.-R., & Rüegg, M. A. (2015). Mechanisms Regulating Neuromuscular Junction Development and Function and Causes of Muscle Wasting. *Physiological Reviews*, 95, 809–852. doi: 10.1152/physrev.00033.2014

309. Todi, S. V., Franke, J. D., Kiehart, D. P., & Eberl, D. F. (2005). Myosin VIIA defects, which underlie the usher 1B syndrome in humans, lead to deafness in Drosophila. *Current Biology*, 15(9), 862–868. doi: 10.1016/j.cub.2005.03.050

310. Tolias, K. F., Duman, J. G., & Um, K. (2011). Control of synapse development and plasticity by Rho GTPase regulatory proteins. *Progress in Neurobiology*, 94(2), 133–148. doi: 10.1016/j.pneurobio.2011.04.011.Control

311. Trevillyan, J. M., Chiou, X. G., Chen, Y. W., Ballaron, S. J., Sheets, M. P., Smith, M. L., Wiedeman, P. E., Warrior, U., Wilkins, J., Gubbins, E. J., Gagne, G. D., Fagerland, J., Carter, G. W., Luly, J. R., Mollison, K. W., & Djuric, S. W. (2001). Potent Inhibition of NFAT

Activation and T Cell Cytokine Production by Novel Low Molecular Weight Pyrazole Compounds. *Journal of Biological Chemistry*, 276(51), 48118–48126. doi: 10.1074/jbc.M107919200

312. Trivedi, N., Stabley, D. R., Cain, B., Howell, D., Laumonnerie, C., Ramahi, J. S., Temirov, J., Kerekes, R. A., Gordon-Weeks, P. R., & Solecki, D. J. (2017). Drebrin-mediated microtubule-actomyosin coupling steers cerebellar granule neuron nucleokinesis and migration pathway selection. *Nature Communications*, 8(14484). doi: 10.1038/ncomms14484

313. Valdez, G., Tapia, J. C., Kang, H., Clemenson, G. D., Gage, F. H., Lichtman, J. W., & Sanes, J. R. (2010). Attenuation of age-related changes in mouse neuromuscular synapses by caloric restriction and exercise. *Proceedings of the National Academy of Sciences of the United States of America*, 107(33), 14863–14868. doi: 10.1073/pnas.1002220107

314. Veillat, V., Spuul, P., Daubon, T., Egaña, I., Kramer, I., & Génot, E. (2015). Podosomes: Multipurpose organelles? *International Journal of Biochemistry & Cell Biology*, 65, 52–60. doi: 10.1016/j.biocel.2011.01.007

315. Verschuuren, J., Strijbos, E., & Vincent, A. (2016). Neuromuscular junction disorders. In *Handbook of Clinical Neurology* (1st ed., Vol. 133). Elsevier B.V. doi: 10.1016/B978-0-444-63432-0.00024-4

316. Wagner, W., Lippmann, K., Heisler, F. F., Gromova, K. V., Lombino, F. L., Roesler, M. K., Pechmann, Y., Hornig, S., Schweizer, M., Polo, S., Schwarz, J. R., Eilers, J., & Kneussel, M. (2019). Myosin VI Drives Clathrin-Mediated AMPA Receptor Endocytosis to Facilitate Cerebellar Long-Term Depression. *Cell Reports*, 28(1), 11-20.e9. doi: 10.1016/j.celrep.2019.06.005

317. Wang, A., Liang, Y., Fridell, R. A., Probst, F. J., Wilcox, E. R., Touchman, J. W., Morton, C. C., Morell, R. J., Noben-Trauth, K., Camper, S. A., & Friedman, T. B. (1998). Association of unconventional myosin MYO15 mutations with human nonsyndromic deafness DFNB3. *Science*, 280(5368), 1447–1451. doi: 10.1126/science.280.5368.1447

318. Wang, H. W., & Nogales, E. (2005). Nucleotide-dependent bending flexibility of tubulin regulates microtubule assembly. *Nature*, 435(7044), 911–915. doi: 10.1038/nature03606

319. Wang, J., Jing, Z., Zhang, L., Zhou, G., Braun, J., Yao, Y., & Wang, Z. Z. (2003). Regulation of acetylcholine receptor clustering by the tumor suppressor APC. *Nature Neuroscience*, 6(10), 1017–1018. doi: 10.1038/nn1128

320. Webb, B. A., Eves, R., & Mak, A. S. (2006). Cortactin regulates podosome formation: Roles of the protein interaction domains. *Experimental Cell Research*, 312(6), 760–769. doi: 10.1016/j.yexcr.2005.11.032

321. Webster, R. G. (2018). Animal Models of the Neuromuscular Junction, Vitally Informative for Understanding Function and the Molecular Mechanisms of Congenital Myasthenic Syndromes. *International Journal of Molecular Sciences*, 19(1326). doi: 10.3390/ijms19051326

322. Weissgerber, T. L., Savic, M., Winham, S. J., Stanisavljevic, D., Garovic, V. D., & Milic, N. M. (2017). Data visualization, bar naked: A free tool for creating interactive graphics. *Journal of Biological Chemistry*, 292(50), 20592–20598. doi: 10.1074/jbc.RA117.000147

323. Wells, A. L., Lin, A. W., Chen, L. Q., Safer, D., Cain, S. M., Hasson, T., Carragher, B. O., Milligan, R. A., & Sweeney, H. L. (1999). Myosin VI is an actin-based motor that moves backwards. *Nature*, 401(6752), 505–508. doi: 10.1038/46835

324. Wen, Y., Eng, C. H., Schmoranzer, J., Cabrera-Poch, N., Morris, E. J. S., Chen, M., Wallar, B. J., Alberts, A. S., & Gundersen, G. G. (2004). EB1 and APC bind to mDia to

stabilize microtubules downstream of Rho and promote cell migration. *Nature Cell Biology*, 6(9), 820–830. doi: 10.1038/ncb1160

325. Weston, C., Gordon, C., Teressa, G., Hod, E., Ren, X. D., & Prives, J. (2003). Cooperative regulation by Rac and Rho of agrin-induced acetylcholine receptor clustering in muscle cells. *Journal of Biological Chemistry*, 278(8), 6450–6455. doi: 10.1074/jbc.M210249200

326. Willadt, S., Nash, M., & Slater, C. R. (2016). Age-related fragmentation of the motor endplate is not associated with impaired neuromuscular transmission in the mouse diaphragm. *Scientific Reports*, 6(1), 24849. doi: 10.1038/srep24849

327. Willmes, C. G., Mack, T. G. A., Ledderose, J., Schmitz, D., Wozny, C., & Eickholt, B. J. (2017). Investigation of hippocampal synaptic transmission and plasticity in mice deficient in the actin-binding protein Drebrin. *Scientific Reports*, 7(February), 1–11. doi: 10.1038/srep42652

328. Wong, M. Y., Liu, C., Wang, S. S. H., Roquas, A. C. F., Fowler, S. C., & Kaeser, P. S. (2018). Liprin-α3 controls vesicle docking and exocytosis at the active zone of hippocampal synapses. *Proceedings of the National Academy of Sciences*, 201719012. doi: 10.1073/pnas.1719012115

329. Woolner, S., & Bement, W. M. (2009). Unconventional myosins acting unconventionally. *Trends in Cell Biology*, 19(6), 245–252. doi: 10.1016/j.tcb.2009.03.003

330. Worth, D. C., Daly, C. N., Geraldo, S., Oozeer, F., & Gordon-Weeks, P. R. (2013). Drebrin contains a cryptic F-actin-bundling activity regulated by Cdk5 phosphorylation. *Journal of Cell Biology*, 202(5), 793–806. doi: 10.1083/jcb.201303005

331. Wu, H., Nash, J. E., Zamorano, P., & Garner, C. C. (2002). Interaction of SAP97 with minus-end-directed actin motor myosin VI: Implications for AMPA receptor trafficking. *Journal of Biological Chemistry*, 277(34), 30928–30934. doi: 10.1074/jbc.M203735200

332. Xing, G., Xiong, W. C., & Mei, L. (2020). Rapsyn as a signaling and scaffolding molecule in neuromuscular junction formation and maintenance. *Neuroscience Letters*, 731, 135013. doi: 10.1016/j.neulet.2020.135013

333. Xu, A., Nepliouev, I., Zhang, Z.-S., & Stiber, J. A. (2012). The Role of Drebrin in Skeletal Muscle Regeneration and Repair. *Cureus*. https://www.cureus.com/posters/119-the-role-of-drebrin-in-skeletal-muscle-regeneration-and-repair

334. Yaffe, D., & Saxel, O. (1977). Serial passaging and differentiation of myogenic cells isolated from dystrophic mouse muscle. *Nature*, 270, 725–727. doi: 10.1038/270725a0

335. Yamazaki, H., Kojima, N., Kato, K., Hirose, E., Iwasaki, T., Mizui, T., Takahashi, H., Hanamura, K., Roppongi, R. T., Koibuchi, N., Sekino, Y., Mori, N., & Shirao, T. (2014). Spikar, a novel drebrin-binding protein, regulates the formation and stabilization of dendritic spines. *Journal of Neurochemistry*, 128(4), 507–522. doi: 10.1111/jnc.12486

336. Yang, X., Arber, S., William, C., Li, L., Tanabe, Y., Jessell, T. M., Birchmeier, C., & Burden, S. J. (2001). Patterning of muscle acetylcholine receptor gene expression in the absence of motor innervation. *Neuron*, 30(2), 399–410. doi: 10.1016/S0896-6273(01)00287-2

337. Yano, H., Ninan, I., Zhang, H., Milner, T. A., Arancio, O., & Chao, M. V. (2006). BDNF-mediated neurotransmission relies upon a myosin VI motor complex. *Nature Neuroscience*, 9(8), 1009–1018. doi: 10.1038/nn1730

338. Zakrzewski, P., Lenartowski, R., Rędowicz, M. J., Miller, K. G., & Lenartowska, M. (2017). Expression and localization of myosin VI in developing mouse spermatids. *Histochemistry and Cell Biology*, 148(4), 445–462. doi: 10.1007/s00418-017-1579-z

339. Zhang, B., Luo, S., Dong, X. P., Zhang, X., Liu, C., Luo, Z., Xiong, W. C., & Mei, L. (2007). B-Catenin Regulates Acetylcholine Receptor Clustering in Muscle Cells Through Interaction With Rapsyn. *Journal of Neuroscience*, 27(15), 3968–3973. doi: 10.1523/JNEUROSCI.4691-06.2007

340. Zhang, M. Y., Zhang, W. J., & Medler, S. (2010). The continuum of hybrid IIX/IIB fibers in normal mouse muscles: MHC isoform proportions and spatial distribution within single fibers. *American Journal of Physiology - Regulatory Integrative and Comparative Physiology*, 299(6), 1582–1591. doi: 10.1152/ajpregu.00402.2010

341. Zhao, B., Meka, D. P., Scharrenberg, R., König, T., Schwanke, B., Kobler, O., Windhorst, S., Kreutz, M. R., Mikhaylova, M., & Calderon De Anda, F. (2017). Microtubules Modulate F-actin Dynamics during Neuronal Polarization. *Scientific Reports*, 7(9583), 1–16. doi: 10.1038/s41598-017-09832-8

342. Zhao, X., Moloughney, J. G., Zhang, S., Komazaki, S., & Weisleder, N. (2012). Orai1 Mediates Exacerbated Ca2+ Entry in Dystrophic Skeletal Muscle. *PLoS ONE*, 7(11). doi: 10.1371/journal.pone.0049862

343. Zong, Y., Zhang, B., Gu, S., Lee, K., Zhou, J., Yao, G., Figueiredo, D., Perry, K., Mei, L., & Jin, R. (2012). Structural basis of agrin – LRP4 – MuSK signaling. *Genes & Development*, 26(3), 247–258. doi: 10.1101/gad.180885.111